

University of Bremen  
Faculty 1 of Physics and Electronics  
Institute for Biophysics

**Measuring creep response of soft samples by magnetic force microscopy**

(Revised edition 2023)

Dr. rer. nat. Achu Yango

## Abstract

In this work, we propose a setup for applying large controlled external magnetic fields in magnet on force transducers by Atomic Force Microscopy. We describe how the novel magnetic AFM setup significantly enhances the capabilities of the scanning probe microscopy technique when samples are to be studied under appropriate experimental conditions in the laboratory. The external forces in magnet might be applied directly to magnetic material deposited behind the AFM in order to orient the material in the direction of the magnetic field through the homemade current carrying coil. The ability to concentrate the magnetic fields on commercial force transducers of interest with a high sensitivity provided a way to derive quantitative information on the nature of the soft spring cantilever and sample interaction by AFM. Here, different modes for applying forces have been proposed: Oscillating the magnetic field causes the magnetic soft spring cantilever to oscillate. Oscillating the magnetic cantilever in the proximity of the soft cell/ tissue samples produces a small indentation on the samples which when measured and quantified gives a measure of the spring constant of the soft samples and diseased cells/tissues. In addition to the magnetic force controlled modulation AFM technique, two other novel modes for applying a forces have been proposed: (1) by raising the sample height an indirect force step is being applied, or (2) by employing magnetic cantilevers a direct force step can be applied. Both (technique (1) and (2)) lead to similar responses, whereas the latter seems to be better defined since it resembles closely a constant strain mode. The former is easier to implement in most instruments, thus it may be preferable from a practical point of view. Most motile live and diseased cells, in comparison with similar soft gels, are much more viscous, as has been qualitatively observed in conventional AFM force curve data before. The creep response and the stress relaxation of soft gel and tissue/cell samples after applying a step in loading and unloading force by means of the external magnetic fields has been directly measured by Atomic Force Microscope. By analysing the creep data with the standard linear solid model, we can quantify the viscous and elastic properties of soft samples independently. With the novel step response experiments the spring constant and the viscous damping coefficient of friction from the creep response data have been quantified. Interestingly, this work might facilitate (when appropriately quantified) the laboratory studies of intrinsic properties of soft live cells, diseased tissues and polymer gel samples in order to elucidate their role of molecular components and their role in visco-elasticity by AFM.

## Acknowledgement

Foremost, I would like to express my sincere and deepest gratitude to my advisor Prof. Dr. Radmacher Manfred for his continuous support of my Ph.D work and the research work, for his patience, motivation, enthusiasm, and immense knowledge on the diverse exciting projects. My three years of research in his lab in the biophysics Institute in the university of Bremen contributed to my professional life and especially my personal growth. Your unconventional guidance helped me in all the time of the work. I could not have imagined having a better mentor for my Ph.D work.

Besides my advisor, I would like to thank Prof. Dr. Dorothea Brüggemann and the dissertation committee, Prof. Dr. Stefan Bornholdt, and Prof. Dr Martin Eickhoff who generously took without hesitating the academic responsibility for this work

My sincere thanks also go to Prof. Dr. Monica Fritz, her working group for their continuous encouragement, inter-disciplinary collaborations, insightful comments, refreshment activities, very constructive feedback and many interesting questions. My appreciations are extended to Holger Doschke, for his valuable assistance.

I thank in general my fellow laboratory mates and all my colleagues in Biophysics Group: Dr. Meike Gummich, Katherina Gärtner, Dr. Carmela Rianna, Dr Jens Schäpe, as well to Prem Kumar for the stimulating discussions, for the sleepless nights we were working together before deadlines, and for all the fun we have had in the time of my work. It was great sharing laboratory with all of you during last four years.

Also I thank my friends in the University and to Marie-Ann for enlightening me the first glance of the work and introducing me to the laboratory, most of all the insightful and friendly discussions. Last but not the least, I would like to thank my entire family: my wife Cathy-Armelle and sisters for their support and encouragements throughout till date.

And finally, last but by no means least, also to everyone in the Biophysics Institute especially Janka Heitz who spent some difficult times while prove reading the initial version of the work.

## Table of content

Abstract.....	i
Acknowledgement.....	ii
Table of content.....	iii
List of Figures .....	v
<b>1.0 GENERAL INTRODUCTION AND STATE OF THE ART .....</b>	<b>1</b>
<b>1.1 What is an Atomic Force microscope? .....</b>	<b>10</b>
<b>1.2 Working principle of the AFM.....</b>	<b>10</b>
<b>1.3 Implementation of the AFM technique .....</b>	<b>14</b>
1.3.1 The AFM cantilevers probe.....	14
1.3.2 Contact mode AFM .....	20
1.3.3 Dynamic mode in AFM.....	27
1.3.4 Force volume .....	29
1.3.5 Vibration response .....	30
1.3.6 Sensitivity of the AFM technique.....	32
1.3.7 Indenting force.....	38
<b>1.4 Mechanical properties and analysis techniques .....</b>	<b>42</b>
<b>1.5 Motivation and summary of critical issues .....</b>	<b>60</b>
1.5.1 Theoretical fundamentals and an experimental approach.....	63
1.5.2 Magnetic properties, force and the choice of magnetic particles.....	67
<b>1.6 Research goals, objectives and overview.....</b>	<b>68</b>
<b>2.0 MATERIALS AND METHODS .....</b>	<b>71</b>
<b>2.1 The AFM apparatus and description .....</b>	<b>71</b>
<b>2.2 Sample preparation.....</b>	<b>72</b>
2.2.1 Cell culture .....	72
2.2.2 Gel preparation.....	72
2.2.3 Magnetic cantilever preparation.....	73
<b>2.3 Descriptions of setup with magnetic cantilevers .....</b>	<b>75</b>
2.3.1 AFM force curves.....	79
2.3.2 AFM z step response:.....	79
2.3.3 AFM magnetic step response .....	80
<b>3.0 DATA ANALYSIS AND MODELLING .....</b>	<b>81</b>
<b>3.1 Spring constant of the sample derived from the force curves .....</b>	<b>82</b>
<b>3.2 Analysis of Creep Response Data from z response experiment .....</b>	<b>84</b>
<b>3.3 Conventional step by increasing z-height: z-step.....</b>	<b>86</b>
<b>3.3 Analysis of Creep Response Data from magnetic force steps.....</b>	<b>90</b>
<b>3.4 Spring constants from the force modulation experiment.....</b>	<b>94</b>
<b>3.5 The phase lag between free and in contact motions of the cantilever.....</b>	<b>96</b>
<b>4.0 RESULTS .....</b>	<b>98</b>
<b>5.0 DISCUSSION.....</b>	<b>109</b>
<b>6.0 CONCLUSIONS AND OUTLOOK.....</b>	<b>115</b>
<b>APPENDIX .....</b>	<b>117</b>
<b>A1. Spring constant of the sample derived from force curves .....</b>	<b>118</b>
<b>A2. Analysis of Creep response Data from z steps and magnetic step on gel sample ...</b>	<b>119</b>
<b>A3. The magnetic force in modulation of the live cell sample .....</b>	<b>120</b>
A3.1 Calibration of the deflection sensitivity of the optical lever system .....	121

A3.2 Calibration of the optical lever deflection sensitivity of the magnetic force AFM.....	122
<b>A 4.0 The mechanical properties of the soft samples from force modulation experiments .....</b>	<b>123</b>
<b>A5.0 Cytosol and Cytoskeleton .....</b>	<b>128</b>
A5.1 The cytoskeleton.....	130
<b>A6.0 The magnetic coil .....</b>	<b>135</b>
<b>A7.0 summary of the viscous properties of the cell derived from creep response data after application of force steps (loading and unloading steps) a magnetic step in force and the z step response experiments.....</b>	<b>138</b>
<b>BIBLIOGRAPHY .....</b>	<b>150</b>





## List of Figures

Figure 1: Schematic diagram of the conventional Atomic Force Microscope head with the addition of a feedback loop. The motion of the soft spring magnetic cantilever is obtained from the difference output of the split photodiode detector together with the optical beam method (design). The AFM combines high sensitivity in applying force, high precision in positioning the tip relative to the sample in three dimensions and the possibility to be operated in an aqueous environment. (Adapted from [9] and [13]) ..... 12

Figure 2: The AFM soft spring cantilever and tip. Typical cantilevers have a diving board shape. These are used for both the contact mode and the dynamic mode AFM. Triangular cantilevers have been used in contact mode AFM with the idea that they may be typically more sensitive. Figure shows a diagram of an AFM probe with 5 AFM cantilevers (four triangular and a rectangular shaped cantilever) with the sharp tip. The tip material can be chosen for specific properties of the sample it will interact with. The soft spring AFM cantilever shown on image employs a pyramidal tip with asymmetrical tip geometry[21]. ..... 15

Figure 3: Typical sequences (steps 1- 5) of an AFM probe movement during a force curve data acquisition. The AFM cantilever deflection (when free and when in contact (2) relative to a stiff sample surface) is recorded versus the z-height piezo scanner. Left panel shows the z piezo fully retracted to the original position (1) and not interacting with the cantilever and the tip (red). The applied load (cantilever spring force) corresponds to the soft spring AFM cantilever deflection signal and the spring constant of the soft spring cantilever. As the z-piezo extends, there is a sudden jump and the AFM cantilever is pulled down (2) by attraction to the sample surface. This attraction decreases with increasing z-height scanner position. As the cantilever tip is pressed into the surface the orientation of the cantilever changes (3). The z-piezo distance increases the cantilever ascends and then begins to pull up the tip (4). The applied load corresponds to the soft spring AFM cantilever deflection and the spring constant of the soft spring cantilever. At the maximum of the applied force load the z-height motion retracts and the cantilever momentarily returns to its free position (5). As shown on the figure forces obtained in air, may reveal an observable hysteresis (typically not seen in aqueous solutions) when the soft spring AFM cantilever is retracted from the sample surface and procedure requires a definite point of contact. Right panel shows corresponding output: force curve plot (adapted from [30]). ..... 21

Figure 4: Comparison of the force curve (approaching regime) on a soft and a stiffer sample as function of the z-height motion. In a force curve we will ramp the force to a certain value by ramping the z-position  $z_1$ . The figure illustrates the contact portion and the non-contact portion of the approaching force curve. The indentation  $\delta$  is represented as the difference in change in z-height and change in the deflection values. Varying the soft spring AFM cantilever with tip movement on the sample can give further information about the soft sample response. The elastic response of the soft sample in question requires an appropriate model like the Hertz model to correlate the z-height motion and the measured deflection of the AFM cantilever. On stiff samples the force curve exhibits a transition of the regimes of the force curve at the contact point, where the slope typically jumps from 0 (free cantilever) to 1 (in contact) with the sample. .... 25

Figure 5: Thermally driven motion of a magnetic cantilever in an aqueous environment. The figure shows several higher modes due to thermal noise of the AFM cantilever. The spring constant of the cantilever obtained from the SHO and Lorentz fits to the first

bending mode to the thermal noise data in the frequency domain. The AFM measures tilt and the sensitivity decreases for higher modes. The figure shows x-axis with the first and the second spectral peaks of the deflection data, which are obtained at approximately 850 Hz and 10 kHz for a wide range of frequencies respectively. The amplitudes (intensity in the thermal noise) of the deflection data on the y-axis span a wider range of  $1021 \dots 1024 \text{ m}^2 \cdot \text{Hz}^{-1}$  with the first frequency fit width smaller size than for the second bending modes. .... 31

Figure 6: Thermal force and deflection fluctuations as a function of AFM cantilever spring constants respectively. These numbers shown on the graph will give a lower limit for noise in the quantities force and deflection. .... 32

Figure 7: Illustration of the AFM optical lever beam bounce technique. The deflection of the cantilever is sensed with the optical detection. Image shows a side view of the reflection at the very end of the soft spring cantilever as it changes orientation upon contact with the sample surface, which is considered as the deflection. The reflected laser light from the very tip end of the AFM triangular cantilever creates a push pull error signal when the spot moves on the position sensitive photodiode (PSD). When the soft spring cantilever is at the neutral deflection the laser light spot falls on the center of the PSD. .... 34

Figure 8: Illustration of an approach-based indenting force versus the resulting indentation relationship obtained on the live cell sample. The raw experimental deflection data (red trace) has been compared with the fitted (blue trace) curve on the soft substrate. The loading force, which is proportional to the contact area of the cantilever tip was the deflection multiplied by the spring constant of the cantilever. The indentation is the deflection subtracted from the z height. The indenting force and the resulting indentation in the cells often will follow the prediction of the Hertz model. Once the contact point has been identified the cell sample stiffness can be derived while assuming linearity. Analysing the approach-load relationship proves linearity for the pyramid tip at larger penetration depths on the live cell. The lower force range (ca. 0 nN -0.1 nN) indicates the considerable noise introduced in the system upon contact between the tip and the cell sample surface..... 41

Figure 9: Comparison force curve of a living cancer thyroid cell sample in an aqueous medium showing the approach and the retracting force curve ramps. (A) Hertz model fit on approaching ramp and retracting ramp of the force curves on a thyroidal cell. For cancer cells (B) a large hysteresis between the two curves could be seen; consequently, thus the spring constants of the cell samples extracted from the mechanical data will be different.[46] ..... 48

Figure 10 Association of the springs to determine the spring constants of the soft sample in terms of the spring constant of the cantilever and the oscillation amplitudes i) no contact A0 and 2) in contact A1 ..... 64

Figure 11: Schematic setup of magnetic AFM cantilever including the electrical assembly. The coil has been connected to a voltage/current transducer. The AFM controller links the transducer to the personal computer. The sample is mounted on the x-y piezo of the AFM. A coil is attached firmly to the microscope objective lens, which is placed under the AFM tip in the combined optical/force microscope (panel A) and a 3 mm gap spacing below the AFM sample holder. The core material of the coil has a sharp pin in order to concentrate the gradient of the magnetic field. In panel B three AFM cantilever with varied lengths. The longest (middle)  $320 \mu\text{m}$  triangular AFM cantilever shows an glued magnetic particle to the tip..... 76

- Figure 12: Typical force curve recorded after ramping cantilever on top of a cell. The figure shows plot of the approach (red trace) and the retract (blue trace) curves for contact mode cantilever in an aqueous environment. The deflection of the cantilever is recorded versus elongation of the piezo-electric scanner in the vertical direction. The simulated fit (green and black) is drawn on the approach and the retract regime of the force curves respectively..... 82
- Figure 13: The Standard Linear Solid Model. The sample is modelled by a Zener element, where a spring  $k_1$  is in parallel to a Maxwell element, consisting of a spring  $k_2$  and a viscous damping element  $f$ . The soft spring AFM cantilever is characterized by its spring constant  $k_c$ . Motion of the sample height  $z$  is resulting in a deflection  $d$  of the cantilever or indentation  $d$  of the sample. .... 84
- Figure 14: Typical conventional force curve obtained on a cell sample. The deflection data (A) and the loading step in  $z$  height (B) for duration of 1 second. The  $z$ -height motion is reversed at  $t = 0.5$ s. The indentation is the difference between the change  $z$  height and the change in the soft spring cantilever deflection signal..... 85
- Figure 15: Typical creep response of a cell after applying a  $z$  step. Panel A shows the deflection data, while the  $z$  height (B) is first ramped as in a conventional force curve (approach ramp), then kept constant for 2 seconds, except a small step force step in magnetic force, which is applied after the creep of the cell, caused by the approach ramp, has relaxed appreciably. Then, finally the sample is retracted again (retract ramp). After the step (applied from time 1.5 to 2.0 seconds) the creep response to the loading and unloading step is analysed in detail. The indentation is the difference between the  $z$  height and the cantilever deflection. .... 86
- Figure 16: Creep response at dwell after applying a loading step in  $z$  height at  $t = 1.5$ s and an unloading step at  $t = 2.0$ s. The indentation is calculated as the difference between  $z$  height and deflection. The deflection data are fitted with an exponential function, which will give  $k_1$ ,  $k_2$  and  $f$  as results. The creep response at the dwell time is zoomed for better visibility. .... 87
- Figure 17: Typical creep response of a cell after applying a magnetic step. Panel A shows the deflection data, while the  $z$  height (B) is first ramped as in a conventional force curve (approach ramp), then kept constant for 2 seconds, except a small step in  $z$ -height, which is applied after the creep of the cell, caused by the approach ramp, has relaxed appreciably. Then, finally the sample is retracted again (retract ramp). After the step (applied from time 1.5 to 2.0 seconds) the creep response to the loading and unloading step is analysed in detail. The indentation is the difference between the  $z$  height and the cantilever deflection. .... 90
- Figure 18: Creep response on the cell sample during 400 pN magnetic step force step starting at  $t = 1.5$ s. The deflection changes slowly resulting to the sample indentation, which is then followed by an unloading step at  $t = 2.0$  s. For the loading step the change of deflection  $\Delta d$  is negative, since the indentation (30 nm) change is positive. The change in  $z$  height is zero during the direct step in force experiment. By applying an exponential fit we gain the spring constants  $k_1$ ,  $k_2$  of the cell sample and the viscous properties of the cell sample. .... 91
- Figure 19: An equivalent mechanical circuit of the sample spring in series with the cantilever spring in the in contact motion. The motion (oscillations) of the cantilever spring in contact with the viscoelastic sample with amplitude  $A_1$ . The elastic properties could be described until the preset loading force of the conventional force curve, ..... 94
- Figure 20: Figure shows stress relaxation data on a gel sample after a modulation force. The upper panel shows the  $z$  height profiles versus the time. The  $z$ -motion was stopped ( $t =$

0.5 seconds) for 2 seconds. During this time the stress relaxation after the approach ramp of the cell has relaxed (with displacement  $A_1$ ) and then retracted at  $t = 2.5$  seconds. The magnetic force modulation is directly applied to the soft spring magnetic AFM cantilever. The modulation of the soft spring magnetic AFM cantilever around an equilibrium indentation leads to a modulation of the force between the soft spring AFM magnetic cantilever and the soft sample. The bottom panel shows the deflection data in nm versus the time off and the in contact with the gel sample after the application of the modulation force in magnet for 3.5 seconds. Before contact the displacement of the free cantilever is  $A_0$ . The effective modulation spring constant of the sample is an indicator of the overall viscoelastic property of the sample. The force modulation may reveal a set of material responses over specific frequencies. For the in-contact system since the same force has to deform two springs, we obtain a smaller displacement  $A_1$  ( $A_1 < A_0$ )..... 95

Figure 21: Typical creep response of a cell after applying a z step. Panel A shows the deflection data, while the z height is first ramped as in a conventional force curve (approach ramp), then kept constant for 2 seconds, except a small step in z-height, which is applied after the creep of the cell, caused by the approach ramp, has relaxed appreciably. Then, finally the sample is retracted again (retract ramp). After the step (applied from time 1.5 to 2.0 seconds) the creep response to the loading and unloading step is analysed in detail (see panel B & D for a zoom in). The deflection data is fitted with an exponential function, which is analysed in terms of the standard linear solid model. .... 100

Figure 22: Creep response of a cell after a magnetic force step. Here the z height is kept constant for 2 seconds, after the approach ramp (22A and B). At time 1.5 s (after 1 second of dwell) a magnetic force is applied to the cantilever (fig. 22C), which leads to a change in indentation of the sample (Fig 22D), which in this case can be read directly from the deflection signal. As in the z-step, we can see an instantaneous jump in deflection followed with a slow creep. Here, due to the different experimental scheme, both effects go in the same direction, and thus appear to the eye very different than the equivalent creep response process in fig 21D. (same cell as in figure 21) ..... 102

Figure 23 Comparison of the elastic spring constants values of the live cell sample calculated from force curve data ( $k_{\text{approach}}$  and  $k_{\text{retract}}$  are the values from the corresponding branch of the force curve) and from step response data ( $k_1$  loading step and unloading step). The graph is a compilation of all 36 force curves from a 6 by 6 force volume over an area of 600nm..... 104

Figure 24: Comparison of the spring constant (A) and viscous properties (B) of the live cells derived from a magnetic step and z step response experiments respectively. The values correspond to the medians of the respective quantity from the 36 values measured in a force volume over a square area of 600nm. The spring constants derived from the step ( $k_1$  loading and  $k_1$  unloading) are very similar for both methods (z step and magnetic step), whereas the spring constant ( $k$ 's) derived from approach and retract force curves deviate largely due to the neglect of viscous response in this type of analysis. The viscous properties (the relative strength compared to the elastic properties is measured by  $k_2$ , whereas  $\tau$  is the relaxation time) are also determined reproducibly in both step methods (z step and magnetic) for loading and unloading steps. .... 104

Figure 25: Stress relaxation response data obtained on a diseased tissue soft sample during the force modulation experiment to test the sensitivity of setup. The figure shows the

- deflection versus the time traced for ca. 3.5 s. The z-motion was stopped ( $t = 0.5$  seconds) and the direction reversed after 2 seconds. During this time the stress relaxation after the approach ramp of the cell has relaxed considerably. .... 106
- Figure 26: Comparison of the spring constants of a soft sample (elastic values) to test magnetic AFM force setup. The spring constant derived by analysing force curve (Conv.), the magnetic step (Magn) and the z step response experiments on cell sample by AFM experiments. The graph is a compilation of all 46 force maps each obtained over an area of 600 by 600 nm..... 107
- Figure 27: Experiment designed to characterize (testing) a AFM magnetic AFM force control design by force modulation experiments. The figure shows the derived spring constants (figure A and B) and the response amplitudes ratio (C) at varied drive frequencies in magnetic force to test the AFM magnetic force setup. Results represent are the median values derived from a force curve and modulated creep data over physiological relevant frequency ranges on soft samples. .... 108
- Figure 28: Force curve on a cell while at maximum force a z step is performed (see yellow circle). The figure shows the same data as in figure 16, here in the conventional scheme of deflection versus z height as is usually done in force curves. The slopes and the corresponding spring constant of the cell sample, which can be calculated from the approach and retract part of the data are also indicated in the annotation..... 118
- Figure 29: Force curve on a cell while at maximum force a magnetic step is performed. The figure shows the same data as in figure 17, here in the conventional scheme of deflection versus z height as is usually done in force curves. Since in a magnetic step, only the deflection changes due to the magnetic force (z is kept constant) the effect of the step is harder to see than in fig 17. The slopes and the corresponding spring constant of the cell sample, which can be calculated from the approach and retract part of the data are also indicated in the annotation..... 118
- Figure 30: Analysis of step response data on polyacrylamide gels. Panel A shows a comparison of spring constant values calculated from approach and retract curve with the spring constant  $k_1$  values from step response. Panel B shows the creep response time and the spring constant of the sample  $k_2$  values. All values are very close for loading and the unloading, except the approach and retract data calculated from the force curves, as expected..... 119
- Figure 31: Schematics of the viscoelastic measurement of soft samples via modulation of the magnetic cantilever tip position with the magnetic force microscopy. The modulation of the cantilever around an equilibrium indentation leads to a modulation of the force between the AFM cantilever and the soft sample. Similar to a constant strain experiment in which the z-height is kept constant for  $t = 2$  seconds of the approach ramp, except  $t = 1.5$ s a jump in the modulation force with an amplitude is applied to the viscoelastic sample by the magnetic cantilever which leads to a modulation indentation with the same frequency. The contact force will oscillate around the equilibrium indentation depth. This results in an effective oscillatory response of the viscoelastic sample. The magnetic force modulation is directly applied to the soft spring magnetic AFM cantilever for duration of 3.5 seconds (B). The magnetic force modulation experiment enabled the drive signals to be directly related to the force and the response of the magnetic cantilever. The amplitude and the phase shift (fitting parameters) between the drive signals and the response due to the sample could be analysed in terms of a linear viscoelastic theory. The time scale is defined by the modulation frequency due to the sample.

By observing the response at a range of frequencies the relative contribution of the elastic and the viscous response can be characterized at varied time scales. The effective modulation spring constant is an indicator of the overall viscoelastic property of the sample. The force modulation may reveal a set of material responses over specific frequencies. .... 120

Figure 32: Calculating the inverse optical lever sensitivity (InvOLS) by obtaining force curves on stiff substrate. Force curve at maximum force performed on clean petri dish substrate in air. The force curve contains information about the long- and the short ranged interaction and also represents the basis for estimation of the Young's modulus of the sample [Pa] to estimate the InvOLS of the system. Calculating the InvOLS typically requires that a force measurement be performed on a hard surface to measure the voltage response of the PSD as a function of the known distance moved by the z-piezo. A resistive force on the stiffer substrate determines how easy the deformation may be performed by the soft spring magnetic AFM cantilever during testing phase. The force curves were obtained on an area of 600 nm x 600 nm. The soft spring magnetic cantilever is subjected to the change in the orientation by the application of an external force. .... 121

Figure 33: Comparison of the spring constants values of the live cell sample calculated from force curve data ( $k_{appr.}$  and  $k_{retr.}$  are the values from the corresponding branch of the force curve) and from the branch of magnetic step response data ( $k_1$  loading and unloading steps). The spring constant ( $k_{approach}$  and  $k_{retract}$ ) derived by analysing the magnetic step response data at an average magnetic force step is shown for a visual comparison demonstrative purposes. The graph is a compilation of all 36-force curves from a 6 by 6 force volume over an area of 600nm. .... 126

Figure 34: Comparison of spring constants values of the stiffer polymer gel sample calculated from a force curve data and from the magnetic step response data. The spring constants calculated from the force curve data (the spring constants  $k_{approach}$  and  $k_{retract}$  are the values from the corresponding branch of the force curve) at an average force step and from the magnetic step response data ( $k_1$  loading step and unloading step). The spring constant ( $k_{approach}$  and  $k_{retract}$ ) derived by analysing the magnetic step response data at an average magnetic force step is shown for a visual comparison demonstrative purposes. The graph is a compilation of all 14-force curves from a 4 by 4 force volume over an area of 600nm. .... 127

Figure 35: Summary of viscous properties derived by independently analysing gel data from the magnetic step response data. The upper panel shows a comparison of the coefficient of friction values from magnetic step response. The lower panel shows the spring constant  $k_2$  values. All values are very close for unloading as expected. .... 127

Figure 36: A network of fibrillar proteins (A) organized into the filaments and the tubules. The distributed cytoplasmic structural actin network is formed by cross-linked actin fibers. The inter-linked polymeric protein filaments (actin filaments in green) and the tubules (highlighted in red) extend throughout a cell cytosol (the blue dots are the cellular nuclei). An electron micrograph shown on (B) shows three filament types. .... 129

Figure 37: Image shows an elastic modulus image (array of elastic force curves at different sites on the soft sample) acquired by indenting a living cell. Morphological changes in the live cell characterized by the variation in the elastic modulus in its

natural environment. The cytoskeleton is related to the cell shape, the change of this shape and the migration of the cells. The array of elastic values of the sample is calculated from the z-height base movement and the measured deflection of the soft spring constant values. The elastic modulus of the FM was calculated by employing the Hertz model. The left panel show the measured height data of the cell sample with the small variation of 'the surface height. .... 132

Figure 38: Image of the AFM coil setup employed for the loading and unloading force control in step and in modulation magnetic force. Image shows a side view of magnetic adapted on the 20 X objective lens of the AFM. The strip of the sharp transformer metal core with copper wire windings is shown in image. The core material aided to create the large gradient of the magnetic field. The apparatus offers an advantage and a non-invasive method to apply force to very end of the magnetic AFM cantilever/magnetic particles placed on the AFM stage in a fluid cell. .... 135

Figure 39: The magnetic force exerted on the cantilever depends on the spatial relation between the coil and the magnetic cantilever in an aqueous medium. The figure shows data obtained after calibrating of the coil voltage into force in magnet as a function of distance to the soft spring magnetic AFM cantilever. The calibration of the coil voltage into force is obtained from the motion of the free cantilever. The force was dependent on the size of the magnetic fragment and the position on the back of the cantilever with respect to the position of the coil. Displacement of the free cantilever in combination with the measured soft AFM cantilever spring constant gives values of the force applied per volts through the coil in use. The calibration was required every time a magnetic fragment was glued to the back of the cantilever was changed or the laser position was changed. For coarse approach the entire coil is firmly attached to objective of the inverted microscope. Graph shows a decrease in the response of the soft spring magnetic cantilever as the gab size is increased. The graph has been zoomed (sensitivity [nN/V] axis) for better visibility. .... 135

Figure 40: Calibration of the coil voltage into force in magnet in an aqueous medium and in air. The calibration of the coil voltage into force is obtained from the motion of the free cantilever. The Comparison shows a reduction in the sensitivity in aqueous medium when compared to air data obtained after a step drive. The values on each point are an average of 19 experimental rounds. The y-axis shows the sensitivity [nN/V] while the x-axis shows the average values from nineteen-experiment measured repeatedly at longer time intervals on the same day. The magnetic cantilever was place at large fields and large distances relative to the AFM sample stage. Figure shows considerable hysteresis and drift in values due to drift in magnetic coil design. .... 136

Figure 41: Figure shows the relationship between the coil current as a function of drive voltage for an example coil prepared for the work. The force modulation technique provides large amplitude of the soft spring magnetic cantilever oscillations of the order of tens of mV/ nm. The graph shows an initial increase of output current as amplitude of drive signal increases. For this coil the figure depicts saturation for larger drive signals values. .... 136

Figure 42: Preparation of magnetic fragments in its fluid suspension. In oder to characterize the swystem we first introduced purely viscous fluids in the form of mixtures. The sytem was first calibrated at low frequencies in the quasi-static operation to set the ratio between the force in magnetic and current through coil. The behavior of magnetic framents under a small magnetic force (coil tip not shown) in a magnetic field and thier tiny aggregates revealed under the light microscopy. By observing the induced motion of due to the local field generated gradient of the coil on the magnetic paticles and beads,

the system was analysed and characterized adequately. The figure shows dark field and phase contrast images of an assembly of nanoclusters of magnetic fragments in with small spacings between them in their suspension. Left panel (A) includes magnetized clusters of the nano particles aligned in the inhomogeneous magnetic field. Paramagnets keep moving in the direction of strongest field. Right panel (B) includes an agglomerate of nano paramagnetic particles in the suspension..... 137

- Figure 43: The magnetic force microscope measurements were performed using a commercial MFP-3D- atomic force microscope mounted on an inverted optical microscope. The AFM soft spring magnetic cantilever is on the piezo-ceramic so that it may be moved in all the three directions. The coil is connected to the computer through a voltage/current converter and the drive signal from the AFM controller. The motion of the magnetic AFM cantilever is measured as a function of the drive current. The magnetic fragments were glued to the end of the cantilever using 2-component glue under control of the inverted optical microscope. Force calibration was only possible if the spring constant of the magnetic AFM cantilever was accurately measured. The relationship between the photodiode signal and the magnetic cantilever deflection (sensitivity factor S) was calibrated by recording several force curves before and after the AFM measurements, at a bare region of the glass coverslip and averaging its slope..... 138
- Figure 44: Summary of viscous values obtained by analysing the magnetic step response data on cell sample. The graph is a compilation of all 36 force curves from a 6 by 6 force volume over an area of 600 nm. The left column represents the loading steps and the right column represents the unloading step on one force volume..... 139
- Figure 45: Summary of viscous values of a cell sample derived by analysing a z step response data on polymer gel sample. The graph is a compilation of all 16-force curves from a 6 by 6 force volume over an area of 600 nm. The left panels are the loading steps and the right panel represents the unloading step analysed on one force volume..... 140
- Figure 46: Summary of spring constants and the viscous damping values obtained from a z step response data on cell sample. The graph is a compilation of all 36-force curves from a 6 by 6 force volume over an area of 600 nm. The left column represents the loading steps and the right column represents the unloading step on one force volume..... 141
- Figure 47: Summary of spring constants and viscous values obtained from a step response data on stiffer polymer gel sample. The graph is a compilation of all 16 force curves from a 6 by 6 force volume over an area of 600 nm. The left panels are the loading steps and the right panel represents the unloading step on one force volume. .... 142
- Figure 48: Summary of viscous values on soft polyacrylamide gels. Figure shows comparison of the spring constants values (panel A) and the relaxation times (panel B) derived by analysing the magnetic (Magn.) steps and the z step response (Z step) data respectively. The initial data obtained from both setups was summarized during the testing phase of the experiment. .... 143
- Figure 49: Comparison of the viscous values obtained from the magnetic step (Magn.) and the z step response (Z step) setups on the gel sample by AFM. The viscous properties from both setups could be quantified compared in terms of the creep response for both experimental designs. .... 144
- Figure 50: Summary of the spring constants and viscous values of the polyacrylamide gels sample derived by analysing the magnetic step response data. The graph is a





## 1.0 GENERAL INTRODUCTION AND STATE OF THE ART

The invention of the microscope and subsequent improvement about four centuries ago hasn't only contributed to improve our sense of seeing but it also revolutionized our understanding of the world through important break through in biology and medicine. In human for example, sight is often considered the most important sense, as it is the one that they would least want to lose. Our eyes, despite being a significant product of human evolution, still have significant limitations. The quest to enhance our perception, particularly through scientific endeavours, has served, in part, as a principal motivator behind most scientific advancements. On the other hand, interestingly, the local probe techniques extend the sense of touch in the micro and nano-world. Thus, by locally probing the surface of materials, scientist may acquire, new complimentary new and reproducible information at microscopic scales employing microscopic techniques. Numerous techniques and experimental approaches are now available in other to explore the mechanical properties of soft samples like polymer gel and live diseased cells. The sensitivity of most techniques may typically be dependent on the characteristics or the properties of the sample as well as on the sample preparation. It is challenging to accurately measure the mechanical properties of the soft samples like living cells, which have important applications in medicine. While we can now collect and now interpret our mechanical data directly by AFM, comparing and interpret our collected data quantitatively with alternative methods in literature seems to be very challenging.

As shown in figure 2a and 2b, an AFM cantilever is a springboard or triangular shaped beam (soft spring cantilevers) fixed (clamped) at one end, which is usually positioned over a deposited sample to be probed. The soft spring AFM cantilevers are mostly for the AFM applications are made of Silicon Nitride and may be manufactured by photolithography or by the wet etching techniques, which offers the possibility to fabricate the varied AFM cantilevers with the desired force sensitivity. The magnetic soft spring AFM cantilever is important for the force application and the viscoelastic creep measurements because it carries the load to the support where it is forced against by a moment or shear stress. The soft spring AFM cantilevers are force transducers made of an elastic material with spring constants often in the down to 0.01 N/m for measuring soft samples like most live and diseased cells including polymer gels. The soft spring AFM cantilever has a tip that interacts with the sample. This is the working end of the AFM (see figure 2b). The major advantage of employing the soft spring AFM cantilevers as a force transducer to study the viscoelastic and

the mechanical properties include its sensitivity and its fast response to the external loading force in the magnet. Application of forces causes this soft spring AFM cantilever to deflect and thus tries to achieve a mechanical force balance with the sample being indented. In some special cases, spherical particles are attached to the soft spring AFM cantilever to achieve specific surface properties and a controlled geometry.

In order to employ the soft spring AFM cantilevers to perform accurate measurements, the sensitivity to forces and displacements of the system are required to be calibrated. This is because the ability to obtain and quantify mechanical information at a single cell level is of central importance to numerous biological questions and still seems to represent a major challenge that requires the development of new and capable measurement tools. In addition, this typically requires analysis of the AFM indentation data obtained from experiments performed at different depths. This argument has been derived from the fact that the AFM capabilities expand beyond abilities to measure the viscoelasticity, the compression modulus, and adhesion forces from soft samples like most motile diseased cells.

In a typical AFM application performed by several authors the electrostatic, van der Waals, and hydration forces with high resolution in electrolyte solutions was measured.[1] Direct information of van der Waals forces became possible in 1970's with the surface force apparatus to explore their magnitude and the surface distance dependence.[2] Their technique was restricted because it required smooth, semi-transparent, macroscopic surface as part of the experimental set-up.[3] However, in many cases, especially in biological applications, the AFM is required to be operated in a medium (aqueous solution like cell culture medium), which has great influence on its dynamic properties.[4, 5] A recent and promising technique used to measure the viscoelastic properties of a wide variety of soft samples is rheology. The application of the AFM in this category is direct and the measurement of viscoelastic properties of soft samples by inferring the elastic constants from the monitored time-dependent deflection displacement curves. The AFM employs a measurement model that relates the soft spring constants of the system response to the deformation of the soft samples in aqueous solutions. Therefore, if knowledge of the spring constants and the true elastic and viscous quantities of the soft samples like the live diseased cell is of much interests, its application will typically require measuring and controlling the force which are applied to the soft sample. A significant factor that challenged the extraction of reliable material properties (information) had been the absence of physical accurate biophysical models for viscoelastic samples. Significant progress has been recently achieved with regards to obtaining the

simultaneous elastic and viscoelastic properties of the live samples like cells. Our AFM can be employed to study the interior of soft samples like live cells.

The change in the orientation or bending of the soft spring AFM cantilever due to the interaction force between cantilever tip and the sample surface is described by the deflection of the soft spring AFM cantilever due to a concentrated load exerted on the AFM tip. However, due to the sharpness (blunt/finite) of the soft spring cantilever tip, the interaction area or the contact compliance can be determined by a variety of local effects, including adhesion, the local hardness and the meniscus effects, which are wholly internal to the contact. The individual displacements are separately identified from the static measurement of the soft spring AFM cantilever positions to which the experiment is confined.

For the soft samples like cells and polymer gel, soft spring AFM cantilevers are required for the mechanical properties measurements involving local deformation because the force step loads of interest are very small. The motion of the soft spring AFM cantilever is recorded and subsequently analysed in terms of a well-established model of viscoelasticity. This employed approach yields the local information on the elastic properties and the viscosity of the cell cytoplasm/cytosol. The contribution to various intracellular components can be assessed by the controlled modification of the interior of the cell. By using soft spring AFM cantilevers of various sizes/shapes information can additionally be gained on the local intracellular geometry. Systematic measurements of the local viscoelastic parameter can be employed to monitor possible abnormal transformations inside the cell. Because mechanical forces are inherent in the cellular environments, the force is a signal that live cells must take advantage of to carry out its functions.[6, 7] Thus, the AFM should allow for the highly accurate positioning of the cantilever, the loading/unloading ramps (jumps) in force steps and of course the use of different soft spring AFM cantilevers with different indenter geometries in the live cells natural environment. The force-distance curves are typically used to determine the force resolution by varying step-wise, the magnitude of the force between the soft sample and the sharp tip (tip geometry), which is the working end of the micro-cantilever. This is relevant because the AFM can be tuned not only to provide superior performance in terms of its resolution or its force sensitivity but also to provide adequate information about the live cell, the mechanical properties from the approach ramp and the retract ramps of the force curves. Even though a variety of methods have been proposed to calibrate the spring constants there are still some sources of errors, which may limit the sensitivity of the AFM vertical output signals. Amongst these are (i) thermal vibrations of the soft AFM cantilever, (ii) the noise in the displacement sensor, originating from the fact that the tip is ramped on the sample surface,

and (iii) the noise generated by the electronics where both the cantilever and the electronic circuits may respond differently and therefore the sensitivity of the system may be different. For mechanical properties involving the local deformations of the soft samples, well-established soft micro-cantilevers, which act as soft springs for the AFM, are however available commercially for the creep measurements by AFM. At large penetration depths in soft samples like live cells, the soft spring cantilevers can resolve better sensitivity measurements after applying small force steps of around 500 pN. Thus in this work, the sensitivity is markedly improved by analysing a smaller fraction of this applied force step by AFM. This is a major step towards satisfying accurately the experimental conditions and the novel setups.

This dissertation is divided into 7 chapters. **In Chapter 1** an introduction into pertinent theoretical background, reviews of many other physical works on soft samples in literature and how it may apply to important activities of live or diseased cells (not in depth) including the current state of the art of measuring visco-elastic properties of soft samples by AFM is given. It is followed by a brief summary of the critical issues with the AFM and motivations. In this work, the magnetic AFM setup has been employed to measure the response of the cell sample in an environment, which mimics its natural environment. Interestingly, the novel magnetic AFM setup has been employed to apply forces to load and unload live cells and to measure reproducibly the creep response of the cell sample in an environment, which mimics its natural environment. Interpretation of the AFM force curves almost entirely relies on force laws and in comparison to typical materials such as metals; glass; the live and diseased cells are small soft objects. These force laws describes forces as a function of the probe –sample separation distance. In addition, for the proposed magnetic setup by AFM, which may employ commercial magnetic particles requires knowledge of the magnetic content for experimental purposes. On one hand, if the magnetic content of the particles or fragments are known, and the smaller magnetic particle is known, the magnetic susceptibility may be read directly from relationship of magnetisation curves provided to experimenters by the vendors. On the other hand, the thermally driven motion of the soft spring triangular shaped AFM magnetic cantilever in an aqueous environment. The spring constants of the soft spring AFM cantilever in an AFM experiment are typically measured by inferring the results of the integral of the thermal noise and the temperature of the aqueous solution. When applied appropriately in the system and if the measured soft sample responses to an applied force are adequately quantified may significantly facilitate the laboratory studies of the intrinsic properties of soft

live cells, diseased tissues and polymer gel samples elucidating their roles of molecular components and their roles in visco-elasticity by AFM. **Chapter 2 describes** the materials and methods, which have been used in this work. In this section the mechanism of the actual measurements process, the laboratory prepared samples and the AFM experiments will be described. Most measurements have been performed on adhering live cells in a stiff petri dish. We present a setup for applying large controlled external magnetic fields in magnet on force transducers by Atomic Force Microscopy by modulating the external fields in magnet (see figure 19). Two additional setups for measuring the creep response of live cells and gels to small force load and unload by AFM has been evaluated. A soft cell sample subjected to a sinusoidal varying stress will respond by a sinusoidal varying strain, which may be out of phase with the applied stress. At a single frequency the material properties could be described. A sinusoidal modulating force in magnet can be applied by attaching a magnetic material to the end of the soft cantilever (back of the cantilever). When placed in the vicinity of the soft samples, the force in magnet modulates the force on the tip end of the cantilever, which transmits a sinusoidal-like indentation to the live cells. As a comparison, a model system gel sample was chosen because it could be routinely prepared in the laboratory and it has a spring constant values, which could be experimentally tuned to a range similar to that of the cell values. We employed cancer cells tissues of the interstitial lumen for the testing of both the magnetic AFM setup and z response AFM setups as well the magnetic force modulation setups. The idea behind the methodology involved choosing an appropriate soft AFM cantilever and monitoring the time dependent response to deformation by AFM for all setups for well-defined and separate experimental conditions. The AFM acting as indenter performs force measurements on live cell samples, detecting sufficient deformation in response to the applied force. For alternative purposes, the magnetic coil has been modelled in our group for direct force load and unloads on soft diseased and healthy soft samples via magnetic fields. Routinely prepared soft spring magnetic AFM cantilevers have been employed to load and to unload the soft sample. To illustrate the method of the magnetic force AFM setup, the creep response measurements were performed with the magnetic cantilevers placed above the magnetic coil. The direction of the force load is the axis perpendicular to the surface of all the soft cells and gel samples, which are placed in petri dishes on the AFM stage. The pyramid indenter with a  $35^\circ$  opening angle and the indentation of the tip has defined the mechanical contact between the tip and the ultra-soft samples. To apply the force load and unload during the creep response measurements by magnetic force AFM, the cantilever deflections to force must be known and the deflection sensitivity should be calibrated. These mechanical readouts

are particularly useful when the soft sample experiences changes in mechanical properties with time as creep or relaxation. The optical lever beam bounce setup by AFM presented in this section determines the bending angle or its inclination rather than the deflection, by considering only the normal force (axis perpendicular to soft sample surface) load direction. Through this work the force curve based calibration can also be used to determine the deflection sensitivity in aqueous solution. Additionally, the soft spring AFM cantilevers' backside can be metalized with aluminium or gold. The metallized gold/aluminium coatings on the backside (the side not facing the sample) of the soft spring cantilevers are employed for AFM experiments in order to enhance its' reflectivity in the aqueous environment. The section is followed by a description of the measurements that have been performed partially with the aid of the software provided by the manufacturer and in addition to in house programmed routines. The principle of obtaining a conventional force curves, z step response, and magnetic step response as well as force modulation data by AFM has been discussed. To address drawbacks, our magnetic AFM apparatus was additionally designed to operate in the force modulation control mode where the user can freely define the quasi-static or the magnetic force modulation indentation profiles in the indentation or the load and unloading control modes. For calibration purposes the polymer gels and the cancer tissues from the interstitial lumen were employed as specific samples. As a result, in addition to commonly used the spring constants values of the soft samples, which are derived from quasi-static experiments, other mechanical values can be extracted such as the storage, loss moduli, and damping factor as a function of strain and frequency or the relaxation time constants could be derived. Depending on the experimental conditions or the physical quantity of interest, the experiments by AFM could performed in many folds: for instance, the magnetic force modulation loading and the unloading of the soft sample has been performed in a conventional fashion by AFM on interstitial cancer cell and the gel samples. Secondly by employing an indirect force in step in z height or direct force steps load in magnet by utilizing the coil's external magnetic field to generate the required force on the soft magnetic AFM cantilever. The novel magnetic force setup allows controlled movements of the magnetic cantilevers to directly measure the creep response of the live cell. In this section the rational and the description of the magnetic force microscope setup, the cantilever including an example of employed magnetic cantilever will be shown and described. The magnetic coil was a type of magnet in which the magnetic field is produced by an electric field such as a wire wound around a magnetic core material. The optimum applied field in magnet has generally been the largest magnetic field at which the core material operates below saturation.

The main advantage of the magnetic coil over a permanent magnet is that the magnetic field strength and the magnetizing fields can be varied or maintained by controlling the supply of the drive alternating current. The magnetic sensitivity permitting orientation of the magnetic cantilever in aqueous solution with respect to the coils external magnetic field form is useful for a wide variety of magnetic particles. The chapter ends with a very brief description and background of all three-measurement modes (magnetic AFM response and the z step response including the force modulation modes) that can be performed on deformable samples to derive the material properties. **Chapter 3** readdresses the objectives of this work in terms the mechanical frameworks employed to analyse the obtained mechanical data, which were correctly obtained in the sub chapters presented in the chapter 1.3 and chapter 2.3. The mechanical analog circuit was employed on all obtained creep response data in order to analyse or derive the visco-elastic properties of the soft gel and diseased cell samples. The spring constant and the friction coefficient (viscous coefficient of friction) and the time constants from the from the loading and unloading curves creep response data of the soft and diseased samples have been derived for the z step response and the magnetic step response experiments respectively. Analysis with an alternative analog circuit was employed for all the diseased samples and soft gels per condition where a step in loading and unload force in magnet by means of magnetic fields via the home-made current carrying coil placed at the base of the AFM in order to demonstrate the finesse in terms of the temporal and spatial sensitivity of the novel technique by force modulation experiments in magnet and in comparison to the other hand with the z-steps steps which were indirectly applied by AFM. By magnetic AFM, the spring constants values of the soft samples were derived from the curves for the different modes of applying the force steps. By considering the balance of the forces in the system after the application of the step in force, one is able to characterize the response of the soft samples considered. In particular, the spring constant and viscous values from a portion of the creep curves after the approach ramps on soft cells and polymer gels were shown. For interstitial cancer tissues, the soft and stiffer polymer gel samples and the soft live cells (diseased) samples the spring constants were derived. The framework that was employed in analysing the creep response of all soft samples after applying a small magnetic force loading step and the z step response data was by a simple mechanical model, which provided a link between the viscous and the elastic properties of the soft samples like the live cell simultaneously. Based on the viscous contribution of the soft sample in its aqueous solution a theoretical framework has been attempted for the magnetic step force load and unloads for determining the relationship between the coefficient of friction and viscous

response of the soft sample. In the first part of the data analysis framework is assigned to the conventional force curve as it describes the response of the live cell. The analysis was performed on two samples per conditions. Analysis of stress relaxation data and the direct force modulation data obtained from the diseased interstitial cells/samples were performed in many separate steps. A procedure to analyse starts with deriving spring constants of the soft samples from the measured slopes of the force curves obtained in a conventional fashion. Secondly, in this section a proposed analysis framework for the creep response data will be described. The magnetic force setup will not only provide the high resolution in the time domain but it is also a high sensitivity setup to characterize the cell mechanics. The resultant creep response to a local deformation has been quantified in terms of the friction coefficient and the experimentally observed relaxation times for the spring constants of the soft samples. The mechanical analog circuit has been employed to analyse the deflection displacement data obtained on the soft samples because it is a simple mechanical model that reproduces the creep response of the soft samples. It is a simple, yet an accurate to characterize the live cell samples viscoelastic properties and diseased cells. For testing, the spring constants derived from the force modulation experiments and magnetic response experiments were additionally linked to the structural features of the brush border microvilli racing the intestinal lumen. The spring constant and the friction coefficient (coefficient of friction) and the time constants from the from the loading and unloading curves creep response data of the soft and diseased samples have been quantified for the z step response and the magnetic step response experiments respectively. **Chapter 4** is the results section. The spring constants and the friction coefficients due to the creep of the mechanical data on the soft samples can be derived using the proposed model. In order to get a better understanding of the two different setups for measuring the viscoelastic creep of living cells by AFM have been described and evaluated. The tabulated results for example samples are tabulated and presented graphically in this section. The resultant local deformation performed by the magnetic AFM step loading and unloading setup of the live cell by the step response setup is suggestive of the local cellular viscosity. The results of the creep response by employing a simple mechanical circuit, the spring constant values and the viscous quantities from the loading and the unloading force steps are described from the data obtained by the magnetic step and the z-step response AFM analysis. Furthermore, to test the validity and the accuracy of the results, the spring constants measured by the conventional scheme has been compared to the magnetic step and the z step response setup. Specifically, two sets of values have been obtained, one for the loading step, and another one for unloading step. The spring constants including the viscous properties of

the cell and gel samples can be quantified accurately from the response experiments. To test the reliability of the setups, comparisons have been made in the system for soft samples and when employing slightly stiffer samples and stiffer magnetic cantilevers on the gel sample. The experimental results from the measured force volumes have been presented with a descriptive statics, which represents the median values obtained from the force curves. The experimental findings have been validated and have been presented in a tabular manner to illustrate the derived values as an example. To address drawbacks, our magnetic AFM apparatus was additionally designed to operate in the force modulation control mode as described before by which the user can freely define the quasi-static or the magnetic force modulation indentation profiles in the indentation or the load and unloading control modes. For calibration purposes the polymer gels and the cancer tissues from the interstitial lumen were employed as specific samples. As a result, in addition to commonly used the spring constants values of the soft samples, which are derived from quasi-static experiments, other mechanical values can be extracted such as storage, loss moduli, and damping factor as a function of frequency, relaxation time constants. The spring constant and the friction coefficient (coefficient of friction) and the time constants from the creep response data of the soft samples from the loading and unloading curves have been derived. These quantities are interesting and can be employed to investigate the role of mechanics in diseases as they might contain important information about structure and the function. **Chapter 5** is the discussion chapter. In this work the step response data is presented in an array of force curves by z step and the magnetic step setups to prove that viscoelastic creep response can be measured reproducibly by magnetic step response AFM in its liquid environment or other appropriate and well-characterized laboratory experimental conditions by AFM. The objective of this section was to evaluate the magnetic step and the z step response setups and show that the setups can be employed to measure the creep response in terms the friction coefficient and the relaxation times of the soft samples by AFM. The rational reported in my work assumes that the force applied, and the indentation change resulting from that force thus the mode, is small such that the mechanical properties do not change considerably. The force sensitivity should be increased as much as possible to be able to apply very small force steps in magnet. A portion of the loading and the unloading steps were analysed for the spring constants for the single relaxation time to obtain two sets of values for the step and the magnetic response AFM setup. Both types of creep data were analysed in the framework of the linear solid model, neglecting hydrodynamic damping of the moving cantilever, which is a combination of two springs and one dashpot. This may not always be given, especially with highly

structured samples like cells. **Chapter 6** concludes this work and states a brief outlook. In this work, the creep response of soft gel and cell samples has been directly measured after applying a step in loading force by means of magnetic fields and indirect step in loading and unloading force in z step by AFM. By employing a more accurate model to the creep response the spring constants values and the relaxation time constants have been derived accurately from the loading and the unloading steps. The viscous response and the elastic values have been quantified in terms of the coefficient of friction and the relaxation time constant from the creep response experiments by magnetic step response and the z step response AFM. The elastic and viscous values derived from the loading and unloading steps are identical for the magnetic step response when compared to the conventional way of obtaining the mechanical data. Using the approach that allowed for magnetic response measurements not only helped us better understand the important limitations of the current AFM approach, but showed us that we can improve it. The chapter includes briefly the future prospects or it gives the potential future directions for research in this area as an outlook. **Chapter 7** is the appendix where we show results, which are relevant to my work. **Chapter 8** is the bibliography containing a list of publications in numerical order.

## 1.1 What is an Atomic Force microscope?

The Atomic Force Microscope (AFM) developed by Binnig, Quate and Gerber [8], enabled investigation of biomaterial surfaces at very high resolution and measuring interaction forces with high sensitivity. As shown on the schematics in figure 1, the AFM is made of three major components: a force transducer (a cantilever beam), an optical detection system to sense the cantilever deflection and the piezo element to position the sample (or the tip). The force transducer is a cantilever, which acts as a soft spring.[9] Initially, it served for the purposes to extend the use of scanning probe techniques beyond electrically conducting samples, it was soon understood by Paul Hansma that this opened the route to visualize biological samples in physiological conditions. In a very early application[10], it was understood and used to determine the elastic properties of living cells.[11] The magnetic force microscope is operated for example in aqueous buffer solutions in direct contact with a substrate (sample) surface and exerts a force on the surface which otherwise is impossible by electron microscopy methods. The atomic force AFM is operated under constant force mode, which incorporates optical beam deflection for sensing the soft spring AFM cantilever motion.

## 1.2 Working principle of the AFM

The AFM operates in the liquid and the air medium by measuring the force between the sample and the cantilever tip. The AFMs are controlled dedicated electronics and control software that allows setting force curve parameters and data acquisition. The schematic diagram in Figure 1 shows an AFM and its' integrated electronics. Our AFM for measurement the creep response soft samples by magnetic AFM was operated in direct contact with a substrate surface and exerts a force on the surface. In addition to the conventionally scheme as described before, I applied well-defined step forces to the soft sample. The spring constants [Pa] of most samples can be measured with high resolution in the range several GPa down to a few kPa, which is the range of the spring constants of common viscoelastic samples like the live cells and polymer gel.[12] The AFM allows for a very good control of the tip position and loading/unloading speed and the use of different probe geometries. The soft spring AFM cantilever can be moved in all three X-Y and Z-directions and is positioned with nm accuracy relative to the sample surface by a piezo electric actuator. With the ability to both load soft spring AFM cantilever in all the three XYZ-axes and then sense how far it actually moved, the controller closes the feedback loop for precise motion control. The AFM feedback controller has kept the cantilever so that the distance between the soft spring cantilever and the sample is held constant. By monitoring the z height, the force curves such that additional creep and non-linearity are ruled out. The primary output of the system is the deflection signal from the PSD. The variations in the PSD output voltage from the segmented (different) quadrants of the photodiode have been used to determine the force exerted on the soft spring cantilever. The PSD output voltage signals are sent out to the piezo scanner on each axis, and read back from the corresponding nano-positioning sensor (NPS™ sensor). The low voltage signals from the PSD output have been amplified by a factor of 15X at high voltage amplifiers. Applying a well-defined voltage pattern typically with turning points to the electrodes for the z-axis scanner caused the z piezo scanner to expand and then contract in the vertical direction, generating the relative vertical motion between the soft spring cantilever and the sample. The deflection signal as a result of the change in orientation (bending) of the loaded end of the soft spring cantilever has been measured and then plotted at many points as the z-axis scanner extends the soft spring cantilever towards the surface and then retracts it again. These high voltage signals range from -10V to +150V on the piezo translator. The filters for the X and Y Sensors are set to 1 kHz and 2 kHz for the Z Sensor to eliminate higher frequency noise while performing the AFM experiments. The change in the deflection signal of the soft spring cantilever was used to trigger a change in the vertical position or the base of the cantilever relative to the sample

typically referred to as the z height position in order to maintain the constant deflection at a chosen pre-set value. The set point of the controller was proportional to the force that is exerted on the sample. A force measurement with the magnetic force microscope required control software very different from many other conventional AFMs employed. While this was an important limitation in early AFM systems, mechanical characterization has become a usual demand, and most systems provide now dedicated environments for advanced force measurements. Indeed, current control software provides tools for custom design of the force ramp routine. For example, the mechanical (creep response) measurements require particular force curve protocols including approach to the sample until a desired applied force is achieved, followed by tip oscillation at different frequencies around a constant indentation and finally return to the initial position out of contact. During an AFM experiment, a probe attached to the soft spring AFM cantilever is brought in contact with the soft sample and may be driven thermally. For precise quantitative data analysis during lateral scanning of the sample, it is crucial to accurately position the soft spring magnetic cantilever at the tip-end over the soft sample to enable a physical interaction that can be captured effectively. In the experimental setting the laser beam is positioned at the rear of the magnetic AFM cantilever and directed towards a photodetector. The deflection is measured by an optical beam deflection setup, which delivers an electrical signal that is proportional to the cantilever deflection.

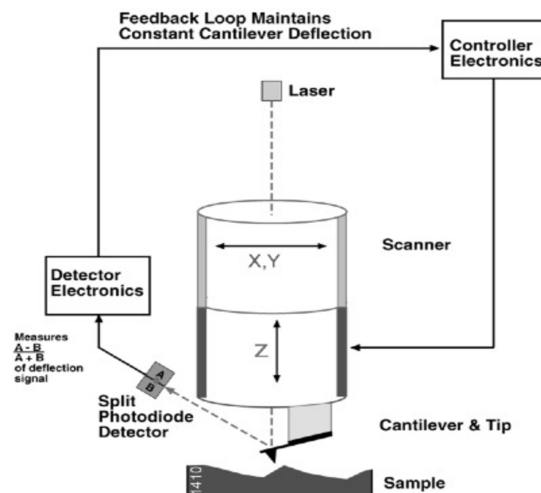


**Figure 1: Schematic diagram of the conventional Atomic Force Microscope head with the addition of a feedback loop. The motion of the soft spring magnetic cantilever is obtained from the difference output of the split photodiode detector together with the optical beam method (design). The AFM combines high sensitivity in applying force, high precision in positioning the tip relative to the sample in three dimensions and the possibility to be operated in an aqueous environment. (Adapted from [9] and [13])**

The theories of the AFM, and the technological aspects have been the topic of many publications and our group (see references herein). Therefore only the aspects necessary for

understanding the contents of this chapter, and not aspects just briefly described in other publications, will be discussed. As seen in the Figure 1, the FM technique requires the addition of electronics that may provide additional drive signals to the piezo sensors and to the driving magnetic field. In general, a feedback system for position control consisting of hardware and a software-based control unit is nowadays employed for the accurate control of the height ( $\Delta z$ ) movements. Positional control was implemented in each of the three axes through an actuator and a sensor, both of which require specific data signals. This is important because the interaction between the tip and the substrate allows enables the AFM experimenters to acquire force curves (see force curves section below).[9] The mechanical properties historically have been analysed from AFM force curves. This is because soft samples will deform in response to cantilever force. This provides a way to experimentally measure the mechanical properties. When the forces and distances involved corresponds to the thermal energy, the thermal fluctuations of the AFM cantilevers become significant. The quantity most characteristic for a soft spring cantilever is the spring constant. The spring constants of cantilevers can also be expressed in more helpful size ranges. For example soft cantilever for AFM force spectroscopy with spring constant value of  $k_c$  0.01 with units in  $[\text{N}\cdot\text{m}^{-1}]$  is equivalent to  $k_c$  10  $[\text{pN}\cdot\text{nm}^{-1}]$ . AFM applications extend into applications ranging from measuring colloidal forces to monitoring enzymatic activity in individual proteins to analysing DNA mechanics. The AFM indentation experiments on metastatic cancer cells discovered a significantly soft magnetic spring constant of the cancer cells compared to the healthy cells.[14] [15] Furthermore, despite the morphological similarities of the cancer cells to the normal cells, it is suggested that the AFM and it derivatives might be more effective for cancer screening than visual examination of the diseased cells.[16] [17] The deflection of the soft spring AFM cantilever is the another directly measured quantity in AFM setup as this quantity provided a measure of the interaction force between the tip and the sample being investigated. The AFM cantilevers are usually made of several materials. Although a variety of methods have been proposed to calibrate the soft springs there are still some challenges, which may limit the sensitivity of the AFM output signals. Amongst these are (i) the AFM cantilever velocity in the aqueous medium (ii) the thermal noise (fluctuation) of the AFM cantilever. The thermal noise method has been based on the fact that the free end of the soft cantilever is continuously in motion. The random motion gives rise to thermal noise of the cantilever bending or a typical change in the orientation. Martin et al. in 1987 [18] performed the another practical demonstration of the cantilever setup in an AFM microscope with a vibrometer to measure the amplitude of the stiff spring cantilever vibration. [19] [18] At large

penetration depths in the soft samples like live cells, the soft spring cantilevers can resolve better sensitivity measurements by applying smaller force steps of around 500 pN. This is a major step towards satisfying accurately the experimental conditions and the novel setups. To understand these challenges associated with these experiments using the AFM, it is important to review the AFM technique itself.

### **1.3 Implementation of the AFM technique**

Since its invention in 1986, the AFM has been a relatively non-destructive microscope in comparison to the conventional scanning electron microscopy and transmission electron microscopy. One of the most exciting results of the AFM has been the discovery that high resolution as well as slow highly sensitive measurements can be performed when the cantilever tip is in contact with the live cell in its natural environment. Martin et al. in 1987 [18] performed the first practical demonstration of the cantilever design in an AFM microscope with an optical interferometer to measure the amplitude of the soft spring cantilever vibration.[19] The required complexity of AFM control software, home-made systems are commonly adapted to the requirements in the development laboratory. However, open software packages to control home-made (routinely programmed modules) or commercial systems are becoming available, and we expect it to be the trend in the following decades. Although one of the most important applications of the AFM is the study of the mechanical properties of the soft samples like the cell sample [20], the extent to which the small loading force indents the sample will depend on the soft sample viscoelasticity.[11] Many other recent applications now require that the AFM spring constants be measured adequately. As we will see in the subsequent sections we will give a brief background of the AFM technique. We will start with the description of the AFM cantilever probe.

#### **1.3.1 The AFM cantilevers probe.**

The key of the AFM is the cantilever. The AFM cantilevers are usually manufactured and supplied in wafers containing six ready to use probe chips for AFM experiments. An image of five AFM cantilevers attached to a cantilever probe chip of length ca. 1.5 mm is shown in Figure 2. The image in the figure 2a shows the four triangular AFM cantilevers on a rectangular chip (from bottom left edge to upper right edge in figure 2a) and one rectangular cantilever. The example cantilevers employ a pyramidal tip as shown in Figure 2b. The AFM cantilevers additionally offer the advantage that they may be produced thinner and therefore made more flexible. The spring constants of the soft spring AFM cantilever values within one

wafer may differ within 10% and may even span up to four times smaller and four times larger than the nominal value when compared between different wafers [21].

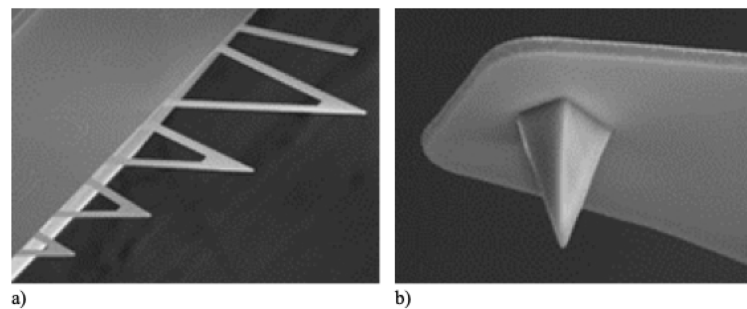


**Figure 2: The AFM soft spring cantilever and tip. Typical cantilevers have a diving board shape. These are used for both the contact mode and the dynamic mode AFM. Triangular cantilevers have been used in contact mode AFM with the idea that they may be typically more sensitive. Figure shows a diagram of an AFM probe with 5 AFM cantilevers (four triangular and a rectangular shaped cantilever) with the sharp tip. The tip material can be chosen for specific properties of the sample it will interact with. The soft spring AFM cantilever shown on image employs a pyramidal tip with asymmetrical tip geometry[22].**

The AFM cantilever may be coated on one side with the magnetic materials in order to enhance its sensitivity to changes magnetic field of the working environment. On the other side, it has been reported that silicon nitride do not process perfect manufacturability for the tip machining. The tip is made out of the same material as the cantilever with the radius ranging from 20 - 35 nm (as provided by the manufacturer [22]), which gives a high sensitivity to small forces. The tip manufacturing reproducibly seems to be a major concern when obtaining force measurements with the AFM. Its merits however are the flexibility and the sharpness of the tip geometry. The well-established soft spring AFM cantilevers may be tipples or having a tip of varying radius of curvature that do not actually exhibit sufficient sharpness. Manufacturers may adjust the production parameters to provide a range of commercially available dimensions on soft spring AFM cantilevers with varying spring constants and soft spring AFM cantilever properties. For example the soft spring AFM cantilevers may be equipped with a bulk shaped pyramidal indenters, which may generally be blunted. They may have three or four sidewalls with a tip opening angle of ca.  $35^\circ$  and protruding length about 3-17  $\mu m$ . The small size and the structure of the soft spring AFM cantilever together with the ability to operate in conditions such as liquid and air makes cantilevers interesting as a force transducer and sensing tool. For the AFM applications, any mechanical interactions between the tip and the surface changes the deflection of the cantilever, which in turn is measured by the reflected light detected by the position segmented detector (PSD). As shown in the Figure 2b, the point where the force is applied on samples is usually a few microns away from the end of the cantilever, as the tip is not exactly at the end

of the cantilever.[23] The most preferable amongst the researchers are the rectangular and the triangular lever shaped soft spring AFM cantilevers. Transmission electron microscopy (TEM) have also been used to image uncoated tips by some researchers to determine the tip radius.[24] The coulomb force and the double layer force measurements have also been used to determine the tip size and shape.[25] The colloidal probe technique has been widely used to in acquiring force versus distance in order to overcome lack of information about the tip shape.[26] But these techniques compromises the high temporal resolution offered by AFM and impedes the mapping of physical properties using force distance curves due to large tip radius. However the shape of the soft spring AFM cantilever tip may be directly determined by the application and specific needs of the experiment. In this work the AFM tip geometry and shape has not been measured, rather it has been determined by the plan and its indentation compared to theory such that manufacturer specifications matches my data. When using 50  $\mu m$  cantilevers the approximation that the force acting is an end loading force is no longer valid.[25] In order to perform force measurements requires the individual calibration of the cantilevers spring constants.

Relevant to my work on the biological samples, as long as the AFM probes employed were commercial AFM probes, they were not calibrated in terms the true spring constants values. The values of the soft spring constants of the soft spring AFM cantilevers and the resonant frequency characterize the mechanical properties of the soft spring magnetic AFM cantilever. Thus, the first important phase of the experimental work was deriving the spring constants of the soft spring cantilevers as accurately as possible. This is because one intends to employ the soft springs to measure accurately viscous values and the true spring constants of the soft samples by applying a force on the tip. More importantly, the calibration approaches neglects the possibility of variations in the spring constants of the individual soft spring AFM cantilevers due to structural defects and the variations in the lever geometry and the composition. In the literature, many techniques have been proposed to calibrate the spring constants of the soft spring AFM cantilevers. Such techniques have typically been grouped into three categories: theoretical techniques (dimensional models), static deflection measurements, and dynamic deflection measurements. The widely used theoretical techniques are based on the prediction of the spring constant of the AFM cantilevers typically from its geometric information. To get more insights, example references and some moderately completed reviews can be read in the work of Ohler [21], or Burnham et al., [27]. While working on biological samples, such as cells, these configurations may be particularly appreciable in AFM measurements. The AFM probes with the sharp tips, with their small

contact area, can induce high stresses upon contact, may have to be accounted for and controlled during experimentation, making them typically advantageous when a strong modulation of the contact area of the soft sample upon interaction with the nanometer-sized features of the cell sample are required. Furthermore as it has been previously mentioned, the quantity most characteristic for a soft spring AFM cantilever is however the spring constant  $k_c$  with units in  $[\text{N}\cdot\text{m}^{-1}]$  necessary to determine the applied force during the experiments and this is typically done or performed using the thermal tuning methods. The AFM however, has now been employed for the direct and high sensitive measurements of the true elastic spring constants and the damping coefficient of friction (friction coefficient) values of the live cell and polymer gel samples with the routinely prepared soft magnetic soft spring AFM cantilevers. As it has been discussed, the tip, the soft spring AFM cantilever and the probe (carrier tip) are typically fabricated on one piece of wafer. As such due to the manufacturing processes, the dimensions of the soft spring AFM cantilevers are difficult to control along the length of the soft spring cantilever and may even vary between each individual soft spring AFM cantilever in the same batch. The spring constants of the soft spring AFM cantilevers as well as the sensitivity are required to be derived accurately before experimenting because the uncertainty in the thickness along the length of the soft spring AFM cantilevers may have an effect on the overall accuracy.

Additionally, the soft spring AFM cantilevers' backside can be metalized with aluminium or gold. The metallized gold/aluminium coatings on the backside (the side not facing the sample) of the soft spring cantilevers are employed for AFM experiments in order to enhance its' reflectivity in the aqueous environment. Such highly reflective surfaces or the coatings on the backside may as well have some problematic effects on the spring constants and viscous values of the soft samples by AFM. For reliability purposes, it has always been additionally required in the course of this work to verify experimentally the manufacturers plan-sheet spring constant of the AFM cantilever values. Producing short, silicon nitride cantilevers with integrated sharp silicon tip is a good strategy to obtain soft high-frequency, high-quality factor cantilevers, which provide high force sensitivity, and can be driven inertially at kHz frequencies, far from the natural resonances of the AFM cantilevers. The theoretical techniques without any experimental verification may not be always very reliable because theoretical techniques are often based on the rectangular beam approximation. The AFM setup however has now been employed for the direct and high sensitive measurements of the true elastic spring constants values and the damping coefficient of friction of the soft samples like the live cells with the routinely prepared magnetic soft spring cantilevers. For

applications to benefit low contact force of about 0.5 nN for our magnetic response experiments, soft spring AFM cantilevers are modified on the backside by equipping with a magnetic sensitivity. Several other methods exist for the calibration of the AFM cantilever spring constants. In 1995, Sader et al., [28] introduced an alternative method to calculating the spring constant of the soft spring AFM cantilever from an unloaded resonance frequency.[29] The mass of the soft spring AFM cantilever was inferred from the geometrical dimensions. The thickness measurements requires typically the use of scanning electron microscopy (SEM) which is time consuming and cannot be routinely carried out separately for each AFM cantilever [28]. The method has additionally required the determination of the mass and the density, which could increase the amount of difficulty during the calibration process. This method is not used in this work because it requires the knowledge of geometrical parameters and may perform best for a very stiff AFM cantilever. The same author has proposed a subsequent method whereby; the spring constants of the cantilever have been determined solely by its resonant frequency and the quality factor in air medium.[29] Experimentally, the soft spring cantilever calibration provided two parameters required for the analysis of the force versus the indentation curve.

Furthermore, by considering the spring constants and the deflection sensitivity of the soft spring AFM cantilever one may typically obtain a maximum load of the corresponding indenter. For the rectangular (single leg) AFM cantilever the nominal spring constants  $k_c$  will be a function of the geometric parameters, the length  $l$ , and the cross sectional width  $w$ , including its the thickness  $t$ , is given by the analytical equation:

$$k_c = \frac{w * t^3}{4 * l^3} * E \quad (1.0)$$

Where  $E$  the elastic (Young's) modulus [Pa] of the cantilever tip geometry. The thickness of the soft spring cantilever can be determined accurately by scanning electron microscopy and has not been done in this work. The regular cantilever through its dimensions and the mechanical properties define its fundamental frequency  $f_0$ . The commonly employed spring constants of the soft spring AFM cantilever in the contact mode of operation are typically in the range from  $0.01 \dots 10 \frac{N}{m}$ . The dimensions may be additionally measured by scanning electron microscopy and the thickness is assumed to be constant over the entire length  $l$ . The spring constants of the soft spring cantilevers vary with a cube to its thickness. The spring constants values seem to be sensitive to the differences in the soft spring AFM cantilever thicknesses between the batches, thus indicating the importance of calibrating the cantilever spring constants by a more appropriate method.[21] The most preferable amongst the

researchers are the rectangular and the triangular cantilever. To localise and to choose the region of interest for the AFM measurements, the AFM cantilever might be supplied with varied shapes. The V-shaped cantilevers are typically employed in the contact mode of operation because the twisting of the soft spring AFM cantilever is not desired. To access different ranges of force on different samples, the experimenter is usually required to change the cantilever (as provided by the manufacturer and reviewed publications). [22] For the soft spring magnetic AFM cantilevers employed in this work, a large contribution to the experimental noise has been due the acoustic noise. For that reason, the AFM equipment employed in this work has been kept in an acoustic to reduce external noise from building and floor. In the same line, the soft spring magnetic AFM cantilevers employed in this work where susceptible to thermal noise and the AFM can be used to measure or to analyse the movement. The thermal noise calibration method has been preferred because it was quick and can be readily performed in liquid conditions immediately after calibrating the deflection sensitivity.[28] In order to obtain the natural frequencies of the magnetic cantilever the thermal noise method has been performed. The random motion gives rise to noise fluctuations of the magnetic cantilever bending. By means of the equi-partition theorem, one can use the magnitude of the thermal fluctuations to estimate the stiffness of the cantilever[24]. The thermal fluctuations of the soft spring cantilever have been analysed after being recorded for ca. 60 seconds. The spring constant of the soft spring magnetic AFM cantilever has been readily estimated by fitting a model to the obtained powers spectrum. The thermal energy in the AFM cantilever results in a cantilever motion described by

$$\frac{1}{2}k_c\langle d^2 \rangle = \frac{1}{2}k_B T \quad (1.1)$$

Where  $k_B$  is the Boltzmann constant ( $1.38 \cdot 10^{-23} \text{ J/K}$ ,  $T$  is the temperature, and  $\langle d^2 \rangle$  is the mean square displacement of the fluctuating AFM cantilever. Thus the force resolution, if only thermal noise is considered, will be given by: [24]

For systems that exhibit simple harmonic motion there is a characteristic frequency that depends on the physical quantities involved. The characteristic frequency of vibration  $\omega$  is given by,  $((2\pi f_0)^2 = k_c/m^*)$ , and an effective mass  $m^*$ . With the fundamental frequency of the rectangular soft spring AFM cantilever given by:

$$f_0 = 0,1615 \cdot \frac{t}{L^2} \cdot \sqrt{\frac{E}{\rho}} \quad (1.2)$$

With,  $\rho$  being the density of the AFM cantilever material. The thickness of an AFM cantilever can be determined accurately by scanning electron microscopy and has not been done in this work. In some special cases, magnetic or spherical particles are attached to the cantilever to achieve specific surface properties and a controlled geometry. This also indicates the importance of calibrating the cantilever spring constants by a more appropriate method.[21] Although this calibration step is very time consuming, technically the calibration step is very relevant because the AFM may be tuned not only to provide a superior performance in terms of its resolution [11] or its force sensitivity but also to provide adequate information about the live cell, the mechanical properties or viscoelastic properties. If we assume that the largest uncertainty arises from the thickness of the AFM cantilever beam, one may, if required, try to estimate the spring constant of the soft spring AFM cantilever by eliminating the thickness and measuring the resonance frequency. Eliminating the thickness from the above equation leads to:

$$k_c = 59,31 \cdot w \cdot l^3 \cdot \omega_0^3 \cdot \sqrt{\frac{\rho^3}{E}} \quad (1.3)$$

Thus by comparing the nominal resonance frequencies and the measured resonance frequencies, one can estimate actual spring constants of the cantilever.

### 1.3.2 Contact mode AFM

Force [N] is measured in AFM by obtaining a force curve. The force curve is a plot of the cantilever deflection as a function of sample position along the z-axis (i.e., towards or away from the probe tip). To obtain topological map using AFM the cantilever with tip is brought to contact or near the surface and it is raster scanned over the region of interest. The AFM continuously monitors the deflection of the AFM cantilever and then adjust in real time the vertical position of the cantilever with respect to the sample, to keep the vertical deflection constant. Figure 3 shows a typical sequence of an AFM probe movement during the acquisition of a force curve. To the best of my knowledge the typical operating modes of a conventional AFM microscope are based on the detection of interatomic forces (capillary, electrostatic, Van der Waals, friction) exerting between a soft spring AFM cantilever-mounted probe and the sample surface. Generally, in a typical force versus distance curve from which the deflection sensitivity can be obtained is shown in figure 3. The relationship between the quantities is an adaptation of the Hooke's law in which the deflection may be

comprised of the magnetic sensitivity, the deflection sensitivity as measured in meter per volt and the deflection as measured in volt. It assumes a relationship between force and the deflection of the soft spring AFM cantilever. As illustrated in the figure 3, there are two traces recorded for a given soft spring AFM cantilever and the sample distance. One curve represents the approaching sample towards the soft spring AFM cantilever and tip and one for the retracting of the sample away from the soft spring cantilever with tip. Time-resolved force curves revealed information about the tip-sample interaction in the contact mode of operation. When obtaining force curves in air a layer of water condensation and other contaminants both cover tip and the sample, forming a meniscus that pulls the two together. Thus the soft spring AFM cantilever has to exert an upward force (negative) to pull the tip free of the meniscus. The lowest point of this curve indicates the strength of the meniscus attraction. Having pulled free, the soft spring AFM cantilever returns to zero deflection and remains there as the z continues to increase. The rate of increase in the repulsive forces during the indentation is proportional to the spring constants (stiffness) of the soft sample. The magnitudes of the (negative) forces depend partly on the van der Waals parameters of the tip – sample ensemble, as well as the capillary forces due to the liquid meniscus acting on the cantilever with tip.

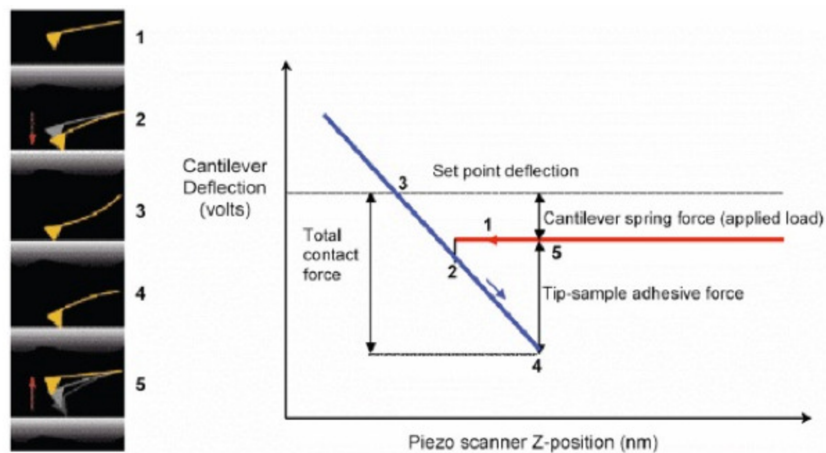


**Figure 3: Typical sequences (steps 1- 5) of an AFM probe movement during a force curve data acquisition. The AFM cantilever deflection (when free and when in contact (2) relative to a stiff sample surface) is recorded versus the z-height piezo scanner. Left panel shows the z piezo fully retracted to the original position (1) and not interacting with the cantilever and the tip (red). The applied load (cantilever spring force) corresponds to the soft spring AFM cantilever deflection signal and the spring constant of the soft spring cantilever. As the z-piezo extends, there is a sudden jump and the AFM cantilever is pulled down (2) by attraction to the sample surface. This attraction decreases with increasing z-height scanner position. As the cantilever tip is pressed into the surface the orientation of the cantilever changes (3). The z-piezo distance increases the cantilever ascends and then begins to pull up the tip (4). The applied load corresponds to the soft spring AFM cantilever deflection and the spring constant of the soft spring cantilever. At the maximum of the applied force load the z-height motion retracts and the cantilever momentarily returns to its free position (5). As shown on the figure forces obtained in air, may reveal an observable hysteresis (typically not seen in aqueous solutions) when the soft spring AFM cantilever is retracted from the sample surface and procedure requires a definite point of contact. Right panel shows corresponding output: force curve plot (adapted from [30]).**

At large separation, the soft spring cantilever is well represented by a simple harmonic oscillator model, whereas the interaction with the substrate seems to add a nonlinear contribution to the potential of the soft spring cantilever as the (average) tip-sample distance is reduced. These cycles can be divided roughly in three regions: the contact regime, the non-contact regimes and a zero force line regime. Generally, at the start of a conventional AFM experimentation, no interaction (no interaction force that deflects the soft spring cantilever) occurs when the soft spring AFM cantilever is well separated from the sample (typically the zero deflection line). This non-contact regime is typically a straight line except for optical effects (which may be sinusoidal oscillation or a straight slope). This segment of the force curve allows one to define the initial value of the loading forces or the soft spring AFM cantilever sample distance.

In the diagram of figure 3 is shown a typical force versus distance curve typically obtained in ambient environment with a soft cantilever on a hard sample. Segments 1-3 is the first half cycle (approach curve) while segments 3-5 is the second half cycle (retract curve). The contact between the soft spring AFM cantilever probe and the sample is made at the border between segments 2 and 3 (technically, depending on the experimental conditions and settings, might be at times challenging to see with the naked eye when obtaining real measurements). The downward deflection is often steep and is typically associated to a jump to contact event. The forces involved may also typically depend on the soft spring AFM cantilever tip, the sample and medium composition. In air, as an AFM tip approaches the sample surface (substrate) the capillary forces on the tip is nearly near zero until the tip contacts a thin layer of water condensation on the sample surface. When contact is made water may be adsorbed around the bridge to form a meniscus bridge between the tip and the substrate.[31] The soft spring AFM cantilever has to exert an upward force to pull the tip free of the meniscus. As illustrated in the figure 3, the interactions in the segment 1-2 as the soft spring AFM cantilever approaches are likely due to the summation the surface forces. Numerous experiments with capillary force measurement in air using soft spring cantilevers indicate that a significant capillary adhesion force is present.[32] These interactions are either negative (attraction between the probe and the sample surface), or positive (repulsion). Here, the probe is not in contact with the sample. The force distance curves shows two transitions as the sample surface approaches and touches the cantilever tip. Once in contact, the attractive pull off forces measured by AFM, given by the sum of the van der Waals component, the chemical bonding component and electrostatic component, and the Laplace force together with the line tension force. One of the most widely used models for mechanical indentation that has been

applied for AFM force curve data is the Hertz model which gives the force on a spherical probe as a function of the elastic properties of the viscoelastic material, the soft spring cantilever radius and the indentation depth (see force curves illustrate in figure 4). When studying viscoelastic samples, considerations must be made to the time dependent viscous contribution of these samples. Thus the Hertzian fit is typically applied to the force indentation data to take into account the cantilever tip geometry. From the results of the Hertz fit (spring constants), then determine the spring constant for a loading force by analytically the derivative of the force indentation relation.

The retraction portion of the force curve sometimes follows the approach curve. (see regime 3 in the figure 3) this segment of the force curves describes the mechanical interactions of the AFM cantilever and/or the sample. Through nonlinearities, the material properties such as adhesion, elasticity, or viscoelasticity may influence the soft spring AFM cantilever dynamics. Indeed, the experimental force curves are measured in a relative fashion, i.e. in terms of both cantilever probe motion and the recorded force values. For a deformable sample, compression and/or indentation processes may lead to linear or non-linear behaviours. During the retraction, an occurrence of hysteresis between the approach and retraction curves may occur. Important adhesion forces may be embedded in the retraction curves, depending on the surface of contact, the contact duration, and mainly on the surface forces between the sample and the soft spring cantilever probe. For microorganisms, this region may be composed of several discontinuities. The most type of hysteresis is due to some adhesion, which appears in the force curve as a deflection below the zero line. In the ideal case of a sphere interacting with the flat surface, the adhesion force can be related to the radius of the sphere and the surface charge energies of the two surfaces.[33] However, under ambient conditions, the main source of adhesion is the formation of capillary bridge between the tip and the sample. In air, most samples have several nanometers of water absorbed to the surface. This water layer typically wicks up to and forms a bridge between the tip and sample. Pulling the tip out the bridge requires a large force to overcome the surface tension. In fluid the adhesive force depends on the interfacial energy between the tip and the sample, in the solution. Varying the solution can change the force of adhesion.

Furthermore, the typical characteristic features of the soft spring AFM cantilever dynamics, such as changes of the resonance frequency, the existence of oscillation regimes with predominantly attractive or predominantly repulsive tip-sample interaction were properly explained and their relation to sample properties could be established in many cases. In special cases, depending on the experimental conditions, experiments related to soft samples,

such as polymers-gels or some biological samples, may typically be carried out in an ambient atmosphere. Under these conditions, the ambient humidity may lead to the formation of the thin film of water covering both the soft spring cantilever tip and the soft sample.[34] If the sample surface comes close to AFM soft spring cantilever a capillary neck may form between soft spring AFM cantilever tip and the sample surface.[35, 36] [37-39]

### *Force curve on stiff sample*

Interpretation of the AFM force curves almost entirely relies on force laws and in comparison to typical materials such as metals; glass; the live and diseased cells are small soft objects. These force laws describes forces as a function of the probe –sample separation distance. In my work, as shown on the figure 3, the AFM records the change in the AFM cantilever deflection ( $\Delta d$ ) in volts as a function of the change in the  $Z$  height. For a very stiff surface zero separation is defined as the region of the force curve in which the soft spring AFM cantilever deflection is coupled in an approximate  $\Delta d \approx \Delta Z$  relationship with the sample movement. This appears on the force curve as a straight line of unit slope (see figure 4). A corrected curve is called force distance curve. The soft spring AFM cantilever is ramped over a stiff sample surface. Accordingly, all the downward piezoelectric motion will be more or less equal to soft spring AFM cantilever bending (left part of the graph) or the change in the orientation of the AFM cantilever. Typically, the inverse of the measured slope (red line) corresponds to the deflection sensitivity (in nm/V). For clarity, a sequence of a typical AFM experiment carried out in ambient environment on a hard sample is illustrated in figure 3. The conventional AFM force curve is a point-wise analysis of the sample, obtained by measuring the cantilever deflection as a function of the distance  $Z$  between the AFM cantilever probe and the soft sample surface. A force curve shows a sequential progress of this force as a function of  $z$  at a specific location on the sample. A position  $Z_0$  required for processing obtained mechanical data by AFM is typically defined as the most distant point to the sample surface. The force plot is plot from relative measurements of the soft spring cantilever deflection, as a function of the relative motion of the cantilever probe distance  $\Delta Z$ . For our analysis and quantitative interpretation reasons these plots are typically detrended in to regimes. Basically, an AFM force curve is composed of two curves, corresponding to the approach regimes (trace) and the retraction regimes (trace) of the probe (blue and red lines, respectively) and the determination of the indentation requires that the cantilever tip makes contact with the sample. A complete force curve thus includes the forces measured as the cantilever probe approaches the sample and is retracted from the sample its starting position.

The obtained data after z-step or magnetic force step) were analysed offline using home-written routines for signal processing in IGOR (Wavemetrics, Lake Oswego, OR, USA) and adapted to the commercial software for conversion of these raw data, i.e. photodiode sensor output [V] vs. linear variable differential transformer (LVDT). In literature, the stiffer property of the sample can be described by the spring constants ( $Pa$ ). Thus, the material (the stiffer sample like the glass dish) under studies is defined as elastic when its response to the application of an external force, in terms of deformation and recovery, is instantaneous and there is no energy dissipated. In the general theory of elasticity, the sample is solid and regarded as a continuous material.

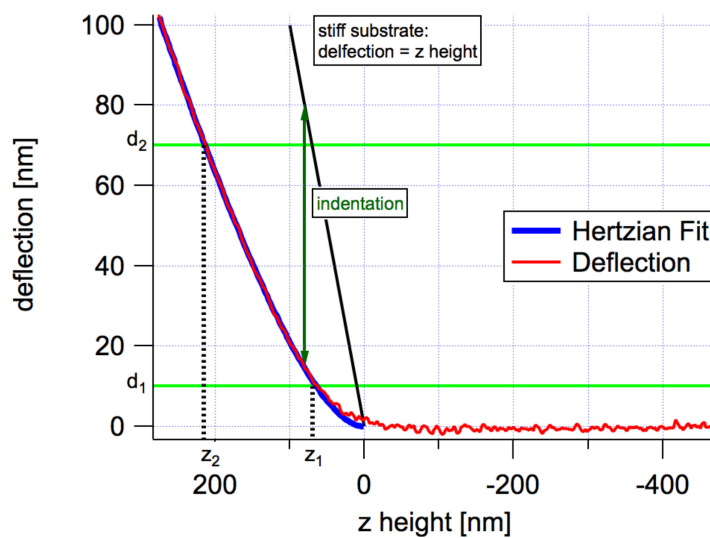


**Figure 4: Comparison of the force curve (approaching regime) on a soft and a stiffer sample as function of the z-height motion. In a force curve we will ramp the force to a certain value by ramping the z-position  $z_1$ . The figure illustrates the contact portion and the non-contact portion of the approaching force curve. The indentation  $\delta$  is represented as the difference in change in z-height and change in the deflection values. Varying the soft spring AFM cantilever with tip movement on the sample can give further information about the soft sample response. The elastic response of the soft sample in question requires an appropriate model like the Hertz model to correlate the z-height motion and the measured deflection of the AFM cantilever. On stiff samples the force curve exhibits a transition of the regimes of the force curve at the contact point, where the slope typically jumps from 0 (free cantilever) to 1 (in contact) with the sample.**

### **Force curve on a soft sample**

In contrast to force curve obtained on a stiffer sample, over the soft sample such as polymer gel or the living cell, the overall shape of the force curve will be quite different from the stiff sample examples illustrated before. It is known that most biological materials are viscoelastic, that is, they exhibit both solid- and fluid-like features. In contrast with elastic solids, the stress–strain relationships of viscoelastic materials are time dependent. The force curves are more likely to show gradual increase in the force. Rheological studies show how materials

deform in time under an applied external force. The deflection ( $\Delta d$ ) of the soft spring cantilever is smaller than the movement in the sample height ( $\Delta Z$ ), due to an indentation ( $\Delta \delta$ ) of the soft sample. When a viscoelastic body is suddenly stretched, and the strain is maintained constant afterward, the resulting stress decreases with time. This property is called the stress relaxation. If a constant force is suddenly applied, by the magnetic AFM cantilever the strain increases with time, a property known as *creep*. As can be seen in the Figure 4 where the approach portion of the force curve is fitted to the contact elastic model. For typical indenter shapes used in the AFM, this may typically result in a non-linear force curve in the contact portion of the AFM force curve. In addition to the presence of adhesive features that may be present on the sample as observed in the example figure 3, the approach and the retract curves may not even overlap, most likely due to viscoelastic properties of the soft samples. Recent AFM applications and theoretical developments as demonstrated in this work by analysing of the motion of the soft spring magnetic cantilever for the loading and the unloading steps of the force curves (or approach or retract), we can quantify the elastic properties and the viscous values of the soft samples like cell and polymer gel independently.

Force curve data (the conventional approach and the retract, as well as the creep response and stress relaxation data after z-step, magnetic force modulation or magnetic force step) were analysed offline using the home-written routines in IGOR (Wavemetrics, Lake Oswego, OR, USA). Figure 3 and figure 4) shows a representative AFM force curves. The distance  $z$  between the sample and the base probe may increase from left to right towards the sample surface. At the left edge of the curve, the tip and the sample touch. As  $Z$  increases, the force on the sample (deflection of cantilever) decreases, and eventually becomes negative (see figure 3). The force-distance curves are acquired, irrespectively of sample topography; over a given distance range  $\Delta Z$  beginning from a fixed distance at  $Z_0$ . At the beginning the soft spring cantilever is away from the sample surface. Then the sample is approached to the soft spring cantilever, acquiring deflection values at each pre-assigned step. This process stops at the  $z$  height ( $F_{max}$ ), when the force exerted on the soft spring cantilever with tip reaches the pre-assigned maximum loading force  $k_c * d_{max} = F_{max}$ . The maximum deflection signal after an approach ramp saved by digitally means and readout with the house routine software that is adapted to the commercial AFM software. However, experimentally the maximum loading force, or the maximum deflection is the control parameter instead of the indentation ( $\delta_{max}$ ). The sample is further retracted sequentially for a  $z$ -height distance  $\Delta Z$  and the deflections in the next withdrawal segments are obtained and then stored digitally. After the acquisition of these deflection values, the sample is withdrawn for a further short distance in order to insure

that the vertical distance between the soft spring AFM cantilever and the subsequent point on the two dimensional plane is never less than  $\Delta Z$ . In the same line, the offered advantage of the use of force curves technique is the possibility of doing the lateral movement with the soft spring AFM cantilever and tip away from the soft sample surface, and hence ruling out the capability of dragging the soft samples like the live cell during the acquisition of the conventional AFM force curve data. Indeed, as explained previously, in the contact mode of operation employed in this work, it was technically possible to generate a sample's height profile simultaneously from the recorded deflection signal values with feedback turned off once the AFM soft spring is close to the sample during experimentation. The limitation in employing such a technique includes small  $Z$  range, variable tip/sample force, and unique  $Z$  calibration for each probe and each laser alignment. The selected scanned force volume typically will follow the soft sample surface. Spatial variation of the soft spring cantilever versus sample interaction can be represented using the AFM force volume (AFM force map). Possible applications of the force volume technique include studies of the electrostatics, the adhesion, or the viscoelastic creep response properties of the soft samples like live and diseased cells as well as polymer gel. In the following, we will describe the specific regions of interest on these curves. In this work force curves will be referred to as the time-resolved contact mode force curves. A force curve as illustrated in Figure 3, will exhibit two regimes: (1) as the soft spring AFM cantilever moves towards the sample, the deflection is constant as long the tip does not touch the sample and (2) the deflection maybe proportional to the  $z$ -height while the tip is in contact with a stiff substrate. The  $z$ -height ( $z$ ) in our AFM with a typical extension range has positioned the soft spring cantilever with a high resolution. The feedback controls the measurable force range  $F = k_c * \Delta d$  while compensating for different  $z$ -heights during experiments.

### 1.3.3 Dynamic mode in AFM

By employing the soft magnetic AFM cantilevers to apply small amplitudes in force on the ultra soft samples the viscous-elastic properties can be separated at a defined frequency (see figure 30 and results in appendix). The third design that may be employed for characterizing the live cells viscoelastic properties is the magnetic force modulation experiment (see figure 19). A soft cell sample subjected to a sinusoidal varying stress will respond by a sinusoidal varying strain, which may be out of phase with the applied stress. At a single frequency the material properties could be described. A sinusoidal modulating force in magnet can be applied by attaching a magnetic material to the end of the soft spring AFM cantilever (back of

the cantilever). The force in magnet modulates the force on the tip end of the soft spring magnetic AFM cantilever, which transmits a sinusoidal-like indentation to the live cells. Here, the soft spring AFM cantilever tip is modulated while in contact with the soft sample. In this design a sinusoidal magnetic force is applied to the cantilever plus the sample and the response of the cell maybe observed over an extended off resonance frequency range (see results in appendix). The magnetic force modulating AFM technique takes advantage of the sensitivity to a range of the indenting force and the precision of the cantilever tip relative to the soft sample under study. In the magnetic force modulation experiment the total force of the system will be a function of the drive force, the AFM cantilever force and the viscous force of the medium. Experimentally, the measurements of the system response to the sinusoidal load in magnet can be expressed with defined parameters and employing an appropriate model, which will represent the data and to quantify the spring constant of the soft sample and the viscous properties. The viscoelasticity could be determined from the definition of the phase difference between the direct drive load at the force end of the soft spring AFM cantilever tip and the response of the cell sample around an average indentation. As has been discussed in the previous section the elastic properties (E) of the cell may be estimated from the quasi-static analysis of the measurements performed by vertical output signals to the deformation. Applicability of the magnetic force modulation design depends on the consistency of the magnetic AFM cantilever to drive coil current and the defined frequency range. It becomes particularly interesting if one could define the experimental parameters and the conditions such that the response of the system could be, when required, reasonably quantified by the ratio of the measurable parameters, i.e., the amplitude during the contact (deflection amplitude in contact  $A_1$ ) and out of contact with the cell sample (free deflection amplitude  $A_0$ ).

$$k_s = -k_c \int \left( \frac{A_n}{A_{n+1}} - 1 \right) dz + konst \quad (1.4)$$

Where „*konst*“ denotes the force at the point where the force modulation the analytical integration began. The modulation signal has been monitored as well as the bending of the cantilever as the sample is being indented. As a soft spring in series with the cantilever spring, the variation of the cantilever modulation amplitude that results from this oscillation will vary according to the elastic properties of the soft sample. The observed creep may originate from the superposition of the soft samples like the live cells viscous and the elastic contributions. If for example under the same force on a stiff sample, no indentation occurs, the amplitude ratio should be zero. This is because larger bending's of the soft spring magnetic AFM cantilever

response has been measured. As a consequence, the spring constant of the sample may be infinite. For a very soft sample the amplitude in contact  $A_1$  will become almost equal to the free amplitude  $A_0$  thus the spring constant sample will approach the spring constant of the soft spring cantilever constant. On a stiffer sample, no indentation will occur, thus the amplitude when in contact should be zero. As a consequence, the spring constant of the sample will be infinite. The variation of the deflection the amplitude of the modulation is a measure of the spring constant of the cell sample. The amplitude of the oscillation might depend on the nature/mechanical properties of sample being studied or the distance to sample. In the dynamic mode, the interaction of the between the tip and the sample is reduced. An excitation maybe kept constant during the whole the acquisition of the force curve

#### 1.3.4 Force volume

Possible applications of the force volume technique include studies of electrostatics, adhesion, and magnetics. As shown above, a single AFM force curve records the force as the cantilever tip approaches and retracts from the surface. When the force reaches a user specified trigger point, the system records the height for that pixel and soft spring AFM cantilever retracts. The AFM force volume associates each position with a force curve in  $Z$  for some specified or selected range. By plotting this  $x$  and  $y$  coordinates, one may view layers of the interaction force at various  $z$ -axis heights above the soft sample surface. The value at the points in a volume is the deflection (force) of the soft spring AFM cantilever at that position in space. The height data is composed of relative  $z$  positions of the trigger points. Many scientists have used the AFM to acquire data or map of interactions from various samples. In order to study the spatial variation of the soft sample interactions, force curves may be typically acquired on several points or a single point over the scanned area. Specifically, when the probe contacts the surface the soft spring AFM cantilever bends upward. The laser spot moves upward on the photo detector and the deflection signal increases. While the cantilever is raster scanned over a sample from pixel to pixel, a force curve is recorded at each point. To compensate different sample heights the range of force curve is moved up and down accordingly (trigger mode). The force curves are taken on definite intervals on the sample forming a grid of equally spaced force curves across the sample surface. This type of force plot acquisition is used to obtain a map of interaction forces for heterogeneous sample. The visualisation of the three dimensional force volume maps is not very obvious. A basic process considers each force curve separately and then estimates the contact point between the cantilever probe tip and the

soft sample in question. By reproducing the preceding point-wise analysis and by scanning the sample surface we obtain a force-volume. This force volume is a collection of force curve  $f(z)$  on a grid in the  $(x, y)$ -plane representing the soft sample surface. This estimation provides a 2D topological reconstruction and the spatial variation of the cantilever-sample interactions of the sample.

Our commercial MFP 3D microscope has an adapted built in force volume acquiring technique for signal processing using home-written routines in IGOR (Wavemetrics, Lake Oswego, OR, USA) for obtaining force curves. The user can put in the number of points in both the  $x$  and  $y$  directions of the sample surface, where the force curves will be acquired in the force volume mode. In the force volume mode, all the force curves starts at a fixed height. An approach (load the cantilever in a forward direction towards the sample) and the retract ramp (unload the cantilever from the sample surface in the reversed direction) are performed, then a lateral displacement away from the surface, again an approach withdrawal cycle and so forth till the end of the experiment. Usually in an AFM experiment, the first force curve will always be obtained from the left bottom of the force volume. An interesting observation on the force volume technique is that the sample is not damaged during the lateral displacements. The acquisition of force curves at every point on the scanned surface may be very time (several minutes) consuming. From the force curves the force versus indentation relation is calculated and a theoretical curve fitted into the data. The spring constant of the soft sample is typically calculated from the fitting procedure. A method of modifying the commercially available AFM is in principle to employ the magnetic cantilevers. The AFM can be modified with a fluid cell, which allows experimenters to measure under almost any kind of aqueous environment. For example during experiments, a drop of fluid on top of a laboratory glass slide such that the sample is covered is by experience enough volume for the AFM experiments to be performed. The laser beam path can be focused to pass through the glass slide and the fluid in order to operate under fluids.

### **1.3.5 Vibration response**

The Figure 5 shows the thermally driven motion of the triangular shaped AFM magnetic cantilever in an aqueous environment. The spring constants of the soft spring AFM cantilever can typically be measured by inferring the results of the integral of the thermal noise and the temperature of the aqueous solution. The first step is typically to obtain the power spectrum of the freely vibrating cantilever with no excitation acting on it. In this method the soft spring AFM cantilever is treated as a simple harmonic oscillator. Although the Sader method, which

has been employed by many scientist can also be performed for a driven cantilever, the thermal tune methods relies only on the thermal excitation. The measurement for the thermal spectrum can be performed with the AFM itself. In many cases it is useful to employing an oscilloscope with higher sampling rate. The captured signal is Fourier transformed to the detector voltage power spectral density (PSD). The required natural frequency and the quality factor can be obtained from this voltage PSD by fitting a SHO model with the added background term the signal. The thermal noise calibration method, [40] has been preferred because it was quick and can be readily performed in the aqueous environment immediately after calibrating the deflection sensitivity.[28]

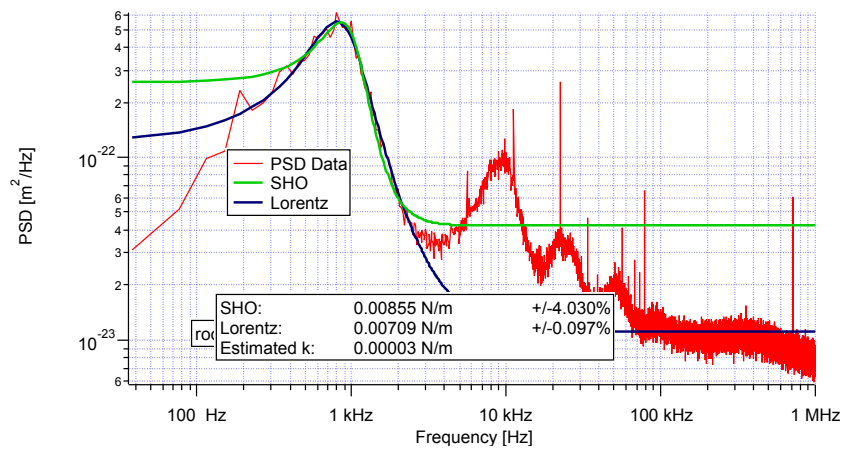


**Figure 5: Thermally driven motion of a magnetic cantilever in an aqueous environment. The figure shows several higher modes due to thermal noise of the AFM cantilever. The spring constant of the cantilever obtained from the SHO and Lorentz fits to the first bending mode to the thermal noise data in the frequency domain. The AFM measures tilt and the sensitivity decreases for higher modes. The figure shows x-axis with the first and the second spectral peaks of the deflection data, which are obtained at approximately 850 Hz and 10 kHz for a wide range of frequencies respectively. The amplitudes (intensity in the thermal noise) of the deflection data on the y-axis span a wider range of  $10^{21} \dots 10^{24} m^2 \cdot Hz^{-1}$  with the first frequency fit width smaller size than for the second bending modes.**

The obtained thermal data as well as the force curve data were analysed offline using home-written routines in IGOR (Wavemetrics, Lake Oswego, OR, USA). The equipartition theorem, which says that if a system is in equilibrium, each mode of the cantilever on average contains an amount of energy  $1/2 (k_B T)$ , is used to find the spring constant of the soft spring AFM cantilever  $k_c$  by relating the thermal motion of the cantilever's fundamental mode to its thermal energy (equation 1.4). Where  $k_B$  is the Boltzmann constant ( $1.38 \cdot 10^{-23} J/K$ ),  $T$  is the temperature (K). The (time averaged) thermal noise in the deflection signal is given by:

$$\frac{1}{2} k_c \langle d^2 \rangle = \frac{1}{2} k_B T \quad (1.5)$$

Where  $\langle d^2 \rangle$  is the mean square deflection caused by thermal vibrations. The force resolution (force fluctuations), if only thermal noise is considered, is be given by: [24]

$$\langle F^2 \rangle = k_B * T * k_c \quad (1.6)$$

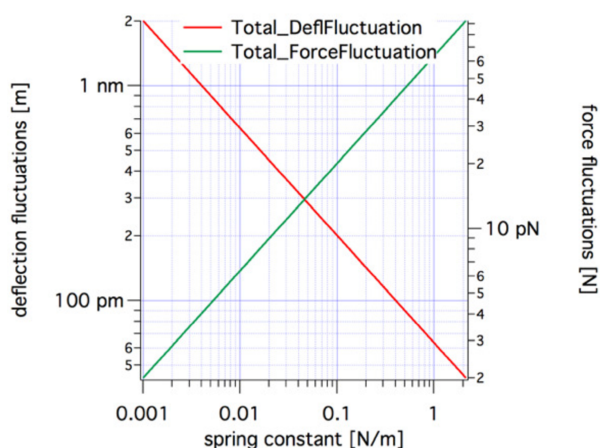


**Figure 6: Thermal force and deflection fluctuations as a function of AFM cantilever spring constants respectively. These numbers shown on the graph will give a lower limit for noise in the quantities force and deflection.**

### 1.3.6 Sensitivity of the AFM technique

The AFM cantilever deflection signal has been the output in volts of the PSD. Among the many detection setups for the indentation experiments, the AFM optical lever design is commercially available and has been widely employed to measure the AFM cantilever deflection in order to characterize mechanical properties of live cells and the tissues. As shown in figure 7 the cantilever bending has been detected via the optical lever detection scheme, which has employed a laser light source and a position sensitive diode (PSD). This is a setup that spatially separates the position sensitive detector (PSD) and the soft spring cantilever. The laser beam is focused on the back of the AFM cantilever and a 4-quadrant position sensitive detector collects the reflected light. With this design either the cantilevers deflection or the torsion can be detected. The instrument used has been equipped with a super luminescent diode (SLD) (laser light) that emits light of low coherence source of ca. 860 nm on the back of the cantilever. The optical beam deflection setup is a design that spatially separates the position sensitive detector (PSD) and the soft spring AFM cantilever. It collects the laser light from the cantilever-sample environment. Generally, the force between the tip and the soft spring AFM cantilever has been measured using the laser and the detector to monitor the cantilever vertical motion. A lens focuses the light beam of the SLD at the back of the cantilever. The light reflects off the soft spring AFM cantilever and up to a collimation lens and mirror to the PSD. The collimated light beam is reflected at the backside of the cantilever, which is tilted at an angle of 12° with respect to the sample plane. The soft spring AFM cantilever reflectivity has been enhanced by coating the backside of the cantilever with

a thin Gold (Au) layer and projected to the photo detector. [23] Accuracy for measuring the displacement is very important in order to obtain a good resolution. The soft spring AFM cantilevers have been employed in transparent liquids and buffer solutions. The photo diode is composed of four smaller detectors addressed A to D. The variations of the detected voltage signals from the segmented detector have been used to determine the cantilevers deflection in the vertical directions. The voltage is generated from each quadrant that is proportional to the intensity of the laser light beam reaching or hitting it and it is used in different combination to find the deflection relative to its unloaded position, usually corresponding to reflected spot on the centre of the photo detector. The photo-detector position was adjusted at the start of the experiment such that the vertical and horizontal voltages are zero when the soft spring AFM cantilever is at rest. Due to the long distance between the soft spring AFM cantilever and the photo detector a geometric gain is acquired. The optical lever detection design has been used in the AFM to sense the small and the well-controlled loading/ unloading force on the soft spring AFM cantilever (generally equipped with a magnetic material) by recording the change in voltage. A small change in the angle of the cantilever leads to a measurable change of the position of the laser on the detector. The optical lever is so sensitive enough such that it can detect the thermal noise. The slope at the point where the laser beam has been focused determines the angle at which the beam is reflected. The noise power spectrum due to thermal noise is obtained with the Fourier analyser.[24] The piezo electric with a z travel range of 10  $\mu\text{m}$  positions the soft spring AFM cantilever tip with the high resolution. The position of the reflected beam depends on the angle of the deflected soft spring AFM cantilever. Due to the difference in bending shapes of different soft spring AFM cantilever modes proportionality constant is required for each mode.[9, 23, 41] [25, 42] As shown on figure 7, the AFM probes the surface of a soft sample typically by moving the sample beneath a tip attached into a weak cantilever spring while the tip is in contact with the soft sample, or near contact to the soft sample with the surface

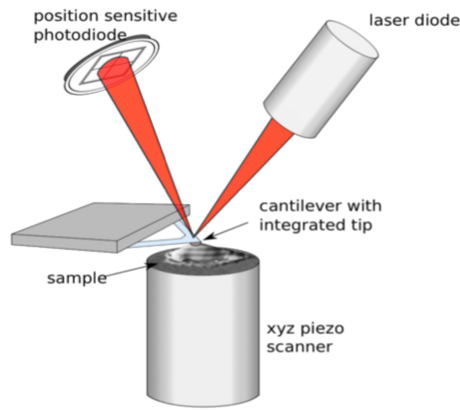


**Figure 7: Illustration of the AFM optical lever beam bounce technique. The deflection of the cantilever is sensed with the optical detection. Image shows a side view of the reflection at the very end of the soft spring cantilever as it changes orientation upon contact with the sample surface, which is considered as the deflection. The reflected laser light from the very tip end of the AFM triangular cantilever creates a push pull error signal when the spot moves on the position sensitive photodiode (PSD). When the soft spring cantilever is at the neutral deflection the laser light spot falls on the center of the PSD.**

All atoms and molecules exhibit weak, short-ranged attractions due to van der Waals forces. [43] The van der Waals forces arise from fluctuations in the electric dipole moments of molecules, which become correlated as the molecules come closer together, giving rise to an attractive force. [44]

An AFM force curve may contain information about the long- or the short-range interactions. The van der Waals forces between any two atoms or molecules may be separated into orientation, induction and dispersion forces. Orientation forces arise only in the case of polar molecules, that is molecules having permanent multipole moments and may be explained in terms of the interaction between, for example, the static dipoles, and the quadrupoles. A polar molecule may induce polarity in the nearby neutral molecule and this results in an attractive induction force between them.

With non-polar molecules none of the interactions, which are caused by permanent dipole can arise. However, the non-polarity of such molecules is a time average: if they are studied at very short intervals they are found to possess finite fluctuating dipole and higher multipole moments. These instantaneous moments induce polarity in the neighbouring atom or molecules to give an attractive force. The fluctuations involved have a frequency in the ultraviolet range and play an important role in the so called optical dispersion (the origin of the name has to do with the fact that a distinct spectra is seen when light is split up into its individual colours in the UV and visible region): for this reason forces arising from this mechanism are known as dispersion van der Waals forces. For a separation greater than about one nanometer the forces due to dipole-dipole dispersion interaction generally overshadow

those due dipole-dipole dispersion interactions and higher multipole interaction, but for smaller separations multipole interaction assume increasing importance. Dispersion forces (quantum mechanical of origin) makes up the third and perhaps most important contribution to the total van der Waals force between atoms and molecules and because they are always present they play a role in a host of phenomena such as adhesion; surface tension; wetting; physical adsorption; the properties of gases, liquids; and the structures of condensed macromolecules such as proteins and polymer. Among other properties, the dispersion forces thus are not additive; that is the force between two bodies is affected by the presence of other bodies nearby both directly and by “reflection” from other molecules, since they too are polarized by the field. The overall effect of quadrupole or multipole interaction usually results in an overall reduction in the strength of the summed pair of interactions. But although small, many-body effects can be important because they do involve all the molecules in a lattice. However, both three-dimensional and two-dimension van der Waals equation of state can be applied to more complex systems for example, to interactions of small colloidal particles in liquid and surfactant molecule on the surface of water or at an oil-water interface. Both equations predict the existence of a gas-liquid coexistence regime at some particular pressure as long as the temperature is below critical temperature. Dispersion forces generally exceed the dipole-dependent induction and orientation forces except for small and highly polar molecules such as interactions between two dissimilar molecules of which one is non-polar and water!

As mentioned before, this has been used by many researches in literature to quantify the elastic properties of soft samples like gel and diseased cells. The spring constants of the soft samples may contribute to an improved understanding of the local mechanical properties of the soft samples. The physiological functions of soft samples like live cells and the diseased cells can typically change in response to their mechanical environment and therefore must be discussed from the viewpoint of biomechanics. In the same line, the mechanical properties of the soft samples like the live and the diseased cell will include its internal stiffness (the spring constants of the sample, the spring constant (stiffness) values and the viscous properties of the sample), the nonlinearity, the anisotropy, the heterogeneity as well as several structural aspects of the sample. These include their relation with individual component of the cytoskeleton and organelles that control the soft live cells and soft polymer gel responsiveness to external mechanical force as well as the remodelling effects. The importance of AFM [8], for measuring the creep response of soft samples like cells in their aqueous solutions mimicking their physiological environment has steadily increased over the last three decades.

[14, 17, 45-48] In my work, in order to determine the mechanical properties (viscoelastic creep) from the force curves on biological soft samples, amongst many other models mentioned before, one of the contact elastic theories namely the Hertz model, has been employed to know the dependence of the contact radius and the soft sample deformation on force. In their work they showed the limits but most importantly the possibilities of the AFM measurements of the mechanical response of soft samples like cells. Force curve methods in the contact mode based on AFM provides a more reliable spring constant of the soft sample at low loading speeds and large indentations. Our group employs the Hertz model and its derivatives by AFM and it has been widely employed by many other scientists in the literature to evaluate the elastic properties of soft samples. The Hertz model describes the simple case of elastic deformation of two perfectly homogeneous smooth bodies touching under a load.[49, 50] Amongst other important points to consider when employing the Hertz model formulation, to my best knowledge, four important other assumptions typically considered by the Hertz model are: (i) the indenter should have a parabolic shape and (ii) adhesion contributions of the soft samples like cells are ignored (iii) the indented sample is assumed to be thick in comparison to the indentation depth and (iv) the homogeneity of the samples being studied is ignored. The first assumption remains a valid one for the case when a spherical tip radius is much larger than the indentation depth.[51] Amongst other theoretical models used in AFM-based evaluation of cell mechanical characteristics we should mention the finite element model, which is among many others in the literature and our group a popular model for analysis of elasticity problems in engineering as described by Ohashi et. al. 2002 [52] The mechanical properties of soft samples exhibits nonlinearity and a viscoelasticity that results in depth, soft spring AFM cantilever tip radius, and the speed-dependent properties that may arise from the complex material architecture and the solid–fluid interactions. As the soft spring AFM cantilever is moved closer to the sample, the soft spring AFM cantilever will deflect because of long-range cantilever sample interactions. In the case where the AFM is operated in an ambient environment or in vacuum with an electrically neutral sample, the only long ranged force will be the van der Waals (vdW) attraction. The mechanism leads to an attractive interaction potential. When the distance is reduced further (a distance of approximately  $10^{-7}$  m), the repulsion of the atoms sets in due to Pauli exclusion principle which can be tentatively described by a distance dependent  $U_{vdW} = -C/R^6$ . With  $C$  being the interaction parameter describing the molecular diameter. However, between a larger sphere of radius  $R$  and a flat surface the force is  $F = -AR/6D^2$  and it is long ranged. The interactions between the macroscopic bodies can always be described in terms of the

Hamaker constant,  $A$ . For the soft spring AFM cantilever sample system, if the soft spring AFM cantilever with tip is far from the sample surface, its' motion may only be due to the thermal noise. The sum of these contributions as is read from equation 1.5 is called the Lennard-Jones potential and it describes the interaction between two atoms separated by the distance  $R$ .

$$U_{LJ} = -\frac{C}{R^6} + \frac{B}{R^{12}} = 4\epsilon \left( \left(\frac{\sigma}{R}\right)^{12} - \left(\frac{\sigma}{R}\right)^6 \right) \quad (1.5)$$

the tip in contact with the surface. The magnitude of the capillary force depends on the cantilever to sample forces. The magnitude and sign of the cantilever force depends on the calibrated soft spring cantilever spring constant and the change in the measured deflection value. Force curve data (conventional approach and retract, as well as the creep response data after z-step or magnetic force step) were analysed offline using home-written routines in IGOR (Wavemetrics, Lake Oswego, OR, USA). As previously described one measures the AFM cantilever deflection when it scans the soft and stiff sample surface. How much signal that is generated in the photodiode for a given amount of the cantilever deflection is called the optical lever sensitivity. The inverse optical lever sensitivity (invOLS) for the tilted soft spring magnetic AFM cantilevers is typically obtained from a portion of the height data after obtaining a force curve on a clean cantilever glass slide. The cantilever deflection [nm] in the repulsive regimes of the force curve equals the inverse slope of the voltage output of the position sensitive sensor,  $\left[\frac{V}{nm}\right]$ , vs. the linear variable displacement transformer curves acquired on the samples. The voltage change is due to the same amount of deflection of the soft spring AFM cantilever as the movement of the piezoelectric element  $\Delta z$ . The cantilever deflection in the retraction part force curve is given by:  $\Delta z = V \cdot InvOLS^{-1}$ . Where  $V$  is the potential difference from a position sensitive detector. Here  $InvOLS \left[\frac{nm}{V}\right]$  is the inverse optical sensitivity. The inverse optical lever sensitivity depends on the dimensions and the shape of the laser spot on the photodiode and hence depends on the refractive index of the medium in which the measurements are performed. The z-height of the feedback loop keeps the soft spring AFM cantilever at a constant deflection, such that the calibrated motion of the z piezoelectric transducer scales the height data. In order to show the linear regions of the force curves, the deflection of the soft spring AFM cantilever was approximately 2 micrometres. The proportionality factor is checked and recalibrated each time before acquiring force curves or when the experimental conditions like change in medium is changed. In a force curve the retract regime is considered for the values in the range of the measured voltage change. The

sensitivity in the tilt is taken into account during calibration and is not a problem, especially as one operates the AFM in closed loop feedback. For the data collected in this work, the magnetic sensitivity of the cantilever was calibrated individually. Many researchers have used the optical interferometer setups (vibrometer) as detection method to supplement the optical lever setups by the manufacturers in order to determine the small displacements of the cantilever with a good resolution.[9] To address drawbacks, our magnetic AFM apparatus was additionally designed to operate in the force modulation control mode where the user can freely define the quasi-static or the magnetic force modulation indentation profiles in the indentation or the load and unloading control modes. For calibration purposes the polymer gels and the cancer tissues from the interstitial lumen were employed as specific samples. As a result, in addition to commonly used the spring constants values of the soft samples, which are derived from quasi-static experiments, other mechanical values can be extracted such as storage, loss moduli, and damping factor as a function of frequency, relaxation time constants. The spring constant and the friction coefficient (coefficient of friction) and the time constants from the creep response data of the soft samples from the loading and unloading curves have been measured. These quantities can be employed to investigate the role of mechanics in diseases as they might contain important information about structure and the function.

### 1.3.7 Indenting force

It is possible to correlate a change in the mechanical properties with the structural changes on the soft samples by AFM because the indentation that is created due to a loading force can now be quantitatively and qualitatively analysed. The AFM contact force or normal force is the most important attribute of the mechanical data obtained by AFM, which is directly related to contact reliability. The elastic response corresponds to the compression in the direction of the force. The deformation of the body may be quantified by the difference between the resulting size and the steady-state size. The relation that links these physical quantities is known as the Hooke's law. The intuitive meaning is that in order to deform a body by a certain percentage of its size, one must apply a force that will be higher for stiffer material compared to softer ones, and the spring constant is a quantification of this property. Accurate determination the samples mechanical and the viscoelastic response requires a specific force measuring design be capable of sensitive detection of the initial point of contact between the indenter and the soft sample. The indentation experiments by AFM employs an indenter with geometry, which is typically unknown to push into the cell and the cantilever response is then monitored. This is an essential tool for the characterization of the lateral

variation of sample mechanical properties and hence for the study of the soft samples. The spring constant of the cell sample in this work has been determined on the basis of the force versus the indentation curves. As a soft sample spring being in series with the soft spring AFM cantilever spring, the indenting force and its resulting indentation in the cells often follow the prediction of the Hertz contact model, which is linear. As theory suggest [53], Hertz model relates and describes the indenting force as a function indenting contact cantilever tip area,[54] which is increased by the spring force for different contact tip geometries. Till date, most of the stiffness data collected in literature by AFM has been currently collected using the pyramidal, the conical or the spherical tip geometry. Based on the tip geometry (pyramidal, spherical or a conical tip) for contact measurements, the spring constant of the soft samples, and the elastic properties can be described. Understanding the effects on the indenter geometry on soft samples opens the possibility to more directly compare data obtained with different indenter geometries [11]. Assuming the live cell is a homogeneous and isotropic material (for at least relatively small indentation) the live cell can be characterized by its Young's modulus and an assigned Poisson ratio. [55] For example in the case for a pyramidal tip geometry with a tip opening angle  $\alpha$ , the elastic modulus  $E$  and the Poisson ratio  $\nu$ , we find widely cited relationship between indentation  $\delta$  and indenting force  $F_{pyramid}$ :

$$F_{pyramid} = \frac{1}{\sqrt{2}} * \frac{E}{1 - \nu^2} * \tan \alpha * \delta^2 \quad (1.7)$$

The contact angle  $\alpha$  is always defined with respect to the advancing sample substrate. From an experimental point of view, the contact angle occurs only visually. Experimental evidence reveals that for perfectly elastic samples the spring constant of the sample increase with increasing contact angles and was proven by a separate experiment. However, for the perfectly elastic sample like the gel a single spring constant value [Pa] seems only to define the response of the sample to deformation. In this work the force curves cycle is the deflection in dependence to the time plot. In applying the extended model usually requires visual inspection of the deflection in dependence to the z height motion. Accurately quantifying the spring constant of the soft samples requires determining the initial force, which typically is a flat baseline between the soft sample and the employed soft spring cantilever tip. In our software, the spring constant [Pa] (material parameter) value which characterizes the materials elastic properties, have been additionally estimated by fitting the obtained deflection data in the frame work of the Hertz contact mechanics, while taking into account the

geometry of the infinitely stiff probe with the soft spring AFM cantilever tip modelled either by cone or a pyramid. It requires however a minimum height adjustment in  $z$  typically in the range of 1-3 micrometres in the approaching and the retracting regimes of the force curves respectively. This is because on each force curve in a force volume the soft spring AFM cantilever indenting force as well the soft sample thickness when in contact has to be accurately determined in order to quantify the material properties. The spring constant however is the soft sample material property and should only vary considerably in dependence to the sample homogeneity and as well as the heterogeneity. Depending on the experimental conditions the slope of the force curve obtained by the loading in force provides information about the spring constants of the sample. The response of the sample force will depend on the soft sample mechanical properties and the information about the soft spring AFM cantilever employed. By averaging the slopes of these small additional steps, one can quantify the soft stiffness of the samples by AFM. The spring constant of the soft samples like the live and the diseased cells apparently will decrease if one does not incorporate accurately the values of the final contact point in the acquired AFM force volume. The experimental data is fit to a theoretical model of the tip deflection in the region where contact is made. As shown in figure 8 the sample force in dependence of the indentation by employing soft springs AFM cantilever as an example. Note that the theoretical curve given by the best fit extends above the experimental values in indentation indicating that the contact was made apparently at larger distances than that predicted by the model. Some sources of noise may limit the deflection output signals, which may have to be corrected in order to analyse accurately the mechanical properties of the sample. Note the small discrepancies in the loading force of ca. 0.1nN that seems to indicate the presence of randomly generated noise in the system and thus affecting its sensitivity during the approach ramp on the soft sample. Most of the uncertainty in this range was largely in the sample spring constants. It is therefore relevant to determine the spring constant e.g., for the soft sample accurately by employing a more suitable model. It is also possible that the tip deforms while it is in contact with the live cell sample. As the tip and the soft sample distance is decreased the tip and the sample moves together, which causes an indentation. To avoid the uncertainties due to the system noise, one might fit the raw deflection data after (during) the contact with the soft sample has been made at defined in the defined range the measured deflection values to obtain the force. The spring constant values of the different samples are indications of different force values in the indentation of a single deflection versus the displacement curve (force curve). It is calculated from the difference of the deflection between the reasonably flat deflection displacement

value and the sloped deflection value (not shown). Eventually the z height piezo is retracted in order to drive the soft spring cantilever back its original (undeflected) position (not shown). The value of the slopes at the large penetration depths allows one to obtain by the quasi-static analysis (e.g., ca. 1 nN) the stiffness and the elastic modulus (E) of the soft samples from the force curve.

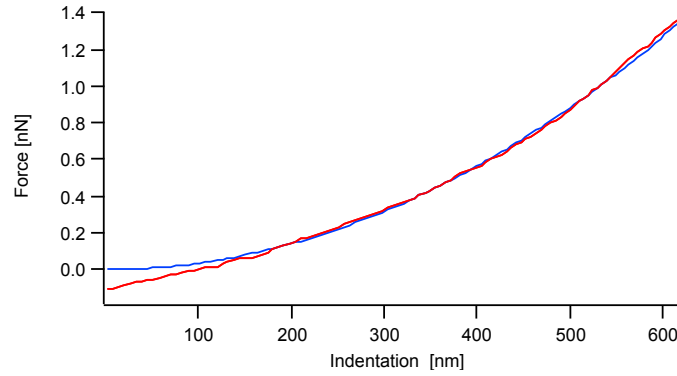


**Figure 8: Illustration of an approach-based indenting force versus the resulting indentation relationship obtained on the live cell sample. The raw experimental deflection data (red trace) has been compared with the fitted (blue trace) curve on the soft substrate. The loading force, which is proportional to the contact area of the cantilever tip was the deflection multiplied by the spring constant of the cantilever. The indentation is the deflection subtracted from the z height. The indenting force and the resulting indentation in the cells often will follow the prediction of the Hertz model. Once the contact point has been identified the cell sample stiffness can be derived while assuming linearity. Analysing the approach-load relationship proves linearity for the pyramid tip at larger penetration depths on the live cell. The lower force range (ca. 0 nN -0.1 nN) indicates the considerable noise introduced in the system upon contact between the tip and the cell sample surface.**

In the AFM the computational model like the Hertz model (blue trace on the force versus the indentation) requires additional assumptions including infinite sample thickness, isotropy and homogeneity. It also requires small stresses (i.e. indentations) to be applied to guarantee a linear response of the sample. Other models have been developed and have been employed by authors in the literature [56] and thin samples [47] by employing sharp tips. Spherical tips have been used to measure the response of the whole live cell. The indentation  $\delta$  and the loading force  $F_{cone}$  for a conical tip shape is given by:

$$F_{cone} = \frac{2}{\pi} * \frac{E}{1 - \nu^2} * \tan \alpha * \delta^2 \quad (1.8)$$

#### 1.4 Mechanical properties and analysis techniques

A quarter of a century ago, the cell and its many internal compartments were still thought of as microscopic reaction vessels containing complex chemical mixtures held at constant temperature and pressure.[57] When developing his famous equation, Robert Hooke devised the compound microscope to study thin slices of cork. Looking at dead cellular walls of plant tissues he was revolutionary and he observed the little pores that he termed “cells”.[57] All living organisms are based on cells as the individual unit of biological organization. These cells typically come in a wide variety of shapes, sizes, and lifestyles such that choosing one representative of the cell type to tell their structural story might be very misleading. Interestingly, understanding mechanical properties of these structured-network organisms in the field of biophysics (physical point of view) has long been a topic of interest for many researchers. The spatial scale associated to with biological structures run from the nanometer all way to the scale of the earth. Most soft samples like motile cells have a spring constants of typically of a few\_ and this value may vary depending on the environment. As the intricate pathways of the intermediate metabolism became available, scientists hoped to described cellular processes as the result of a complex series of parallel and sequential second-order chemical reactions brought about by the diffusion and random collisions of chemical species in these confined spaces. During the intervening time, this view has changed dramatically. Most cells are polar structures, and their interior is neither homogeneous nor isotropic. Moreover, most of the essential cellular functions for membrane bounded cells such as chromosomal segregation during cell division, translocation of organelles from one part of the cell to another, or the maintenance of a voltage across the membrane all involve directional movement and transport of chemical species. Processes such as replication, transcription, and translation require the information encoded in the sequence of linear polymers to be read and copied in a directional manner, and cells must often move and orient themselves in response to the external chemical gradients and other signals. To overcome the randomizing effect of Brownian motion and carry out these directional processes, cells typically possess molecular structures that behave as tiny machine-like devices. These devices operate as molecular motors, converting chemical energy into mechanical work used to drive the internal activities of the live and diseased cell. However, they are unlike macroscopic engines in that, because of their dimensions, the many small parts that make up these molecular motors must operate at energies only marginally higher than that of the thermal bath and hence are subjected to large fluctuations. Sitting astride the line that separates stochastic from deterministic phenomena, the function of these molecular motors can be thought to be that of refining the randomness of the molecular events and generating directional processes in the live and the

diseased cell. Live cells have hundreds of different types of molecular motors; each specialized for a particular function. Many biological motor-like proteins have been discovered and characterized in recent years. Although there is much variation in design and performance amongst them, several lines of evidence suggest that many such mechanochemical proteins share fundamental underlying features that can be understood with the same basic concepts and theories. Such theories seek to describe the physical principles that govern the behaviour of molecular motors, to explain the role of fluctuations in their operation, to describe the nature of the coupling between chemical reaction and physical coordinates, and to understand specific aspects of this conversion, such as its efficiency and reversibility.

Mechanical properties of live cells, have gained a large interest and have seen rapid development in the last decade for two reasons. Firstly, the availability of the technics to measure cell mechanics with high spatial resolution and high sensitivity by AFM. For animal cells the mechanical response is mainly caused by the actin cytoskeleton[58] and internal stresses in this fluid-filled network.[59] Secondly, the field is very interesting because it has been discovered that mechanical measurements have some biomedical applications like monitoring and diagnosis of diseased most cells.[60] For instance changes in spring constant of a live cell can indicate disease or injury. This advances that stemmed from many observations of the dynamics of cell properties of deformability. The cytoskeleton, known as the system of protein filaments that enable the cell to insure it's structural integrity and morphology, exert forces and to produce motion, It has been shown in previous works that the monolayers of the live cells typically change shape dynamics when stimulated with laminar flow. Accompanying any changes in such morphology are probable changes in intracellular ionic fluxes, gene regulation, transcription, translation and the cytoskeletal structure. The eukaryotic cells display an ability to organize their actin filaments into higher-order, cross-linked structures that have a profound influence on cellular shape, division, adhesion, motion and/ or signalling, many of which are essential for the survival of the healthy cell. The core constituent of the actin cytoskeleton is monomeric globular (G)-actin, a 43-kDa ATPase that self-organizes to form a two stranded helical polymer around itself every 37nm, approaching several micrometers in length with characterized rate constants for these transitions.[61]. The non-muscle cells controls actin via a large amount of regulatory proteins that shift actin between the polymeric to monomeric (5.4 nm in size) structures as required by the motile cell. The monomeric globular actin is composed of two major subunits, Each of these subunits can be further partitioned into two additional subunits.[62] It was initially through the study of the

stepwise assembly of the brush border microvilli that a role for multiple actin-bundling proteins in the construction of parallel actin bundles was first recognized. Numerous and highly regular, finger-like projections dramatically increase the apical plasma membrane of absorptive epithelial cells. Microfilaments in motile healthy and diseased cells are typically grouped with and other actin binding proteins to form 200-500 nm thick actin bundles. Parallel actin bundles, at the core of the brush border microvillus have additionally been found to contain yet another kind actin-bundling protein.[63, 64] Small espin (110kDa) is a member of what appears to be a new family of high affinity actin- bundling proteins, the espins and displays intriguing similarities to the forked proteins of *Drosophila*. One study proposed that magnesium is the cation bound to actin in native myofibrils because-the treatment with ethylenediaminetetraacetate seems not to diminish the magnesium levels in the myofibril preparations.[65] Recombinant small espin elicits the formation of parallel actin bundles in vitro under physiological conditions and, when expressed ectopically in transiently transfected cells, espin decorates actin stress fiber-like structures and appears to cause their bundling and/or accumulation.[64] In response to stimulus, most motile cells may not only do they respond robustly to dynamic gradients as a result of the perturbations, but may also adapt the migration direction by integrating and resolving competing spatial signals, or prioritizing newly encountering attractants.[66-71] Conversely, in order for the cell body to follow, contraction may be coupled with de-adhesion at the rear of the cell. Particular progress has been made with cytoplasmic gels isolated from macrophages and amoeboid cells and with the more highly organized structure of the intestinal microvillus. Numerous models based on positive feedbacks, incoherent feed-forward, excitable or Turing-like networks have been proposed to describe the down-streamed polarized signalling activity of the cell-surface.[68, 72, 73] In literature, to the best of my knowledge more than 100 focal adhesion specific proteins have been identified including enzymes namely (e.g., focal adhesion kinase, FAK protein of 12 kD),[74] [75] scaffolding proteins (e.g., paxillin), adaptor proteins (e.g., zyxin) [76], structural proteins (e.g., talin) [77] [78], F-actin binding proteins (e.g.,  $\alpha$ -actinin) [79] [80] [81], as well as the integrin linker proteins (the major and best characterized trans-membrane receptors proteins that mediate dynamic interaction during cell migration), which will mediate inside-out and outside-in signalling process, micro-environmental sensing[82], and coordinated cell migration.[82] The proteins, known as integrin, are heterodimers that are known to be typically composed of  $\alpha$  (size in the range of 120-180 kilo Dalton) and  $\beta$  (size in the range of 95-117 kilo Dalton) subunits and it is included in the glycoprotein family.[83] [84] [85] Although there are no genetic relations between subunits, they share similarity in the

domain structure.[86] Talin, vinculin,  $\alpha$ -actinin, and integrin, have been shown to interact in vitro and positioned on 2D extracellular matrix such that they suggested that there may be potential link between actin filaments and the membrane. However, little attention has been paid to cellular interior.[65] To my best knowledge, other protein families that contain proteins previously purified exist and have been found to have functional similarities to the founding proteins. Over the past five years much effort has been directed towards these goals. Many new actin-binding proteins have been identified, initially in crude cell-free extracts, but many of these have now been purified and partially characterized. Filaments have been additionally shown to be dynamic and can translocate fuelled by nucleotide hydrolysis even without the typical motor proteins.[87] Polymerized actin seems to move centripetally in motile cells. Monomeric actin apparently preferentially at or near the membrane at the extreme leading edge of the cell cytoskeleton and is then transported backwards towards the cell nucleus. The general assumption was that the stress fibres reinforce the cell against a external shearing forces that is applied via by blood flow.[88] Conversely, in response to stimulus the actin cytoskeleton may undergo morphological changes. This involves disassembly of the existing meshwork as well as nucleation of new filaments and an actin wave is typically a spatially segregated assembly and disassembly cycle.[88] In vivo, their assembly-disassembly processes lead to a dynamic pattern of organization in concert with many different motile activities of the living cell. Experimental observations have shown that cells as diverse as social amoeba, neutrophils, leukocytes, fibroblasts, and nerve cells maintain the acquired orientation even when signals are disrupted or noisy.[89-94] The polymerization is an intrinsic property of actin. An interesting consequence of adenosine triphosphate (ATP) hydrolysis in actin polymerization was for seen by Wegner et al, who showed that this irreversible polymerization introduced the possibility of irreversible energetic difference between the two ends, while in case of reversible polymerization the critical concentrations are identical at the two ends. In the presence of ATP, monomer concentration can be defined at subunits which the net rate of polymer growth is zero, pending a slow association of subunits and an equivalent dissociation at the other end. The condensation processes have been studied in detail, particularly by Oosawa and Asakura and by Wagner. They showed that the rate of the microfilament assembly is typically controlled by the formation of a nuclei and their production is favoured by the presence of magnesium cations. [65] ATP hydrolysis in the filament is tightly coupled to polymerization and regulates the kinetics of dynamic assembly as well as the proteins. Thus will typically depends on the ATPase activity; ATP binds with affinities in the nanoMolar range in the central subunit in

the enzyme, but actin exhibits only very weak ATPase activity in its monomeric form. Polymerization triggers a conformational change in the nucleotide binding subunit that allows actin to hydrolyse ATP within seconds of the filament formation. The cleaved inorganic phosphate is not released immediately after hydrolysis yielding the intermediate ADP-P<sub>(i)</sub> (adenosine diphosphate inorganic phosphate) state of F-actin [88] Polymerization cycle may be separated from the ATP hydrolysis by reducing the rate of ATP hydrolysis by lowering its' temperature or by increasing the monomer concentration. After the release of the inorganic phosphate, which typically leads to ADP-bound filamentous-actin represents the matured - state of the filament, which can then be depolymerized back to an aged monomeric form. The interface between the major subunits forms the nucleotide binding pockets. It is known that equilibrium between the globular and the filamentous form of actin depends on the state the bound adenosine nucleotide.[95-97] Adenosine triphosphate and adenosine diphosphate inorganic phosphate bound (ATP- and ADP-P<sub>(i)</sub>- bound) actin is more stable in the filamentous form than the ADP-bound state.[98] Molecular dynamic simulations revealed that nucleotide binding cleft remains closed in the ATP and ADP-P<sub>(i)</sub>- bound states, but typically prefers an open conformation after the release of the inorganic phosphate.[99] These biochemical properties are very integral to the non-muscle cellular activities of the actin because each asymmetric filament possesses a fast growing barbed end and a slower growing pointed-end that are distinguishable by their structural characteristics and kinetic properties. As I earlier pointed out, there exist numerous evidences in previous works that the directed behaviour in response to external perturbations may rely on generating polarized signalling activity at the leading edge of the motile cell that is translated to an elongated cell shape, and subsequent persistent migration in the direction of the signal.

The first application of the AFM on cancer cells was performed by Lekka et al., in 1999 [17]. In their work they suggested that cancer cells are softer than normal cells in AFM measurements, and this change in cellular spring constant are attributed to the changes in the organization of the cytoskeleton [17]. The argument that cancer cells seem to be softer than normal cells in AFM measurements has also been validated in subsequent studies [100], [46]. This rational has been additionally applied to numerous studies in the investigations of rheological properties of tissues like the lung epithelial cells [101], heart cells [102], the lamina of cell nuclei [103] and vascular endothelium [104]. A recent study shows that the property of the extracellular matrix like the spring constant modulates the viscoelastic properties of the live and the diseased cells thus normal cells appear softer than cancer cells on soft substrates. [48]. Nevertheless, their mechanical fingerprint or phenotype [14] is very

different and clearly distinguishable from normal cells. So, the general idea using cell mechanics as a tool to detect the state of a cell, including its pathological state, or in the case of cancer cells its malignancy still holds and has been understood, and will have potentially many applications in the biomedical industries. The feedback of the spring constant of the local matrix on the cell state likely has important implications for development, differentiation, disease and regeneration. [105]

The deformation of soft samples like live cells or the diseased cells is as a result of an applied stress or strain evolving over time.[12] How cells respond to deformation has been investigated with many techniques in the laboratory and to the best of my knowledge the first reports on single cell mechanics were using the micropipette aspiration technique [106, 107]. The micropipette aspiration technique offers the advantage that it may be performed using equipment available in the laboratory to study the viscosity of the entire live cell. In this technique the micromanipulator is used to bring a micropipette into contact with the cell surface. The suction pressure is applied in the micropipette to deform the soft sample like the live cell surface. The live cells are not adherent to the stiffer substrate when employing this setup. However, the resultant deformation of the cell by the micropipette setup is suggestive of the global cellular mechanical properties, like viscosity since the entire cell sample is deformed.[107] In 1950, Crick et al., [108], pioneered a novel magnetic force experiment in which they employed controlled movements of micro magnetic particles of arbitrary shapes to measure the viscoelastic response of live cell. However, due to technical challenges and the lack of magnetic beads quantitative measurements were challenging. Following the rational performed by Crick et al., [108], Valberg et al., in 1987 [109] have extracted the viscoelastic properties of cells by studying the relaxation of the remnant magnetization or by tracking the translational motion of single particles. [110] [109]. Many other methods have been used to study soft samples including Scanning Acoustic Microscopy [111], magnetic twisting cytometry (MTC) by the application of the torque and no force [112, 113], the application of force by magnetic tweezers [110, 114], AFM [45], optical tweezers [115] and hydrodynamic stretcher [116]. The MTC however typically applies a magnetic field to generate the torque on the magnetic materials attached to the live cell surface. It is challenging to control the force and characterize the twisting with high resolution. The cellular spring constants have been derived from the applied torque and the twisting deformation relationship. [112] As compared to the loading techniques like magnetic tweezers or magnetic bead cytometry experiments where contact is made with the live cell sample by employing a magnetic bead, the contact between the sharp tip of an AFM can be reasonably well defined when the cell is indented in

an almost vertical direction, normal to the petri dish or the support on which the cells are cultured. The conventional AFM method strongly relies on the knowledge of the area function of the indenter as a function of the tip geometry, which is known to a few degrees when the experiments are being performed. For the optical tweezers, the forces applied on the soft samples depend on the spring constants of the optical trap and range roughly 1-100 pN. In a typical optical tweezers experiment a soft sample is specifically brought close to a bead in contact with the cell and trapped bead is controlled externally at the focal point of the laser. The force exerted on the soft sample may be determined from the offset of the trapped bead from the centre of the trap. Both the AFM and the optical tweezers are capable of generating relatively high forces, but generally have lower sensitivity in the low force regime partly because of the inherent challenges in measuring the slopes due to the noise. The AFM combines the capabilities of high force sensitivity with a quantitative mechanical probing at larger indentation depths. However, depending on the experimental setup (creep or modulation type) the analysis and the models employed vary strongly, and need to be refined accordingly. For a comprehensive review and discussion the reader may be inferred for instance to this review: [117]. Most importantly the difference between active and passive microrheology has also been emphasized, which gives the basis for detecting active processes in cells.[118]

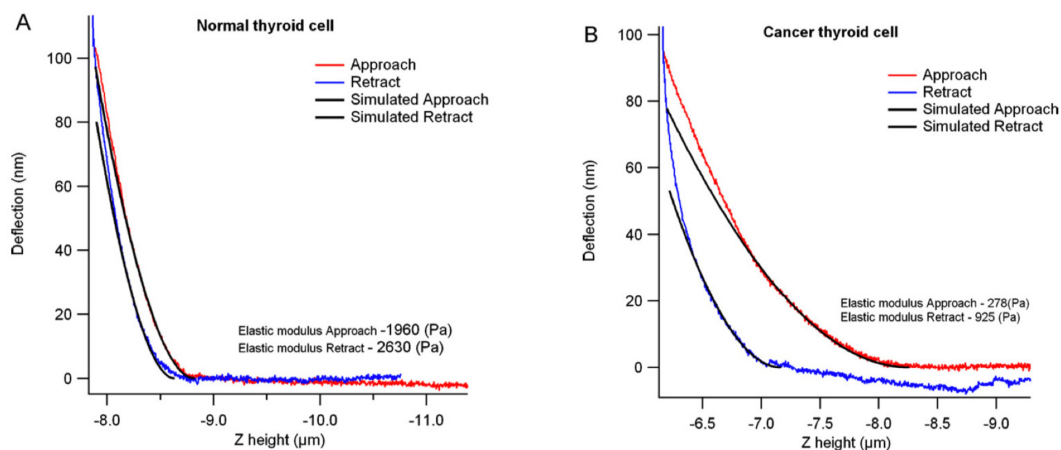


**Figure 9: Comparison force curve of a living cancer thyroid cell sample in an aqueous medium showing the approach and the retracting force curve ramps. (A) Hertz model fit on approaching ramp and retracting ramp of the force curves on a thyroidal cell. For cancer cells (B) a large hysteresis between the two curves could be seen; consequently, thus the spring constants of the cell samples extracted from the mechanical data will be different.[46]**

In a modulating experiment the timescale of the response can be set by the experimental parameters, since the frequency is swept over a given range. This allows seeing multiple relaxation processes, which may then result in power law behaviour of the viscoelastic properties.[119] In creep experiments only the most prominent relaxation process will be visible. However, this may very well be the most relevant time scale or process with which

cells interact with their environment. This confirms the practical need to use creep experiments to complement other possibly more sophisticated methods.

In AFM, usually mechanical data, i.e. force curves, are analysed in terms of the Hertz model [120, 121], which only considers elastic properties of the sample as shown in figure 1 and figure 9. The use of the Hertz model is necessary, since due to the tip geometry (typically pyramidal or spherical tips are used), the contact area between the tip and the sample will increase while loading the cell, and hence the spring constant of the soft samples will be a function of loading force (and tip geometry and sample properties). The Hertz model is widely used when analysing mechanical data of cells by AFM [45]. However, analysing force - indentation data with the Hertz model neglects the contribution of viscous properties of soft samples, which is very important in the case of cells. In force curves, their contribution can be seen by a separation between the approach (loading) and retract (unloading) curve. The difference may also be due to plastic deformation, which does not seem to be an issue in cells, as can be seen by recording several force curves in the same area, which are identical to each other. Thus by applying the Hertz model, we will get different spring constants of the soft samples from the loading and unloading curve, which shall rather be called apparent spring constants of the soft samples. Often only approach data are analysed to achieve comparable data between experiments and groups. In some reports - including one from our group [122] - it has been argued, without a strict and convincing derivation, that the average of the apparent stiffness's of the soft samples, shall be close to their true elastic spring constants, and the difference shall be a measure of the viscous properties. In some reports, the difference between approach and retract curves have been analysed to calculate viscoelastic properties.[119, 122, 123] However, during the approach ramp, the force and indentation are varying at a constantly changing rate, and the response of the live cell is due to the retarded response during the entire approach or retract path, the analysis depends largely on the linearity and homogeneity of the sample. It is essential to compare these data with other data where the force or indentation are changed in a simpler way over a smaller range, where it can be expected that the sample reacts in an approximately linear fashion. An alternative (and scientifically more sound) approach is measuring the stress relaxation after the approach ramp in a force curve [124] or to apply an indirect or direct step in magnet or sample height after the initial creep of the ramp during a force curve has seized respectively.

Modulating the sample position sinusoidally has been used [101, 125] to measure viscoelastic properties of cells as a function of frequency as is done in polymer rheology. A modulating

force can be applied by attaching a small magnetic particle to the very end of the soft spring AFM cantilever. The force in magnet modulates the force on the tip end of the magnetic cantilever, which will transmit a modulating indentation to live cells.[126-128]. In addition the retract curves, adhesion may be present, which will make determination of the contact point difficult and may need to be considered as an offset of the acting curve. However the adhesion, which will be mediated by the extracellular molecules sticking to the tip, it is not clear at which point these molecular bonds are under tension and actually generate a force.

For the leading edge of a migrating cell to advance, protrusion of the membrane must be followed by adhesion to the substratum at the front. The organization of the actin filaments in many types of fully spread tissue-cultured cells has been investigated extensively through the combination of light microscopy and the electron microscopy technique and to my best knowledge, it has been generally accepted that the actin filaments are capable of rapid rearrangement in non-muscle cells both spatially and temporally to the cell requirements. Electron microscopic studies have indicated that bundles of actin filaments may terminate at the plasma membrane in regions where the cell attaches to the underlying substrate or where two cells make contact. As already mentioned, the motile cells possess several mechanisms for exerting force to its immediate environment. In particular a number of mechanochemical enzymes have been identified, including myosin, dynein, and kinesin. A pool of experimental data additionally showed that it was literally possible to follow the actin or microtubules movement along the immobilized kinesin or myosin.[129]

All of these molecules share a common characteristic: they enable the cell to exert, contractile forces. In the same line, it is additionally known from previous works that –and in response to non-conflicting perturbations-, the most influential force in most nucleated cells is widely considered to be the creation of protrusion from the leading edge that seems to be driven by the outward extension of the actin filaments. Force production in the cytoplasm requires an energy source, and in the cytoplasm, this must ultimately be derived from the chemical energy of nucleotide hydrolysis. Most motile cells contain small amounts of contractile bundles that form transiently under specific conditions and are much less well organized than muscle fibers. Interestingly, repeated dendritic nucleation generates branched arrays of filaments as found on the leading edge of most cultured mobile cells. The dendritic nucleation model was originally proposed in 1998 to explain the formation of branched actin networks nucleated by actin-related protein 2/3 complexes in motile cells.[130] The model was later improved to include force generation and monomer recycling in the actin network.[87, 131] In response to stimulus, actin in motile cells typically manifests an interesting cycle of assembly and

disassembly in which it polymerizes near the end of the cell or edge of the cell and depolymerizes further away from the cell edge and an actin wave is a spatially segregated assembly and disassembly cycle.[88, 132-134] Non-muscle contractile bundles are regulated by myosin phosphorylation rather than the troponin mechanism.[135] To my best knowledge, the contractile bundles in the non-muscle cells function has been described by many other works principally to provide the mechanical support, for example, by assembling into cortical stress fibers that connect the cell to its extracellular matrix through the focal adhesions or by forming a circumferential belt in an epithelial cell, connecting it to adjacent cells through adherents junctions.[136] In the skeletal muscle sarcomere actin filaments attach to the Z-line and emerge from either sides with opposing polarities. Following the discovery of conventional muscle myosin; subsequent sequencing showed that it was indeed a myosin-related protein.[137, 138] Kinesin proteins share very similar structural features with myosin in their head domain and are therefore thought to have branched from a common ancestor with myosin, but diverge in their tail structures.[139] Members of the kinesin-13 family are unconventional, in that they can possessively induce microtubule depolymerisation, a process that is essential to chromosome segregation during mitosis.[140] Dynein proteins are less well characterized. Myosin was classified based on its actin-activated ATPase activity from earlier works on the freshwater *Acanthamoeba*. [141] The organization of filaments in vertebrates' skeletal muscle as a well-studied example is highly uniform and rigidly maintained to carry out its functions. The class II myosin found in muscle are by far the most characterized members of the myosin superfamily, but recent comparative studies across classes have provided new insights into myosin's molecular structure and function. Interestingly, the roles of actin, myosin and associated proteins in muscle have since served as a models for certain types of movement in organism because the changes in the intrinsic protein of myosin played a central role in signalling conformational states of myosin and linking these to its catalytic events. Since 1954,[142] the motor that produced filament sliding, the myosin head had been observed both by electron microscopy and X-Ray diffraction. Kinetic studies had shown that ATP dissociated actin from the myosin was detached from actin to four state model of the kinetics of the actin myosin interaction. The cross-bridge model for muscle contraction proposes that the myosin cross-bridge binds to the actin element in an initial conformation and then undergoes a change of state, which moves the actin element past the myosin element. This elemental event, which is part of a cycle driven by ATP hydrolysis, is known as the 'power stroke'. Each stroke of the cross-bridge leads to the hydrolysis of one ATP molecule. The cross-bridges were first studied over five decades ago[143] and a quantitative cross-

bridge theory of muscle contraction with coupled ATP hydrolysis was proposed by A. F. Huxley. Muscle contraction typically depends on two processes that consume enormous amounts of ATP: filament sliding, driven by the ATPase of the myosin motor domain, and calcium ion pumping, driven by the calcium ion pump. For such a highly uniform and rigidly maintained structure, cations that will typically associate with actin-bound nucleotide like magnesium or calcium may also affect the rate polymerization. Evidence has shown that tightly bound cations like magnesium and calcium is bound to ATP with the dissociation constant in the nano-molar range [144], but according to other works the polymerization rates of magnesium actin cations seem to be faster than those of calcium actin cations. [144-146].

Most motile cells navigate to the damaged site by sensing the local chemical cues, which are irregular, conflicting and change over time and space. The structures differ primarily in the way in which the actin is organized by actin-cross-linking proteins. Because of the arrowhead pattern observed when myosin decorates the actin filaments intrinsically, the fast-growing end of the polarised polymer is denoted the barbed end and the slow-growing end is denoted pointed end. This inherent polarity is thought by many other works to drive membrane protrusion on non-muscle cells. However, the organization of the filaments to my best knowledge depends on the type of protrusion. The actin filaments extend when ATP-actin monomers are preferentially incorporated at the barbed end. As the filament matures, ATP bound in the central subunit of actin is hydrolysed, phosphate is released and the resulting ADP-actin filament is disassembled by loss of monomers from the pointed end. The released ADP-actin monomers then undergo nucleotide exchange to generate ATP-actin monomers that can be used for new cycles of polymerisation. Interestingly, a subset of actin-binding proteins is capable of directly sensing the nucleotide state of either globular or the filamentous-actin.[147] As prominent example, actin-binding proteins of the ADF/cofilin family because of their apparent ability to efficiently bind and sever the filamentous-actin (without capping) preferably in the ADP-bound state to promote actin turnover, but bind only with weaker affinity to young actin filaments that harbours ATP or ADP-P<sub>i</sub> in their active site[148, 149] Pollard and Mooseker [150] estimated the rates of assembly and disassembly at each end and they have shown that there is preferred assembly in the barbed end while preferential disassembly occurs in the pointed end. This cyclic process is regulated *in vivo* by a variety of actin-binding proteins that control the kinetics of actin turnover.[151, 152] For instance, globular- actin probably does not exist at significant concentrations as the un-complexed monomer *in vivo*; instead it is essentially always bounded to actin binding proteins (ABPs) such as profilin to prevent uncontrolled nucleation event.[153] In response to an

external signal as a consequence manifest as difference in the assembly rates at the two ends the actin monomers may flux fast through the barbed end to the pointed end.[132] Actin networks involved in dynamic processes such as membrane protrusion assemble and disassemble at rapid time scale. It is known that steps of cell motility and migration may typically express the large family of myosin, the dyneins or the kinesin are actin/microtubule-dependent molecular motors proteins, which have diverse structures and functions like movement and force production in the cell through the hydrolysis of ATP. To my best knowledge, model systems typically used by investigators might differ significantly in terms of both the rate and the persistence of the protrusion. A well-studied model system in the literature is the leading edges of fibroblast cells and that of the amphibian keratocytes.[154-156] As the keratocyte migrates, the lamellipodial network turns over and the components must be transported in the migration direction. The initial hypothesis regarding the mechanism of this turnover and transport was simple: long actin filaments span the lamellipodium and treadmill, with their barbed ends growing at the front, pointed ends shortening at the rear, and actin monomers diffusing from the rear to the front. It is known by many groups that cancer cells may typically adopt morphologies that have been characterized by temporal dominance of particular Rho GTPases. For example activation of cdc42 results in appearance of filopodia, while activation of RhoA induces robust stress fibres and some cases cell spreading. The dynamic assembly and disassembly of filaments and the formation of larger scale filament structures are crucial aspects of actin's function, and are therefore under scrupulous control by over a hundred actin-binding proteins. The coordinated actions of specific subsets of actin-binding proteins regulate the dynamics of distinct arrays of actin filaments at specific times and places within the cancer cell. In many other systems, adhering the cells naturally progresses through several other phenotypes; for example filopodia, lamellipodi and cell spreading controlled by the GTPases cdc42, Rac and Rho, respectively. In cell migration, spatially regulated contractility is typically utilized both in the symmetry breaking and tail retraction. To my best knowledge the keratocytes do not possess filopodia or the stress fibres. In the early nineties, the graded radial extension hypothesis integrated experimental data into a mathematical model that explained the wide, smooth and sloping shape of the leading edge as follows: the protrusion rate at the front of the growing actin network is graded – it is maximal at the center of the leading edge, and gradually decreases towards the sides. For the most studied samples under the light and electron microscopy undergoes rapid constitutive motility and assembles a large extremely thin leading edge. The fibroblast exhibit slow ( $> 1\mu\text{m}/\text{min}$ ) and intermittent movements whereas the keratocytes

exhibit rapid movement ( $> 10\mu\text{m}/\text{min}$ ). The diverse morphogenic changes live cells typically requires large shape changes which may last over seconds to hours. Smilenov et al.,[157] recently suggested the existence of a molecular clutch that couples the traction and to the contractile forces by demonstrating that the focal adhesions are highly motile in immobile live fibroblast cells yet stationary in migrating fibroblast variants. The typical ATP-hydrolysis driven, directional filament growth called actin treadmilling. Tseng Y. et. al., (2004) [158] were able to demonstrate that the actin related proteins 2/3 (Arp2 and Arp3) complex (220kDa) plays the role, in promoting the rapid formation of homogeneous and stiff networks by using real time particles embedded in F-actin networks.[158] When activated its own actin-like subunits, the Arp 2 and Arp 3, typically serves as templates for monomer addition by mimicking the barbed end of a growing polymer.[159, 160] In motile healthy and diseased cells, the actin filaments functions as the force-generating polymer motors, structural scaffolds and tracks for motor proteins. Actin filaments are linked via interactions into a network forming „Y-shaped“ branches, with the pointed end of each filament attached to the side of another mother filament that augment its' nucleation activity with the rapidly growing barbed end facing forward.[131] In previous studies of most mobile cells, which were as well rich in actin, the relative control of actin assembly is essential for motility and rapid changes in the live and diseased cell shape.[133, 161] Different structures are initiated by the action of distinct nucleating proteins: the actin filaments of dendritic networks are nucleated by the Arp 2/3 complex, using this model it was thought by many works in literature to produce forces that drives protrusion structures.[158, 162-165] These bundles are made of the long, parallel filaments produced typically by formins.[158, 163, 166, 167] Although the critical concentration seems to be the minimum concentration for filament formation in vivo, rather than just a simple equilibrium description, on one hand the elongation and the ATP hydrolysis may typically manifest in the dynamics. On the other hand, the formins have additionally been shown in other works to dimerize and to form a structure that acts likes like a barbed end filament cap to stabilize the formation of an adjacent structure, thus nucleate non-branching actin filaments and may typically contribute to lamellopodium or the filopodium formation. The structural organization of different actin networks depends on specialized accessory proteins. According to the models, described in other works the Arp 2/3 nucleates actin polymerization and organizes filaments into a dendritic network by linking the filament minus ends to the side of other filaments. As mentioned previously, it is known that the Arp2/3 complex interacts with the side filaments. In most motile cells, the highest concentration of the contractile element in the actin network seems to be within the lamella hence it has the

capability of pulling against points of adhesion to the substrate. Although the actomyosin-based mechanism of force generation is important it seems not be essential motility of the amoeba.[168] According to authors, the changes might be due to either movement of the whole actin filaments from one place in the cell to another or due to the disassembly of the filaments in one place and assembly in the other. The time scale of these changes is probably too fast to allow for diffusion of actin filaments because by fluorescence after photobleaching actin filaments in live cells and at high concentrations in vitro is to my knowledge, immobile. Alternatively if the cell is stationary, like disc shape sea urchin, the actin filaments assemble at the margin of the cell and move away from the edge reflecting the same relationship of the cell surface as in locomotion. The gram-negative pathogenic bacteria, like *Listeria*, and *Rickettsia* move intracellularly by polymerizing a comet tail of cross-linked actin filaments that propels them fast through their surrounding hosts cytoplasm[167] and to my best knowledge typical amoeboid motility vivo may not require integrin nor other molecular interaction with the extracellular matrix (ECM) [169] but may typically rely on the continuous physical interaction with the environment and the friction mechanism with its environment.[170] Here the properties of the host organism that depend on the spatio-temporal scale comes into play, \_while the velocity of the *Listeria* bacteria (of up to about  $1 \mu\text{m}/\text{s}$ ) in a homogenous environment are typically constant, some mutants progress in a solitary manner. This observation has been later reproduced in vitro motility assays using latex beads coated with bacterium membrane protein, (actin assembly-inducing protein) ActA or directly with viral capsid antigen (VCA) proteins. Additionally, understanding of such actin based propulsion mechanism has been augmented by the molecular and mesoscopic, continuum models. Furthermore, the properties of the actin gels and the *Listeria* propulsion has been studied experimentally with soft samples like endosomes, oil droplets, and liposomes. They show that the actin gel squeezes the object, compressing its sides and pulling its rear, a typical effect that gives a “pear-like” shape. The direct observation that actin comet during its growth on coated beads has shown the actin gel constantly undergoes typical deformation that depend on the protein composition of the motility medium. As a function of bead size and the concentration of crosslinkers or the regulatory proteins, the bead velocity can be limited either via the diffusion of the monomers to the coated surface, the polymerization velocity at the surface of the bead, or by the elastic stress built up in the gel. According to literatures, cancer cell migration and invasion into adjacent tissues and intravasation into blood or the lymphatic vessels are required for metastasis of adenocarcinomas, the most common human cancers.[171, 172] The invasive cells acquire

migratory phenotype that seems to be associated with the increase in the expression of several genes involved in cell motility. This in turn allows the carcinomas to respond to cues from the microenvironment that trigger tumour invasion.[173, 174] Diseased cell migration in primary tumours can be directly observed by multi-photon microscopy with animals carrying green fluorescent protein (GFP)-labelled tumours.[175][7] In the case of breast tumours, most of the migrating cells are solitary with an amoeboid morphology [176, 177][9]. These diseased cells have been observed moving linearly in association with the extracellular matrix (ECM) fibers. Given that some of the extracellular matrix fibers converge onto blood vessels, these fibers may as well function as a path for carcinoma cells to migrate toward blood vessels. In many other works, in which analyzing the migratory behaviour of soft diseased cells like cancer cells have demonstrated the architectural organization of different actin-rich structures (dense array of actin filaments) and molecules within, depending on the environment in which they were grown. For instance, in an environment that promotes sufficient mechanical contacts and loosely organized extracellular matrix (ECM) will encourage an amoeboid-type migration where cells adopt a characteristic polarized rounded shape. This property of cell migration, which relies on the continuous formation of dynamic cellular membrane protrusions, results in rapid locomotion has been typically observed in white blood cells like the leukocyte cells[178] but has also been observed in diseased cells.[179] However, of particular relevance is the distinct polarity, which may not only cause the myosin heads to interact with the filaments at a preferred angle but also account for the different rate of assembly between the ends of the filaments.[180-182] Branching typically occurs during nucleation by Arp 2/3 activated by the Wiskott Aldrich syndrome protein (WASP) or Scar protein[183]; capping protein and profilin act synergistically with Arp2/3 complex to favour branched nucleation and these branches created by Arp2/3 complex are relatively rigid.[184-187] The growing filaments push the plasma membrane forward until they are capped. The filaments then ages automatically by the hydrolysis of bound ATP and the dissociation of inorganic phosphate. The ADF/cofilin accelerate, the rate limiting step. After the phosphate release the branches dissociate from the Arp2/3 complex and the mother filaments and becomes targets for severing and depolymerization. Perksins et al.,[188] formulated a theory that accounts for the force generated by polymerization process it self when the filaments are rigid. They proposed that the addition of subunits to the end of the growing filaments rectified the Brownian motion of any diffusing object inform of the filament and showed that this ratcheting of the diffusive motion could generate sufficient force to account for a number of motile phenomena. Pushing of the load, the actual protrusive event is thought not only to occur by the elongation

of actin filaments but probably by an elastic Brownian ratchet mechanism.[189] In this model, the Brownian motion creates a sufficient gap, and so that the diffusion is biased forward. This physical model allows calculation of the velocity at which the load can be pushed at a polymerizing filament. This model predicted that the loading velocity should depend on its diffusion coefficient, and thereby on its size. If the load is immobile, the filament will not grow and no force will be generated. For a ratchet of this sort operating at optimum efficiency, the amount of force generated is limited only by the free released by the polymerizing reaction; a single actin filament is predicted to be capable of generating a force. As an improvement to the former model, the elastic Brownian ratchet mechanism was proposed by Mogilner et. al., 1996 [190], in which the thermal energy bends the semi-stiff filaments, storing elastic energy. Unbending of an elongated filament against the leading edge would then provide the driving force for protrusion. To my best knowledge, most actin filaments barbed end are not freely available in most cells and are likely blocked from elongation by the barbed end binding proteins, capping proteins. For instance, it is known that the capping protein and profilin have been proposed to maintain a pool of actin/profilin that is able to elongate free barbed ends but not pointed ends [191]. Profilin is also known to inhibit spontaneous actin nucleation more strongly than nucleation by Arp2/3 complex. The capping protein also terminates the elongation of barbed ends [192] and efficiently nucleates actin filaments that grow in the pointed end direction. Filopodia protrusion on healthy live cells has been thought of to occur by filament treadmilling. The peripheral network of most motile cells typically manifest as rapidly moving, morphologically dynamic, cycling structure that is largely unconnected to the substrate and poorly coupled to actin network within the body of the cell. The long unbranched filament organisation seems to be consistent with assembly occurring by elongation rather than nucleation. The basic molecular structure of the lamellipodia and the filopodia provides them with the capacity to perform distinct cellular functions. Biophysical experiments additionally suggest that the dendritic organization of lamellipodia may provide a tight brush-like structure that is able to push along a broad length of plasma membrane. Through localized activation of the Arp2/3 complex, the lamellipodium could be induced to grow in a particular direction, providing a basis for directional migration. In contrast, filopodia, owing to the parallel bundle organization in its cellular network, are in addition particularly well designed to serve as sensors and to explore the local environment, although they seem not to be essential for chemotaxis.

The viscosity of soft samples usually easily shows detectable relaxation phenomena following the perturbation of most motile cells. The viscosity mapping in biological systems is

important for the understanding of the internal biophysical processes. In the past few years several scientific works have aimed to quantify this soft sample property by applying fluorescence imaging techniques, like the fluorescence recovery after photobleaching [193] [194], because by tuning the fluorescent properties of the employed probes, one achieves a high spatiotemporal resolution. However, the introduction of the fluorescent probes, in consequence, seems to interfere with the intrinsic properties of proteins or the amino acids. On the contrary, there are very little direct experimental results on creep response. The magnetic force AFM is a powerful setup that can be used to measure the creep response of the soft samples like the cell. The AFM has the advantage in that the viscous response of the bulk sample can be quantified without the addition of fluorescent probes. Although the AFM which employs a sharp tip has very successfully been employed for analysis of cellular elasticity, the broad range of absolute elastic moduli reported for living cells under same conditions in the literature (100 Pa–100 kPa) is intriguing [195] [196]. The degree of quantitative information that can currently be extracted from the conventional force curve analysis of such ultra soft samples like the cell is still limited and also very challenging. As shown in the recent work of Rianna et. al., in 2016 [48], the properties of the extracellular matrix like the stiffness modulates the viscoelastic properties of the live and the diseased cells. The AFM has been employed to obtain this type of information from ultra-soft samples as well as about the apparent elastic constants. However, it is interesting that the life and the diseased cells will exhibit a sharp change in the viscoelastic properties in response to the varying stiffness of the mechanical environment. Their rationale, which was based on applying an indirect force step by AFM on the diseased and the normal cell types and have reported a change in the storage modulus of the healthy cells from 1.2 to 2.7 kPa and the loss modulus of 300 to 735 Pa s while tuning the stiffness of the polymer gel substrate on which the cells are placed stiffness to higher values respectively. The diseased cells, on the other hand, showed a storage modulus of 1.4 kPa and a loss modulus of 400 Pas, which were virtually independent of the polymer gel substrate stiffness. However, their findings showed the usefulness of the setup in measuring the viscoelastic properties of the normal and diseased cell samples. In contrast, intervening measurement methods such as the bead-tracking microrheology or the micropipette aspiration give values of 100–500 Pa for elasticity.[112] [110] The differences have been ascribed to cell substructure heterogeneity, the viscous properties and the far greater spatial accuracy of AFM measurements.[195] [110] On the other hand, adherent cells have been demonstrated to change their shape from round to fully spread without significantly altering their microfilament mass.

It is known in by many other scientist that normal live cell types may tune their mechanical properties to the stiffness (spring constant) of the underlying substrates [197], however to my best knowledge similar works in which the creep responses are directly quantified after the magnetic step FM have not been performed till date. It is important to carefully measure the viscous response and the elastic properties of live cells in response to the deformation achieved under different force steps and experimental conditions in order to compare the results. The main issue with such novel experimental setups, however, lies in the fact that it is challenging to directly measure the viscous contribution of the soft samples accurately on soft samples. The rheological properties are the key features of living cells [198] and have been also characterized in a few works by obtaining time-dependent measurements for small loading forces in their natural environment. [199]

The relative contributions of the actin polymerisation-depolymerisation dynamics and tensile prestress to the live cells shape and stability are controversial.[199] It has been proven in several studies that cancer cells on such supports are at least one order of magnitude softer than normal cells, because of their different cytoskeleton structure and organization [200], however creep response measurements on the live cells response on the stiff petri dishes with an alternative setup is still missing in literature. This indicates the practical relevance that viscoelastic properties of live cells and tissues need to be quantified directly by a more appropriate experimental setup even though in their natural environment the substrate stiffness may additionally tune the live cells samples mechanical properties.[199] Proper use of the AFM setup with novel methods allows mechanical probing of the soft samples without significant influence of the underlying substrate. There is the need for setups capable of addressing the rheology of the living cells without disrupting the cytoskeletons underneath the cell. [201] [100] [202] [48]

In indirect loading setup such as the conventional AFM, the mechanical data are analysed in a quasi-static manner. The dynamic response from analysis of the force curves and contact mechanics is encircled with a number of challenges especially when characterizing the viscoelastic properties as has been discussed before. This is because a force balance in the conventional way of obtaining the mechanical data implies that a substantially slow measurement has to be performed. It thus seems to suffer from the low-frequency noise, or the drift in the system, hence only one frequency can be employed at a time, and it is generally too slow to probe the cell mechanics. When mechanical measurements are performed rapidly, the viscous contribution of the soft samples associated with the motion of

the soft spring AFM cantilever becomes significant. Viscoelasticity of the soft samples like the cell may also lead to the frequency-dependent response of the soft spring AFM cantilever. This is because, besides their solid-like property, they show fluid-like properties and will have the ability to flow giving rise to entropic forces, capillary forces associated with the surface curvature, and the viscous forces that depend on the mechanical system.

### 1.5 Motivation and summary of critical issues

To the best of my knowledge the determination of the spring constants of the soft spring AFM cantilevers has been a major issue to nano- and biomechanics researchers whose goals have typically been to measure forces down to about ten pN on many structured samples or even some complex soft samples. Micrometer-sized AFM cantilevers, for example, are present in many applications, ranging from chemical to biological sensors and have typically been employed for the diagnosis of broad range of diseased cells [203] and even in glucose monitoring from unhealthy patients.[204] The advantages include the high sensitivity, the quick response and the low power requirement.[205] Moreover the AFM techniques are commonly employed in microbiology for their advantage over electron microscopy when measuring living cells. Although one of the most important applications of the AFM force–distance curves is the study of the mechanical properties of the soft samples[54], the extent to which the loading force deforms the sample will depend on the soft sample viscoelasticity including the AFM tip resolution.[11] In the same line, very significant to most AFMs is the employed soft spring AFM cantilever response. In response to the substrate, the soft spring AFM cantilever may deform when in contact with the, or in the proximity to the soft sample being measured. The measured force in an AFM is simply by multiplying the known cantilever spring constant of the AFM cantilever with the measured deflection ( $\Delta d$ ). In fact, because the manufacturer’s nominal values of spring constants deviations from the nominal values often span over a factor of 3 in error in recent years, there have been for many years now –to my best knowledge- controversies around the need for independent, more precise and accurate methods for calibrating the spring constants of the soft spring AFM cantilever. A variety of these methods have been proposed on other works to calibrate the spring constant of the soft spring AFM cantilever, which have spring constants in the range 0.01 to 1 N/m and among them the thermal noise method is the most preferred by the researchers. More recently, researchers have been using the thermal calibration technique developed for laser Doppler vibrometry (LDV) to calibrate both the torsional and the flexural spring constant of the soft spring cantilever. By direct comparison of their obtained results with commercial referenced

cantilevers using the LDV thermal and the electromagnetic force balance, an agreement of up to 2% or slightly better was demonstrated.[206] By using reference cantilevers with spring constants of the cantilevers determined from the instrumented and the calibrated nanoindenters Grutzyk et al., [207] recently described a method to calibrate stiffer cantilevers (in the range 200 to 250 N/m), which has been based on International traceable chain. Furthermore, the majority of these methods to calibrate the spring constants of the cantilever adapt the soft spring cantilevers to a holder for force balance and the change in the deflection due the cantilevers of a known spring constant by a technique originally proposed by Tortonese et. al., [208], or by the measurements of change in the deflection due to the viscosity of the aqueous medium surrounding the cantilever. This results in a decrease in resonance frequency and to a widening of the resonance peak due to the viscosity of the medium that makes it harder to record good thermal spectra in water.[209, 210] The AFM force distance (deflection displacement) curves have been used for the studies of numerous material properties and for the characterization of surfaces.[20] For different purposes of different results it might be useful to actuate the tip of the soft spring cantilever directly by an external means or the piezo actuator by AFM. When obtaining force curves in the contact mode, lateral forces may act on the tip due to frictional forces in the system [211], although the lateral spring constants for triangular shaped cantilevers has been questioned before.[212] Other recent works explore and measure synchronously in an SI traceable way the influence of AFM cantilevers undergoing torsional bending, which is associated to the torsional spring constants of the employed soft spring cantilever using the electromagnetic balance and the optical lever system.[211] This challenging scenario has led to efforts to standardize conditions and isolate critical variables or values with the hope that unambiguous results not only will demonstrate the existence of the minute changes in spring constants of the soft sample but also will permit the analysis of the underlying mechanisms in cell mechanics. However, the previous studies of the deflection sensitivity are mainly focused on measuring the vibrational or resonance characteristics and using these characteristics to determine the spring constant of the soft spring cantilevers through the mechanical or the thermodynamic relations.[206] [21] In fact, the calibration uncertainties of currently used techniques to the best of my knowledge are still relatively high, e.g., ranging from 10% to 30 % especially for cases where the spring constant of the reference cantilever employed are not guaranteed as compared to the manufacturers prescribed spring constant values.[27] [213]

While scanning, the heterogeneous structures on the soft sample may deflect the tip and thus the soft spring cantilever such that the vertical displacements are recorded. Its vertical

movement is relevant because it allows for simultaneous mapping of the material mechanical properties locally with high spatial resolution and at different positions of the cell. If the position sensitive detector monitors the slow response to the local deformation, analysis of the creep response to the local deformation by a more suitable procedure, the soft sample data will ease repeatability and will not be very prone to inter experiment inconsistencies. Indeed, as a complimentary technique, this will render my novel magnetic AFM setup very suitable for deriving the quantitative measures like the viscous response values and the true elastic properties of the soft sample like live and diseased cells.[9]

Additional motivations for our work were to minimize potential errors, which are z-height scanner and soft spring cantilever-related, that might arise during the force curve measurements by AFM. Consequently, this work aims to offer a possible solution for these problems and to perform or directly measure and quantify the viscoelastic creep response of the soft samples like live cells adhered on substrates with large spring constants by magnetic AFM. This is because the soft samples like cells are capable of storing and dissipating applied mechanical energy through an internal friction mechanism in a way that, to the best of my knowledge, may strongly depend on the rate of the indentation. When measuring the mechanical properties of these soft materials it is important to quantify both the true elastic and true viscous properties.[100] As mentioned earlier, despite the many detailed previous works, the measurements of the mechanical properties on the cell mechanics (live diseased cells) and the polymer gels have not been adequately quantified by AFM. We expect the magnetic force AFM based experiments to play an important role, like choosing the favourable experimental conditions; with newer experimental setups to directly probe live cell samples. Most importantly, it will aid or provides future experimenters to draw more objective conclusions about the cell mechanics of the diseased cells, like cancer cells. Additionally, it should be noted that the initial reports have not systematically analyse the obtained mechanical data with the help of an adequate model for the sample response. Hence, to make more quantitative judgements and conclusions about the live cell sample's viscoelastic properties, new analysis tools/models, highly sensitive setups like the novel magnetic step response AFM setup are required, in which the true spring constants of the soft samples will be directly determined. We modelled a magnetic force setup with the goal of quantifying the spring constants and the viscous coefficient of friction (friction coefficient) of soft samples like cells and polymer gel (gel) samples by AFM. The degree of accuracy of the true elastic properties could be linked to the viscous response of the soft samples from the

measurements at a most probably characteristic time scale imposed by the experimental conditions.

In this work, we propose a setup for applying large controlled external magnetic fields in magnet on force transducers by Atomic Force Microscopy. The viscoelastic creep response of soft gel and cell samples after applying a step in loading and the unloading force by means of magnetic fields has been directly measured by AFM. A second setup has been presented in which the loading and the unloading force is applied indirectly by changing the z height of the AFM. The work is based on understanding of AFM setups, and benefit for more efficient operations and advance applications. Our interest targets quantitative measurements of nanoscale viscoelastic properties by AFM, which can be applied to related practices in the study of soft samples. Efforts are shown to improve the quantitative capabilities of this technique. We expect our results to have broad applications to characterize mechanical properties of soft, biological samples under near-physiological aqueous environment and the accurate force measurements using z step response and the magnetic response AFM respectively.

### **1.5.1 Theoretical fundamentals and an experimental approach**

Magnetic AFM cantilevers (soft springs) was an important and a necessary tool because we wished to apply force to the soft samples. In order to access the effects by which the environment will have on the motion of the soft spring AFM cantilever, I have considered two general cases. When the soft spring AFM cantilever is in (in contact) and not (off/no contact) in contact with the soft sample like the life cells and gels. The figure 10 shows the soft spring AFM cantilever oscillating off and in contact with the sample, with amplitudes of  $A_0$  and  $A_1$ , respectively. The figure also portrays schematically the diagram of the simplified AFM cantilever spring-dashpot model for the cases of a non-contact and the contact measurement typical for my magnetic AFM implementations carried out in an aqueous environment.

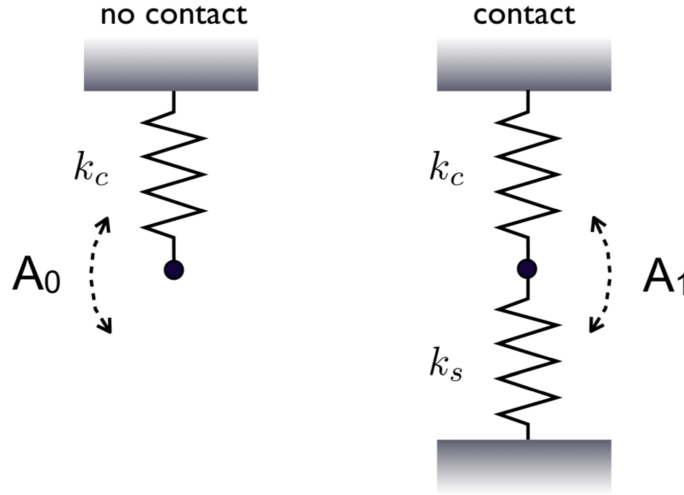


**Figure 10** Association of the springs to determine the spring constants of the soft sample in terms of the spring constant of the cantilever and the oscillation amplitudes i) no contact  $A_0$  and 2) in contact  $A_1$

In the case where the vibrated soft spring AFM cantilever is not in contact with the system has resonance frequency that is related to the soft spring AFM cantilever as  $m_0\omega_0^2 = k_c$ . The soft spring AFM cantilever may be described as a damped harmonic oscillator with effective mass  $m_0$ . When in contact both the systems' effective mass and the resonant frequency changes, such that  $m_1\omega_1^2 = k_c + k_s$ . To be specific  $k_c$  is the spring constant of the soft spring cantilever while  $k_s$  is the spring constant of the employed soft sample. In both cases the motion of the soft spring AFM cantilever and the reaction of the soft spring AFM cantilever to an external force field can be described within a good approximation by a damped and a driven harmonic oscillator. The equation of motion of the free cantilever is:

$$F_{total}^{(free)} = F_{drive} + F_k + F_{viscous} \quad (1.10)$$

Is the oscillating magnetic force,  $F_k$  is the restoration force due to the deflected soft spring AFM cantilever, which can be described by Hooke's law  $F_k = k_c(z - \bar{z})$ , (where  $z$  is the cantilever deflection and  $\bar{z}$  is the equilibrium soft spring AFM cantilever deflection), and  $F_{viscous}$  represents the viscous force due the hydrodynamic interaction of the soft spring AFM cantilever in liquid. The equation for the free cantilever is (assuming,  $\bar{z} = 0$ ):

$$m_0 \frac{d^2z(t)}{dt^2} = F_{drive} - k_c z_0(t) - \eta_0 \frac{dz_0(t)}{dt} \quad (1.11)$$

Where  $m_0$  is the effective mass of the soft spring AFM cantilever,  $k_c$  is the spring constant of the AFM cantilever,  $z_0(t)$  is the free cantilever deflection,  $z_0$  is the free equilibrium deflection. The viscous force was written in the form:

$$F_{viscous} = \eta_0 \frac{dz_0(t)}{dt} \quad (1.12)$$

The resultant force on the magnetic soft spring AFM cantilever magnetic cantilever in contact with a viscoelastic sample and exposed to an oscillating magnetic field will be given by:

$$F_{total}^{(contact)} = F_{drive} + F_{contact} + F_k + F_{viscous}^\dagger \quad (1.13)$$

Therefore, the effective equation of motion of the soft spring AFM cantilever in contact  $z_1(t)$  is given by:

$$m_1 \frac{d^2 z_1(t)}{dt^2} + \eta_1 \frac{dz_1(t)}{dt} + k_c z_1(t) = F_{drive} + F_{contact} \quad (1.14)$$

The surrounding medium and the sample typically exerts a force  $F_{viscous}^\dagger$  when the soft spring AFM cantilever is contact with the soft sample, which is proportional to the velocity given by.

$$\frac{dz_1(t)}{dt} \quad (1.15)$$

The differential equation to be solved for the non-contact scenario will be described by:

$$\frac{d^2 z(t)}{dt^2} + b_0 m_0 \frac{dz_0(t)}{dt} + \omega_0^2 m_0 z_0(t) = F_{drive} \quad (1.16)$$

While the soft spring AFM cantilever is in contact, the scenario can be described in two ways:

1) In the first case we explicitly add the contact force to the resultant force acting in the soft spring AFM cantilever, which be subsequently be labelled CM1.

$$m_0 \frac{d^2 z_0(t)}{dt^2} + b_1 m_0 \frac{dz_0(t)}{dt} + \omega_0^2 m_0 z_0(t) = F_{drive} + F_{contact} \quad (1.17)$$

Where the proportionality coefficient typically written in the non-contact case as  $b_0$  and  $b_1$  for the contact case is the damping coefficient. Again, the viscous force of the contact case is written as:

$$F_{viscous}^\dagger = \eta_1 \frac{dz_1(t)}{dt} \quad (1.18)$$

Here  $\eta_1$  is the effective hydrodynamic viscous coefficient of the liquid + viscoelastic sample when in contact with the soft sample.

2) Alternatively, we can write the effective model equation such that contact is described by a change in the effective soft spring AFM cantilever mass  $m_1$  or resonant frequency  $\omega_1$  of the system. This will be subsequently labelled as CM2.

$$m_1 \frac{d^2 z_1(t)}{dt^2} + b_1 m_1 \frac{dz_1(t)}{dt} + \omega_1^2 m_1 z_1(t) = F_{drive} \quad (1.19)$$

In this equation  $z_0(t)$  denotes the soft spring AFM cantilever motion being off or  $z_1(t)$  in contact with the sample.  $F_{drive} = F_B e^{-i\omega t}$  is the driving magnetic force acting on the cantilever (magnetic) and  $F_{contact}$  represents the force between the soft spring AFM cantilever and the employed soft sample.  $F_B$  is a parameter that depends on the magnetic dipole moment of the coil and the magnetic cantilever, and the distance between the magnetic soft spring AFM cantilever and the coil. As it has been previously described,  $b = \eta/m$  or better written  $b_n = \eta_n/m_n$  is the damping coefficients of the viscous force due to either liquid (off contact regime) and liquid + sample (in contact regime). In steady state, these equations have solution of the type

$$z_n(t) = A_n \exp i(\omega t + \phi_n) + \check{z}_n \quad (1.20)$$

where  $\omega$  is the angular frequency of the AC (alternating current).  $\phi_n$  is the phase shift due to viscous forces.  $\check{z}_n$  is the equilibrium cantilever deflection. The phase shift  $\phi = \phi - \phi_0$  is due to the sample viscoelasticity. By solving the solution  $z_0(t)$  we obtain the following expression for the amplitude of vibration  $A_0$  as function of frequency. The evolution is characterized by a response function of the form

$$A_0 = \frac{F_B}{k_c} \frac{1}{(1 - (\omega/\omega_0)^2) + i(b_0 \omega/\omega_0^2)} \quad (1.21)$$

When the tip approaches the surface, the sample forces may modify the vibration. The contact (surface) forces ( $F[Z+z(t)]$ ) has to be added where,  $Z$  is the distance between the surface and the mean position of the AFM cantilever tip and  $z(t)$  is vibration around this mean position.  $F'_{contact}$  is the derivative of the contact force between the soft spring AFM cantilever and the sample.  $F_{contact}$  has two components: 1) the contribution due to z-step displacement that brings the cantilever into contact  $F_{contact}(\delta_0)$  and causes an indentation  $\delta_0$ . This quantity is

typically estimated as  $F_{contact}(\delta_0) = k_c d_{trigger}/2$ , where  $d_{trigger}$  is the maximum cantilever deflection of the force curve taken before a dynamic measurement. 2) The other force component is due to the oscillation contribution due to the magnetic field  $F_{drive}$ . For the typical modulation experiments the contact force will oscillate around  $F_{contact}(\delta_0)$ . We can expand in a Taylor series to determine the effective modulation of the contact force due to the magnetic field. The solution for the contact and the non-contact cases in the contact mechanics 1 (CM1) and the contact mechanics 2 (CM2) approaches are, respectively

$$A_1^{(CM1)} = \frac{F_B}{k_c} \frac{1}{[1 + (F'_{contact} \delta_0/k_c) - (\omega/\omega_1)^2] + i(b_1\omega/\omega_0^2)} \quad (1.22)$$

$$A_1^{(CM2)} = \frac{F_B}{k_c + k_s} \frac{1}{[1 - (\omega/\omega_1)^2] + i(b_1\omega/\omega_1^2)} \quad (1.23)$$

Where  $b_1 = \eta_1/m$  and  $\omega_1^2 = [\omega_0^2 + F'_{contact}(\delta)/m_0] = \omega_0^2[1 + F'_{contact}(\delta)/k_c]$ . This equation states the contact of the soft spring AFM cantilever with the viscoelastic surface induces a small change of resonance frequency. At a given distance from the surface, there is a resonance at a frequency lower than far away from the surface. The shift of the resonance frequency is directly related to the force gradient. At constant applied frequency, the observed shift in resonance curve results in a decrease of the amplitude of the vibration whose measurement of the spring constants of the sample it self directly.

### 1.5.2 Magnetic properties, force and the choice of magnetic particles

Magnetic AFM cantilevers (soft springs) were employed in this work to apply force to the required soft samples. It is known that magnetic particles when placed in medium and exposed to large enough external magnetic fields are subjected to the induced forces in magnet exerted on them by the magnetic field [214]. The ability to concentrate the magnetic field on the magnetic cantilevers of interest with high sensitivity has been particularly crucial for the success of the novel AFM magnetic step response applications in the laboratory and for the subsequent measurements. The sensitivity of the magnetic cantilever should be large to create a measurable cantilever displacement. In 2016, Tasci et. al. [214] showed that the behaviour of the movement and aggregation of magnetic particles in the magnetic fields could both appear as if they are in the inhomogeneous or in the uniform magnetic fields. Majority of the magnetic particles available for non-invasive work are the weakly ferromagnetic

(composite of 20-90% by weight of  $\text{Fe}_2\text{O}_4$  % or  $\text{Fe}_2\text{O}_3$  nanoparticles embedded in polymer matrix) and this includes the available paramagnetic beads. The paramagnetic particles are defined by the size of the nanoparticles they contain. Even though it holds for all materials including ferromagnets, the relationship between the magnetic field (B) and magnetic field strength (H), may depend on the previous magnetisation of the ferromagnetic material or its magnetic history. The magnetic field is no longer linear with the induced field H. On the other hand, if the magnetic content is known, and the smaller magnetic particle is known, the magnetic susceptibility could be read directly from relationship of magnetisation curves provided to experimenters by the vendors (in the so called B–H curves). [215] The magnetic response to a magnetizing field may differ greatly in the strength and the mass. The magnetic materials employed on the soft spring magnetic AFM cantilevers during this work were interesting for us to employ because they were readily available and could be routinely prepared. Nevertheless, the magnetic particle selection requires not only a good understanding of the desired performance in an applied field, but also the data sheet information available on the magnetic particle provided by the vendors. The bacterial organelles called magnetosomes are promising in enhancing the sensitivity of the force transducers. This is because they are ferromagnetic and possess (fixed magnets) magnetic crystals of sizes between 35 and 120 nm. This is interesting because the ferromagnetic particles are preferred in applications where the external field is weak and the particle size is limited, due to their high saturation magnetisation. The force in magnet induced on the magnetotactic bacteria causes them to align in the presence of an external magnetising field. A vast number of reviews and books have been published on application of magnetic particles. [216] [217] [215]

## **1.6 Research goals, objectives and overview**

In order to accurately quantify the viscoelastic properties of the soft samples, like soft eukaryotic cells, requires accurately quantifying the spring constant quantity. In this work procedures to measure and to analyse the viscoelastic properties of soft samples like diseased cells, tissues and polymer gels, will be presented. For this purpose, experimental setups for modulating the soft samples in magnetic force and two novel setups in which the well controlled force steps were applied to load and then to unload the cell sample by employing a soft spring magnetic cantilever. Specifically, we intend to change the sample base height by introducing a well-defined step, we expect this position change to be transmitted through the soft live cell or tissue samples and to deflect the soft spring AFM cantilever, which may creep to a new equilibrium position. During creep experiments the loading force (which is

proportional to the deflection) and the indentation (which is  $z$  sample height minus deflection) will both change. Thus, the experimental situation is not identical with a relaxation at constant strain, nor at constant stress, which is usually used in polymer rheology. In addition to the conventional  $z$  step scenario, a novel magnetic step response setup has been implemented in which magnetic cantilevers placed in a magnetic field are employed to apply directly a force step at constant  $z$  height, mimicking an experiment which is closer to the constant strain situation.

For the first time, data obtained from the live cell with quantities like samples spring constants, and the relaxation times would be derived from the  $z$  step and the magnetic step AFM creep response curves respectively. The experimental results from a single force curve have been tabulated to show the true elastic spring constants and the viscous values derived from the loading and unloading steps from the live cell sample respectively. Although both approaches are not equivalent with constant strain or constant creep response experiments, the coefficient of friction values from the force volumes (for the loading and the unloading steps) have been additionally derived and quantified from the experimental creep response data in order to elaborate the usefulness of the new experimental setups.

Our objective is to obtain creep response data of live cell samples locally by the magnetic step response AFM (direct) and the  $z$  step response AFM (indirect) setups by raster scanning the soft samples appropriately. (i) The soft spring magnetic cantilevers will be employed to characterize the soft samples viscoelastic properties by AFM. The novel magnetic step response setup has enabled the time dependent response of the creep after a fast magnetic step in loading and unloading force were applied to the soft samples. A localized, concentrated and spatially reconfigurable magnetic field has been necessary to achieve precise, biocompatible and well-defined loading and unloading force steps in magnet. To my knowledge no similar setup was available commercially to perform the experiments. Experimentally, the local response to deformation on the soft samples will be performed in two folds firstly indirectly and then directly to load and to unload the live cell samples and the gel sample respectively. (ii) The measured creep response of cells by the magnetic step AFM setup will be evaluated and the results interpreted by employing the mechanical analog circuit after performing the magnetic step and the  $z$  step response AFM experiments on the cell samples. The circuit employed in quantifying the soft samples response to the loading and the unloading force is the simplest combination of springs and a dashpot, which reproduces the experimental results obtained on cells and polymer-gel. A descriptive statistics of the experimental results, which represents the median values in the range of the measured force curves by AFM have been

presented. The viscous values that described the response and the relaxation time constants including the obtained elastic values have been quantified from the creep response experiments by the magnetic step response AFM. The values have additionally been compared to prove the reliability and reproducibility of the results derived by both setups respectively. (iii) By comparing the measured data to the obtained z-step response AFM data, we prove -in terms of intrinsic material properties by employing an appropriate model that the AFM setup can be employed for measuring the creep response of living diseased cells under near physiological conditions. With the help of this extended model we prove that we could derive the viscous properties of live cell samples in terms of the friction coefficient and the relaxation times.

The key advantage of this magnetic step AFM response setup lies in its capability to perform local measurements cells response to small loading forces directly at a single cell level and in its aqueous buffer solution. This novel magnetic force setup has been based on the direct measurements creep response measurements of the live cells and the polymer gel samples in the loading and the unloading steps in forces, as compared with the conventional indirect way of applying indirect loading of the samples as has been performed before. Due to several technical historical challenges, which has been faced by the AFM technique, its relevance for testing and the comparisons between alternative techniques like the z step response and the conventional steps is revealed and thus to assess which of the two may be more preferable.

## 2.0 MATERIALS AND METHODS

This chapter is the material and method section of the work. The chapter entails firstly the description of the sample cell culture and samples, then the polyacrylamide sample and lastly the magnetic cantilever preparation as employed in the course of this work respectively. For each AFM experiment performed the samples were either polymer gels or cultured cells placed on different glass slides and petri dishes respectively. Working on living cells, apparent elasticity measured by force–distance curves can vary if recorded on edge, in the perinuclear, or nuclear region, because of the heterogeneous intracellular composition and height differences. First, a brief explanation of the AFM employed and the magnetic AFM cantilever will be given. Then follows a short description of the setup as employed for this work. The optical lever design will be described, followed by the explanation of the designs for force measurements. The creep response curves have been recorded by monitoring the deflection of the cantilever after loading and unloading the soft sample in force by the magnet or by increasing the z height. For creep response experiments, the two loading schemes in z step and the magnetic step have been performed and will be described in this section. The pyramid indenter with a 35° opening angle and the indentation of the tip has defined the mechanical contact between the tip and the ultra-soft samples. The measurements of the soft samples material properties will be described. The third experiment could be carried out in the future and briefly described, whereby a sinusoidal force modulates the soft sample to obtain calibrated spring constants of the system. However, the focus was to employ the step response for local measurements of the creep response of the cell sample.

### 2.1 The AFM apparatus and description

In general the Atomic Force Microscope has been operated under constant force mode. Many considerations are made especially if the cantilever becomes heavily damped at the point of the tip due to the relatively large magnetic AFM cantilever tip – sample interaction. The primary experimental requirement was the application of a force in magnet at the very free end on the magnetic AFM cantilever. Therefore, the magnetic force microscope setup incorporated the optical beam deflection scheme for sensing the AFM soft magnetic cantilever motion in the aqueous environment. The schematics diagram in the figure 11 shows the most important components of the magnetic force microscope including its electrical assembly. A laser beam emitted by the laser diode is directed onto the cantilever and reflected

onto an array of four photodiodes. The corresponding output voltage signals from the PSD are acquired and then processed through a feedback electronic system. By subtracting opposite diode signals, the vertical as well as the torsion of the cantilever can be detected. Thus, as with the conventional AFM, the motion of the soft spring magnetic AFM cantilever must be measured with sub angstrom resolution. The most desirable situation is to apply a force directly behind the tip and not at other points along soft magnetic AFM cantilever employed. Due to the difference in bending shapes of different cantilever modes proportionality constant is required for each mode.[24] [9] [41] [23] [25, 42]

## **2.2 Sample preparation**

The live NIH-3T3 fibroblasts cells (cells) and the ultra soft polymer gel (gel) have been subjected for the characterization of the creep response by magnetic force microscope. The results are compared an alternative approach (z step AFM response). The material properties of the gel samples were tuned for biocompatibility and mechanical stability. The local visco-elastic properties (values) derived from the soft sample (gel sample and the live cell sample) with the magnetic AFM cantilevers will be described for the two AFM designs. Depending on the sample in its environment newly prepared magnetic cantilevers have been employed to characterize the soft samples viscoelastic properties.

### **2.2.1 Cell culture**

Cells were cultured in low glucose DMEM (Dulbecco's Modified Eagle Medium), supplemented with 10 % FBS (Fetal Bovine Serum) and incubated at 37°C in a humidified atmosphere of 95% air and 5% CO<sub>2</sub>. Cells were cultured typically for two days after splitting on plastic Petri dishes prior to AFM measurements. The plastic petri dish was then mounted in a home built aluminium holder and fixed with vacuum grease. Experiments were performed at room temperature in 5% CO<sub>2</sub> atmosphere.

### **2.2.2 Gel preparation**

Acrylamide and Bis-acrylamide solutions were purchased from Bio-Rad. N,N,N',N'-Tetramethylethylenediamine (TEMED), TC-119 medium, N-[3-(Trimethoxysilyl)propyl]ethylenediamine silane and dichlorodimethylsilane solution were purchased from Sigma. Sodium hydroxide (NaOH) and ammonium persulphate (APS) were purchased from Merck and circular cover glasses (22 mm diameter) from VWR Scientific.

Glutaraldehyde, ethanol and other solvents were purchased from Panreac AppliChem. Polymerization of the gel solution [218] was carried out between two glass slides, silanized with amino- or chloro- silanes, respectively. In details, for the amino-silanization, round cover slips were first washed in absolute ethanol, then covered with 0.1M NaOH for 3 minutes and finally activated with the amino-silane N-[3-(Trimethoxysilyl)propyl]ethylenediamine for 3 minutes and fixed with 0.5% glutaraldehyde for 30 minutes. For the chloro-silanized glass preparation, a dichlorodimethylsilane solution was poured on the cover slides for 5 minutes; glasses were later extensively washed with ultrapure water (MilliQ systems, Molsheim, FR) and dried. Polyacrylamide gel solution was prepared by mixing 40% Acrylamide with 2% Bisacrylamide in ultrapure water. Polymerization was initiated by APS and TEMED. The solution was dropped on the amino-silanized glass and covered with the chloro-silanized one slide to avoid the presence of oxygen that would inhibit the polymerization. After 30 minutes the upper slide was removed, leaving the gel on the amino-silanized support. The polymer gels (gel as a simple acronym used through out this work) on amino-silanized support were then stored in humid conditions for future use.

### 2.2.3 Magnetic cantilever preparation

The magnetic AFM cantilevers have been prepared by gluing a 20  $\mu\text{m}$  permanent magnetic fragments to the back side of the cantilever opposite to the AFM tip and stored at room temperature for use. The usage is illustrated on figure 3 where the magnetic fragments have been positioned at the rare end to the back of the cantilever. I have employed V-shaped cantilevers (MLCT, Bruker, Germany) [22] with a nominal *spring constant*  $\approx 10$  mN/m (resonant frequency in air  $\approx 7$  kHz) for cell experiments and micro lever (DNP-S, Bruker, Germany) with a nominal *spring constant*  $\approx 60$  mN/m (resonant frequency  $\approx 23$  kHz) for the experiments on gels. Small magnetic fragments of about 20  $\mu\text{m}$  in diameter were prepared by sanding a strong samarium cobalt magnet (IBS, Berlin, Germany) with an electrical tool (Dremel, Breda, NL) [219]. We placed a new cantilever chip into a cantilever chip holder, with the probe of the chosen V-shaped AFM cantilever facing upwards. A tiny drop of 2-component epoxy glue (18g+15g /2 x 15ml, Uhu Plus endfest 300, Uhu GmbH, Bühl, Germany) [220] was mixed and put on a glass slide next to a small amount of magnetic fragments. The glass slide with glue and magnetic fragments was placed on the optical microscope stage (Zeiss, Axiovert 300, Oberkochen, Germany) [221]. The AFM cantilever tip has been carefully dipped into the droplet of glue and then quickly to the region containing magnetic fragments by optical microscopy. Excess glue (if any) was removed by slightly

touching the cantilever tip on a bare portion of the glass slide. An easy way of handling was by micromanipulation. In this way it possible to translate the cantilever tip in three-dimensions on a suitable magnetic fragment and off the glue on the laboratory glass slide in a precise manner. Once the AFM cantilever and the magnetic fragment come in contact, the AFM cantilever was withdrawn by lifting the AFM cantilever chip holder off the surface of the glass slide.

### 2.3 Descriptions of setup with magnetic cantilevers

The AFM enabled the installation of the magnetic cantilevers in air and in aqueous environment like the cell culture medium. A schematic of the force microscope (MFP-3D Asylum Research, Santa Barbara, CA, USA) has been employed for this work. Our AFM has been operated in contact mode whereby the soft spring AFM cantilever exerts a force on the sample surface. The MFP-3D AFM operates both in liquid and air medium and measures the force between the sample and soft spring cantilever. The soft spring AFM cantilever can be moved in the Z directions and it is positioned with nm accuracy relative to the sample surface by a piezo electric transducer. The feedback system for position control consists of a hardware and software based control units. By monitoring the z height, the force curves such that additional creep and non-linearity are ruled out. The magnetic force microscope resides on a commercial optical microscope (Axiovert 200, Zeiss, Oberkochen, Germany). Cell populated PA supports were placed in Petri dishes, fixed to an aluminium holder with vacuum grease and mounted on the AFM stage with two magnets. All the set-up was enclosed in a homebuilt polymethylmethacrylate (PMMA) box in order to inject and maintain 5% CO<sub>2</sub>. As shown on figure 3a, to apply a magnetic force to the soft spring magnetic AFM cantilevers a coil of 100 turns around a soft iron core was attached to a polyvinyl chloride (PVC) tube, which fitted to the microscope objective placed under the AFM. The soft iron had a sharp pin in order to create a large gradient of the magnetic field. Typically, currents of 1.5 A were used in our measurements. The step like voltage signal was generated by the AFM controller and amplified with a home-built high current OP-AMP. Readout, control of AFM cantilever motion (includes all the digital signal processing) and analysis of the signal were done using home written routines in IGOR (Wavemetrics, Lake Oswego, OR, USA).

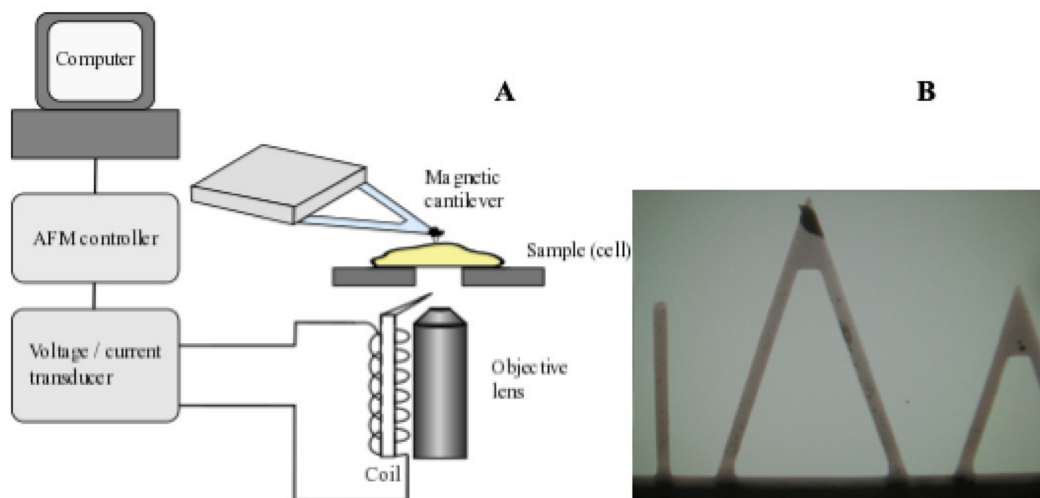


**Figure 11: Schematic setup of magnetic AFM cantilever including the electrical assembly. The coil has been connected to a voltage/current transducer. The AFM controller links the transducer to the personal computer. The sample is mounted on the x-y piezo of the AFM. A coil is attached firmly to the microscope objective lens, which is placed under the AFM tip in the combined optical/force microscope (panel A) and a 3 mm gap spacing below the AFM sample holder. The core material of the coil has a sharp pin in order to concentrate the gradient of the magnetic field. In panel B three AFM cantilever with varied lengths. The longest (middle)  $320\ \mu\text{m}$  triangular AFM cantilever shows an glued magnetic particle to the tip.**

For detection, the laser of the AFM had to be aligned to an area of the soft spring AFM cantilever, not being covered by glue. The deflection sensitivity of the magnetic cantilever was calibrated by obtaining a force curve on a stiff substrate, usually petri dish.[40] The AFM cantilever was then withdrawn a few micrometres from the surface and the thermal motion of the free cantilever was recorded to obtain the spring constant following the method by Butt et al., [24]The soft cantilevers for cells and slightly stiffer ones for the gels have been used. By applying a voltage step to the free cantilever and measuring its deflection the magnetic sensitivity was obtained. Despite the simplicity of this calibration approach, there are some drawbacks in the standard calibration method of the deflection sensitivity: 1) A clean and rigid substrate is required, which is not always available, for example when a soft sample at full coverage (a confluent cell layer, a tissue slice) is studied. This point is critical because it can force the experiment to perform separate experiments for calibrating the deflection sensitivity and for measuring the sample; ideally, one should try to perform both tasks without changing the experimental setup (including the laser alignment on the cantilever, the thermalization of the liquid medium, among others). Therefore, in practice, it is a good practice, whenever possible, to leave a portion of the substrate uncovered and clean to calibrate the deflection sensitivity. The calibration and the linearity of both the z-piezo and

the deflection signals, may directly affect the slope of the force curve, and therefore the deflection sensitivity. Whenever possible, the output of a well-calibrated displacement z-sensor should be recorded and used as z-piezo displacement axis or used to operate the z-scanner in close-loop mode. Other wise the cantilever tip–surface contact may, if at all, reduce the tip sharpness or damage the tip functionalization. 2) When tips with large radii and/or stiffer AFM cantilevers are used, especially on adhesive surfaces, friction forces can produce a torque, which can influence the measured deflection and can result in an apparent deflection sensitivity[222-225]. The z-piezo must be properly calibrated otherwise; the measured deflection sensitivity will be systematically rescaled. The vertical deflection signal must be free of artefacts as much as possible, for instance, due to crosstalk between vertical and lateral segments of the photo sensitive detector[226, 227]; these effects can be important when a large deflection interval is probed, as during the acquisition of a force curve. The deflection signal should be measured well within the linearity range of the photo-detector, which, depending on the system can be as small as one-third of the total range. The linearity of the response was checked to take care that the coil is not operated in saturation. Typical maximum forces were around 0.8 nN. The magnetic force could be increased by using a larger magnetic particle or by bringing the coil closer to the AFM cantilever[114]. Since, for our applications the force was sufficient we did not try to increase further. [25] Essentially, we glued a small magnet in the back of a regular AFM cantilever (referred to as a magnetic cantilever, or MC), and placed a coil below the sample stage such that the magnetic cantilever (MC) is positioned at a distance  $x_{mm}$  close to the coil such that the tip lies in coil axis. Flowing through the coil there is an alternative current of the form:

$$i_{AC}(t) = i_0 \exp i\omega t \quad (2.1)$$

Where  $\omega$  is the oscillation frequency and  $i_0$  is the current amplitude. The magnetic field in the proximity of the magnetic cantilever (MC) can be approximated by the magnetic field of  $N$  loops of a radius  $a$  at a distance  $x$  along the axis, such that:

$$\vec{B}_{AC}(t) = \frac{\mu_0 N i_{AC}(t) a^2}{2(x^2 + a^2)^{3/2}} \hat{x} \quad (2.2)$$

We can also write  $\vec{B}_{AC}(t)$  in terms of the magnetic dipole moment of the coil  $\mu_{coil}(t) = (\pi a^2) N i_{AC}(t)$  as

$$\vec{B}_{AC}(t) = \frac{\mu_0 \mu_{coil}(t)}{2\pi(x^2 + a^2)^{3/2}} \hat{x} \quad (2.3)$$

Where  $\mu_0$  is the vacuum permeability. This AC magnetic field is not uniform since the magnetic field lines outside of the coil are divergent. However, what really mattered here was whether the magnet was glued to the soft spring AFM cantilever will interact with the  $\vec{B}_{AC}(t)$ . Since the MC has a permanent magnetic dipole moment  $\vec{\mu}_{MC}$ , the potential energy of  $\mu_{MC}$  in the presence of  $\vec{B}_{AC}(t)$  is given by:

$$U = -\vec{\mu}_{MC} \cdot \vec{B}_{AC}(t) \quad (2.4)$$

In principle, we do not know which is the direction of  $\vec{\mu}_{MC}$  but it is applicable (it works) as long as we have the vertical component to couple with  $\vec{B}_{AC}(t)$ . Assuming that  $\vec{\mu}_{MC} = \mu_{MC} \hat{x}$  an approximate form of the force acting on the magnetic cantilever (MC) due to  $\vec{B}_{AC}(t)$  is given by:

$$\vec{F}_{AC}(t) = \nabla (\vec{\mu}_{MC} \cdot \vec{B}_{AC}(t)) \quad (2.5)$$

Finally, the approximate vertical force acting on the magnetic cantilever (MC) located at a distance  $x$  above the coil is:

$$\vec{F}_{AC}(t) = -\frac{3}{2\pi} \frac{\mu_0 \mu_{MC} \mu_{coil}(t) x}{(a^2 + x^2)^{5/2}} \hat{x} \quad (2.6)$$

By expanding the above expression around an average distance  $x_0$  between the MC and the coil, we obtain:

$$F_{AC}(x) - F_{AC}(x_0) = -\frac{3\mu_0 \vec{\mu}_{MC} \mu_{coil}(t)}{2\pi} \left[ \frac{1}{(a^2 + x_0^2)^{5/2}} - \frac{5x_0^2}{(a^2 + x_0^2)^{7/2}} \right] (x - x_0) \quad (2.7)$$

Replacing  $\mu_{coil}(t) = \pi a^2 i_0 e^{i(\omega t)}$ , we obtain the effective driving force on the MC has in the form:

$$F_{drive} = G(a, N, i_0, x_0, \mu_{MC}) (x - x_0) \exp(i\omega t) = F_B \exp(i\omega t), \quad (2.8)$$

Where the amplitude of the driving force  $F_B$  depends on a few parameters of the experimental setup namely 1) The geometrical characteristics, 2) the current amplitude of the coil, and 3) the magnetic dipole moment of the cantilever.

### 2.3.1 AFM force curves

The AFM force curves have been a plot of the deflection of the cantilever versus the extension of the z piezo height. The conventional and the stress relaxation curves were recorded on a cell and gel and sample in order to study the viscoelastic property. The conventional and the stress relaxation curves started at a point where cantilever and the sample are far apart and the cantilever were not deflected. Force curves were taken typically at a sample rate of 1 Hz, maximum deflection was set to 100 nm, and a typical travel range of 2 $\mu$ m. The time for a complete cycle was chosen in such a way that the retracting and the approaching part of the force curves in the non-contact part of the force were not separated by the viscosity effects. The forces curves obtained here are ramped up and down with constant speed, except at the turning points. For the stress relaxation force curves, z motion was stopped for a dwell time of 2 s after the trigger threshold was achieved (cantilever deflection of 150 nm). From the slope  $s$  of the force curve and the spring constant of the cantilever  $k_c$ , we calculated the spring constant of the sample  $k_s$ , by:

$$k_s = k_c * \frac{s}{1 - s} \quad (2.9)$$

I have recorded force volumes (6x6, or 10x10 force curves) at a typical spacing of 100nm to test homogeneity of samples and reproducibility of force curve data.

### 2.3.2 AFM z step response:

For step response, we kept the z voltage constant for a prolonged time (2s) after approaching the sample as in a regular force curve described above. After 1s of dwell time, the z height was increased by a small amount (typically 100nm) towards the soft sample and then withdrawn again after 0.5 s, (see figure 16) while the deflection signal was monitored showing the creep response of the sample. The creep response can be modelled by a spring and dashpot combination, usually called the general linear solid model. We could calculate the viscoelastic properties of the sample as described below.

### 2.3.3 AFM magnetic step response

Alternatively, to change the  $z$  height of the sample, we could apply a magnetic force step using magnetic cantilevers during the dwell time as described above. Typically, a force step of 0.4 nN was applied, while the  $z$ -height was kept constant and the deflection signal is recorded showing the creep response of our sample (see figure 17). The soft spring magnetic cantilever comprising of glued magnetic particle of volume  $V$  had magnetic susceptibility  $\chi$  was exposed to the external magnetic field ( $B$ ). The magnetic AFM cantilever experienced a gradient field of the form [228]

$$F_m = \chi * V * \frac{(\nabla \cdot B)}{\mu_0} * \vec{B}_{AC}(t) \quad (2.10)$$

$F_m$  is the force a paramagnetic particle of magnetic susceptibility  $\chi$  feels in a magnetic field. The response of the magnetic cantilever to the drive current a magnetizing field  $B_{AC}$  has been applied to the soft spring magnetic AFM cantilever. In both experimental approaches used in this work, neither the force nor the indentation can be kept constant. Even in magnetic step response, where a constant external force is applied, the indentation is changing and hence the deflection of the cantilever, and hence the force exerted by the cantilever is changing. In  $z$  step response, it is even clearer that force (being proportional to cantilever deflection) and indentation (being  $z$  height change - deflection change) are changing after applying the step during the observed creep response. Technically speaking the stress (i.e. force) and the strain (i.e. indentation) are changing in our experiment. Since normally stress relaxation is used in a condition where the strain is constant, and vice versa, we do not use the terms stress or strain relaxation here for our experimental conditions. Even though, stress and the strain are relaxing (both) in our experiments.

### 3.0 DATA ANALYSIS AND MODELLING

The chapter describes the data analysis of the deflection data obtained from the conventional force curve, z step response and the magnetic response design respectively. The objective of this section is to show that the creep response of cells samples by z step response and the magnetic step AFM design could be adequately quantified by employing the standard solid linear model. The standard linear solid model (SLS) has been employed to analyse the data from the magnetic step and the z step AFM design, which is the simplest combination of springs and a dashpot, which reproduces the experimental results obtained on cells. The viscous properties of the live cell samples will be derived in terms of the viscous damping coefficient of friction (friction coefficient or coefficient of friction) and the relaxation times.

Force curve data (conventional approach and retract, as well as the creep response data after z-step or magnetic force step) were analysed offline using home-written routines in IGOR (Wavemetrics, Lake Oswego, OR, USA). Since in a soft sample (e.g., a live cell data creep even over the dwell time of 2s was still substantial, one subtracted an exponential fit over the entire dwell time (excluding those data when the step has been applied) to subtract the global creep. The loading and unloading step was fitted by a single exponential function to the corrected data. By employing the standard linear solid model (see figure 12), the spring constants of the sample  $k_1$  and  $k_2$ , the friction coefficient  $f$  and the relaxation time constant  $\tau$  can be obtained. One gets two sets of values, one for the loading step, and another one for unloading step.

#### *Nomenclature used here*

Since there are several quantities discussed in this manuscript, which all have units of a spring constant, we use the following nomenclature: We use *spring constant of the soft spring cantilever* when addressing the spring constant  $k_c$  of the cantilever; we use *spring constant of the sample* when addressing the spring constant  $k_s$  of the sample determined by a force curve, and we use  $k_1$  and  $k_2$  when addressing the spring constants of the sample derived from z-step response and magnetic step response data analysed within the framework of the standard linear solid model.

### 3.1 Spring constant of the sample derived from the force curves

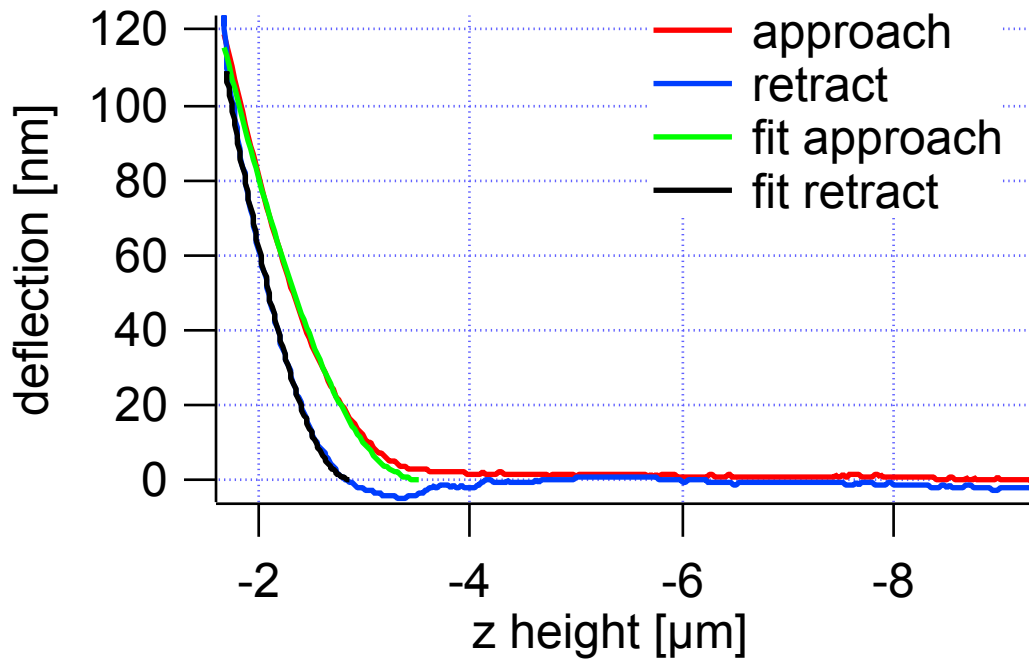


Figure 12: Typical force curve recorded after ramping cantilever on top of a cell. The figure shows plot of the approach (red trace) and the retract (blue trace) curves for contact mode cantilever in an aqueous environment. The deflection of the cantilever is recorded versus elongation of the piezo-electric scanner in the vertical direction. The simulated fit (green and black) is drawn on the approach and the retract regime of the force curves respectively.

When loading the soft sample with an AFM cantilever, at each given loading force  $F_1$ , which can be measured by its deflection  $d_1$ , one will create a sample indentation. In the force curve one measures the deflection as a function of  $z$  height of the sample. From the mechanical data one can derive the spring constants of the sample from the slope of the plot deflection versus  $z$ -height. The slope  $s$  is defined as:

$$s = \frac{\Delta d}{\Delta z} \quad (\text{A3.01})$$

Where  $\Delta d$  is the change in the deflection and  $\Delta z$  is the change in the  $z$  height. From the slope  $s$  of the force curve and the spring constant of the cantilever  $k_c$ , one calculated the spring constant of the sample  $k_s$ , by:

$$k_s = k_c * \frac{s}{1 - s} \quad (\text{A3.02a})$$

Since the slope,  $s$ , may be different on approach or retract, I distinguish both. In cells, due to a high viscous contribution  $k_{approach}$  and  $k_{retract}$  will always be substantially different. This is better illustrated on the deflection time data.

### 3.2 Analysis of Creep Response Data from $z$ response experiment

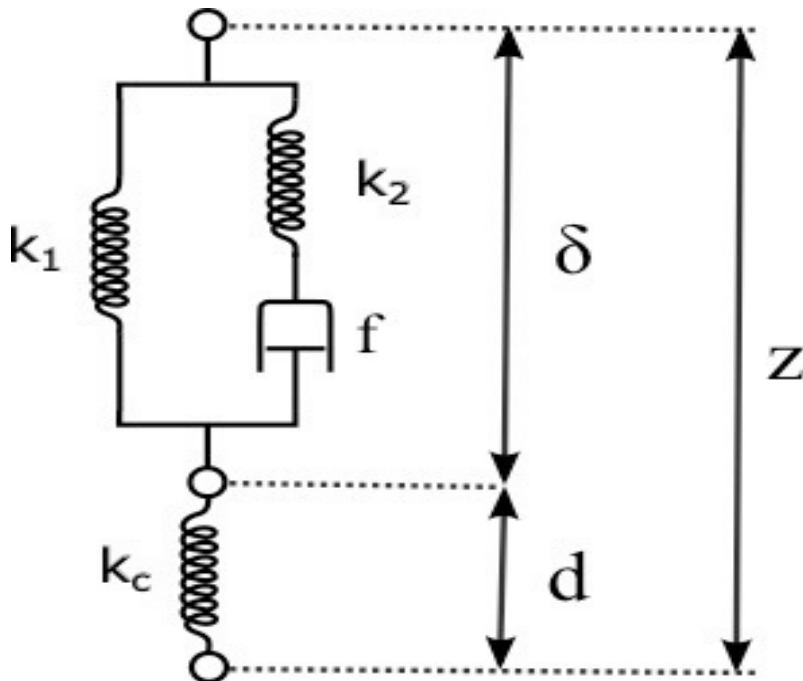
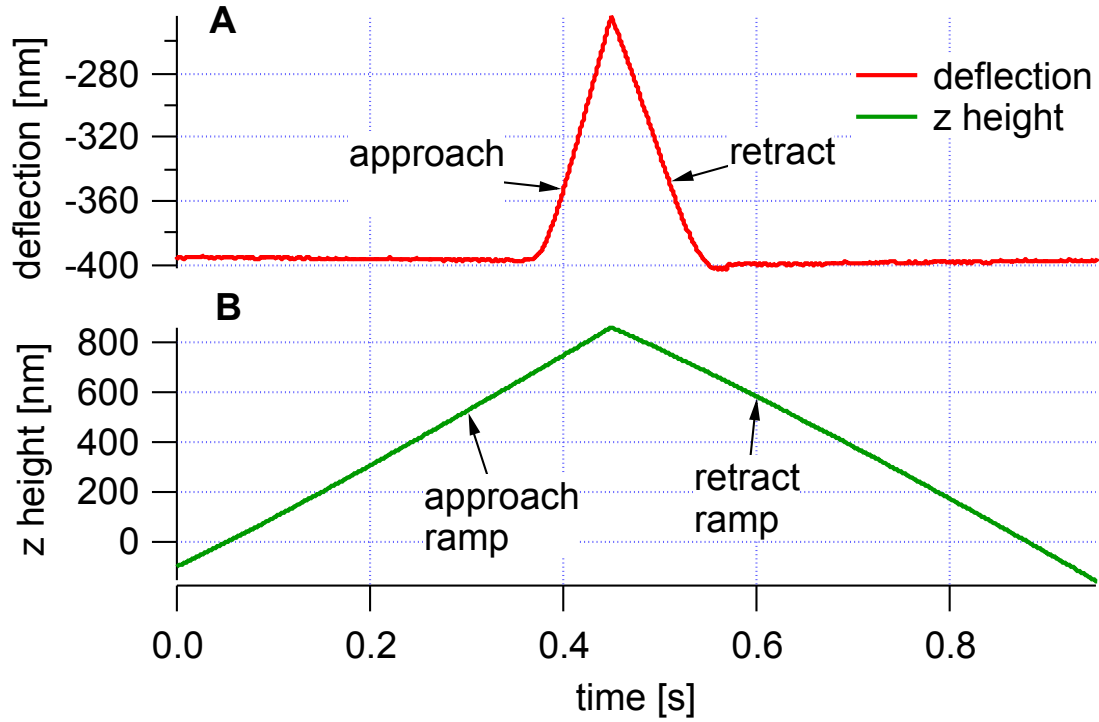


Figure 13: The Standard Linear Solid Model. The sample is modelled by a Zener element, where a spring  $k_1$  is in parallel to a Maxwell element, consisting of a spring  $k_2$  and a viscous damping element  $f$ . The soft spring AFM cantilever is characterized by its spring constant  $k_c$ . Motion of the sample height  $z$  is resulting in a deflection  $d$  of the cantilever or indentation  $d$  of the sample.



**Figure 14: Typical conventional force curve obtained on a cell sample. The deflection data (A) and the loading step in z height (B) for duration of 1 second. The z-height motion is reversed at  $t = 0.5\text{s}$ . The indentation is the difference between the change z height and the change in the soft spring cantilever deflection signal.**

We apply a step force when in contact with the sample at a z-position  $z_1$ , the deflection will be  $d_1$ , and the indentation is  $\delta_1$ . Before the step the force equilibrium will be:

$$k_c * d_1 = k_s * \delta_1 = k_s * (z_1 - d_1) \quad (\text{A3.02b})$$

We have used here the general relation between z-height, deflection and indentation, which will be always obeyed:

$$z = d + \delta \quad (\text{A3.02c})$$

Since the forces are in equilibrium at this point, we can simplify our calculations by redefining the origin such, that

$$d_1 = z_1 = \delta_1 = 0 \quad (\text{A3.02d})$$

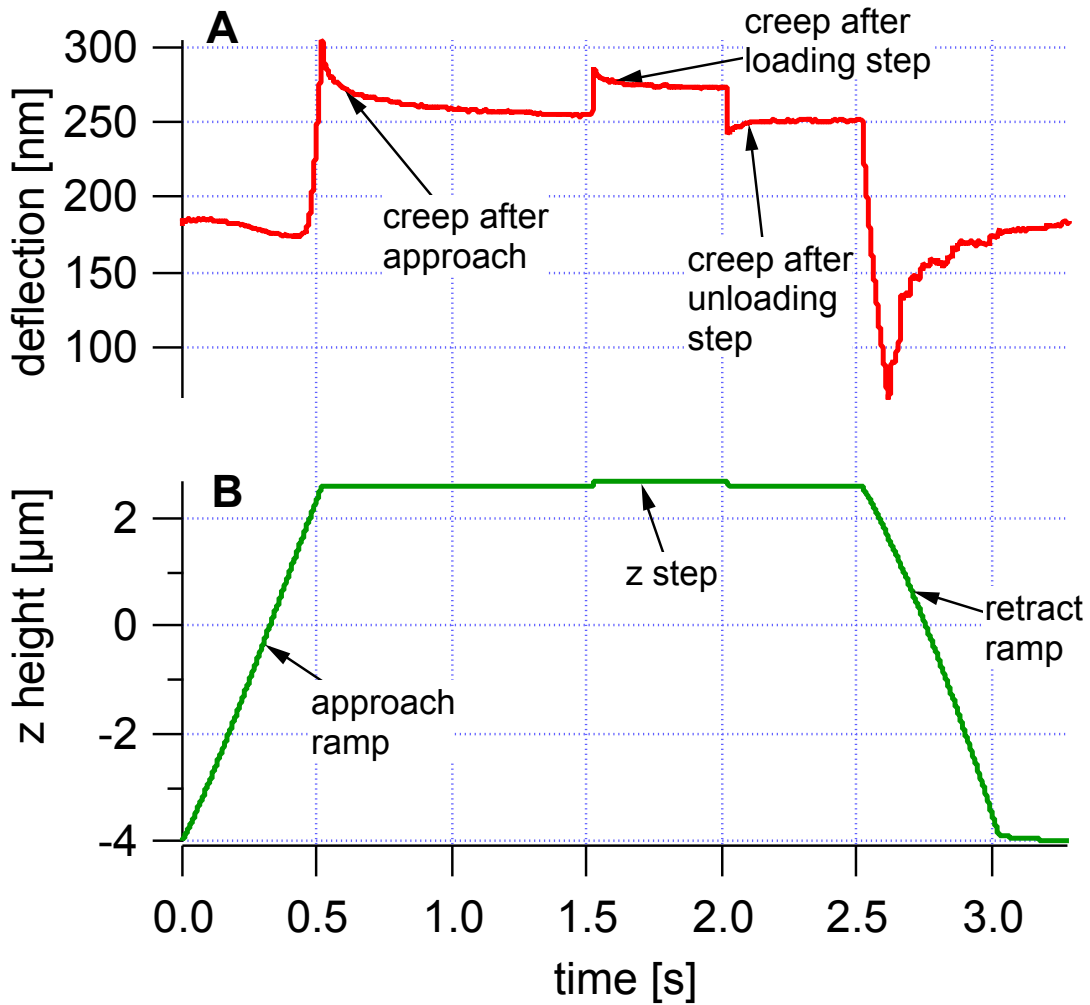


Figure 15: Typical creep response of a cell after applying a z step. Panel A shows the deflection data, while the z height (B) is first ramped as in a conventional force curve (approach ramp), then kept constant for 2 seconds, except a small step force step in magnetic force, which is applied after the creep of the cell, caused by the approach ramp, has relaxed appreciably. Then, finally the sample is retracted again (retract ramp). After the step (applied from time 1.5 to 2.0 seconds) the creep response to the loading and unloading step is analysed in detail. The indentation is the difference between the z height and the cantilever deflection.

### 3.3 Conventional step by increasing z-height: z-step

When externally applying force steps in indentation on the sample with the AFM cantilever at contact during a dwell time, by a jump in z height one will increase the z-height to:

$$z_2 = z_1 + \Delta z = \Delta z \tag{A3.03}$$

After relaxation, the deflection will have a new value  $d_2$ :

$$d_2 = d_1 + \Delta d = \Delta d \quad (\text{A3.03b})$$

One models the sample by a combination of two springs and a dashpot, termed the general linear solid model, which is the minimum model to reproduce the measured creep behaviour above. After relaxation, the spring  $k_2$  will be relaxed due to the creep of the viscous damping element  $f$ , so the force balance looks like:

$$k_c * d_2 = k_1 * \delta_2 = k_1 * (z_2 - d_2) \quad (\text{A3.04})$$

$$k_c * \Delta d = k_1 (\Delta z - \Delta d)$$

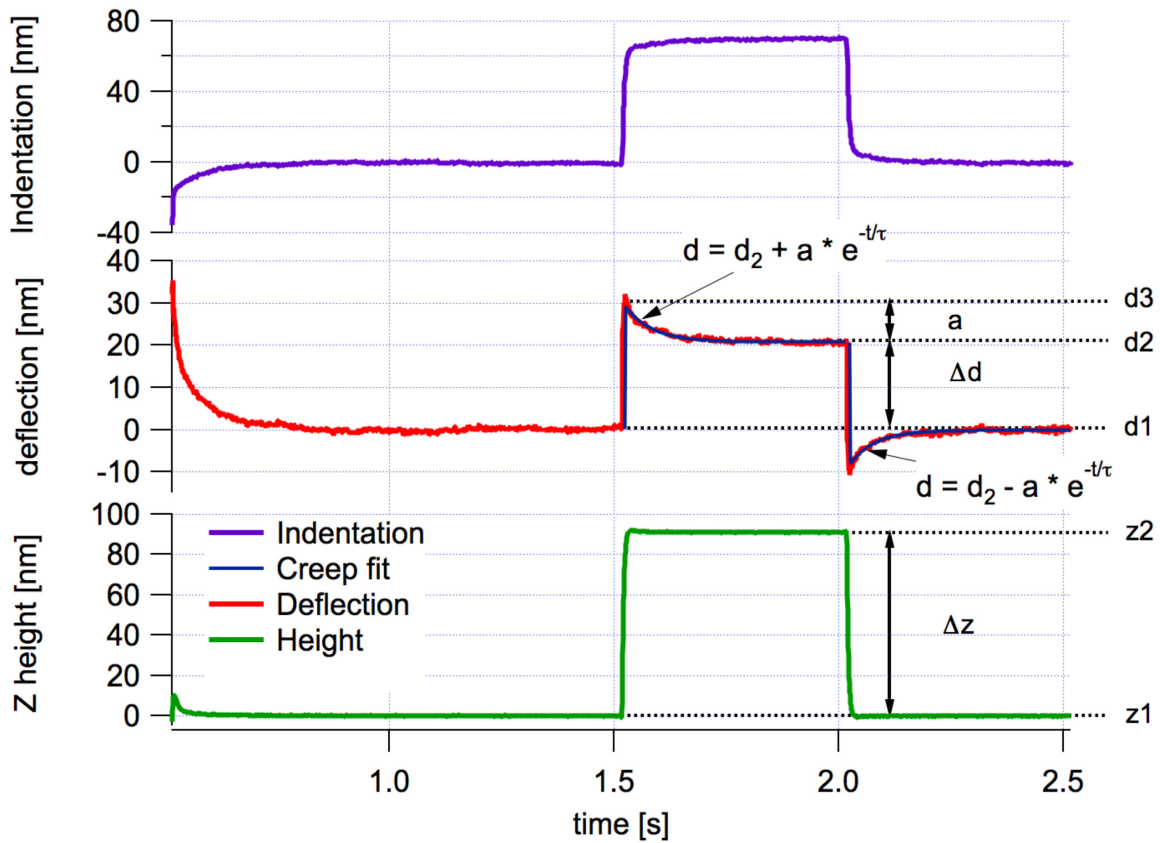


Figure 16: Creep response at dwell after applying a loading step in  $z$  height at  $t = 1.5\text{s}$  and an unloading step at  $t = 2.0\text{s}$ . The indentation is calculated as the difference between  $z$  height and deflection. The deflection data are fitted with an exponential function, which will give  $k_1$ ,  $k_2$  and  $f$  as results. The creep response at the dwell time is zoomed for better visibility.

The spring constant  $k_1$  can be derived from the measurable quantities  $\Delta d$  and  $\Delta z$ :

$$k_1 = k_c \frac{\Delta d}{\Delta z - \Delta d} \quad (\text{A3.05})$$

Right after (the infinitely step) z-step, the viscous element can be considered as a stiff rod. Thus, the force balance looks like:

$$\begin{aligned} k_c * d_3 &= (k_1 + k_2) * \delta_3 & (\text{A3.06}) \\ k_c(\Delta d + a) &= (k_1 + k_2) * (z_2 - d_3) \\ k_c(\Delta d + a) &= (k_1 + k_2) * (\Delta z - \Delta d - a) \end{aligned}$$

So, I can derive the spring constant  $k_2$  from the measurable quantities  $\Delta d$ ,  $\Delta z$  and from the initial value  $a$  of the deflection:

$$k_2 = k_c \frac{\Delta d + a}{\Delta z - \Delta d - a} - k_1 \quad (\text{A3.07})$$

After relaxation, the spring  $k_2$  will be relaxed due to the creep of the viscous damping element  $f$ . For describing the creep responses, one employs the following ansatz for the relaxation process:

$$d = d_2 - d_1 + a * e^{-t/\tau} = \Delta d + a * e^{-t/\tau} \quad (\text{A3.08})$$

The amplitude  $a$ , and the relaxation time  $\tau$  can be obtained by an exponential fit of the data. The force equilibrium for any point in time is given by:

$$\begin{aligned} F_c &= F_1 + F_2 & (\text{A3.09}) \\ F_2 &= k_c * d - k_1 * \delta \end{aligned}$$

The equation implicitly relates the dynamic values, which are a function of coefficient of viscous friction. Further the force in the Maxwell element will follow the following dynamic equation:

$$\dot{\delta} = \frac{\dot{F}_2}{k_2} - \frac{F_2}{f} \quad (\text{A3.10})$$

In the experimental scheme an ideal step loading cannot be achieved. The loading has been accompanied by a very small rise time of the cantilever. The creep in terms of the true sample spring constant could be described by:

$$\delta = z - d \quad (3.11)$$

$$\delta = \Delta z - \Delta d - a e^{-t/\tau}$$

$$\dot{\delta} = a * \frac{1}{\tau} * e^{-t/\tau} \quad (A3.12)$$

The force  $F_2$  in the Maxwell element can be rewritten using our ansatz eq. (A3.09):

$$F_2 = k_c (\Delta d + a e^{-t/\tau}) - k_1 * (\Delta z - \Delta d - a e^{-t/\tau}) \quad (A3.13)$$

$$F_2 = k_c * \Delta d - k_1 * (\Delta z - \Delta d) + k_c a e^{-t/\tau} + k_1 a e^{-t/\tau}$$

Using the above equilibrium of forces (A3.09) this will reduce to:

$$F_2 = k_c a e^{-t/\tau} + k_1 a e^{-t/\tau} \quad (A3.14)$$

$$\dot{F}_2 = -k_c \frac{a}{\tau} e^{-t/\tau} - k_1 \frac{a}{\tau} e^{-t/\tau} \quad (A3.15)$$

Entering the expressions from eq. A3.14, eq. A3.15, and eq. A3.12 in eq. A3.10 we get:

$$\frac{a}{\tau} e^{-t/\tau} = - \frac{k_c \frac{a}{\tau} e^{-t/\tau} + k_1 \frac{a}{\tau} e^{-t/\tau}}{k_2} - \frac{-k_c a e^{-t/\tau} - k_1 a e^{-t/\tau}}{f} \quad (A3.16)$$

$$1 = - \frac{k_c + k_1}{k_2} + \frac{k_c + k_1}{f} * \tau$$

$$f = k_2 * \tau * \frac{k_c + k_1}{k_2 + k_c + k_1} \quad (A3.17)$$

The relaxation time constant  $\tau$  is the apparent time in the experimental setup, which not only depends on the materials properties  $k_1$ ,  $k_2$ , and  $f$ , but also on the cantilever spring constant  $k_c$ , i.e. experimental parameters. The intrinsic relaxation time constant is defined by the ratio of coefficient of friction  $f$  and  $k_2$ :

$$\tau^* = \frac{f}{k_2} = \tau * \frac{k_c + k_1}{k_2 + k_c + k_1} \quad (A3.18)$$

### 3.3 Analysis of Creep Response Data from magnetic force steps

For the magnetic force step eq. (A3.02a) for the situation before the step still holds:

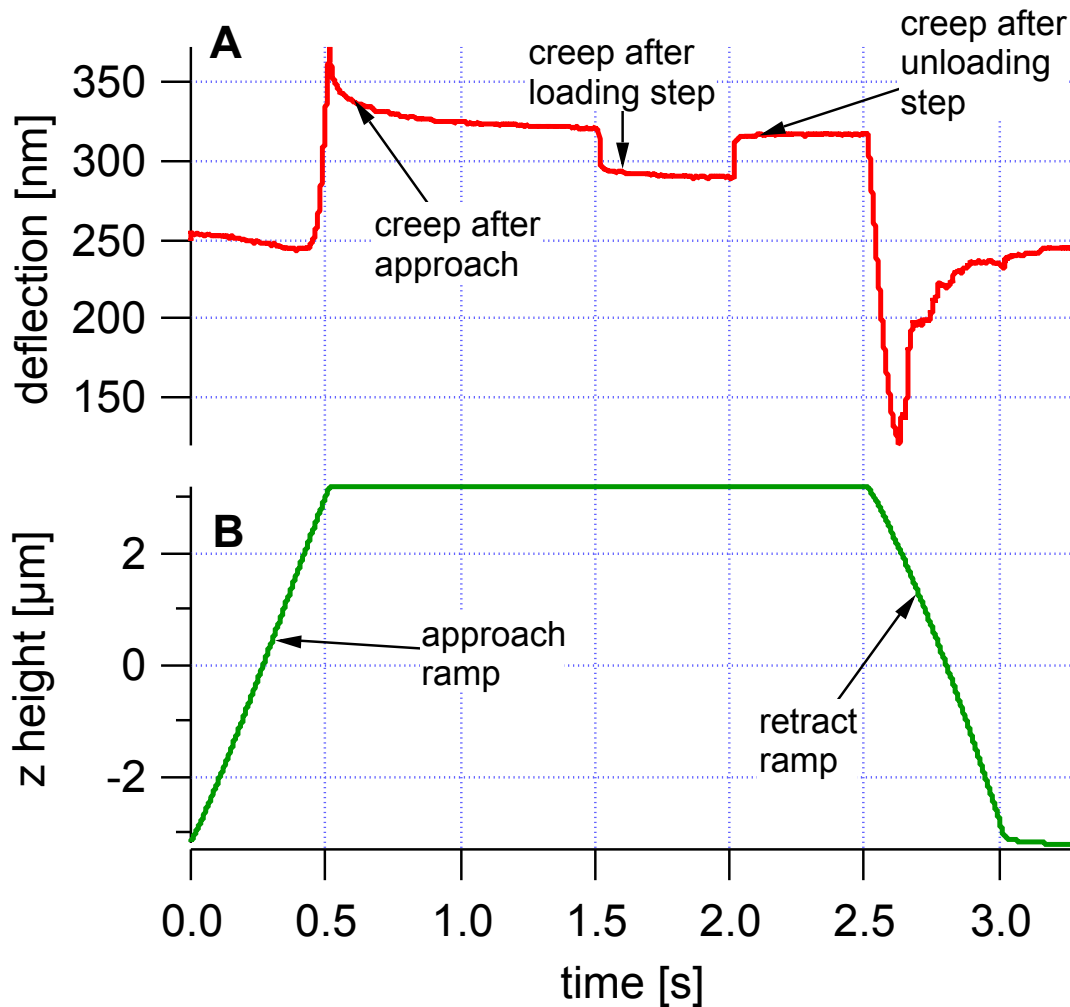


Figure 17: Typical creep response of a cell after applying a magnetic step. Panel A shows the deflection data, while the z height (B) is first ramped as in a conventional force curve (approach ramp), then kept constant for 2 seconds, except a small step in z-height, which is applied after the creep of the cell, caused by the approach ramp, has relaxed appreciably. Then, finally the sample is retracted again (retract ramp). After the step (applied from time 1.5 to 2.0 seconds) the creep response to the loading and unloading step is analysed in detail. The indentation is the difference between the z height and the cantilever deflection.

$$z_1 = z_2 = 0 \tag{A3.19}$$

$$\Delta z = 0$$

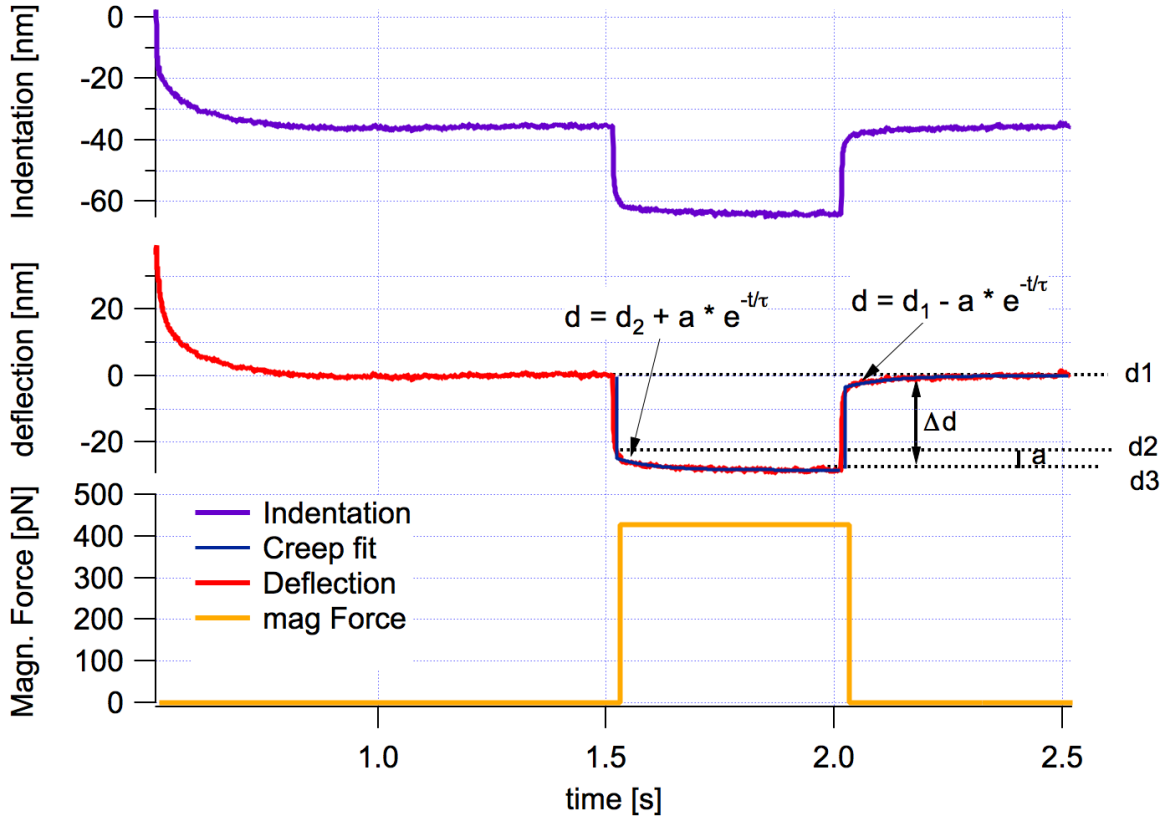


Figure 18: Creep response on the cell sample during 400 pN magnetic step force step starting at  $t = 1.5$ s. The deflection changes slowly resulting to the sample indentation, which is then followed by an unloading step at  $t = 2.0$  s. For the loading step the change of deflection  $\Delta d$  is negative, since the indentation (30 nm) change is positive. The change in  $z$  height is zero during the direct step in force experiment. By applying an exponential fit we gain the spring constants  $k_1$ ,  $k_2$  of the cell sample and the viscous properties of the cell sample.

When applying the external magnetic force  $F_m$ , one will first observe a sudden jump in deflection  $d_3$  and then a relaxation to a deflection  $d_2$ . Since  $z$  is zero during the entire process, the indentations and the deflection are directly linked:

$$\begin{aligned}
 \delta_1 &= -d_1 = 0 & (A3.20) \\
 \delta_2 &= -d_2 & d_2 &= \Delta d + a \\
 \delta_3 &= -d_3 & d_3 &= \Delta d
 \end{aligned}$$

For the loading step the change of deflection  $\Delta d$  is negative, since the indentation change is positive. The creep amplitude  $a$  is positive, since  $d_2$  is larger than  $d_3$ . After relaxation to deflection  $d_2$  the force balance looks like:

$$k_c * d_3 = k_1 * \delta_3 + F_m \quad (\text{A3.21})$$

$$k_c * \Delta d = -k_1 * \Delta d + F_m$$

$$k_1 = \frac{F_m}{\Delta d} - k_c \quad (\text{A3.22})$$

The initial response after the force step obeys the following force balance:

$$k_c * d_3 = (k_1 + k_2) * d_3 + F_m \quad (\text{A3.23})$$

$$k_c * (\Delta d + a) = (k_1 + k_2)(\Delta d + a) + F_m$$

$$(k_1 + k_2) = \frac{F_m}{\Delta d + a} - k_c \quad (\text{A3.24})$$

$$k_2 = \frac{F_m}{\Delta d + a} - k_c - k_1 \quad (\text{A3.25})$$

For the relaxation one employs the same ansatz as above in eq. A3.08

$$d = d_2 + a e^{-t/\tau} \quad (\text{A3.26})$$

$$d = \Delta d + a e^{-t/\tau}$$

The force balance needs to be expanded because of the magnetic force  $F_m$ :

$$F_c = F_1 + F_2 + F_m \quad (\text{A3.27})$$

$$F_2 = k_c * d - k_1 * \delta - F_m$$

$$F_2 = (k_c + k_1) * d - F_m \quad (\text{A3.28})$$

The force dynamics for the Maxwell element is also necessary here.

$$\dot{\delta} = \frac{\dot{F}_2}{k_2} - \frac{F_2}{f} \quad (\text{A3.29})$$

Using the ansatz from equation A3.08 one can calculate  $F_2$ , its time derivative and the time derivative of the indentation:

$$F_2 = (k_c + k_1) * [\Delta d + a e^{-t/\tau}] - F_m \quad (\text{A3.30})$$

$$\dot{F}_2 = (k_c + k_1) * \left(-\frac{a}{\tau}\right) e^{-t/\tau}$$

The indentation and its time derivative are given by:

$$\delta = -d \quad (\text{A3.31})$$

$$\delta = -\Delta d - a e^{-t/\tau}$$

$$\dot{\delta} = -\dot{d} = \frac{a}{\tau} e^{-t/\tau} \quad (\text{A3.32})$$

This will be entered in the dynamic equation of the Maxwell element A3.10:

$$\begin{aligned} \frac{a}{\tau} e^{-t/\tau} = & \frac{k_c + k_1}{k_2} * \left(-\frac{a}{\tau}\right) e^{-t/\tau} + \frac{(k_c + k_1) * \Delta d}{f} \\ & + \frac{(k_c + k_1) * a e^{-t/\tau}}{f} - \frac{F_m}{f} \end{aligned} \quad (\text{A3.33})$$

This relation can be split in its time dependent part and those terms, which do not depend on time:

$$\frac{a}{\tau} e^{-t/\tau} = \frac{k_c + k_1}{k_2} * \left(-\frac{a}{\tau}\right) e^{-t/\tau} + \frac{(k_c + k_1) * a e^{-t/\tau}}{f} \quad (\text{A3.34})$$

$$0 = \frac{(k_c + k_1) * \Delta d}{f} - \frac{F_m}{f} \quad (\text{A3.35})$$

The equation can be simplified and will give us a relation for the friction coefficient:

$$1 = -\frac{k_c + k_1}{k_2} + \frac{(k_c + k_1) * \tau}{f} \quad (\text{A3.36})$$

$$f = k_2 * \tau * \frac{k_c + k_1}{k_2 + k_c + k_1} \quad (\text{A3.37})$$

This relation is identical to the case of the z step. The intrinsic relaxation time constant is defined by the ratio of coefficient of friction  $f$  and  $k_2$ :

$$\tau^* = \frac{f}{k_2} = \tau * \frac{k_c + k_1}{k_2 + k_c + k_1} \quad (\text{A3.38})$$

### 3.4 Spring constants from the force modulation experiment.

In the previous section (section 1.5.1) we have described the motion of the free cantilever and the cantilever in contact with the visco-elastic sample in terms of the driven harmonic oscillator. The free motion is described by a mass connected to a single spring. As shown in figure 19 the in contact motion is described by a mass connected to a single spring.

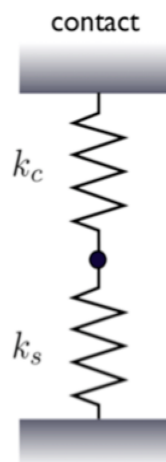


**Figure 19: An equivalent mechanical circuit of the sample spring in series with the cantilever spring in the in contact motion. The motion (oscillations) of the cantilever spring in contact with the viscoelastic sample with amplitude  $A_1$ . The elastic properties could be described until the preset loading force of the conventional force curve,**

The in-contact motion can be described by a mass connected to two springs (representing the cantilever and the sample.) Assuming that we pull down the mass with the given force,  $F_m$ , in both systems (e.g., the magnetic force). In the free cantilever model, forces act on the cantilever immersed in aqueous oscillating with the displacement amplitude is  $A_0$  as well as when the cantilever is in contact with the soft sample.

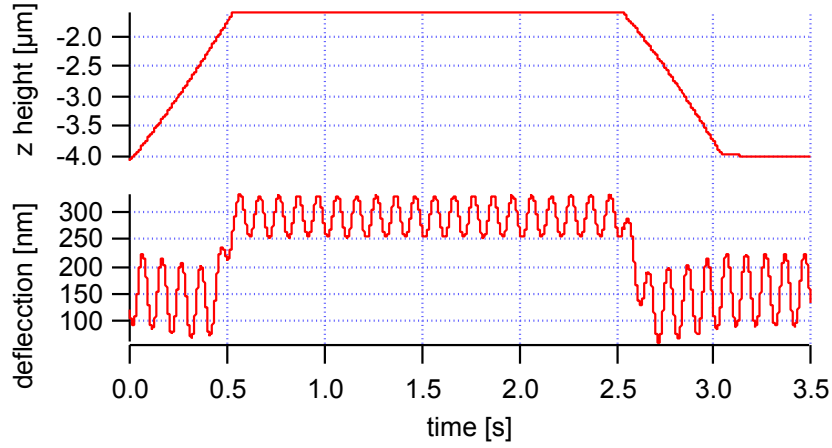


Figure 20: Figure shows stress relaxation data on a gel sample after a modulation force. The upper panel shows the z height profiles versus the time. The z-motion was stopped ( $t = 0.5$  seconds) for 2 seconds. During this time the stress relaxation after the approach ramp of the cell has relaxed (with displacement  $A_1$ ) and then retracted at  $t = 2.5$  seconds. The magnetic force modulation is directly applied to the soft spring magnetic AFM cantilever. The modulation of the soft spring magnetic AFM cantilever around an equilibrium indentation leads to a modulation of the force between the soft spring AFM magnetic cantilever and the soft sample. The bottom panel shows the deflection data in nm versus the time off and the in contact with the gel sample after the application of the modulation force in magnet for 3.5 seconds. Before contact the displacement of the free cantilever is  $A_0$ . The effective modulation spring constant of the sample is an indicator of the overall viscoelastic property of the sample. The force modulation may reveal a set of material responses over specific frequencies. For the in-contact system since the same force has to deform two springs, we obtain a smaller displacement  $A_1$  ( $A_1 < A_0$ ).

We describe the motion of the cantilever free magnetic and in contact with a viscoelastic sample in terms of the solution of the driven harmonic oscillator. When the cantilever is in contact with a viscoelastic sample and also subjected to a magnetic field, the equation of motion will be given by eqn. 1.12. As it has been described, when in contact, we will have the modulating force that makes the cantilever oscillates with the given frequency, the restoration force acting on the deflected the cantilever as well as the viscous forces due to the liquid and the soft sample. The differences between the motions are:

- 1) The oscillations are different, being  $A_0$  for the free cantilever and  $A_1$  for the cantilever in contact with a viscoelastic sample.
- 2) The resonant frequencies and phase angles for both motions are also different ( $\omega_0 \neq \omega_1$  and  $\phi_0 \neq \phi_1$ )

To estimate the spring constants we simplify both free and in-contact motion by a simple arrangement of springs.

For the in-contact system since the same force has to deform two springs, we obtain a smaller displacement  $A_1$  ( $A_1 < A_0$ ). By equating the forces as had been described before, we then obtain  $k_c A_0 = (k_c + k_s) A_1$ , which leads to the spring constants  $k_s$  of the soft sample that can be determined in terms of  $A_0$  and  $A_1$

$$k_s = k_c \left( \frac{A_0}{A_1} - 1 \right) \quad \text{A3.39}$$

On a very stiff sample, no indentation will occur, thus the amplitude in contact  $A_1$  will be zero, leading to  $k_s \rightarrow \infty$ . For every soft sample the amplitude in contact  $A_1 \rightarrow A_0$ , which leads to  $k_s \rightarrow 0$ . In the limit of  $\omega \rightarrow 0$  we only have the elastic response because the viscous components vanishes as  $dy_n/dt \rightarrow 0$ . For  $\omega > 0$ , the viscous effects are present and  $k_s$  represents an effective spring constant.

### 3.5 The phase lag between free and in contact motions of the cantilever.

The phase lags of the cantilever motion are directly related to the internal viscosity of the sample, is calculated by

$$\phi = \phi_1 - \phi_0 \quad \text{(A3.40)}$$

The phase angles of each type of the cantilever motion is

$$\tan \phi_n = I_m [A_n] / R_e [A_n] \quad \text{(A3.41)}$$

For small angles one has within the CM2 approach

$$\tan \phi_n \approx \phi_n = \frac{b_n \omega}{\omega^2 - \omega_0^2} \quad \text{(A3.42)}$$

We can make further approximations assuming  $\omega_1 \approx \omega_0$  to determine the phase difference as

$$\phi \approx \frac{(b_1 - b_0) \omega}{\omega^2 - \omega_0^2} \quad \text{(A3.43)}$$

Since  $b_1$  describes the viscous damping due to the aqueous environment + sample, and by  $b_0$  is only due to the aqueous environment, the phase difference  $\emptyset$  carries only in the information about the viscosity of the sample.

## 4.0 RESULTS

This is the results section. The viscoelastic creep response of living cells and gel was measured by AFM stress relaxation experiments. In addition to this conventional z step scenario, we also implemented here a method to apply directly a magnetic force step at constant z height, which is closer to a constant strain situation. In this section the results are shown and have been described. The spring constants from the cell and the gel sample have been quantified in adequate manner and then summarized in a tabular form. To avoid confusion the viscous property of the soft sample, friction coefficient, which has been derived will be given the acronym,  $f$ , in the rest of the manuscript

### *Nomenclature used here*

Since there are several quantities discussed in this manuscript, which all have units of a spring constant, we use the following nomenclature: We use *spring constant of the soft spring cantilever* when addressing the spring constant  $k_c$  of the cantilever; we use *spring constant of the sample* when addressing the spring constant  $k$  of the sample determined by a force curve, and we use  $k_1$  and  $k_2$  when addressing the spring constants of the sample derived from z-step response and magnetic step response data analysed within the framework of the standard linear solid model.

Figure 21 shows the entire data sequence (z height (fig 20A) and deflection (20B)) as a function of time, as well as a zoom-in in the region of interest during the dwell time ((z height (fig 20C) and the deflection (20D))). As can be seen from the raw data, the relaxation time is on the order of 0.1 seconds, thus we choose to wait for 1s, before the step is applied. Even this prolonged waiting time is not sufficient so some residual creep from the approach is still visible. Thus, we needed to subtract an exponential function, to remove the global creep (green curve in Fig 20B). Here an exponential fit is applied to the entire dataset, excluding those data points next to the loading and unloading step. This detrended data set is actually shown in Fig 20D, which shows the corrected deflection data to be analysed. As can be seen here, after detrending, the loading and unloading step give similar (except sign) results, and the cell achieves - after creep - the same deflection position as before the step is applied. We have fitted then locally an exponential function to describe the creep response after the loading and unloading step (blue curves in Fig 20D). If we model our sample response by the linear solid model, which is the simplest combination of springs and dashpots reproducing the observed creep response data, we find that the deflection shall follow a single exponential behaviour (see analysis section for the derivations). The fit parameters (time constant  $\tau$ ,

deflection plateau after creep has relaxed, and amplitude of the exponential decay) can be converted in the elements of the linear solid model circuit  $k_1$ ,  $k_2$  and  $f$ . Where  $k_1$  will be the spring constant of the sample after relaxation,  $k_1 + k_2$  will be value for the initial elastic constant of the cell sample right after the step has been applied, and  $f$  will be the friction damping coefficient. The apparent relaxation time constant  $\tau$  will be determined by the sample's viscoelastic properties plus the cantilever spring constant. The intrinsic relaxation time constant  $\tau^*$ , defined as  $f / k_2$  will be independent of experimental conditions. Table 1 summarizes the results from analysing the force curve and the step response data presented in figure 20. The values presented in table 1 will depend on the contact area, which is a function of loading force or indentation. By applying a suitable model (like the Hertz model often used in AFM), these values can be converted to materials properties like storage or loss modulus. However, since the validity of these models, especially on the microscopic scale used here, may be questionable we did not refrain to this option within this work.

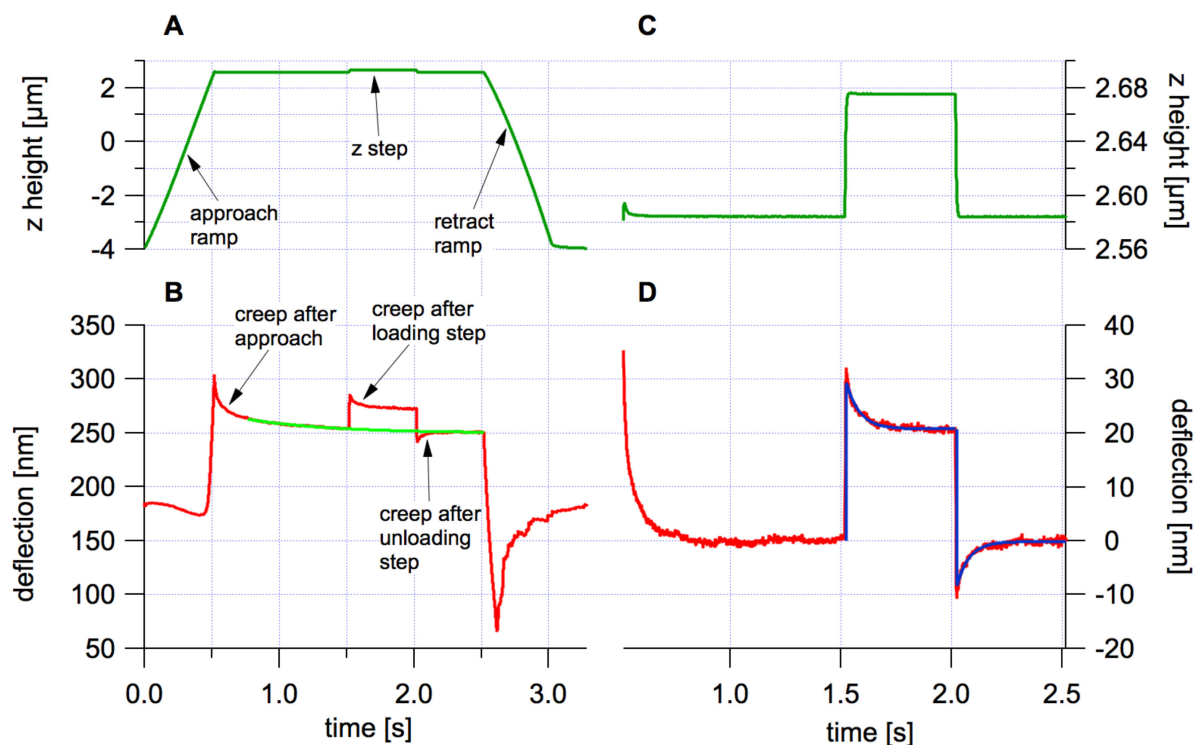


Figure 21: Typical creep response of a cell after applying a z step. Panel A shows the deflection data, while the z height is first ramped as in a conventional force curve (approach ramp), then kept constant for 2 seconds, except a small step in z-height, which is applied after the creep of the cell, caused by the approach ramp, has relaxed appreciably. Then, finally the sample is retracted again (retract ramp). After the step (applied from time 1.5 to 2.0 seconds) the creep response to the loading and unloading step is analysed in detail (see panel B & D for a zoom in). The deflection data is fitted with an exponential function, which is analysed in terms of the standard linear solid model.

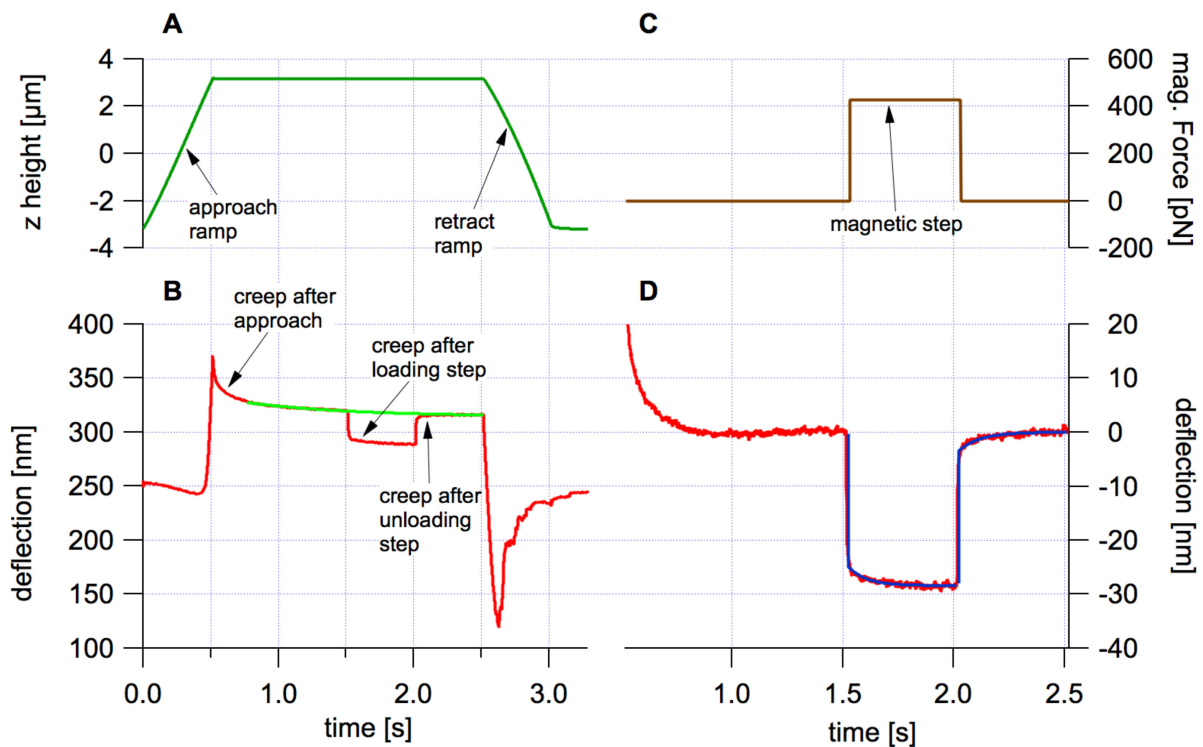
Experiment type		k, k1 [mN/m]	k2 [mN/m]	$\tau$ [ms]	$f$ [ $\mu$ Ns/m]
Force Curve	Approach	3.78			
	Retract	7.99			
z step	Loading	3.42	2.10	52.4	110
	Unloading	3.52	2.01	49.4	99.3

Table 1: Summary of the spring constants of the live cell sample and the viscous properties derived by analysing the force curve and the z step response data presented in Figure 21

As can be seen in table 1, the spring constant derived from the slope of the approach and retract branch of the force curve at a force corresponding to those applied during the step,

deviate largely from each other, since this type of analysis does not consider any viscous contribution of the sample, but rather assumes that the response is purely elastic. Since this is definitely not the case, the numbers will be wrong by some degree and shall rather be called apparent spring constant values. On the contrary, the spring constants of the cell sample derived from the loading and unloading step are very close to each other, demonstrating that the design of this experiment (and the analysis of the data) does handle viscous properties adequately and will result in reliable numbers for the viscous properties of the cell sample.  $K_1$  is the spring constant of the cell sample after creep has seized, so this should correspond to the spring constant of a force curve taking at an infinitely small loading rate, which is not possible. Not surprisingly, the spring constants of the cell sample determined from the force curve are larger than  $k_1$ .  $K_2$  is the additional spring constant of the cell sample in the visco-elastic branch, so somehow the ratio of  $k_1$  and  $k_2$  measures whether the cell sample is purely elastic ( $k_2$  should be zero then), or has both contributions. In our case in cells,  $k_1$  and  $k_2$  are of the same order, so cells are elastic and viscous at the same time at roughly the same proportion. The friction coefficient will be due to the internal viscosity of the cytosol, the organelles, and the cytoskeleton being pulled through the cytosol. From an experimental point of view, the relaxation time  $\tau$  may be more interesting, since this sets the time scale at which viscous contributions will be apparent ( $t \leq \tau$ ) or not ( $t \gg \tau$ ). The observed relaxation time will be the most prominent, in terms of response amplitude and in terms of time scale, i.e. the longest time scale as selected by the experimental scheme and the analysis procedure. It is conceivable that in a cell, there will be many more relaxation processes at a multitude of time scales, depending to different modes of creep response, which have not been analysed or detected within the framework of this work.

In  $z$  step response a sudden change in  $z$  height is applied to the sample base, which will be transmitted through the cell and deflect the cantilever. The cantilever deflection is then slowly relaxing in a new equilibrium position, which implies that the loading force (which is proportional to the cantilever deflection) is changing. The sample deformation, which is the  $z$ -height minus the cantilever deflection, will also be changing (and relaxing slowly). See the results shown in figure 15, where the indentation during a step response has been calculated and plotted. So, this type of experiment will neither be a constant stress (i.e. constant force), nor a constant strain (i.e. constant sample deformation or constant indentation) type experiment, as is usually used in creep experiments in soft matter physics. Thus we designed a variant of this experiment, where the sample  $z$ -height is kept constant, while a magnetic force step is applied directly to the cantilever during the dwell time (see figure 21).



**Figure 22: Creep response of a cell after a magnetic force step. Here the z height is kept constant for 2 seconds, after the approach ramp (22A and B). At time 1.5 s (after 1 second of dwell) a magnetic force is applied to the cantilever (fig. 22C), which leads to a change in indentation of the sample (Fig 22D), which in this case can be read directly from the deflection signal. As in the z-step, we can see an instantaneous jump in deflection followed with a slow creep. Here, due to the different experimental scheme, both effects go in the same direction, and thus appear to the eye very different than the equivalent creep response process in fig 21D. (same cell as in figure 21)**

Figure 21 shows the response of a cell after applying a magnetic force step in contact with the cell. The experimental sequence is very similar to the z step response in figure 20. After approaching the cell the z height is kept constant now for the entire dwell time (0.5 .. 2.5 seconds) and the cantilever tip is retracted after dwell. After 1 s dwell (at  $t = 1.5s$ ) a magnetic force of 400 pN is applied directly to the cantilever, which is turned off after 0.5 s (at  $t = 2s$ ) (see figure 21A and 21B for the z-height and the deflection as a function of time during the entire sequence). The creep response can be observed from the deflection signal. As in the case of z step response the global creep (caused by the approach ramp of the force curve) has to be subtracted (green line in figure 21B) to get the detrended deflection signal to be analysed further (figure 21D). We also fit a single exponential function to the deflection data after the loading (at  $t = 1.5s$ ) and the unloading step ( $t = 2.0s$ ) of the magnetic force (Fig 21D),

which is then also analysed in the frame work of the linear solid model, to get the same spring constants ( $k_1 + k_2$ ) of the cell and the viscous quantities ( $f$  and  $\tau$ ) as in the case of  $z$  step. Table 2 summarizes the results of the analysis for the data presented in figure 21. As in the case of  $z$  step, we observe a large discrepancy for the spring constant values of the cell sample derived from the approach and retract force curve, but very good agreement of the viscoelastic properties derived from the loading and unloading step. As in the case of  $z$  step response, the sample indentation will be the difference between  $z$  height (which is constant in this experimental scheme) and deflection. The data presented in figure 21 have been recorded at the same cell in roughly the same area as the  $z$  step data of figure 20, except for some small drift or movement of the cell, which is inevitable during the time needed for acquiring data and switching from one mode to another (some 20 minutes in this case). Thus the numbers in table 2 are not identical but very similar to those in table 1.

Experiment type		k, k1 [mN/m]	k2 [mN/m]	$\tau$ [ms]	$f$ [ $\mu$ Ns/m]
Force Curve	approach	3.78			
	Retract	7.45			
Magnetic Step	Loading	2.86	2.08	70.2	146
	unloading	2.91	2.04	83.8	171

**Table 2: Summary of spring constants ,  $k$  ,(elastic values) of the live cell sample and the viscous properties derived by analysing the force curve and magnetic step response data presented in Figure 22**

In this work one has recorded step response data in an array of force curves (6 X 6 curves at a spacing of 100nm) to show that viscoelastic properties can be measured reproducibly by these methods. Figure 22 shows the spring constants derived from the loading and the unloading steps,  $k_1$  values of the creep response data as well as spring constant  $k$  of the cell sample calculated from the approach and retract ramp of the force curve. As in the case of single force data above (figure 20, summarized in table 1) we can see that except for the spring constant values of the cell sample,  $k$ , calculated from the retract curves, which shows a large variation, the other quantities, and most importantly the  $k_1$  from loading and unloading step are very accurately determined. To further stress this point, for all the soft samples (cells and gels), one has averaged the spring constants and the relaxation time  $\tau$  determined by  $z$  step and magnetic step data for comparison shown in figure 24. There is some slight deviation

between magnetic and z step data, although they were recorded on the same cell, however there may have been some drift or movement between the two measurements. Other possible error sources will be discussed below. Recording the entire force map took 4 minutes plus some time for switching from one mode to another. This may explain the slight deviation easily.

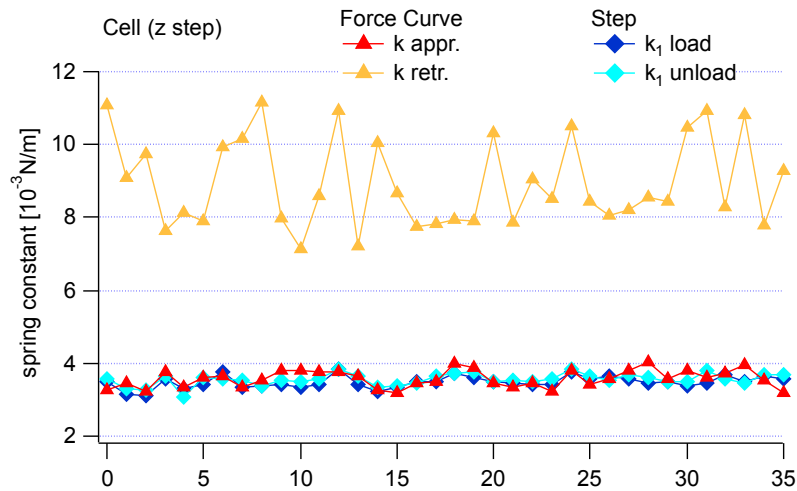


Figure 23 Comparison of the elastic spring constants values of the live cell sample calculated from force curve data ( $k$  approach and  $k$  retract are the values from the corresponding branch of the force curve) and from step response data ( $k_1$  loading step and unloading step). The graph is a compilation of all 36 force curves from a 6 by 6 force volume over an area of 600nm.

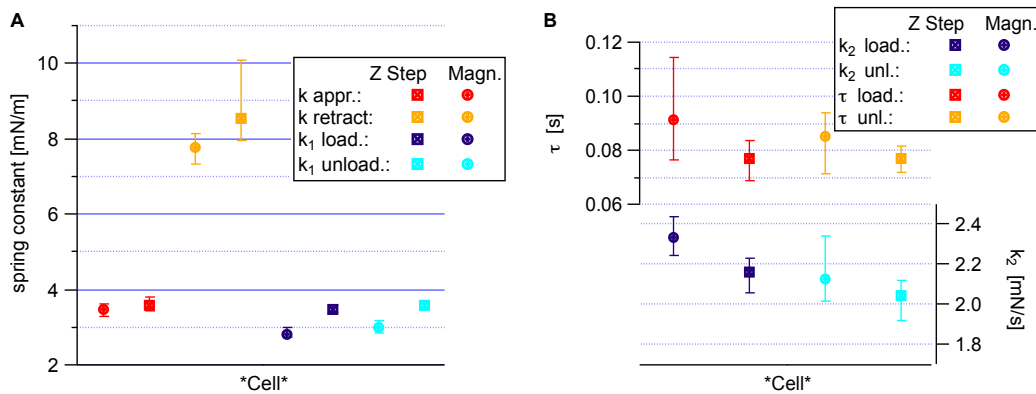
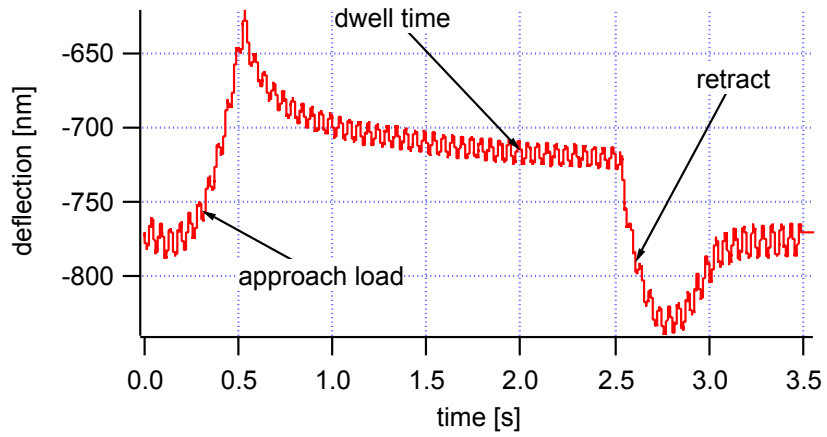


Figure 24: Comparison of the spring constant (A) and viscous properties (B) of the live cells derived from a magnetic step and z step response experiments respectively. The values correspond to the medians of the respective quantity from the 36 values measured in a force volume over a square area of 600nm. The spring constants derived from the step ( $k_1$  loading and  $k_1$  unloading) are very similar for both methods (z step and magnetic step), whereas the spring constant ( $k$ 's) derived from approach and retract force curves deviate largely due to the neglect of viscous response in this type of analysis. The viscous properties (the relative strength compared to the elastic properties is measured by  $k_2$ , whereas  $\tau$  is the relaxation time) are also determined reproducibly in both step methods (z step and magnetic) for loading and unloading steps.

I employed a third design, the magnetic force modulation experiment for characterizing the live diseased cells viscoelastic properties (see figure 24 for the obtained stress relaxation data). A soft diseased cell sample subjected to a sinusoidal varying stress will respond by a sinusoidal varying strain, which may be out of phase with the applied stress. At that single frequency the diseased tissue/cell properties were described. A sinusoidal modulating force in magnet was applied by attaching a magnetic material to the end of the soft cantilever (back of the cantilever). The force in magnet modulates the force on the tip end of the cantilever, which transmits a sinusoidal-like indentation to the live cells. Here, the soft spring AFM cantilever tip was modulated while in contact with the soft sample. In this design a sinusoidal magnetic force is applied to the cantilever plus the sample and the response of the cell maybe observed over an extended off resonance frequency range (see figure 18 and the results in appendix). The magnetic force modulating technique took advantage of the sensitivity the range of the indenting force on the diseased tissue cell and the precision of the soft spring AFM cantilever tip relative to the soft sample under study. During the magnetic force modulation experiment shown on the figure the total force of the system was a function of the drive force, the soft spring cantilever force and the viscous force of the medium. Experimentally, the measurements of the system response to the sinusoidal load in magnet can be expressed with defined parameters and employing an appropriate model, which will represent the data and to quantify the spring constant of the soft sample and the viscous properties. The spring constants and the viscous values of the diseased tissue cell was determined from the definition of the phase difference between the direct drive load at the force end of the cantilever tip and the response of the cell sample around an average indentation.



**Figure 25: Stress relaxation response data obtained on a diseased tissue soft sample during the force modulation experiment to test the sensitivity of setup. The figure shows the deflection versus the time traced for ca. 3.5 s. The z-motion was stopped ( $t = 0.5$  seconds) and the direction reversed after 2 seconds. During this time the stress relaxation after the approach ramp of the cell has relaxed considerably.**

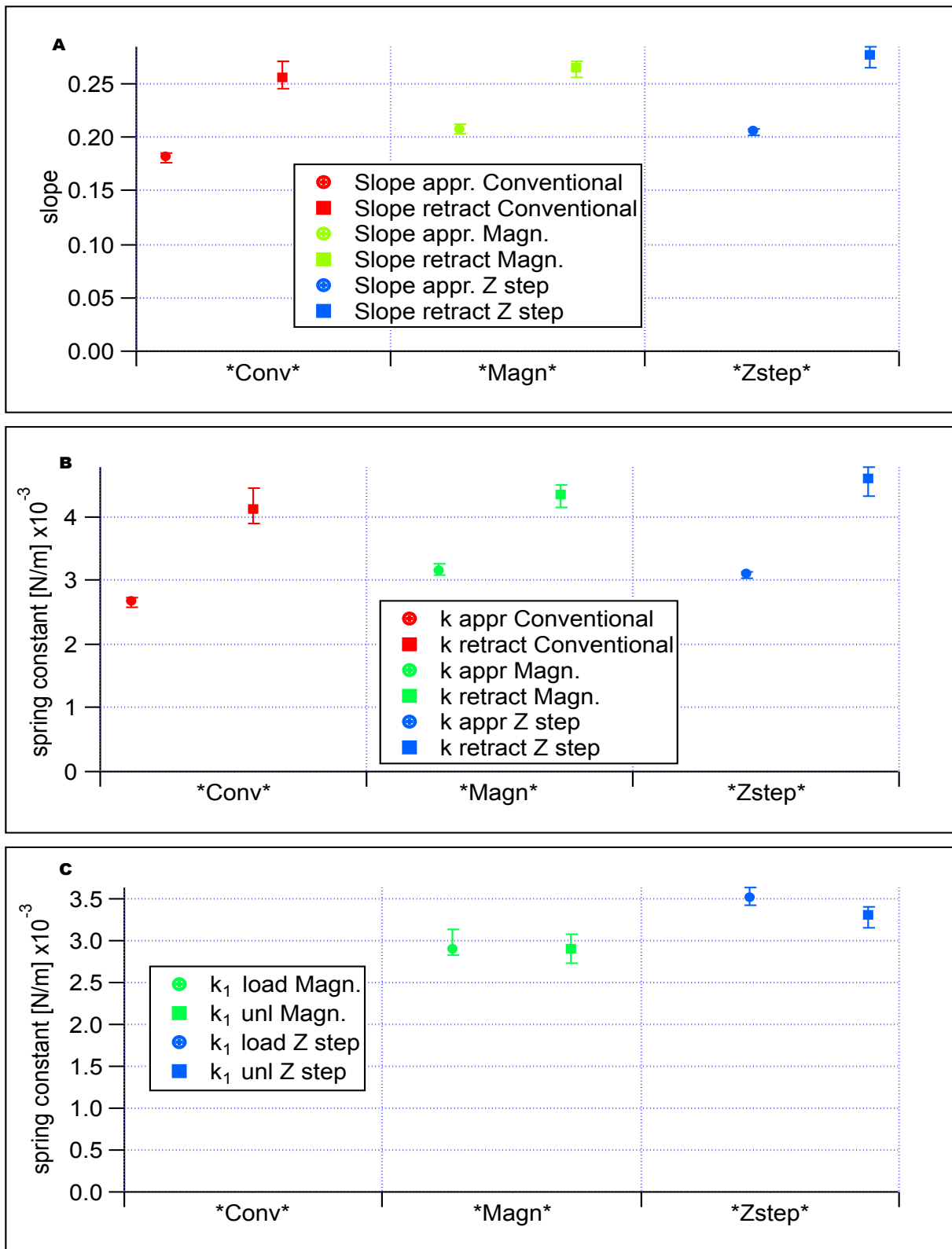


Figure 26: Comparison of the spring constants of a soft sample (elastic values) to test magnetic AFM force setup. The spring constant derived by analysing force curve (Conv.), the magnetic step (Magn) and the z step response experiments on cell sample by AFM experiments. The graph is a compilation of all 46 force maps each obtained over an area of 600 by 600 nm.

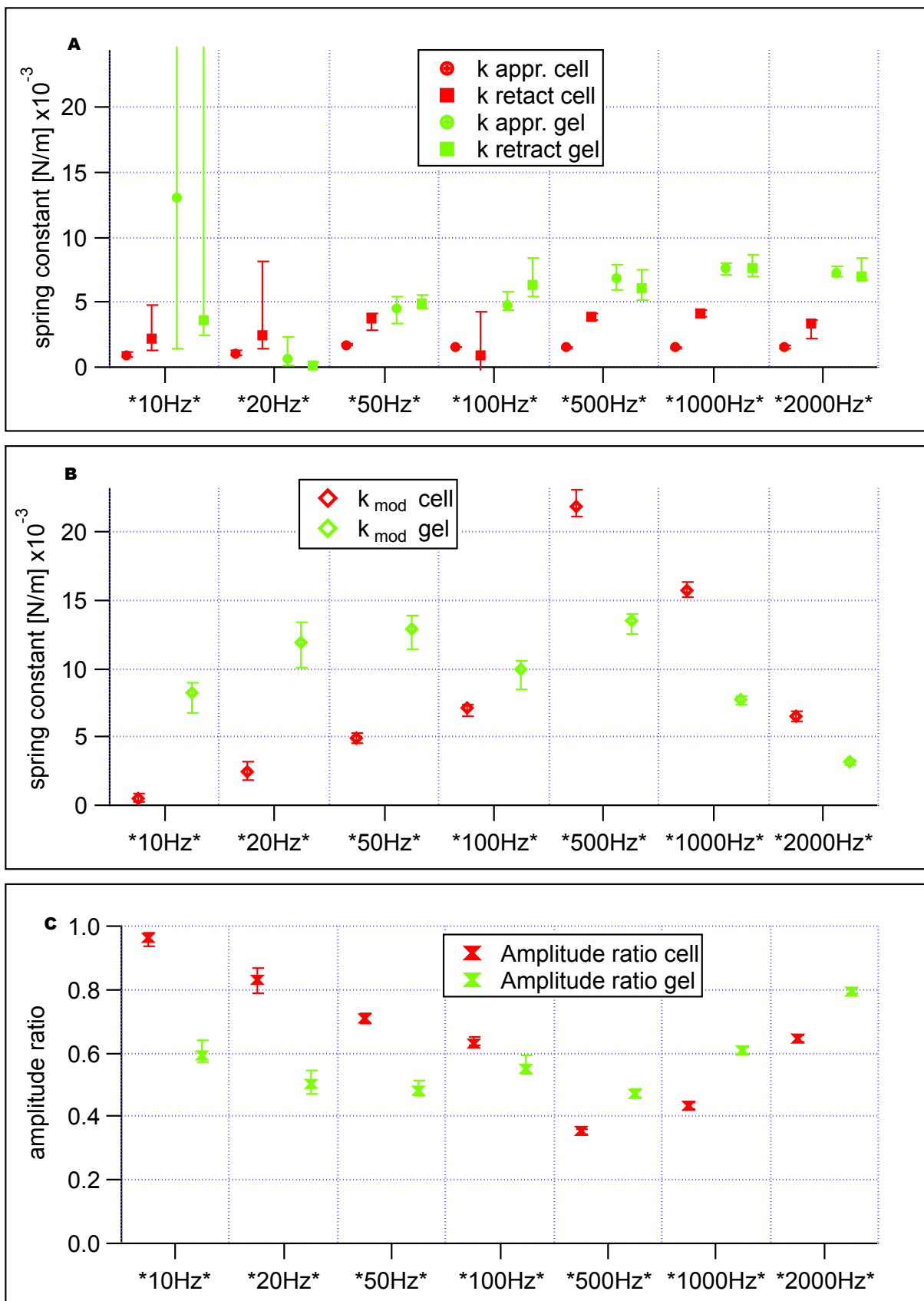


Figure 27: Experiment designed to characterize (testing) a AFM magnetic AFM force control design by force modulation experiments. The figure shows the derived spring constants (figure A and B) and the response amplitudes ratio (C) at varied drive frequencies in magnetic force to test the AFM magnetic force setup. Results represent are the median values derived from a force curve and modulated creep data over physiological relevant frequency ranges on soft samples.

## 5.0 DISCUSSION

The focus of this work was to evaluate and prove that the magnetic step setup can be employed to creep response of living cells by AFM. Two different setups for measuring the creep response have been employed. A third design was employed, the magnetic force modulation experiment for characterizing the live diseased cells viscoelastic properties, However, the focus was to perform local measurements of the creep response of the cell sample.

### *Hydrodynamic drag of cantilever*

The viscoelastic properties of cells by recording the creep response have been analysed after applying a z-step or a magnetic force step. Both types of creep data were analysed in the framework of the linear solid model (figure 9), which is a combination of two springs and one dashpot. This is the simplest model, which reproduces the observed creep response data. The AFM cantilever has been modelled just by its spring constant, neglecting hydrodynamic damping of the moving cantilever. Thus is justified to consider hydrodynamic effects of the cantilever to be small compared to the sample viscous contribution. This assumption was tested by looking at the creep response of polyacrylamide gels under the same experimental conditions. On the gel one only sees very little creep after applying a step. Some creep is visible after the approach ramp, which applies a much larger force than the subsequent steps applied here. On gels, one is not able to separate the hydrodynamic contribution of the cantilever and the viscous contribution of the sample. However, one can consider the combined viscous effect in the gel experiment as an upper limit for hydrodynamics in the cell experiments. And since this combined viscous effect is much smaller than in cells, we can safely say that the predominant viscous effect in cells comes from the sample and hydrodynamics can be neglected in cell data.

### *Error sources in step response data*

Besides systematic errors (like tip shape, changes in cells induced by temperature or pH changes, and so forth), the major experimental error will come from the accuracy of deflection calibration. By measuring force curves on the bare substrate, we have observed that variations in slope of the force curve can be around 5..10% despite the fact that force curves

on a stiff support shall have a value of 1. This problem is very serious when investigating cells, since in cell samples even bare areas of the substrate are coated to some degree with extra-cellular matrix material excreted by cells. But even on ultra-clean samples (like carefully cleaned glass slides) a similar, maybe slightly smaller variation, of slope values is observed. In these samples the effect may be due to tip contamination, stick-slip motion of the tip along the substrate, or other sources. Let's assume that the deflection calibration is off by  $p$  per cent or some factor  $e = 1 + p$  (which will typically be on the order of 0.95 to 1.05 corresponding to a 5% error). The spring constants of the soft spring AFM cantilevers (magnetic or not) have been calibrated by recording thermal fluctuations of the free cantilever, where the calibration of the power spectral density will then be proportional to  $e^2$ . The spring constant will be inverse proportional to the PSD, so it will be off by a factor of  $1/e^2$ . Any mechanical measurements, regardless whether it is based on the slope of the force curve, or step response, will eventually boil down to a relation where the sample spring constant  $k_s$  is proportional to the ratio of loading force and indentation. In AFM the indentation is given by the difference between  $z$  height and deflection. The exact relation may look different (see the analysis section), but for the sake of error propagation, one can write a kind of archetypical equation:

$$k_s = \frac{\Delta F}{\Delta \delta} = \frac{k * \Delta d}{\Delta z - \Delta d}$$

Since the change in deflection is much smaller than the change in  $z$  (in case of a  $z$  step on cells since the slope is on the order of 1/10), one can neglect the error in the denominator, so the total deviation of the elastic properties in  $z$  step will be proportional to  $1/e$ , or also  $p$  per cent.

In magnetic step,  $\Delta z$  is zero, so the errors in  $\Delta d$  will cancel, and we will end up with an error of  $1/e^2$ , which will be proportional to  $2*p$ , if  $p$  is small.

So, magnetic step response will be more prone to errors in deflection calibration. However, if calibrated cantilevers can be used, e.g. those where the spring constant had been measured with the help of a vibrometer, then the only error would be in the deflection signal, which would actually cancel. Other recent developments have also considered the dynamic AFM methods to measure mechanical properties of soft samples like the live (and or the live diseased) cells. In the dynamic methods the AFM cantilever may be excited to oscillate at or near its resonant frequency during movement. The observed quantities are the amplitude and the phase of the cantilever with respect to the excitation signal. Experimentally, many other researchers and works may perform it typically by the piezo electric element mounted on the

AFM cantilever. Typical amplitudes of about tens of nanometres are achieved. When the tip is brought near the sample, the resonance frequency of the soft spring AFM changes slightly due to increased acting between the soft spring AFM cantilever and the sample. This effect is monitored directly by monitoring the changes in the amplitude of oscillation at a fixed frequency or near the resonance peak. The amplitude of the oscillation might depend on the nature/mechanical properties of sample being studied or the distance to sample. In the dynamic mode, the interaction of the between the tip and the sample is reduced. An excitation maybe kept constant during the whole the acquisition of the force curve.

#### *Change in Contact Area during Step*

The rationale behind the experiments reported here assumes that the sample reacts linearly while applying a step. This requires that the force applied, and the indentation change resulting from that force, is small such that the mechanical properties do not change considerably. This may not always be given, especially with highly structured samples like cells. The consequence is to increase the force sensitivity as much as possible to be able to apply very small force steps. Since the main limitation in current state of the art AFMs is not instrumental noise, but rather thermal noise in the cantilevers, it is essential to use very soft cantilevers. For the cantilevers used here, thermal noise levels will be around 7 pN (see appendix). One has used here the softest cantilevers available for cell work, however it would be favourable if softer cantilevers will become available.

When applying a force step, the indentation and hence the contact area between a pyramidal tip and the sample is changing. This will lead to a change in contact spring constant. In our case a typical indentation change was 70 nm for z-step, and 30 nm for a magnetic step, whereas the indentation before the step was applied was about 700 nm in both cases. So, the change in contact area will be 10% for z-step and less than 5% in the case of magnetic step. This will lead to a systematic error in spring constant values of the sample. This situation can be improved by applying smaller steps, if force sensitivity is sufficient. Even better, is the use of blunt (e.g. cylindrical) tips, which will result in a constant contact area regardless of applied force. This has been suggested by Rico et al [229] however these tips are not commercially available despite their merits for mechanical measurements.

#### *Comparison of step response data and force curve data*

When recording a force curve one constantly changed the z height, while the sample is indented. Therefore, one basically apply a continuous series of little steps, each will cause a

relaxation over a time scale of the observed relaxation time. The observed viscous effect will be the superposition of the individual creep response, where retardation has to be taken into account. Since force-loading rate is changing constantly during the approach rate, there is no simple way to disentangle spring constants of the cell and viscous contributions in force curves. Thus, usually force curves are only analysed in terms of elastic properties, which inevitably leads to different values for approach and retract ramps, as can be seen in tables 1 & 2. Analysing step response data with the help of the linear solid model will not only result in identical spring constants of the soft sample for loading and unloading, but it also will quantify the viscous response of the sample in terms of the friction coefficient and the relaxation time  $\tau$ . This is a major improvement compared to the previous conventional way of taking force curve data and analysing them only in terms of apparent elastic properties.

The mechanical data in Table 1 and 2 agree reasonably well, as can be expected from subsequent measurements on cells. Even if technically they have been taken on the same position, there is always motion and shape changes of cells going on, so that you cannot expect exactly identical numbers here. On gels, which are stable and very homogenous, we were able to achieve results, which were reasonably close together (5-10%).

#### *Comparison of z step and magnetic step data*

In soft matter physics creep experiments are usually done after applying a well defined step in force and keeping the applied spring constant (constant stress) and monitoring the creep in strain (corresponding to indentation in our experiment), or operating at a constant strain (after applying a jump there) and following the creep response. Our experimental condition is neither constant strain nor constant stress, since both quantities (force being proportional to deflection and indentation) change. However, as long as the material acts linearly, which needs to be assumed anyhow in the framework of our analysis, we can deal with strain and stress being not constant. The analysis presented in the material methods is based on the actual experimental conditions.

Nevertheless, the magnetic force step approach was designed, to come closer to a constant stress situation. In this approach one does not change the z-height but apply an additional force directly to the tip of the cantilever by a magnetic field. However, since this additional force will indent further the sample, we also see a creep in the deflection. So, again one is not at a constant stress situation, but somewhat closer. AFM would allow keeping deflection constant by adjusting the z height of the sample. Since the response of the system is rather

slow, it would interfere with the relaxation times we observe in cells. Thus, a rather simple approach has been used in this work.

### *Multiple Relaxation times*

You would expect that complicated soft matter like the cytoskeleton of the cell will exhibit multiple relaxation times, which will be linked to different molecular or physical processes, like friction of the cytosol, like internal friction in the bending of actin filaments, or the time scale of the activity of myosin cross-linkers, just to mention a few. This will ask for a more complicated model as the general linear solid model, which will have multiple Maxwell elements, one for each relaxation time. Here, one wanted to follow Ockam's razor and try to use the simplest model, thus implementing only one relaxation time. Since this model fits the data very well, one does not see a need to extend our model, since this will only introduce additional parameters, which cannot be linked easily to molecular or physical processes. In the future, or in different experimental conditions, it may be essential to extend the model used for analysis.

When looking carefully on our creep response data (e.g. in figure 15 and 16) we can clearly see evidence of slower (beyond 0.5s) and faster timescales (below 10 ms). For the very slow processes, it is probably more appropriate to term them active motion or shape changes of the cell, than mechanical creep. They are not caused by the step applied to cell, but occur always in a more random or not predictable fashion as would be expected from active cellular processes. So, one did not follow and record the processes over longer times than 0.5 seconds, since they are due to other processes. The faster processes, which are visible where the exponential fit does not match nicely the data for times close than 5ms to the step, may very well be analysed within the framework of mechanical response of the cells. However, since our soft cantilevers have response times on the order of 1 ms, one do not have the appropriate time resolution to analyse these processes. This, in essence, lead one to focus only on a single exponential fit.

### *Comparison with other data*

The focus of this work was to evaluate two different schemes for measuring the creep response of living cells by AFM. Therefore, we have presented our results as model free as possible, i.e. using the simplest mechanical circuit, which needs to be employed to describe our data. Calculating spring constants of the cell or gel (and dynamic viscosities) will reflect to some part sample properties, but will also depend on tip geometry, or more precisely to

contact area. In conventional force curves, usually the Hertz model (or its variants) is used to get the material's properties (like Young's modulus) from the raw data. This can also be done from step response data, and will be reported in another publication [48]. However, since the Hertz model requires several assumptions (homogeneity, isotropy, linearity of the material, large thickness of sample), which are all questionable to some degree, one would rather omit these issues here in the context of this work. Along the same line, in cell rheology often more complicated models as the standard linear solid model are used, e.g. power law behaviour. Again, this applies to assumptions; specifically here a power law behaviour can be expected by the superposition of an (infinite) number of relaxation processes, each of which will be characterized by its own spring constant and relaxation time. There will be a general relation between the relaxation time and the length scale of these modes, both increasing in a correlated fashion. One believes, that in the data, since we are measuring the slowest modes of cellular mechanics, one is at the extreme end of a (otherwise) continuous spectrum, and thus the application of a power law behaviour may be questionable again.

In future work, one will look into differences in visco-elastic properties of cells and to elucidate the role of certain molecular components of the cytoskeleton (actin, myosin, cross linkers, adhesion sites) and their role in viscoelasticity.

## 6.0 CONCLUSIONS AND OUTLOOK

In this work the viscoelastic properties of live cells with a new experimental approach inspired by polymer rheology has been measured: steps in forces either induced by changing the sample height or applying a magnetic force to the end of the cantilever. Although both approaches are not equivalent with constant strain or constant creep response experiments used in soft matter physics, they can be analysed in the framework of linear elastic theory to yield elastic and viscous properties of the sample. This is a major improvement in comparison to standard force curves, which clearly show the influence of viscous properties, by the difference of approach and retract curves, however usually they are not (cannot easily be) analysed to include this viscous response. If analysed in the standard way, the spring constants derived from force curves will deviate for loading and unloading, and shall rather be called apparent spring constants. The spring constants of the cell and the viscous properties derived from the loading and unloading step are identical, even with experimental errors, and thus reveal in quantitative and reliable manner the true viscoelastic properties of cells.

Although it has been shown in this work that soft magnetic cantilevers could be employed to measure the viscoelastic creep response of the soft samples like cells accurately the work will be improved if different a forms of magnetic materials will be employed in the future. For the controlled movements of the loading and unloading step forces in magnet the soft spring cantilevers have been made more sensitive by equipping them with permanent magnetic fragments to measure the creep response of the live cells and polymer gels. However the magnetic step response AFM experiments performed in this work have not been achieved with the available smallest ferromagnetic materials. The geometries of the magnetic fragment glued to the back of the soft spring cantilevers typically unknown, which leads to complications in the orientation of the step forces in magnet especially the mechanical properties. These magnetic responses for the various cantilevers differ greatly in strength. However, the results in this work demonstrate the usefulness revealing the creep response while employing the soft spring magnetic cantilevers to loading and to unload the of cell samples. The current work has not been performed with the smallest available ferromagnetic materials. There is lack of information about the spring constant and the mass of the

employed cantilever. One will like to employ for the future preferably a smaller ferromagnetic particle in the order of a micron. As a good alternative magnetosomes could be employed because they are small and they are closer to a perfect ferromagnetic material. For this reason the soft spring cantilevers could be prepared in the future with the magnetic materials like the magnetosomes.

More interestingly, the Hertz model could be included to the mechanical equivalent circuit presented in this work in a future work to fit the material properties. Here it might prove to be more useful.

## APPENDIX

This section is the appendix and the chapter aims to provide a brief overview to our understanding of biomechanics with respect to my AFM experiments of the soft samples presented in prior sections.

The PRO-deficient cells were softer, which was attributed to remodelling of the cell cytoskeleton. As a consequence of increasing knowledge on the viscoelastic properties of cells and tissues [101] the idea of mechanics in diseases evolved. The earliest implementation of this idea was the evidence that cancer cells tend to be softer than normal cells by Lekka et al. [17]

Elastic materials typically deform instantaneously in response to external forces and immediately recover their initial shape when unloaded. Moreover, these materials show time-independent mechanical behaviour with no energy dissipation. On the other hand, the application of a constant shear force to a fluid induces constant velocity flow and energy dissipation. Although cell and tissue mechanics are usually studied assuming that they are elastic materials, they exhibit many viscoelastic features. Materials exhibiting both solid- and liquid-like features are known as viscoelastic materials. The cell elasticity could typically be understood in terms of the cytoskeletal dynamics where a number of cross-links, rearrangements and deformation and stress will affect the elastic properties of the cell. On the other hand the viscosity can typically be understood as the internal friction that occurs when all the components in a flowing liquid are forced to slide along each other.

I will give a brief overview the main operational principles, the capabilities and the application of the force modulation mode, to characterize mechanical behaviour in disease. A simple model to characterize mechanical linear viscoelastic behaviour of soft samples was presented in the previous chapters of this work.

## A1.0 Spring constant of the sample derived from force curves

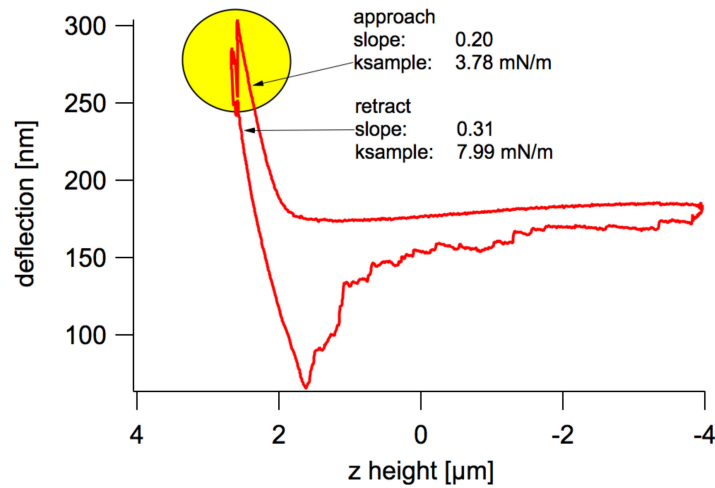


Figure 28: Force curve on a cell while at maximum force a z step is performed (see yellow circle). The figure shows the same data as in figure 16, here in the conventional scheme of deflection versus z height as is usually done in force curves. The slopes and the corresponding spring constant of the cell sample, which can be calculated from the approach and retract part of the data are also indicated in the annotation

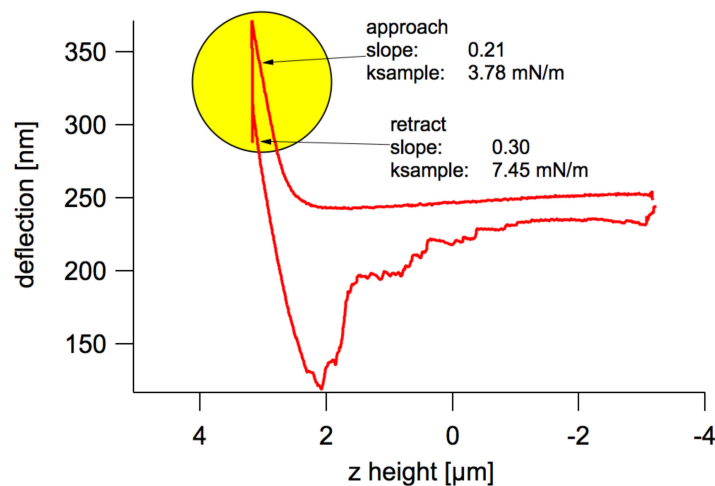


Figure 29: Force curve on a cell while at maximum force a magnetic step is performed. The figure shows the same data as in figure 17, here in the conventional scheme of deflection versus z height as is usually done in force curves. Since in a magnetic step, only the deflection changes due to the magnetic force (z is kept constant) the effect of the step is harder to see than in fig 17. The slopes and the corresponding spring constant of the cell sample, which can be calculated from the approach and retract part of the data are also indicated in the annotation.

### A2.0 Analysis of Creep response Data from z steps and magnetic step on gel sample

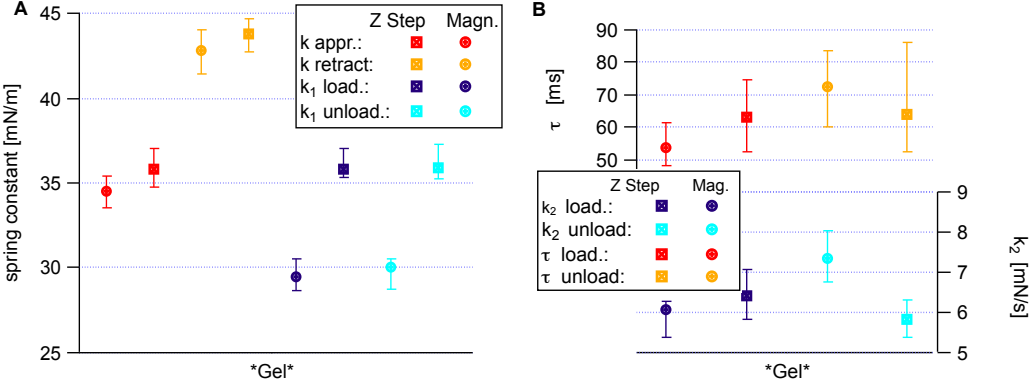


Figure 30: Analysis of step response data on polyacrylamide gels. Panel A shows a comparison of spring constant values calculated from approach and retract curve with the spring constant  $k_1$  values from step response. Panel B shows the creep response time and the spring constant of the sample  $k_2$  values. All values are very close for loading and the unloading, except the approach and retract data calculated from the force curves, as expected.

### A3.0 The magnetic force in modulation of the live cell sample

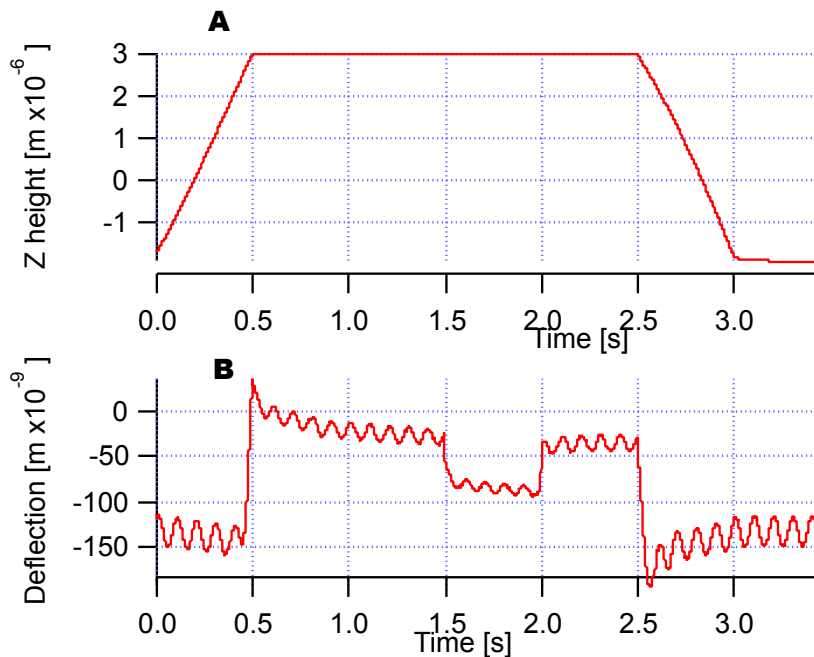


Figure 31: Schematics of the viscoelastic measurement of soft samples via modulation of the magnetic cantilever tip position with the magnetic force microscopy. The modulation of the cantilever around an equilibrium indentation leads to a modulation of the force between the AFM cantilever and the soft sample. Similar to a constant strain experiment in which the z-height is kept constant for  $t=2$  seconds of the approach ramp, except  $t=1.5$  s a jump in the modulation force with an amplitude is applied to the viscoelastic sample by the magnetic cantilever which leads to a modulation indentation with the same frequency. The contact force will oscillate around the equilibrium indentation depth. This results in an effective oscillatory response of the viscoelastic sample. The magnetic force modulation is directly applied to the soft spring magnetic AFM cantilever for duration of 3.5 seconds (B). The magnetic force modulation experiment enabled the drive signals to be directly related to the force and the response of the magnetic cantilever. The amplitude and the phase shift (fitting parameters) between the drive signals and the response due to the sample could be analysed in terms of a linear viscoelastic theory. The time scale is defined by the modulation frequency due to the sample. By observing the response at a range of frequencies the relative contribution of the elastic and the viscous response can be characterized at varied time scales. The effective modulation spring constant is an indicator of the overall viscoelastic property of the sample. The force modulation may reveal a set of material responses over specific frequencies.

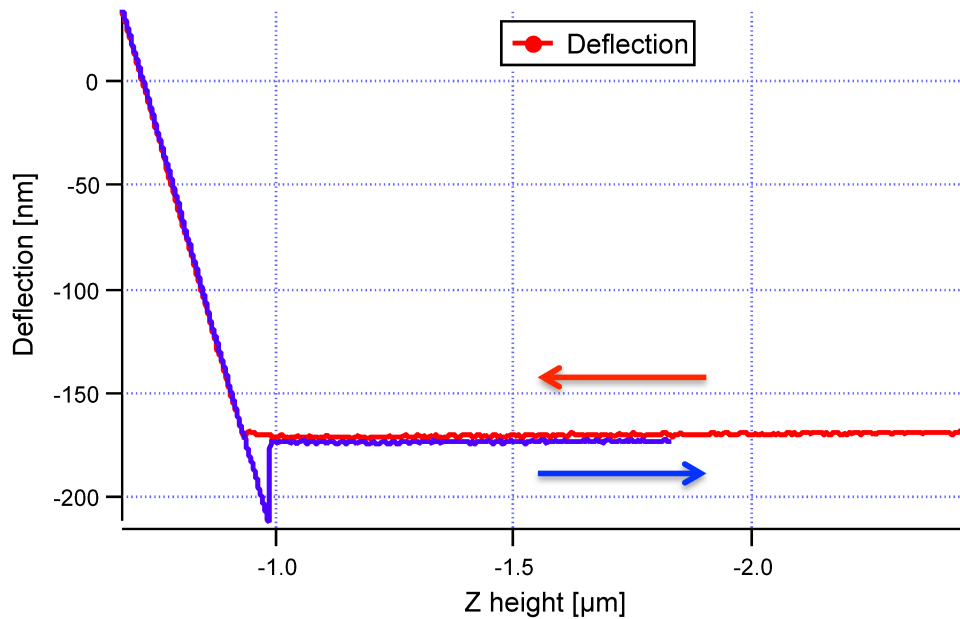


Figure 32: Calculating the inverse optical lever sensitivity (InvOLS) by obtaining force curves on stiff substrate. Force curve at maximum force performed on clean petri dish substrate in air. The force curve contains information about the long- and the short ranged interaction and also represents the basis for estimation of the Young's modulus of the sample [Pa] to estimate the InvOLS of the system. Calculating the InvOLS typically requires that a force measurement be performed on a hard surface to measure the voltage response of the PSD as a function of the known distance moved by the z-piezo. A resistive force on the stiffer substrate determines how easy the deformation may be performed by the soft spring magnetic AFM cantilever during testing phase. The force curves were obtained on an area of 600 nm x 600 nm. The soft spring magnetic cantilever is subjected to the change in the orientation by the application of an external force.

### A3.1 Calibration of the deflection sensitivity of the optical lever system

The thermal method based on the optical lever system requires the accurate calibration of the deflection sensitivity; since the latter parameter enters as a square in the formula for the spring constant, a small relative error in the deflection sensitivity leads to a twice as large relative error in the value of the spring constants of the AFM (magnetic) cantilever. The main parameters for the conventional scheme in AFM experimentation are: 1) z-piezo displacement sensitivity: this parameter converts the z-stage position to the specific output of the microscope software to nanometres (nm). As an example, if the microscope yields the z-height values in micrometres ( $\mu\text{m}$ ), in the special AFM modes, the microscope produces the z-height values expressed in piezo stage steps. In this case, the correct parameter will be the calibrated nm per step value. 2) The AFM soft spring cantilever's spring constant ( $k_c$ ): The exact value of the spring constant of the AFM cantilever used in the experiment, expressed Newton per meter (N/m) is required quantity to be known in all experiments. During the experimentation, this value is typically estimated while taking account of the geometric properties of the soft spring cantilever or by measuring the resonant frequency of the AFM cantilevers by the manufacturers plan sheet. 3) Deflection sensitivity ( $S$ ): The deflection

sensitivity parameter depends on the position sensitive detector and on the optical alignment of the laser on the AFM cantilever. To calculate the sensitivity, one is required to obtain force curves on a stiffer and then calculate the slope (measured in V/nm) of the approach regime of the force curve. 4) The magnetic sensitivity: The deflection of the free soft magnetic AFM cantilever to a loading force in magnet in combination with their measured spring constant values gives the force applied per volt through the prepared magnetic coil. The system was first calibrated at low frequencies in the quasi-static operation to set the ratio between the force in magnetic and current through coil in an inhomogenous magnetic field. The behavior of all magnetic fragments under a small magnetic force and their tiny aggregates in a suspension were tested and additionally revealed under the light microscopy. By observing the induced motion of due to the local field generated gradient of the coil on the magnetic cantilever and the beads, the system was analysed and characterized adequately.

The calibration of the deflection sensitivity,  $S$ , is typically performed by making contact with the AFM tip on a very rigid surface and collecting a series of raw photodiode signal versus z-piezo displacement curves (e.g., see figure 31). Assuming that neither the tip nor the surface are deformed, the deflection sensitivity is calculated as the inverse of the mean slope of the contact region of the  $\Delta V$  versus z-height or equivalently as the mean of the inverse slopes, which leads to the same relative error.

### A3.2 Calibration of the optical lever deflection sensitivity of the magnetic force AFM.

To avoid many possible artefacts encountered during experimenting in the conventional contact method to determine the deflection sensitivity, a contactless approach is suggested. Amongst many other approaches, this approach is based on the same assumptions that the thermal noise procedure directly provides the spring constant rather than the parameters of the simple harmonic oscillator (SHO) fit. If an incorrect value  $S_{temp}$  of the deflection sensitivity is used, an estimation of the spring constant  $k_{temp}$  will be obtained. The correction factor  $\lambda$  for the deflection sensitivity, such that:

$$S = \lambda^2 \sqrt[3]{k} \tag{A3.1}$$

Could be calculated as

$\lambda = \sqrt{\frac{k_{temp}}{k_{tre}}}$	A3.2
---	------

Where in the above equation,  $k_{true}$  in the denominator is the known true value of the intrinsic spring constant of the soft spring AFM cantilever, which is, a value obtained by means of an accurate calibration method. Acquisition of the thermal spectra while experimenting and calculation of the deflection sensitivity with the above equations was used in this work in order to monitor possible variations of the deflection sensitivity due, for example, to the displacement of the laser on the back of the soft spring AFM cantilever.

#### **A4.0 The mechanical properties of the soft samples from force modulation experiments**

The mechanical properties of the soft samples like cells will be briefly described, based on the force indentation curves and modulating the sample by application of a modulation (sinusoidal) loading and unloading force. The spring constants of the live cells can be calculated from the force curves by fitting the conventional AFM data to the Hertz model. This method has been widely applied to test the mechanical properties of the live cells and the tissue despite some limitations like the uncertainty in determining the contact point of the force curves, or whether the Hertz model could be applied and the possibility to damage or kill the live cells while experimenting. [20]

A design to characterize the viscoelastic response (mechanical properties) of the soft samples like the gel has been the magnetic force modulation design. The purpose of employing the broad range of the modulation frequency was to identify the optimal range of settings for the adhesion data on soft samples if steric repulsive polymeric forces are visible on the approach and the retract curves. The magnetic coil and the magnetic AFM soft spring cantilevers for the direct force application employed in this work have been explained before. Briefly, the AFM cantilevers employed were prepared by gluing a magnetic fragments on the very end of the back of the cantilever. This was an advantage. Usually the magnetic moment including the magnetic strength of the newly prepared AFM cantilever cannot be determined or known at time of my routine preparation. The alignment of the laser beam on back of the employed soft magnetic cantilever and the coil sharp tip position were left unchanged during the entire experiment and after the calibration. The spring constants of the cantilever were calibrated using the thermal noise method. The calibration of the magnetic sensitivity required a calibrated magnetic cantilever usually by the thermal tune method and the correction of the PSD sensitivity. Subsequent attempts to experimentally measure the modulated spring constants of the samples and the viscous properties along the direction of the force application

direction on the soft samples revealed inconsistencies in the derived numbers. The force and the spring constants of the soft samples have been monitored by monitoring the modulated tip end of the magnetic cantilever. However, to validate whether the magnetic coil could be employed in the future to characterize the viscoelastic properties of the soft samples, the force modulation experiments have been initially performed for a broad range of low frequencies on the live cell and the polymer gel samples respectively.

With the force modulation one applies the constant amplitude of modulation by the magnetic cantilever driven by external fields. Here  $F_{drive} = F_B e^{-i\omega t}$  is the driving magnetic force acting on the soft spring magnetic cantilever. The model equation to describe the soft spring magnetic AFM cantilever motion is:

$$m_0 \frac{d^2 d(t)}{dt^2} + k_c d(t) = F_{contact} + F_{visco} \quad A4.1$$

The corresponding time dependent cantilever deflection signal is  $d(t) = d + A e^{i(\omega t + \phi)}$  where  $\phi$  is the phase lag while taking into account the internal viscosity of the soft sample. The sample indentation is obtained by  $\delta(t) = z(t) - d(t)$ , is the oscillating quantity in contact with the viscoelastic sample described in an approximated form by  $\delta(t) = \tilde{\delta} e^{i\omega t + \phi}$  due to the oscillating magnetic field at equilibrium. Following the approximation in the system, at each position there exist a mechanical equilibrium of in the system of the cantilever force  $F^c$  and the sample force  $F^s$ , which a function of sample indentation:

$$F_{(z_i)}^c = k_c * d_i = F_{(z_i)}^s = F_{(\delta_i)}^s = F_{(z_i - d_i)}^s \quad A4.2$$

The contact force oscillates around the equilibrium indentation on the viscoelastic sample. In our formalism the sample force  $F^s$ , depends in a non-linear fashion in indentation, because the contact force will be a function of indentation and the sample's mechanical properties may change as a function of indentation. Thus we observe a change in deflection signal and the indentation, by:

$$\Delta F^s = F_{(\delta_2)}^s - F_{(\delta_1)}^s = F_{(\delta_1 + \Delta\delta)}^s - F_{(\delta_1)}^s \quad A4.3$$

The sample force  $F^s$  depends in a non-linear fashion on indentation. The contact force  $F_{contact}$  will be a function of indentation and the sample's mechanical properties may change as a function of indentation. Noting that  $k_s \cdot d(t) = F_{contact}$ . This leads to an alternative form by:  $F_{contact}(\delta) \approx F_{contact}(\delta_0) + F'_{contact}(\delta_0)(\delta - \delta_0)$ . Linearizing the change in the sample force gives the relation where the force and the displacement amplitudes and the harmonic frequency of the applied force are measured by the indentation which subsequently gives quantities that are used to determine the spring constants and the viscous values of the viscoelastic sample in a simple general form by:

$$\Delta F^s = F^s_{(\delta_1+\Delta\delta)} - F^s_{(\delta_1)} = F^s_{(\delta_1)} + \frac{\partial F^s_{(\delta)}}{\partial \delta} * \Delta\delta - F^s_{(\delta_1)} \quad A4.3$$

The oscillatory strain response at the same signal from the oscillating magnetic field (input magnetic in put frequency,  $\omega$ ) is fitted numerically. With the phase angle  $\tan \phi_n = I_m [A_n]/R_e [A_n]$  and the approximations after the relaxation to the general phase shift relation in the CM2 approach given by:

$$\tan \phi_n \approx \phi_n = \frac{b_n \omega}{\omega^2 - \omega} \quad A4.4$$

For small angles this phase shift provides a measure of the solid-like and liquid-like behaviour of the soft sample. At a given frequency the dynamics or the oscillatory force will cause an oscillatory strain response at the same frequency. The oscillatory force lags behind the phase angle by a measurable quantity  $\phi = \phi_1 - \phi_0$ . The measurable quantity is related to the internal viscosity of the sample. The differences between the motions of the magnetic cantilever on the viscoelastic samples are the amplitudes and the changes in the resonant frequency ( $\omega_0 \neq \omega_1$  and  $\phi_0 \neq \phi_1$ ): However, to estimate the spring constants of the cantilever we simplify both free and in-contact motion by a simple arrangement of springs.

$$k_s = -\frac{A_0 k_c}{A_1} - k_c = +k_c \left( \frac{A_0}{A_1} - 1 \right) \quad A4.5$$

Typically in the conventional AFM approach the maximum force is measured and not the maximum indentation which requires attention during the analysis. To estimate  $F'_{contact}(\delta)$ , we may choose the Hertz model for the pyramidal indenters with the following relation by:

$$F_{contact} = \frac{1}{\sqrt{2}} E' \delta^2 \tan \theta \quad A4.6$$

Here in the former equation  $A_0$  denotes the free amplitude and, as introduced above  $A_1$  is the amplitude as a function of AFM cantilever surface distance.  $E'$  is the reduced Young's modulus of the system,  $\delta$  the measured indentation. Integrating this relation yields the general equation shown below as:

$$k_s = -k_c \int \left( \frac{A_n}{A_{n+1}} - 1 \right) dz + konst \quad A4.7b$$

Where „*konst*“ denotes the force at the point where the force modulation the analytical integration began

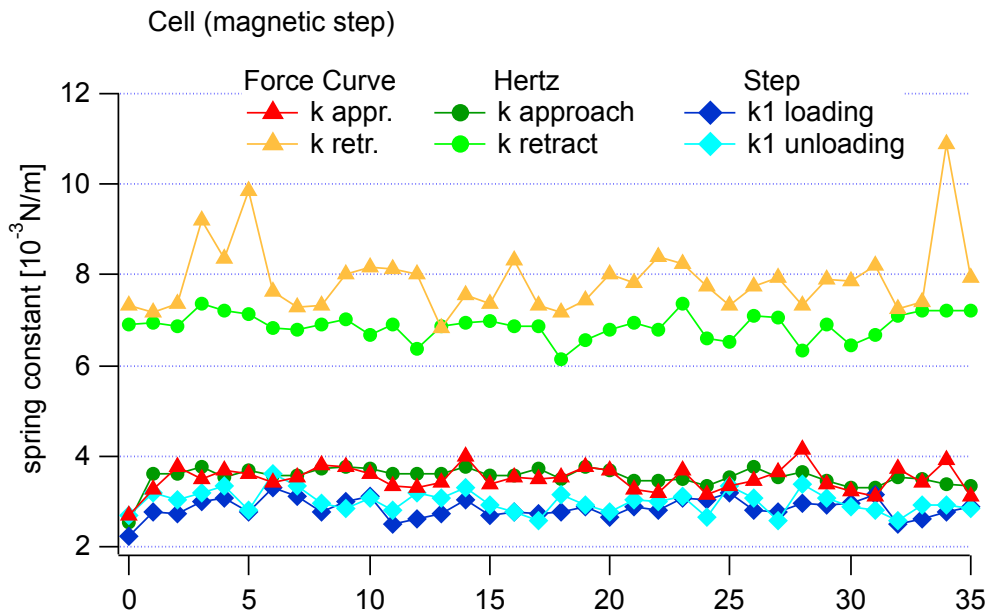


Figure 33: Comparison of the spring constants values of the live cell sample calculated from force curve data (k appr. and k retr. are the values from the corresponding branch of the force curve) and from the branch of magnetic step response data (k<sub>1</sub> loading and unloading steps). The spring constant (k approach and k retract) derived by analysing the magnetic step response data at an average magnetic force step is shown for a visual comparison demonstrative purposes. The graph is a compilation of all 36-force curves from a 6 by 6 force volume over an area of 600nm.

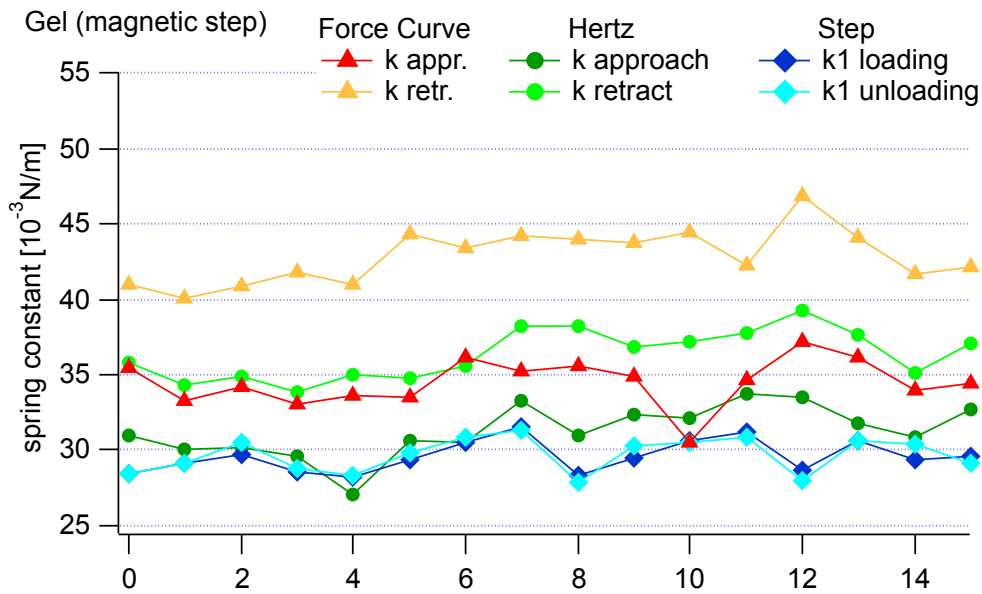


Figure 34: Comparison of spring constants values of the stiffer polymer gel sample calculated from a force curve data and from the magnetic step response data. The spring constants calculated from the force curve data (the spring constants  $k_{\text{approach}}$  and  $k_{\text{retract}}$  are the values from the corresponding branch of the force curve) at an average force step and from the magnetic step response data ( $k_1$  loading step and unloading step). The spring constant ( $k_{\text{approach}}$  and  $k_{\text{retract}}$ ) derived by analysing the magnetic step response data at an average magnetic force step is shown for a visual comparison demonstrative purposes. The graph is a compilation of all 14-force curves from a 4 by 4 force volume over an area of 600nm.

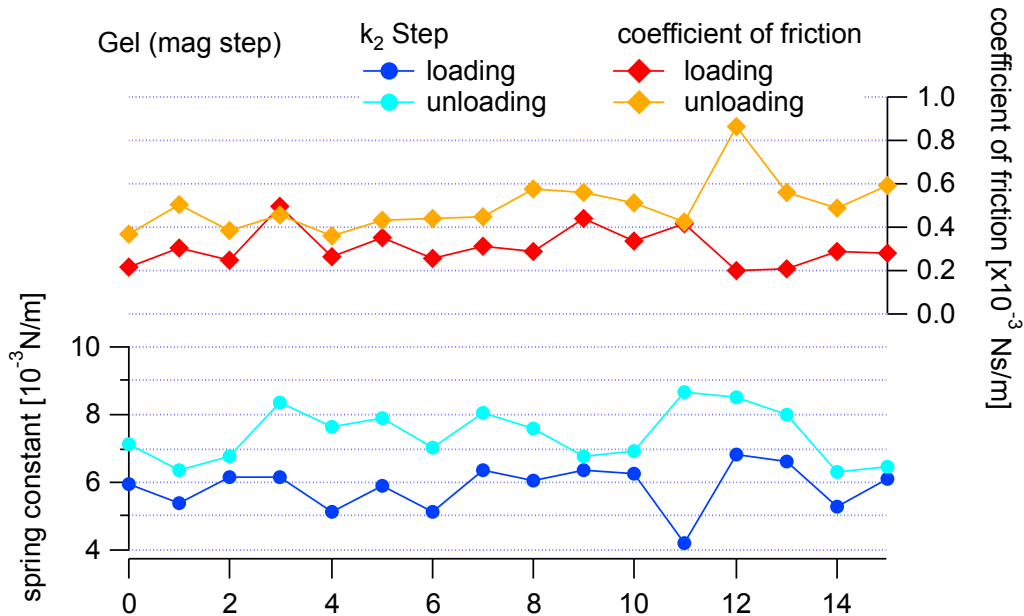


Figure 35: Summary of viscous properties derived by independently analysing gel data from the magnetic step response data. The upper panel shows a comparison of the coefficient of friction values from magnetic step response. The lower panel shows the spring constant  $k_2$  values. All values are very close for unloading as expected.

The force measurements of viscoelastic samples like live cell in its natural environment which mimicking by magnetic step AFM and force modulation is one of the key improvements because quantitative analysis could be made and it allows experimenters to make more objective conclusions about the sample under study. Viscoelastic properties of the soft samples like cells are least understood of all the mechanical properties of the polymers because measurements are typically characterized by elastic and the viscous contributions. Extracellular matrix regulate their size and shape as a result of constantly modulating the local mechanical demands on the soft samples they compromise. It is widely accepted by many researchers in literature that in response to the external mechanical forces, soft samples like cells exhibit a viscoelastic phenomenon such as creep or stress relaxation. [230] These living cells may be considered as soft materials whose rheological properties respond rapidly and reversibly by the application of a loading force [198]. They will exhibit a fast continuous motion and a shape change that sets them apart from other biomaterials like polymer gel thus more sensitive.[231] [202] The cells will therefor have to rely on their viscoelastic properties and deformation behaviour for its survival and proper regulation of a many biological processes at the molecular and cellular levels in the human body. These important characteristics result from coordinated changes in the actin cytoskeleton, which is a scaffolding material that provides mechanical and structural properties required for live cells, that extends from the cells external environment and the underlying actin cortex to deep within the cell. From a biomechanical point of view of interest are also the fibrillar collagen (collagen fibrils type III) typically found in elastic tissues. However, the viscous contributions of the soft samples like live (and diseased) cells are largely ignored, mainly because of technical, instrumental, or analytical limitations.

In the following sections, brief descriptions of the cell structural components will be presented.

### **A5.0 Cytosol and Cytoskeleton**

Each cell is surrounded by a cell membrane that separates the cell interior from the surrounding microenvironment. It is not only a structural scaffold within which cells are embedded but also contains various proteins, proteoglycans, and other molecules that participate in distinct cellular functions like adhesion or migration. The cell membrane consists of a double layer of phospholipids in which proteins are embedded. The interaction of the cell with the ECM mainly happens through the action of integral (going across the cell

membrane) and peripheral (attached to the outer side of the cell membrane) proteins regulating the transport of substances to and from the cell. All intracellular organelles are embedded in the cytoplasm filling the cell interior. The cytoplasm contains two elements, that is, the cytosol (a liquid fraction) and the cytoskeleton (a network of protein filaments).

The cytosol is the intracellular fluid comprised of water, dissolved ions, large water-soluble molecules, smaller molecules, and proteins. Within it, multiple levels of organization can be found. These include concentration gradients of small molecules such as calcium, large complexes of enzymes that act together to carry out metabolic pathways, and protein complexes such as proteasomes that enclose and separate parts of the cytosol.

Adherent cells are anchored via focal adhesions to the extracellular matrix, which is essential for force transduction, cell spreading, and migration. Focal adhesions consist of clusters of transmembrane adhesion proteins of the integrin family and numerous intracellular proteins, including talin and vinculin. They link integrin to actin filaments and are key players of focal adhesions that build up a strong physical connection for transmitting forces between the cytoskeleton and the extracellular matrix. These proteins consist of a globular head and a tail domain that undergo conformational changes from a closed, auto-inhibited conformation in the cytoplasm to an open, active conformation in focal adhesions, which is regulated by phosphorylation.

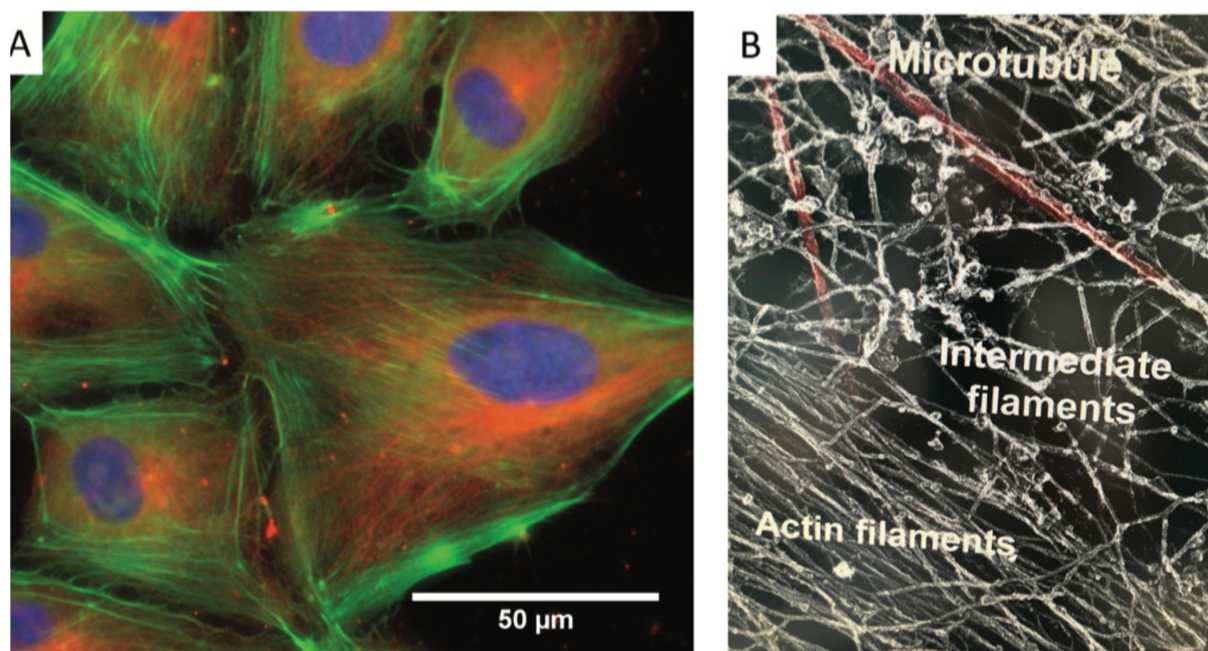


**Figure 36: A network of fibrillar proteins (A) organized into the filaments and the tubules. The distributed cytoplasmic structural actin network is formed by cross-linked actin fibers. The inter-linked polymeric protein filaments (actin filaments in green) and the tubules (highlighted in red) extend throughout a cell cytosol (the blue dots are the cellular nuclei). An electron micrograph shown on (B) shows three filament types.**

## A5.1 The cytoskeleton

The network of fibrillar proteins in eukaryotic cell sample is called the cytoskeleton and they form higher order meshes and bundles that endow individual cells with their ability to sustain external mechanical forces. The cytoskeleton is highly dynamic, and a multifunctional network that connects all compartments of the cell in a three-dimensional space. This intracellular network provides eukaryotic cells with structural support to maintain cell shape and directional locomotion. At the same time, it provides the opportunity for active, directed transport, such as organelles or the separation of chromosomes in mitosis. Three cytoskeletal proteins are of specific interest to cell mechanical properties. In addition to actin fibers (7 nanometers thick), the cytoskeleton consists of two other types of protein filaments, microtubules (fibers at about 23 nm), and intermediate filaments (Ifs, about 8-12 nm wide). All three comprise dynamic protein components that polymerize into spiral-shaped fiber bundles. Actin filaments (F-actin), with their flexible, double-helical structure of polymerized globular monomers (G-actin) have a diameter of 7–9 nm. The properties of the cell are largely determined by their morphology and maintenance like the cell shape, size during cell growth and cell division. In addition to its important role in eukaryotic cells, actin network growth across organisms highlights its versatility and robustness as a cellular mechanism to generate forces and drive cellular movement.

The actin is the most abundant proteins in eukaryotes that form polarized filaments that interact with an array of annularly proteins. Microfilaments or the actin filaments are polar structures composed of globular molecules of actin arranged as a helix and account for many mechanical properties of the cytoplasm (the liquid part of the cytoplasm, a viscoelastic material). They are the smallest protein fibers in the cytoskeleton, about 7 nanometers thick, making them the thinnest filaments in the cytoskeleton. Microfilaments, aid in cytokinesis, which is the division of a cytoplasm of a cell when it is dividing into two daughter cells, in cell motility and allow single-celled organisms like amoebas to move, as well as being very involved in cytoplasmic streaming, which is the flowing of cytosol throughout the cell. Cytoplasmic flowing transports nutrients and cell organelles.

Microfilaments are also part of muscle cells and allow these cells to contract, along with myosin. Actin and myosin are the two main components of muscle contractile elements. In tissues, actin structures are responsible for the polarity of the cells and the cohesion of the

epithelial cells or serve as mechanical support for microvilli on the cell surface. During cell division, actin is used in the form of contractile rings to cut off daughter cells from each other. In the role cell motility, the assembly and disassembly of actin regulate filopodia and lamellipodia at the cell front of migrating cells, and forces are generated by ATP hydrolysis of the myosin motor proteins at actin fibres. Several actin-binding proteins precisely regulate the growth and the branching of Filamentous actin. They are found below the plasma membrane as a network (cortical actin) and also in the cytoplasm as discrete fibre bundles (stress fibres) starting from adhesion complexes to the membrane. This type of filament also shows orientation, as polymerization takes place at both ends, but at different rates. Actin plays a role in the biochemical network organization with consequence for viscoelastic properties of the cytoplasm and the mechanical integrity of the cells and tissues.

**Microtubules** are the largest of the cytoskeleton's fibers at about 23 nm. They are hollow tubes made of alpha and beta tubulin. Microtubules form structures like flagella, which are "tails" that propel a cell forward. They are also found in structures like cilia, which are appendages that increase a cell's surface area and in some cases allow the cell to move. Most of the microtubules in an animal cell come from a cell organelle called the centrosome, which is a microtubule-organizing centre. The centrosome is found near the middle of the cell, and microtubules radiate outward from it. Microtubules are important in forming the spindle apparatus (or mitotic spindle), which separates sister chromatids so that one copy can go to each daughter cell during cell division. They are also involved in transporting molecules within the cell and in the formation of the cell wall in plant cell.

**Intermediate filaments** are about 8-12 nm wide; as the name reads the intermediate because they are in-between the size of the microfilaments and the microtubules. Intermediate filaments are made of different proteins such as keratin (found in hair and nails, and also in animals with scales, horns, or hooves), vimentin, desmin, and lamin. All the intermediate filaments are found in the cytoplasm except for lamins, which are found in the nucleus and help support the nuclear envelope that surrounds the nucleus. The intermediate filaments in the cytoplasm maintain the cell's shape, bear tension, and provide structural support to the cell.

In eukaryotic cells, the cell shape is important for the functioning the single cell and tissues that they form. This makes it interesting to study. The shape of the given cell can be thought of as governed by extrinsic forces, the mechanical properties of its constituent components

and the intrinsic forces generated by the cell which both are cell shape determinants, the mechanics including the intracellular spatial organizations.

From a mechanical perspectives actin filaments are semi flexible on length scale of the cell, having persistent length in the order of the cellular length ca. 20 microns. Furthermore, the actin filaments are highly dynamic and rapidly re-organize enabling the cell to migrate and change its shape. Despite their flexibility and the high turn over rate, actin has long been known to be vital for cell mechanically.

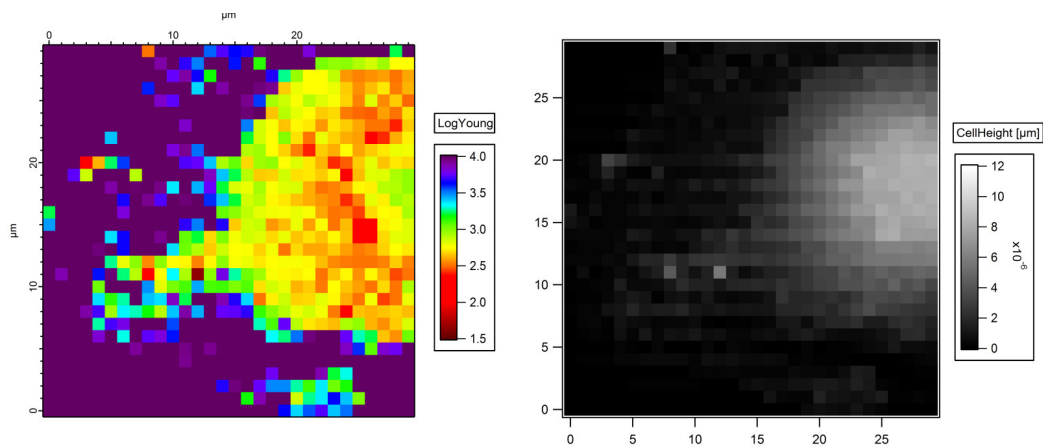


**Figure 37:** Image shows an elastic modulus image (array of elastic force curves at different sites on the soft sample) acquired by indenting a living cell. Morphological changes in the live cell characterized by the variation in the elastic modulus in its natural environment. The cytoskeleton is related to the cell shape, the change of this shape and the migration of the cells. The array of elastic values of the sample is calculated from the z-height base movement and the measured deflection of the soft spring constant values. The elastic modulus of the FM was calculated by employing the Hertz model. The left panel show the measured height data of the cell sample with the small variation of the surface height.

The ability for the actin cytoskeleton to sustain mechanical stress is therefore not strongly influenced by a single filament rigidity but a consequence of the higher lever structures that the form and their polymerisation dynamics. The microtubules typically form hollow tubes based on spiral like assembly of the tubules heterodimers in a GTP dependent manner. Microtubules have the ability to engage motor proteins, which are the force generating molecules that either move cargo along the filaments or move the filaments in relation to each other. Cytoskeletal motor proteins have been characterized into 2 groups including myosin, which form dynamic assemblies with the F-actin and the kinesin and dynein, which associate with microtubules. Unlike actin filaments, microtubules, IF do not interact with specialized groups of motor proteins. Cytoskeletal aspects are an integral to many aspects of the cellular homeostasis and their function is independent on regulatory signals network and accessory proteins that link them to cellular components. The eukaryotic cells perform a wide range of

complex reactions/functions to maintain tissues, and for the ultimate well being of the whole organism. For this purpose, the various intracellular processes and biochemical reactions are tightly controlled and integrated. The division of a cell into two daughter cells is a typically example of the orderly occurrence of an integrated series of cellular reactions.

Apoptosis is typically referred to as the programmed cell death in the literature. This occurs when the cell has fulfilled its biological functions. Apoptosis may be regarded as a natural cell death and it differs from the cell death caused by injury due to radiation, anoxia etc. Programmed cell death is a highly regulated process. A wealth of recent research has shown that cells are able to sense mechanical signals and forces in their environment. The mechanical properties of culture substrates determine cell differentiation and fate. Cells tune their mechanical properties to match that of their substrates and migrate towards particular conditions. The importance of sustaining, generating sensing mechanical forces at cellular level is brought largely into context when examining diseases that target the cytoskeleton. Genetic disorders that disrupt the cytoskeleton or the binding of actin to membrane of RBC lead to abnormal cell shape and compromised functions in disease such as malaria and sickle cell. Many recent clinical examples and the literature suggest that changes in cell rheology may have consequences for health in patients in constant mechanical stress from their external environments and they have shown a property to deform and an ability to squeeze through tissue matrix to access the circulatory system and subsequently move through small leaks in blood vessel walls. The ability of blood cells (neutrophils), a cascade of events, which involves several different types of cell adhesion molecules, ensures the attachment of the blood cells to the walls of blood vessels and subsequent penetration will occur only at sites where leukocyte invasion is required. When the neutrophils interact with an inflamed venule endothelium, an interaction occur between other molecules on the surfaces of the two types of cells and as a consequence leads to an increase in the binding activity of certain integrin suited on the neutrophils surface. The activated endothelial cells that line these venules become more adhesive to circulating. When neutrophils encounter the selectins, they form transient adhesions that dramatically slow their movement through the vessel. The bound neutrophils then change their shape and squeeze between narrow capillaries or adjacent endothelial cells into the damaged tissue. The ability of blood cells to change shape and return to their original shape after the application of external loads suggests that live cells are viscoelastic. [107] [232] [233] The time dependent response of these samples is the nanoscale equivalence of the creep response observed in the bulk materials used to determine their viscoelastic properties. In fact, deflection distance curves are used for the characterization of a

wide variety of material properties like the viscoelastic of the live and the diseased cells because of the improved AFM designs. These improved designs may be of advantage to measuring the small fluctuating forces in the viscous medium.[24] In the same line it is known in many works in the literature that alteration in the spring constants of the live cell could have significant effects in their ability to squeeze through the surrounding tissue invade and metastasize. The cell mechanical properties were closely associated with various disease conditions such as tumour formation and metastasis in the human body. Thus an exciting avenue amongst many other goals in the cell mechanics research and related works is to make links between the cellular level mechanosensitivity, the force generation mechanical properties together with their underlying molecular mechanism.

For instance, one recent study suggested that metastasis of cancerous cell involves a complex sequence of interlinked biochemical and biomechanical events, including adhesion, migration and deformation during tumour cell invasion. Although, the cytoskeleton's elastic properties have been extensively studied by other methods, and to the best of my knowledge the internal friction characteristics have still not been fully understood. Measuring the internal friction of cells is also of interest because this property is closely linked with the dynamics and the nanomechanical properties of the cells. Similarly, the interplay of cellular components enables adaptation to changing demands of mechanical strength and stability. As such, the understanding of how cell mechanically respond to physical forces may be a key and an important step to further explore how the transmission and the distribution of these mechanical signals are eventually converted to biological and chemical responses in the cell. In order to develop an accurate understanding of properties of the methods to probe the cell mechanics (interconnection between the ECM and cytoskeleton measuring) and accurately quantify the internal friction parameter are required. Furthermore, force measurements of soft cell samples which are adhered to a substrate by AFM is one of the key improvements because quantitative analysis could be made and it allows experimenters to make more objective conclusions about the sample under study. However, the viscous contributions of cells are largely ignored, mainly because of technical, instrumental, or analytical limitations.

## A6.0 The magnetic coil



Figure 38: Image of the AFM coil setup employed for the loading and unloading force control in step and in modulation magnetic force. Image shows a side view of magnetic adapted on the 20 X objective lens of the AFM. The strip of the sharp transformer metal core with copper wire windings is shown in image. The core material aided to create the large gradient of the magnetic field. The apparatus offers an advantage and a non-invasive method to apply force to very end of the magnetic AFM cantilever/magnetic particles placed on the AFM stage in a fluid cell.

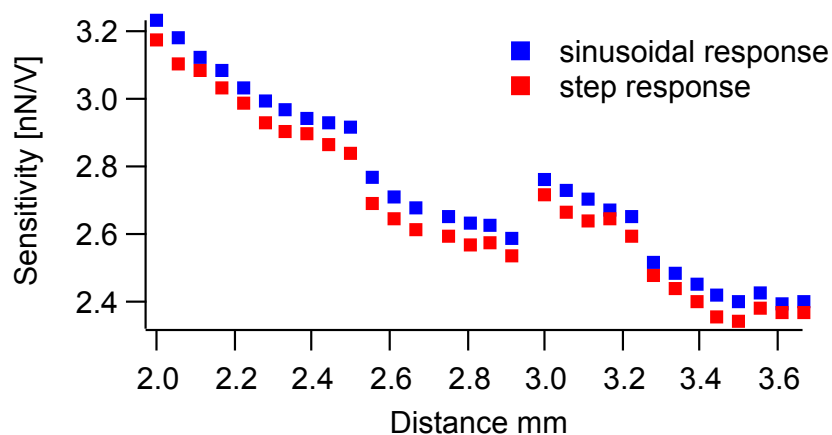


Figure 39: The magnetic force exerted on the cantilever depends on the spatial relation between the coil and the magnetic cantilever in an aqueous medium. The figure shows data obtained after calibrating of the coil voltage into force in magnet as a function of distance to the soft spring magnetic AFM cantilever. The calibration of the coil voltage into force is obtained from the motion of the free cantilever. The force was dependent on the size of the magnetic fragment and the position on the back of the cantilever with respect to the position of the coil. Displacement of the free cantilever in combination with the measured soft AFM cantilever spring constant gives values of the force applied per volts through the coil in use. The calibration was required every time a magnetic fragment was glued to the back of the cantilever was changed or the laser position was changed. For coarse approach the entire coil is firmly attached to objective of the inverted microscope. Graph shows a decrease in the response of the soft spring magnetic cantilever as the gap size is increased. The graph has been zoomed (sensitivity [nN/V] axis) for better visibility.

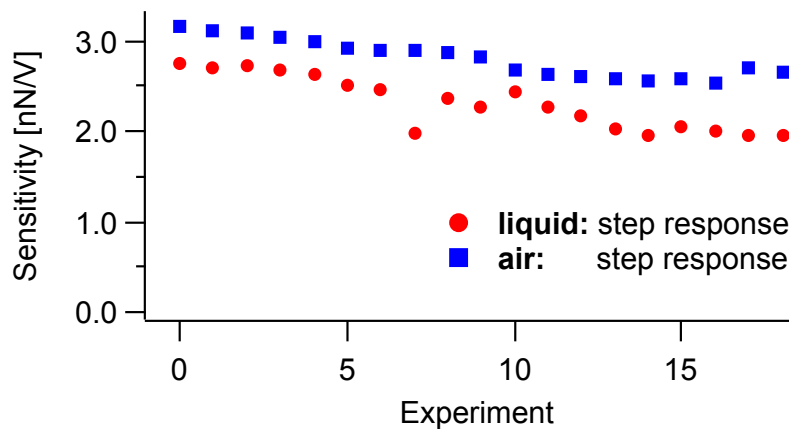


Figure 40: Calibration of the coil voltage into force in magnet in an aqueous medium and in air. The calibration of the coil voltage into force is obtained from the motion of the free cantilever. The Comparison shows a reduction in the sensitivity in aqueous medium when compared to air data obtained after a step drive. The values on each point are an average of 19 experimental rounds. The y-axis shows the sensitivity [nN/V] while the x-axis shows the average values from nineteen-experiment measured repeatedly at longer time intervals on the same day. The magnetic cantilever was placed at large fields and large distances relative to the AFM sample stage. Figure shows considerable hysteresis and drift in values due to drift in magnetic coil design.

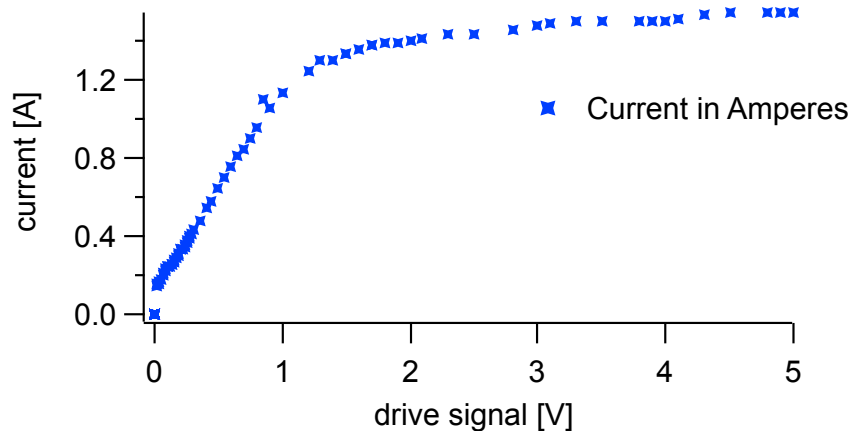
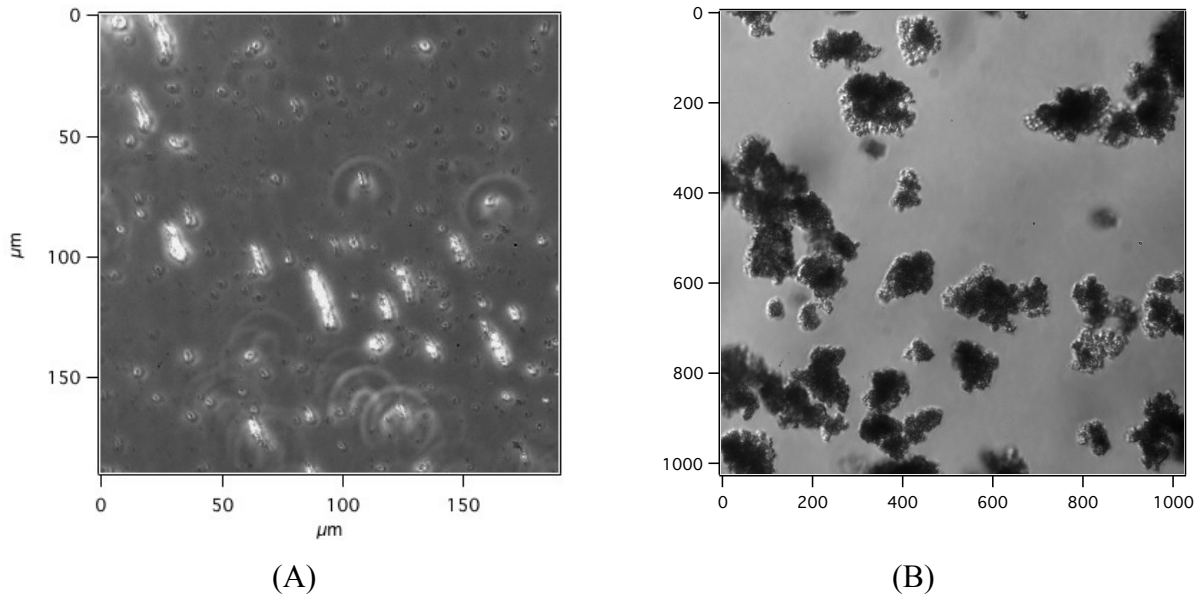


Figure 41: Figure shows the relationship between the coil current as a function of drive voltage for an example coil prepared for the work. The force modulation technique provides large amplitude of the soft spring magnetic cantilever oscillations of the order of tens of mV/ nm. The graph shows an initial increase of output current as amplitude of drive signal increases. For this coil the figure depicts saturation for larger drive signals values.



**Figure 42: Preparation of magnetic fragments in its fluid suspension. In order to characterize the system we first introduced purely viscous fluids in the form of mixtures. The system was first calibrated at low frequencies in the quasi-static operation to set the ratio between the force in magnetic and current through coil. The behavior of magnetic fragments under a small magnetic force (coil tip not shown) in a magnetic field and their tiny aggregates revealed under the light microscopy. By observing the induced motion of due to the local field generated gradient of the coil on the magnetic particles and beads, the system was analysed and characterized adequately. The figure shows dark field and phase contrast images of an assembly of nanoclusters of magnetic fragments in with small spacings between them in their suspension. Left panel (A) includes magnetized clusters of the nano particles aligned in the inhomogeneous magnetic field. Paramagnets keep moving in the direction of strongest field. Right panel (B) includes an agglomerate of nano paramagnetic particles in the suspension.**

The system was first calibrated at low frequencies in the quasi-static operation to set the ratio between the force in magnetic and current through coil in an inhomogeneous magnetic field. The behavior of magnetic fragments under a small magnetic force in a magnetic field and their tiny aggregates revealed under the light microscopy. By observing the induced motion of due to the local field generated gradient of the coil on the magnetic particles and beads, the system was analysed and characterized adequately.

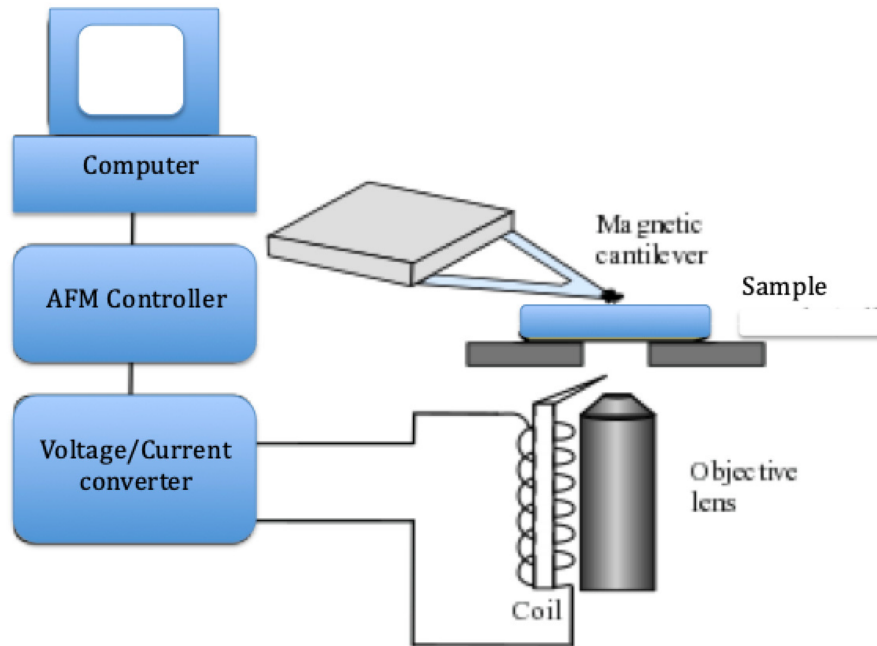


Figure 43: The magnetic force microscope measurements were performed using a commercial MFP-3D- atomic force microscope mounted on an inverted optical microscope. The AFM soft spring magnetic cantilever is on the piezo-ceramic so that it may be moved in all the three directions. The coil is connected to the computer through a voltage/current converter and the drive signal from the AFM controller. The motion of the magnetic AFM cantilever is measured as a function of the drive current. The magnetic fragments were glued to the end of the cantilever using 2-component glue under control of the inverted optical microscope. Force calibration was only possible if the spring constant of the magnetic AFM cantilever was accurately measured. The relationship between the photodiode signal and the magnetic cantilever deflection (sensitivity factor  $S$ ) was calibrated by recording several force curves before and after the AFM measurements, at a bare region of the glass coverslip and averaging its slope.

**A7.0 summary of the viscous properties of the cell derived from creep response data after application of force steps (loading and unloading steps) a magnetic step in force and the z step response experiments**

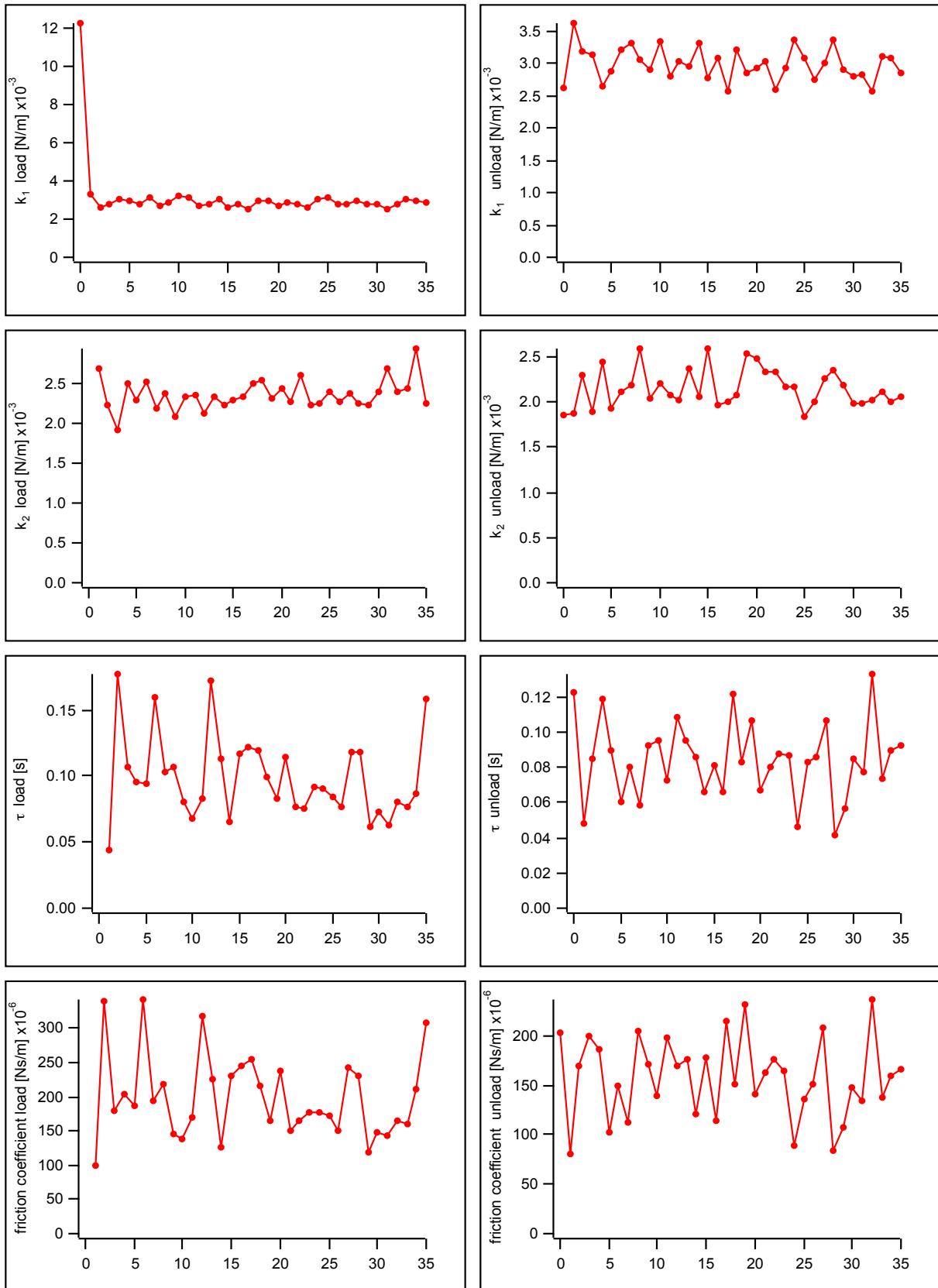


Figure 44: Summary of viscous values obtained by analysing the magnetic step response data on cell sample. The graph is a compilation of all 36 force curves from a 6 by 6 force volume over an area of 600 nm. The left column represents the loading steps and the right column represents the unloading step on one force volume.

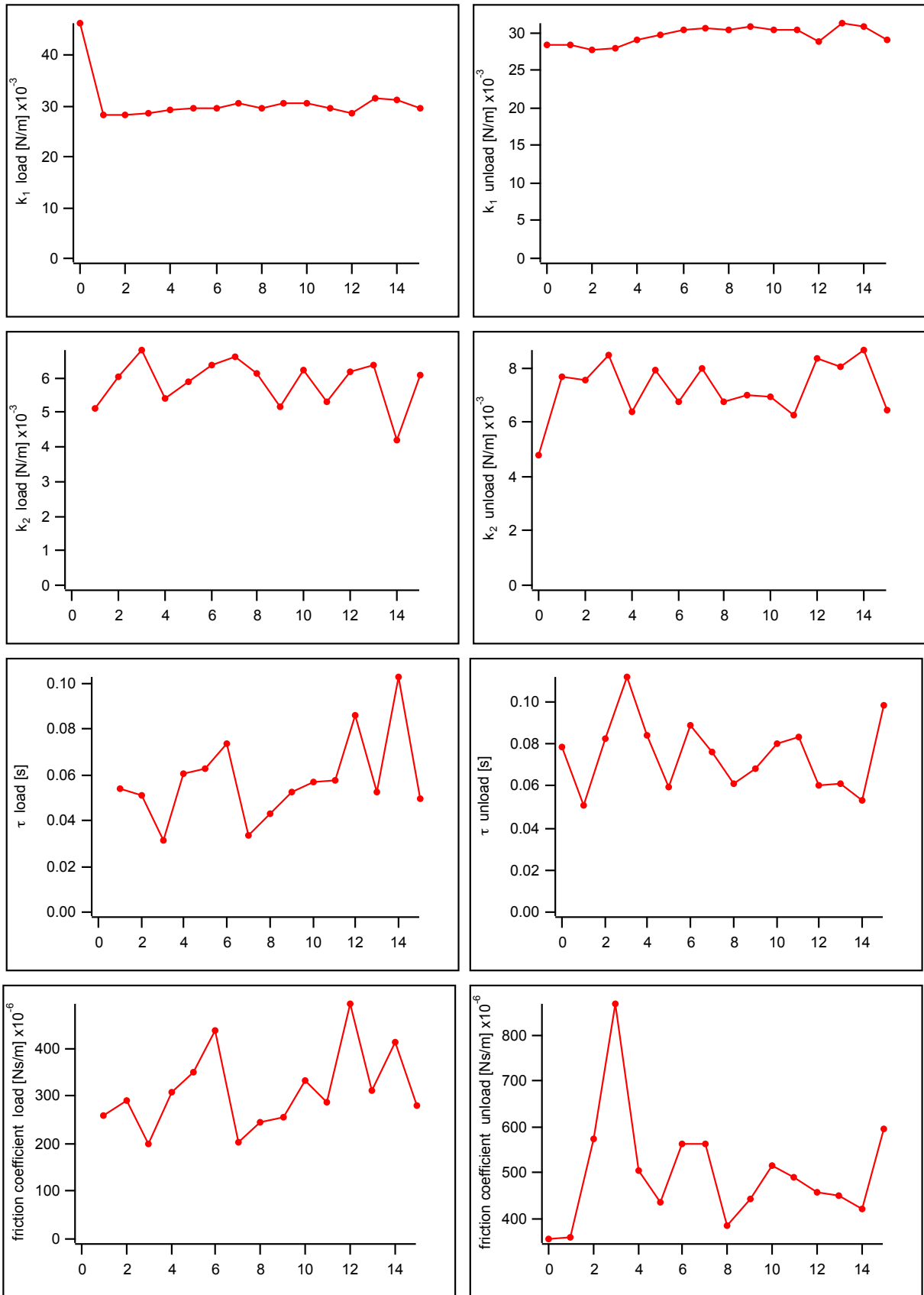
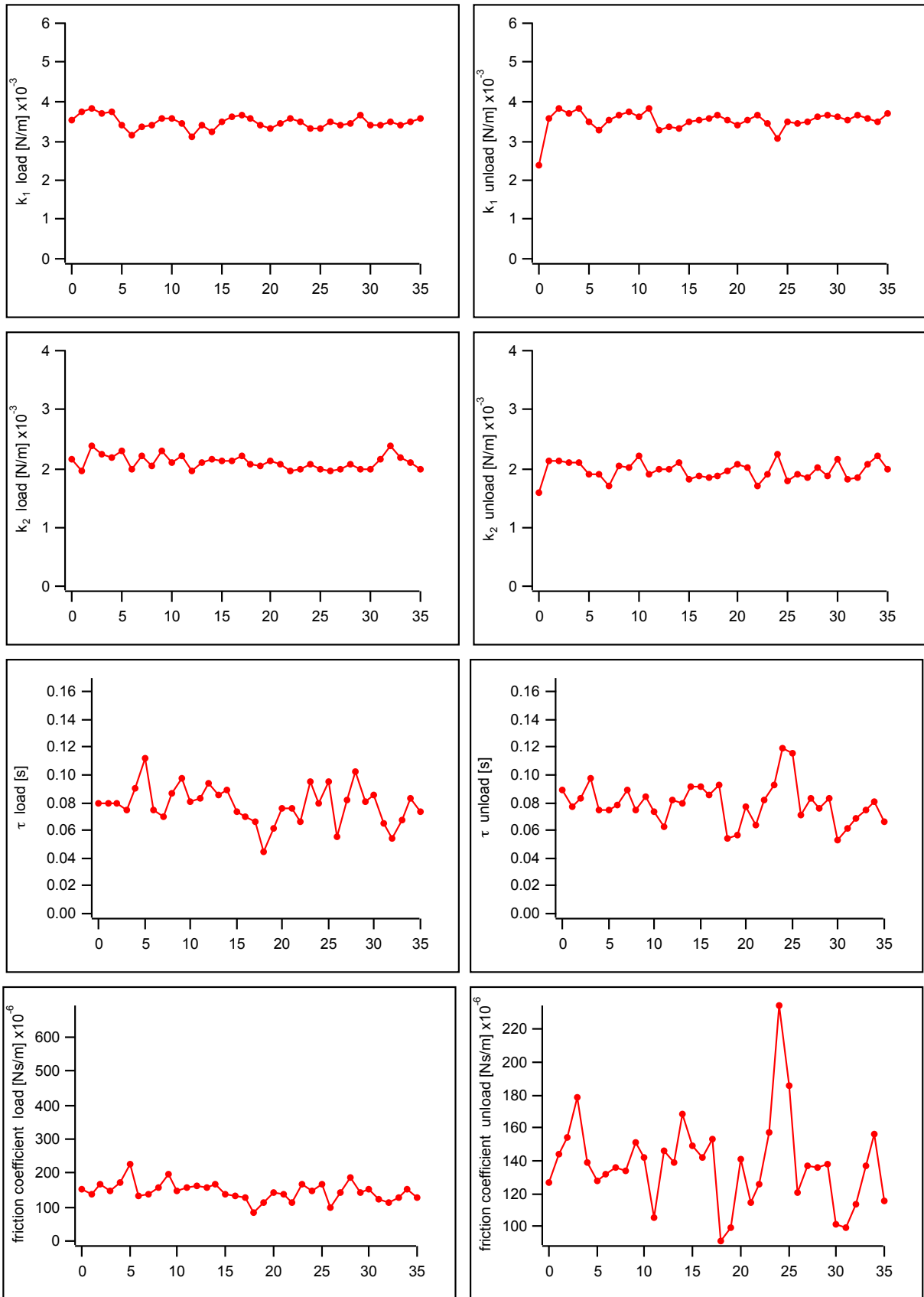


Figure 45: Summary of viscous values of a cell sample derived by analysing a z step response data on polymer gel sample. The graph is a compilation of all 16-force curves from a 6 by 6 force volume over an area of 600 nm. The left panels are the loading steps and the right panel represents the unloading step analysed on one force volume.



**Figure 46: Summary of spring constants and the viscous damping values obtained from a z step response data on cell sample. The graph is a compilation of all 36-force curves from a 6 by 6 force volume over an area of 600 nm. The left column represents the loading steps and the right column represents the unloading step on one force volume.**

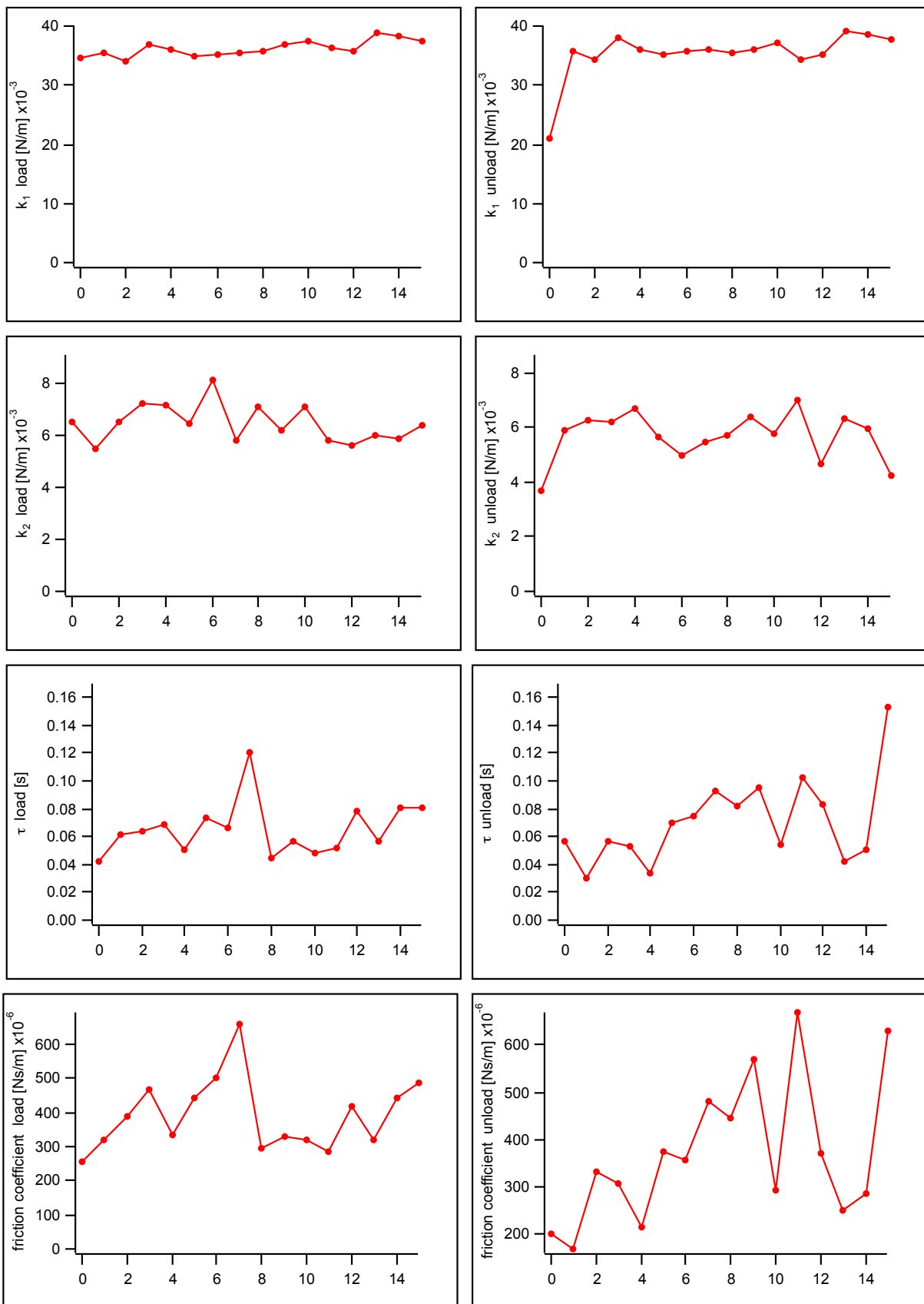


Figure 47: Summary of spring constants and viscous values obtained from a step response data on stiffer polymer gel sample. The graph is a compilation of all 16 force curves from a 6 by 6 force volume over an area of 600 nm. The left panels are the loading steps and the right panel represents the unloading step on one force volume.

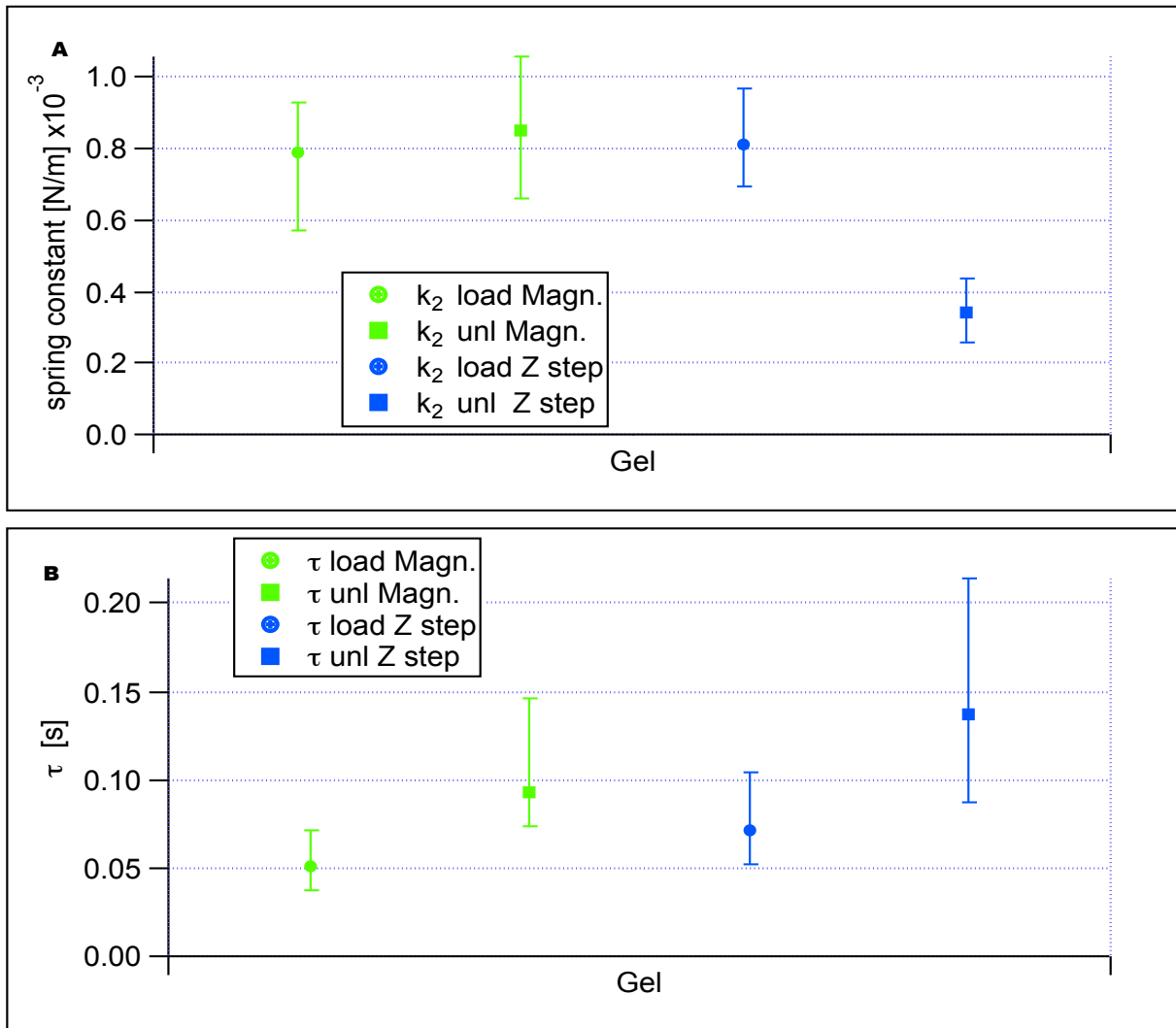


Figure 48: Summary of viscous values on soft polyacrylamide gels. Figure shows comparison of the spring constants values (panel A) and the relaxation times (panel B) derived by analysing the magnetic (Magn.) steps and the z step response (Z step) data respectively. The initial data obtained from both setups was summarized during the testing phase of the experiment.

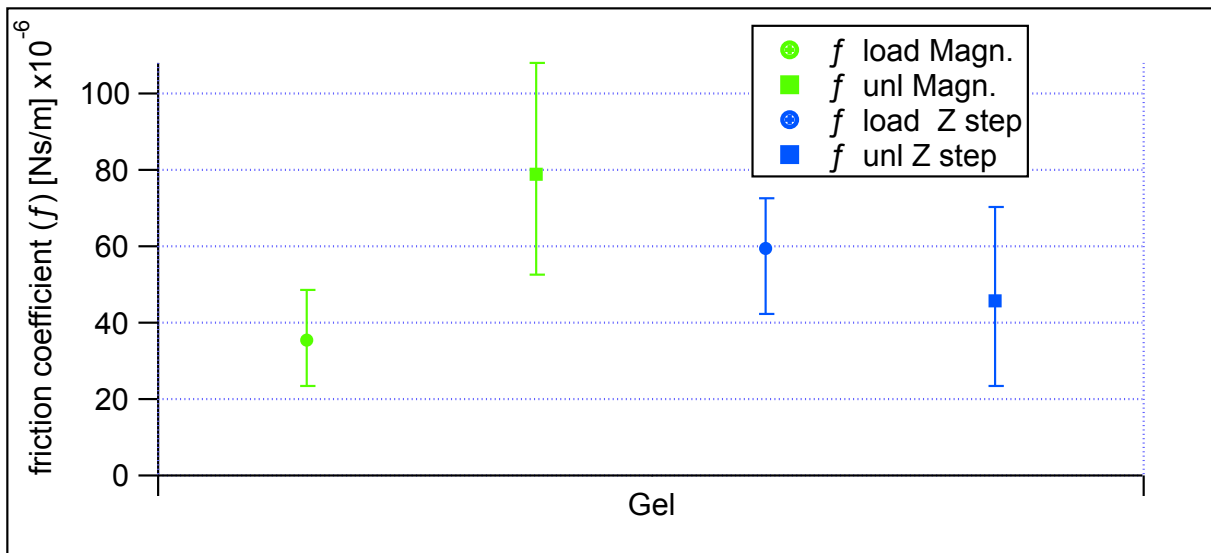
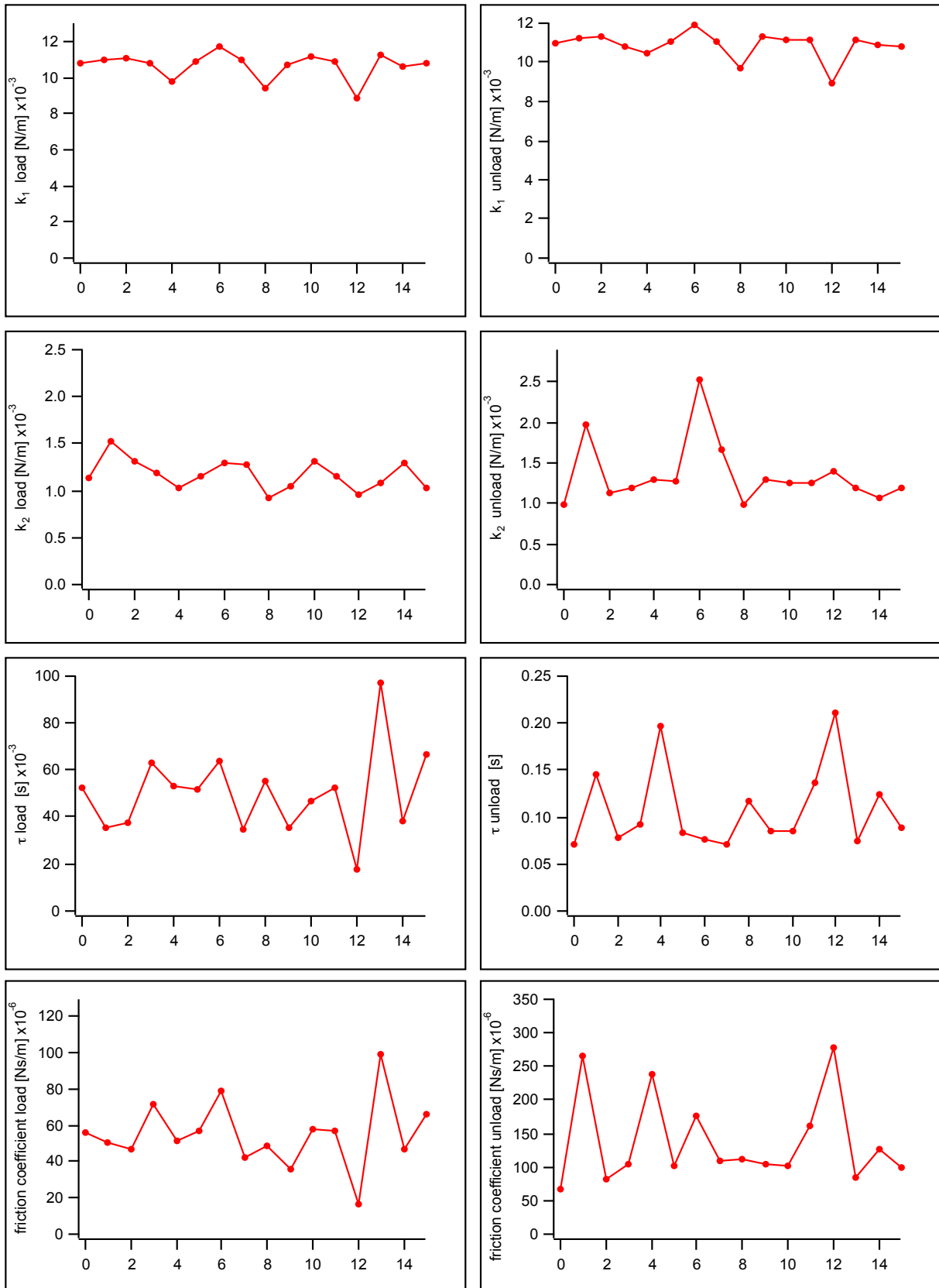


Figure 49: Comparison of the viscous values obtained from the magnetic step (Magn.) and the z step response (Z step) setups on the gel sample by AFM. The viscous properties from both setups could be quantified compared in terms of the creep response for both experimental designs.



**Figure 50: Summary of the spring constants and viscous values of the polyacrylamide gels sample derived by analysing the magnetic step response data. The graph is a compilation of all 16-force curves from a 6 by 6 force volume over an area of 600 nm. The left panel show loading step, and the right panel shows the unloading step on one force volume.**

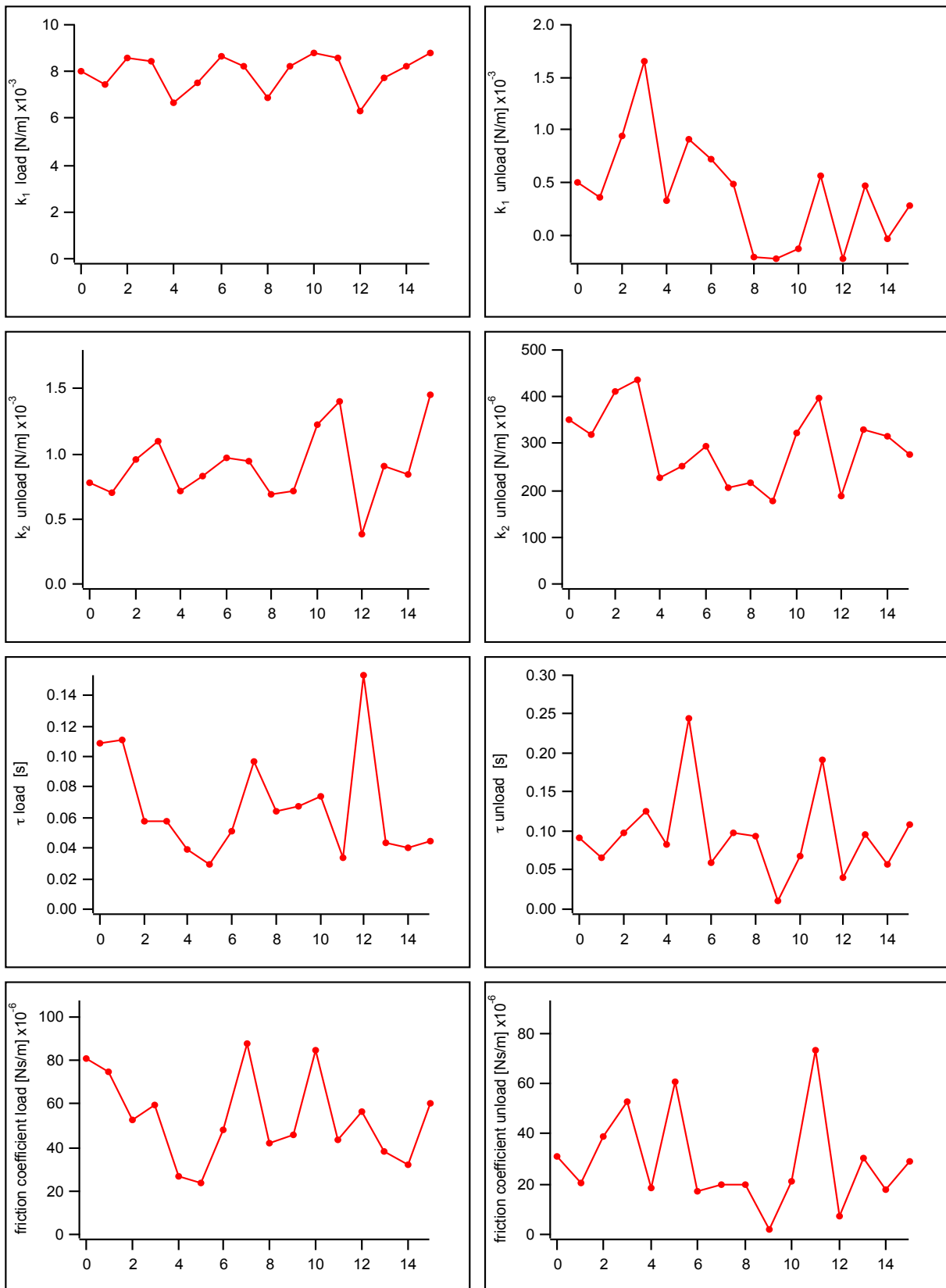
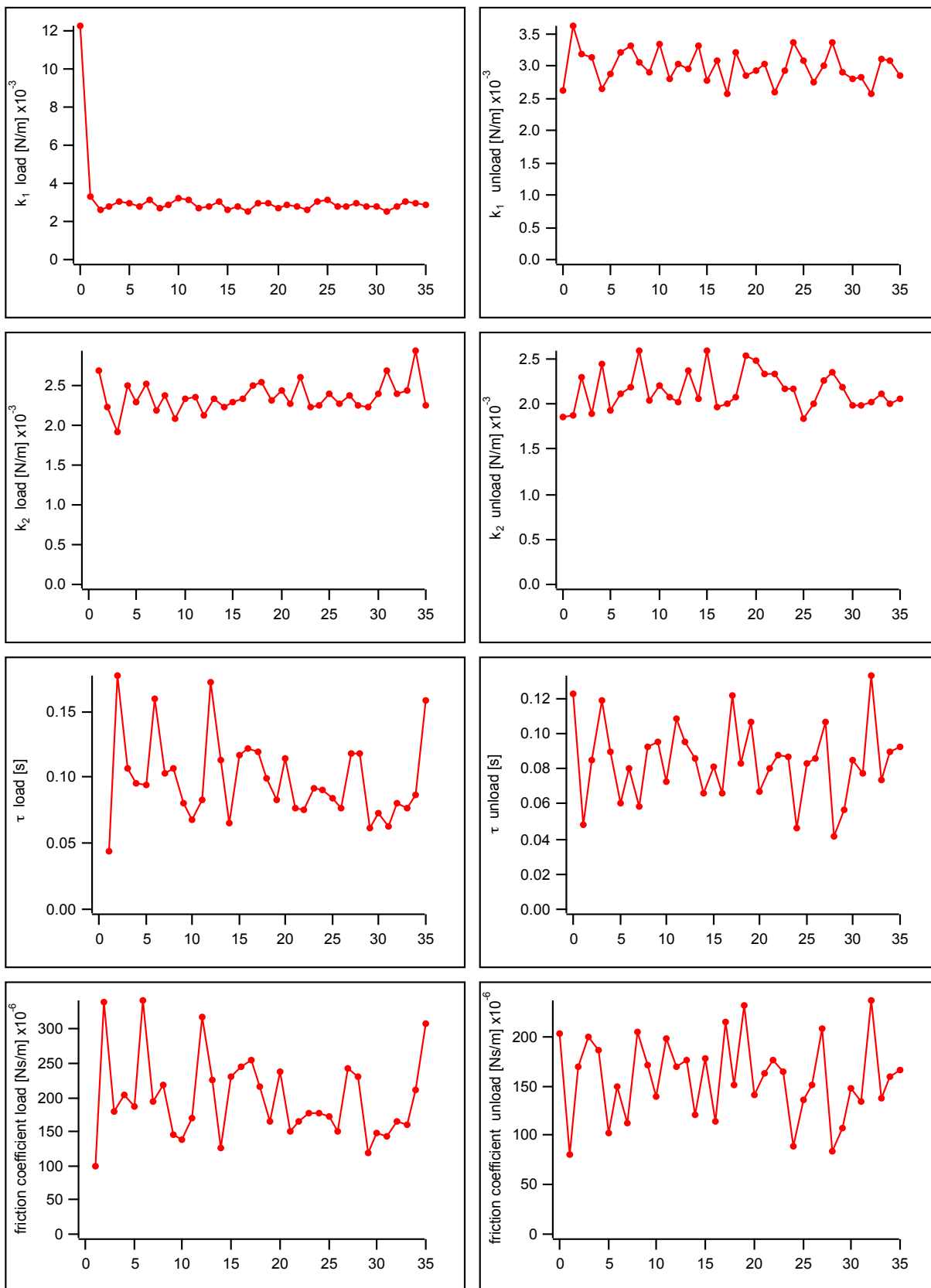


Figure 51: Summary of spring constants and viscous values on soft polyacrylamide gels sample derived by analysing the z step response data. The graph shown is a compilation of 16 force curves over an area of 600nm x 600nm on a soft gel. Derived values are very close for unloading and unloading steps, when compared to the approach and retract data derived from the force curves, as expected.



**Figure 52: Summary of spring constants and viscous values of the cell sample derived by analysing the magnetic step response data. The graph is a compilation of all 36-force curves from a 6 by 6 force volume over an area of 600 nm. The left panel show loading step, and the right panel shows unloading step on one force volume.**

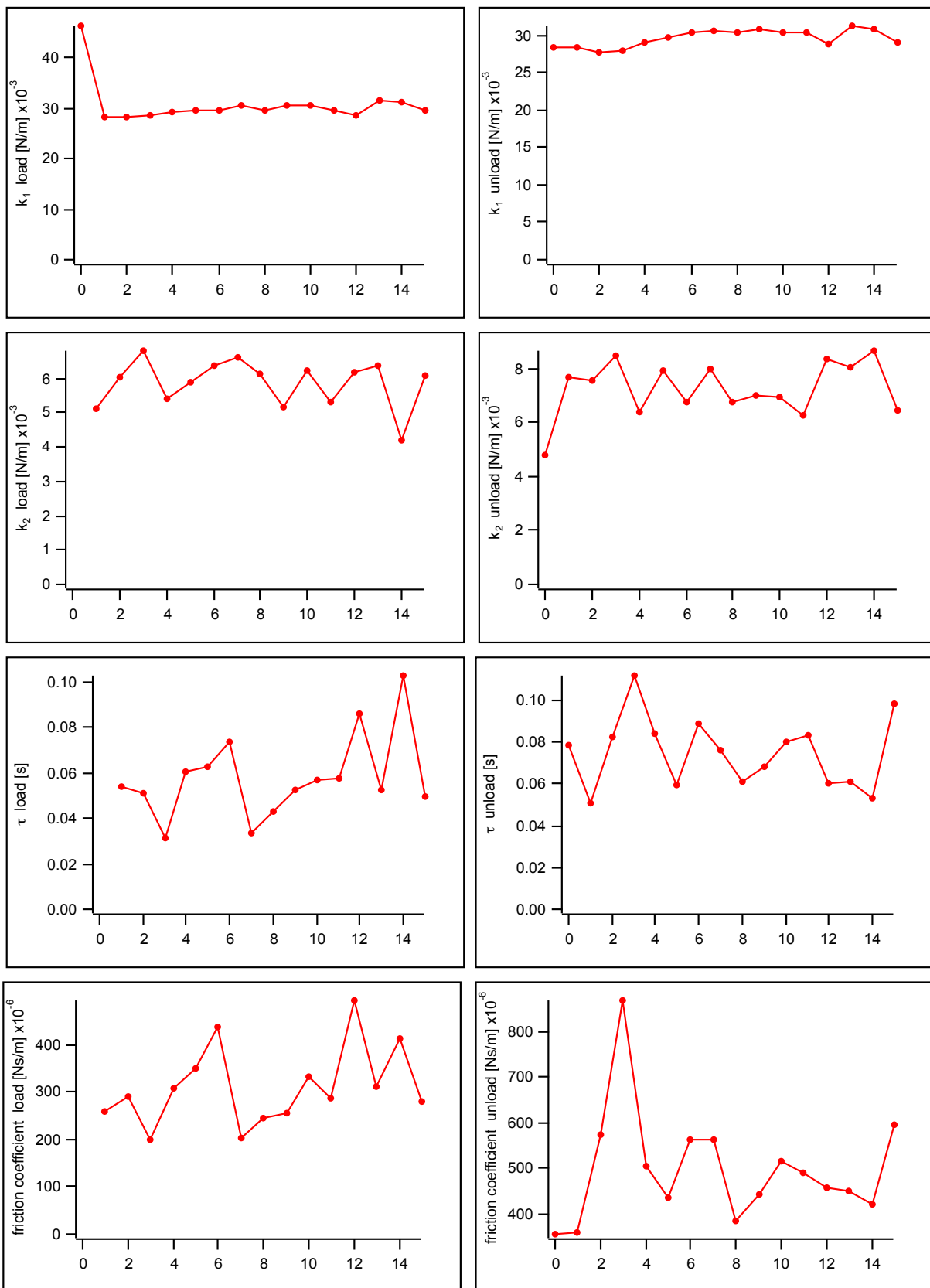


Figure 53: Summary of the spring constants and viscous values from the soft polyacrylamide gel sample derived by analysing the z step response data. The graph is a compilation of all 16-force curves from a 6 by 6 force volume over an area of 600 nm. The left panel show loading step, and the right panel shows unloading step on one force volume. Data has been zoomed for better visibility.

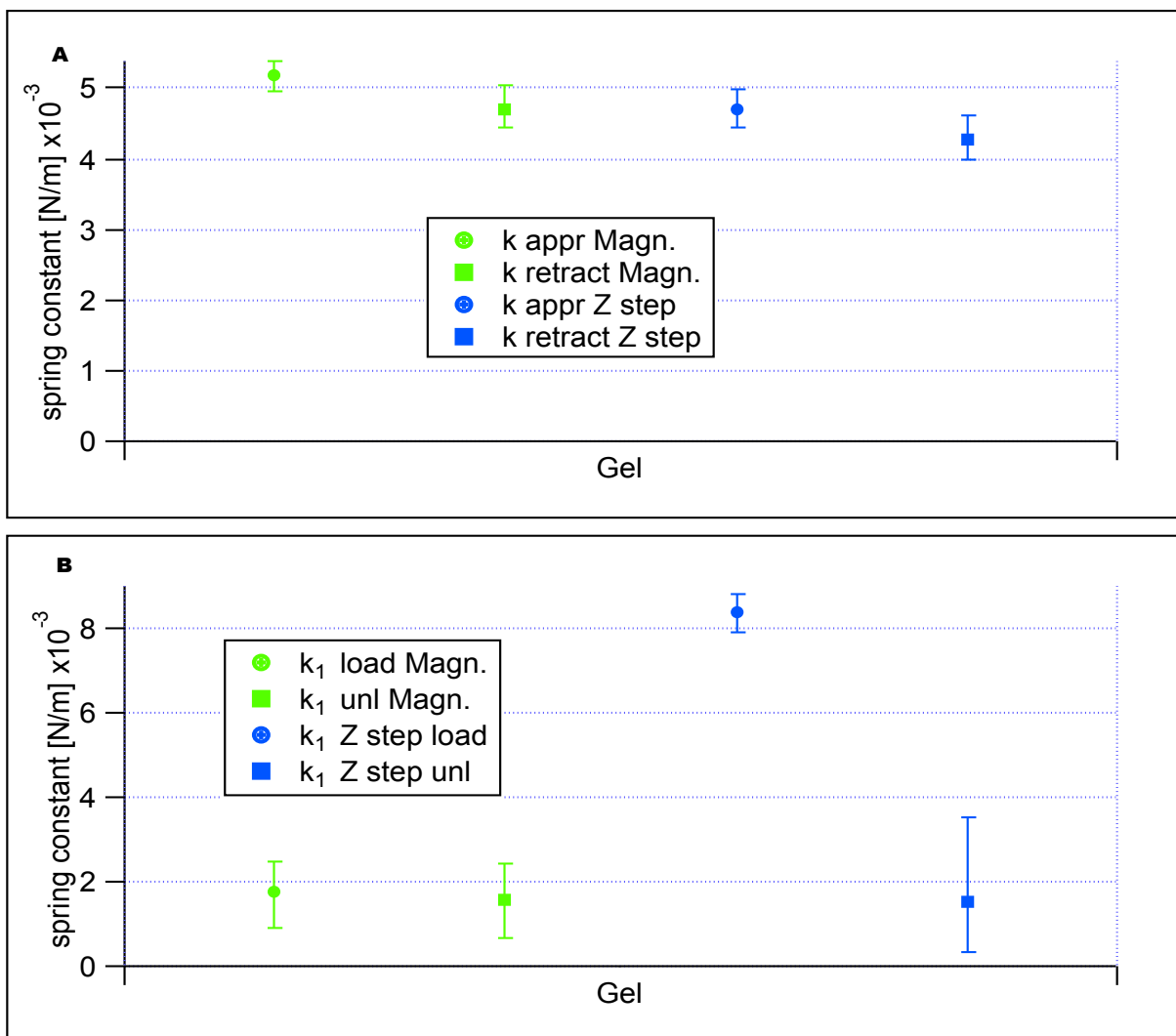


Figure 54: Summary of spring constants on the soft polyacrylamide gel sample derived by analysing the force curve and magnetic step (Magn.) response data. The determined spring constant from the loading and the unloading steps are reasonably close together in numbers for magnetic step setup. The spring constants obtained by analysing the z step response data deviates largely in numbers and observation emphasizes the need for careful consideration on the experimental design and the selection of the measurement technique with soft AFM cantilevers.

## BIBLIOGRAPHY

1. Butt, H.-J., *Measuring electrostatic, van der Waals, and hydration forces in electrolyte solutions with an atomic force microscope*. Biophysical Journal, 1991. **60**(6): p. 1438-1444.
2. Israelachvili, J.N., *Surface forces*, in *The Handbook of Surface Imaging and Visualization*. 2022, CRC Press. p. 793-816.
3. Israelachvili, J.N. and G.E. Adams, *Measurement of forces between two mica surfaces in aqueous electrolyte solutions in the range 0–100 nm*. Journal of the Chemical Society, Faraday Transactions 1: Physical Chemistry in Condensed Phases, 1978. **74**: p. 975-1001.
4. Lyubchenko, Y.L., et al., *Atomic force microscopy imaging of double stranded DNA and RNA*. Journal of biomolecular structure and dynamics, 1992. **10**(3): p. 589-606.
5. Lindsay, S., et al., *STM and AFM images of nucleosome DNA under water*. Journal of Biomolecular structure and Dynamics, 1989. **7**(2): p. 279-287.
6. Vogel, V., *How Cells Exploit Forces to Sense and Respond to their Environments*. Biophysical Journal, 2014. **106**(2): p. 3a.
7. Yusko, E.C. and C.L. Asbury, *Force is a signal that cells cannot ignore*. Molecular biology of the cell, 2014. **25**(23): p. 3717-3725.
8. Binnig, G., C.F. Quate, and C. Gerber, *Atomic force microscope*. Physical review letters, 1986. **56**(9): p. 930.
9. Bhushan, B. and H. Fuchs, *Applied scanning probe methods VII*. 2007: Springer.
10. Weisenhorn, A.L., et al., *Deformation and height anomaly of soft surfaces studied with an AFM*. Nanotechnology, 1993. **4**(2): p. 106.
11. Radmacher, M., M. Fritz, and P.K. Hansma, *Imaging soft samples with the atomic force microscope: gelatin in water and propanol*. Biophysical journal, 1995. **69**(1): p. 264.
12. Levental, I., P.C. Georges, and P.A. Janmey, *Soft biological materials and their impact on cell function*. Soft Matter, 2007. **3**(3): p. 299-306.
13. AZONANO. *Atomic Force Microscopy and Using It for Investigating Gene Delivery Vehicles*. 2006, 05, 12 [cited 2015; Available from: <https://www.azom.com/article.aspx?ArticleID=3278>].
14. Lekka, M., et al., *Cancer cell recognition–mechanical phenotype*. Micron, 2012. **43**(12): p. 1259-1266.
15. Lekka, M. and P. Laidler, *Applicability of AFM in cancer detection*. Nature nanotechnology, 2009. **4**(2): p. 72-72.
16. Lekka, M., et al., *Cancer cell detection in tissue sections using AFM*. Archives of biochemistry and biophysics, 2012. **518**(2): p. 151-156.
17. Lekka, M., et al., *Elasticity of normal and cancerous human bladder cells studied by scanning force microscopy*. European Biophysics Journal, 1999. **28**(4): p. 312-316.
18. Martin, Y., C.C. Williams, and H.K. Wickramasinghe, *Atomic force microscope-force mapping and profiling on a sub 100 - Å scale*. Journal of Applied Physics, 1987. **61**(10): p. 4723-4729.
19. Martin, Y. and H.K. Wickramasinghe, *Magnetic imaging by “force microscopy” with 1000 Å resolution*. Applied Physics Letters, 1987. **50**(20): p. 1455-1457.

20. Cappella, B., *Physical Principles of Force–Distance Curves by Atomic Force Microscopy*, in *Mechanical Properties of Polymers Measured through AFM Force-Distance Curves*. 2016, Springer. p. 95-230.
21. Ohler, B., *Practical advice on the determination of cantilever spring constants*. Application Note AN94, Veeco Instruments Inc, 2007.
22. Bruker. *MLCT - Bruker AFM Probes*. 2016; Available from: <http://www.brukerafmprobes.com/p-3444-mlct.aspx>.
23. Braga, P.C. and D. Ricci, *Atomic force microscopy: biomedical methods and applications*. Vol. 242. 2004: Springer Science & Business Media.
24. Butt, H.-J. and M. Jaschke, *Calculation of thermal noise in atomic force microscopy*. *Nanotechnology*, 1995. **6**(1): p. 1.
25. Butt, H.-J., B. Cappella, and M. Kappell, *Force measurements with the atomic force microscope: Technique, interpretation and applications*. *Surface science reports*, 2005. **59**(1): p. 1-152.
26. Hillier, A.C., S. Kim, and A.J. Bard, *Measurement of double-layer forces at the electrode/electrolyte interface using the atomic force microscope: potential and anion dependent interactions*. *The Journal of Physical Chemistry*, 1996. **100**(48): p. 18808-18817.
27. Burnham, N., et al., *Comparison of calibration methods for atomic-force microscopy cantilevers*. *Nanotechnology*, 2003. **14**: p. 1-6.
28. Sader, J.E., et al., *Method for the calibration of atomic force microscope cantilevers*. *Review of Scientific Instruments*, 1995. **66**(7): p. 3789-3798.
29. Sader, J.E., J.W. Chon, and P. Mulvaney, *Calibration of rectangular atomic force microscope cantilevers*. *Review of Scientific Instruments*, 1999. **70**(10): p. 3967-3969.
30. AZONANO. *Fundamentals of Contact Mode and TappingMode Atomic Force Microscopy*. 2012, 18, 05; Available from: <https://www.azonano.com/article.aspx?ArticleID=3010>.
31. De Gennes, P.-G., *Wetting: statics and dynamics*. *Reviews of modern physics*, 1985. **57**(3): p. 827.
32. Jinesh, K. and J. Frenken, *Capillary condensation in atomic scale friction: how water acts like a glue*. *Physical review letters*, 2006. **96**(16): p. 166103.
33. Noy, A., et al., *Chemical force microscopy: exploiting chemically-modified tips to quantify adhesion, friction, and functional group distributions in molecular assemblies*. *Journal of the American Chemical Society*, 1995. **117**(30): p. 7943-7951.
34. Beaglehole, D. and H. Christenson, *Vapor adsorption on mica and silicon: entropy effects, layering, and surface forces*. *The Journal of Physical Chemistry*, 1992. **96**(8): p. 3395-3403.
35. Colchero, J., et al., *Observation of liquid neck formation with scanning force microscopy techniques*. *Langmuir*, 1998. **14**(9): p. 2230-2234.
36. Zitzler, L., S. Herminghaus, and F. Mugele, *Capillary forces in tapping mode atomic force microscopy*. *Physical Review B*, 2002. **66**(15): p. 155436.
37. He, M., et al., *Critical phenomena of water bridges in nanoasperity contacts*. *The Journal of Chemical Physics*, 2001. **114**(3): p. 1355-1360.
38. Stifter, T., O. Marti, and B. Bhushan, *Theoretical investigation of the distance dependence of capillary and van der Waals forces in scanning force microscopy*. *Physical Review B*, 2000. **62**(20): p. 13667.
39. Xiao, X. and L. Qian, *Investigation of humidity-dependent capillary force*. *Langmuir*, 2000. **16**(21): p. 8153-8158.

40. Hutter, J.L. and J. Bechhoefer, *Calibration of atomic - force microscope tips*. Review of Scientific Instruments, 1993. **64**(7): p. 1868-1873.
41. Kodera, N., et al., *High-resolution imaging of myosin motor in action by a high-speed atomic force microscope*, in *Molecular and Cellular Aspects of Muscle Contraction*. 2003, Springer. p. 119-127.
42. Proksch, R., et al., *Finite optical spot size and position corrections in thermal spring constant calibration*. Nanotechnology, 2004. **15**(9): p. 1344.
43. Burnham, N.A. and A.J. Kulik, *Surface forces and adhesion*, in *Handbook of micro/nano tribology*. 2020, CRC Press. p. 247-271.
44. Leckband, D. and J. Israelachvili, *Intermolecular forces in biology*. Quarterly reviews of biophysics, 2001. **34**(2): p. 105-267.
45. Radmacher, M., *Studying the mechanics of cellular processes by atomic force microscopy*. Methods in cell biology, 2007. **83**: p. 347-372.
46. Prabhune, M., et al., *Comparison of mechanical properties of normal and malignant thyroid cells*. Micron, 2012. **43**(12): p. 1267-1272.
47. Gavara, N. and R.S. Chadwick, *Determination of the elastic moduli of thin samples and adherent cells using conical atomic force microscope tips*. Nature nanotechnology, 2012. **7**(11): p. 733-736.
48. Rianna, C. and M. Radmacher, *Comparison of viscoelastic properties of cancer and normal thyroid cells on different stiffness substrates*. European Biophysics Journal, 2016: p. 1-16.
49. Hertz, H., *Ueber den kontakt elastischer koerper*. J. Reine Angew. Math, 1881. **92**(156).
50. Johnson, K., *Contact mechanics cambridge univ. Press, Cambridge, 1985*. **95**(365): p. 922.
51. Mahaffy, R., et al., *Scanning probe-based frequency-dependent microrheology of polymer gels and biological cells*. Physical review letters, 2000. **85**(4): p. 880.
52. Ohashi, T., et al., *Experimental and numerical analyses of local mechanical properties measured by atomic force microscopy for sheared endothelial cells*. Biomedical materials and engineering, 2002. **12**(3): p. 319-327.
53. Fischer-Cripps, A.C., *Introduction to contact mechanics*. 2000: Springer.
54. Cappella, B., *Physical Principles of Force-Distance Curves by Atomic Force Microscopy*, in *Mechanical Properties of Polymers Measured through AFM Force-Distance Curves*. 2016, Springer. p. 3-91.
55. Rico, F., et al., *Probing mechanical properties of living cells by atomic force microscopy with blunted pyramidal cantilever tips*. Physical Review E, 2005. **72**(2): p. 021914.
56. Rico, F., et al., *Nanomechanics of lung epithelial cells*. International journal of nanotechnology, 2005. **2**(1-2): p. 180-194.
57. Hooke, R., *Micrographia*. 1968: Holzer.
58. Rotsch, C. and M. Radmacher, *Drug-induced changes of cytoskeletal structure and mechanics in fibroblasts: an atomic force microscopy study*. Biophysical journal, 2000. **78**(1): p. 520-535.
59. Schäfer, A. and M. Radmacher, *Influence of myosin II activity on stiffness of fibroblast cells*. Acta Biomaterialia, 2005. **1**(3): p. 273-280.
60. Rianna, C., et al. *Cell mechanics as a marker for diseases: Biomedical applications of AFM*. in *AIP Conference Proceedings*. 2016. AIP Publishing.
61. Pollard, T.D., *Rate constants for the reactions of ATP-and ADP-actin with the ends of actin filaments*. The Journal of cell biology, 1986. **103**(6): p. 2747-2754.

62. Kabsch, W., et al., *Atomic structure of the actin: DNase I complex*. Nature, 1990. **347**(6288): p. 37-44.
63. Bartles, J.R., A. Wierda, and L. Zheng, *Identification and characterization of espin, an actin-binding protein localized to the F-actin-rich junctional plaques of Sertoli cell ectoplasmic specializations*. Journal of cell science, 1996. **109**(6): p. 1229-1239.
64. Bartles, J.R., et al., *Small espin: a third actin-bundling protein and potential forked protein ortholog in brush border microvilli*. The Journal of cell biology, 1998. **143**(1): p. 107-119.
65. Weber, A., R. Herz, and I. Reiss, *Role of magnesium in the relaxation of myofibrils*. Biochemistry, 1969. **8**(6): p. 2266-2271.
66. Albrecht, E. and H.R. Petty, *Cellular memory: neutrophil orientation reverses during temporally decreasing chemoattractant concentrations*. Proceedings of the National Academy of Sciences, 1998. **95**(9): p. 5039-5044.
67. Jilkine, A. and L. Edelstein-Keshet, *A comparison of mathematical models for polarization of single eukaryotic cells in response to guided cues*. PLoS computational biology, 2011. **7**(4): p. e1001121.
68. Tracqui, P., *Biophysical models of tumour growth*. Reports on Progress in Physics, 2009. **72**(5): p. 056701.
69. Mori, Y., A. Jilkine, and L. Edelstein-Keshet, *Asymptotic and bifurcation analysis of wave-pinning in a reaction-diffusion model for cell polarization*. SIAM journal on applied mathematics, 2011. **71**(4): p. 1401-1427.
70. Loomis, W.F., *Cell signaling during development of Dictyostelium*. Developmental biology, 2014. **391**(1): p. 1-16.
71. Skoge, M., et al., *Cellular memory in eukaryotic chemotaxis*. Proceedings of the National Academy of Sciences, 2014. **111**(40): p. 14448-14453.
72. Onsum, M.D. and C.V. Rao, *Calling heads from tails: the role of mathematical modeling in understanding cell polarization*. Current opinion in cell biology, 2009. **21**(1): p. 74-81.
73. Goehring, N.W. and S.W. Grill, *Cell polarity: mechanochemical patterning*. Trends in cell biology, 2013. **23**(2): p. 72-80.
74. Burridge, K., C.E. Turner, and L.H. Romer, *Tyrosine phosphorylation of paxillin and pp125FAK accompanies cell adhesion to extracellular matrix: a role in cytoskeletal assembly*. The Journal of cell biology, 1992. **119**(4): p. 893-903.
75. Lee, B.Y., et al., *FAK signaling in human cancer as a target for therapeutics*. Pharmacology & therapeutics, 2015. **146**: p. 132-149.
76. Hirota, T., et al., *Zyxin, a regulator of actin filament assembly, targets the mitotic apparatus by interacting with h-warts/LATS1 tumor suppressor*. The Journal of cell biology, 2000. **149**(5): p. 1073-1086.
77. Gilmore, A.P. and K. Burridge, *Regulation of vinculin binding to talin and actin by phosphatidylinositol-4-5-bisphosphate*. Nature, 1996. **381**(6582): p. 531-535.
78. Calderwood, D.A. and M.H. Ginsberg, *Talin forges the links between integrins and actin*. Nature cell biology, 2003. **5**(8): p. 694-696.
79. Otey, C.A., F.M. Pavalko, and K. Burridge, *An interaction between alpha-actinin and the beta 1 integrin subunit in vitro*. The Journal of cell biology, 1990. **111**(2): p. 721-729.
80. Crawford, A.W., J.W. Michelsen, and M.C. Beckerle, *An interaction between zyxin and alpha-actinin*. The Journal of cell biology, 1992. **116**(6): p. 1381-1393.
81. Kreis, T. and R. Vale, *Guidebook to the cytoskeletal and motor proteins*. Vol. 2. 1999: Oxford University Press Oxford.

82. Geiger, B., J.P. Spatz, and A.D. Bershadsky, *Environmental sensing through focal adhesions*. Nature reviews Molecular cell biology, 2009. **10**(1): p. 21-33.
83. Berman, A., N. Kozlova, and G. Morozovich, *Integrins: structure and signaling*. Biochemistry (Moscow), 2003. **68**: p. 1284-1299.
84. Green, L.J., A.P. Mould, and M.J. Humphries, *The integrin  $\beta$  subunit*. The international journal of biochemistry & cell biology, 1998. **30**(2): p. 179-184.
85. Plow, E.F., et al., *Ligand binding to integrins*. Journal of Biological Chemistry, 2000. **275**(29): p. 21785-21788.
86. Takada, Y., X. Ye, and S. Simon, *The integrins*. Genome biology, 2007. **8**: p. 1-9.
87. Quinlan, M.E., et al., *Drosophila Spire is an actin nucleation factor*. Nature, 2005. **433**(7024): p. 382-388.
88. Carlier, M. and D. Pantaloni, *Direct evidence for ADP-inorganic phosphate-F-actin as the major intermediate in ATP-actin polymerization. Rate of dissociation of inorganic phosphate from actin filaments*. Biochemistry, 1986. **25**(24): p. 7789-7792.
89. Ridley, A.J., *Life at the leading edge*. Cell, 2011. **145**(7): p. 1012-1022.
90. Ridley, A.J., et al., *Cell migration: integrating signals from front to back*. Science, 2003. **302**(5651): p. 1704-1709.
91. Foxman, E.F., E.J. Kunkel, and E.C. Butcher, *Integrating conflicting chemotactic signals: the role of memory in leukocyte navigation*. The Journal of cell biology, 1999. **147**(3): p. 577-588.
92. Wojciak-Stothard, B. and A.J. Ridley, *Shear stress-induced endothelial cell polarization is mediated by Rho and Rac but not Cdc42 or PI 3-kinases*. The Journal of cell biology, 2003. **161**(2): p. 429-439.
93. Parent, C.A. and P.N. Devreotes, *A cell's sense of direction*. Science, 1999. **284**(5415): p. 765-770.
94. Mataraza, J.M., et al., *IQGAP1 promotes cell motility and invasion*. Journal of Biological Chemistry, 2003. **278**(42): p. 41237-41245.
95. Otterbein, L.R., P. Graceffa, and R. Dominguez, *The crystal structure of uncomplexed actin in the ADP state*. Science, 2001. **293**(5530): p. 708-711.
96. Belmont, L.D., et al., *A change in actin conformation associated with filament instability after Pi release*. Proceedings of the National Academy of Sciences, 1999. **96**(1): p. 29-34.
97. Graceffa, P. and R. Dominguez, *Crystal structure of monomeric actin in the ATP state: structural basis of nucleotide-dependent actin dynamics*. Journal of Biological Chemistry, 2003. **278**(36): p. 34172-34180.
98. Korn, E.D., M.-F. Carlier, and D. Pantaloni, *Actin polymerization and ATP hydrolysis*. Science, 1987. **238**(4827): p. 638-644.
99. Pfaendtner, J., et al., *Nucleotide-dependent conformational states of actin*. Proceedings of the National Academy of Sciences, 2009. **106**(31): p. 12723-12728.
100. Kumar, S. and V.M. Weaver, *Mechanics, malignancy, and metastasis: the force journey of a tumor cell*. Cancer and Metastasis Reviews, 2009. **28**(1-2): p. 113-127.
101. Alcaraz, J., et al., *Microrheology of human lung epithelial cells measured by atomic force microscopy*. Biophysical journal, 2003. **84**(3): p. 2071-2079.
102. Andreu, I., et al., *Heterogeneous micromechanical properties of the extracellular matrix in healthy and infarcted hearts*. Acta biomaterialia, 2014. **10**(7): p. 3235-3242.

103. Kaufmann, A., et al., *Amphibian oocyte nuclei expressing lamin A with the progeria mutation E145K exhibit an increased elastic modulus*. *Nucleus*, 2011. **2**(4): p. 310-319.
104. Oberleithner, H., et al., *Potassium softens vascular endothelium and increases nitric oxide release*. *Proceedings of the National Academy of Sciences*, 2009. **106**(8): p. 2829-2834.
105. Discher, D.E., P. Janmey, and Y.-l. Wang, *Tissue cells feel and respond to the stiffness of their substrate*. *Science*, 2005. **310**(5751): p. 1139-1143.
106. Yeung, A. and E. Evans, *Cortical shell-liquid core model for passive flow of liquid-like spherical cells into micropipets*, in *Biophysical journal*. 1989. p. 139-149.
107. Evans, E. and A. Yeung, *Apparent viscosity and cortical tension of blood granulocytes determined by micropipet aspiration*. *Biophysical journal*, 1989. **56**(1): p. 151.
108. Crick, F. and A. Hughes, *The physical properties of cytoplasm: A study by means of the magnetic particle method Part I. Experimental*. *Experimental Cell Research*, 1950. **1**(1): p. 37-80.
109. Valberg, P. and H. Feldman, *Magnetic particle motions within living cells. Measurement of cytoplasmic viscosity and motile activity*. *Biophysical Journal*, 1987. **52**(4): p. 551.
110. Bausch, A.R., W. Möller, and E. Sackmann, *Measurement of local viscoelasticity and forces in living cells by magnetic tweezers*. *Biophysical journal*, 1999. **76**(1): p. 573-579.
111. Kundu, T., J. Bereiter-Hahn, and K. Hillmann, *Measuring elastic properties of cells by evaluation of scanning acoustic microscopy  $V(Z)$  values using simplex algorithm*. *Biophysical journal*, 1991. **59**(6): p. 1194.
112. Bausch, A.R., et al., *Local measurements of viscoelastic parameters of adherent cell surfaces by magnetic bead microrheometry*. *Biophysical journal*, 1998. **75**(4): p. 2038-2049.
113. Fabry, B., et al., *Scaling the microrheology of living cells*. *Physical review letters*, 2001. **87**(14): p. 148102.
114. Kollmannsberger, P. and B. Fabry, *BaHigh-force magnetic tweezers with force feedback for biological applications*. *Review of Scientific Instruments*, 2007. **78**(11): p. 114301.
115. Guck, J., et al., *The optical stretcher: a novel laser tool to micromanipulate cells*. *Biophysical journal*, 2001. **81**(2): p. 767-784.
116. Mietke, A., et al., *Extracting Cell Stiffness from Real-Time Deformability Cytometry: Theory and Experiment*. *Biophysical journal*, 2015. **109**(10): p. 2023-2036.
117. Kollmannsberger, P. and B. Fabry, *Linear and nonlinear rheology of living cells*. *Annual review of materials research*, 2011. **41**: p. 75-97.
118. Ahmed, W.W., É. Fodor, and T. Betz, *Active cell mechanics: Measurement and theory*. *Biochimica et Biophysica Acta (BBA)-Molecular Cell Research*, 2015. **1853**(11): p. 3083-3094.
119. Hecht, F.M., et al., *Imaging viscoelastic properties of live cells by AFM: power-law rheology on the nanoscale*. *Soft matter*, 2015. **11**(23): p. 4584-4591.
120. Hertz, H., *Über die Berührung fester elastischer Körper*. *Journal für die reine und angewandte Mathematik*, 1882. **92**: p. 156-171.
121. Sneddon, I.N., *The relation between load and penetration in the axisymmetric Boussinesq problem for a punch of arbitrary profile*. *International journal of engineering science*, 1965. **3**(1): p. 47-57.

122. Rebelo, L., et al., *Comparison of the viscoelastic properties of cells from different kidney cancer phenotypes measured with atomic force microscopy*. Nanotechnology, 2013. **24**(5): p. 055102.
123. Wu, H., T. Kuhn, and V. Moy, *Mechanical properties of L929 cells measured by atomic force microscopy: effects of anticytoskeletal drugs and membrane crosslinking*. Scanning, 1998. **20**(5): p. 389-397.
124. Moreno-Flores, S., et al., *Stress relaxation and creep on living cells with the atomic force microscope: a means to calculate elastic moduli and viscosities of cell components*. Nanotechnology, 2010. **21**(44): p. 445101.
125. Radmacher, M., R. Tillmann, and H. Gaub, *Imaging viscoelasticity by force modulation with the atomic force microscope*. Biophysical journal, 1993. **64**(3): p. 735.
126. Florin, E.L., et al., *Atomic force microscope with magnetic force modulation*. Review of scientific instruments, 1994. **65**(3): p. 639-643.
127. Puig-De-Morales, M., et al., *Measurement of cell microrheology by magnetic twisting cytometry with frequency domain demodulation*. Journal of Applied Physiology, 2001. **91**(3): p. 1152-1159.
128. Rebêlo, L., et al., *Microrheology of cells with magnetic force modulation atomic force microscopy*. Soft matter, 2014. **10**(13): p. 2141-2149.
129. Nelson, P.C., et al., *Biological physics: energy, information, life*. 2008: WH Freeman New York.
130. Mullins, R.D., J.A. Heuser, and T.D. Pollard, *The interaction of Arp2/3 complex with actin: nucleation, high affinity pointed end capping, and formation of branching networks of filaments*. Proceedings of the National Academy of Sciences, 1998. **95**(11): p. 6181-6186.
131. Doubrovinski, K. and K. Kruse, *Cytoskeletal waves in the absence of molecular motors*. Europhysics Letters, 2008. **83**(1): p. 18003.
132. Vicker, M.G., *F - actin assembly in Dictyostelium cell locomotion and shape oscillations propagates as a self - organized reaction-diffusion wave*. FEBS letters, 2002. **510**(1-2): p. 5-9.
133. Gerisch, G., et al., *Mobile actin clusters and traveling waves in cells recovering from actin depolymerization*. Biophysical journal, 2004. **87**(5): p. 3493-3503.
134. Vicker, M.G., *Eukaryotic cell locomotion depends on the propagation of self-organized reaction-diffusion waves and oscillations of actin filament assembly*. Experimental cell research, 2002. **275**(1): p. 54-66.
135. Cohen, P., *The origins of protein phosphorylation*. Nature cell biology, 2002. **4**(5): p. E127-E130.
136. Cuerrier, C.M., et al., *Real-time monitoring of angiotensin II-induced contractile response and cytoskeleton remodeling in individual cells by atomic force microscopy*. Pflügers Archiv-European Journal of Physiology, 2009. **457**: p. 1361-1372.
137. Jung, G., E.D. Korn, and J. Hammer 3rd, *The heavy chain of Acanthamoeba myosin IB is a fusion of myosin-like and non-myosin-like sequences*. Proceedings of the National Academy of Sciences, 1987. **84**(19): p. 6720-6724.
138. Berg, J.S., B.C. Powell, and R.E. Cheney, *A millennial myosin census*. Molecular biology of the cell, 2001. **12**(4): p. 780-794.
139. Miki, H., et al., *All kinesin superfamily protein, KIF, genes in mouse and human*. Proceedings of the National Academy of Sciences, 2001. **98**(13): p. 7004-7011.

140. Hunter, A.W., et al., *The kinesin-related protein MCAK is a microtubule depolymerase that forms an ATP-hydrolyzing complex at microtubule ends*. Molecular cell, 2003. **11**(2): p. 445-457.
141. Pollard, T.D. and E.D. Korn, *Acanthamoeba myosin: I. Isolation from Acanthamoeba castellanii of an enzyme similar to muscle myosin*. Journal of Biological Chemistry, 1973. **248**(13): p. 4682-4690.
142. Huxley, H. and J. Hanson, *Changes in the cross-striations of muscle during contraction and stretch and their structural interpretation*. Nature, 1954. **173**(4412): p. 973-976.
143. Huxley, H.E., *The Mechanism of Muscular Contraction: Recent structural studies suggest a revealing model for cross-bridge action at variable filament spacing*. Science, 1969. **164**(3886): p. 1356-1366.
144. Selden, L.A., L.C. Gershman, and J.E. Estes, *A kinetic comparison between Mg-actin and Ca-actin*. Journal of Muscle Research & Cell Motility, 1986. **7**: p. 215-224.
145. Selden, L.A., J.E. Estes, and L.C. Gershman, *The tightly bound divalent cation regulates actin polymerization*. Biochemical and Biophysical Research Communications, 1983. **116**(2): p. 478-485.
146. Tobacman, L.S. and E.D. Korn, *The kinetics of actin nucleation and polymerization*. Journal of Biological Chemistry, 1983. **258**(5): p. 3207-3214.
147. Pollard, T.D., L. Blanchoin, and R.D. Mullins, *Molecular mechanisms controlling actin filament dynamics in nonmuscle cells*. Annual review of biophysics and biomolecular structure, 2000. **29**(1): p. 545-576.
148. McGough, A., et al., *Cofilin changes the twist of F-actin: implications for actin filament dynamics and cellular function*. The Journal of cell biology, 1997. **138**(4): p. 771-781.
149. Blanchoin, L. and T.D. Pollard, *Mechanism of interaction of Acanthamoeba actophorin (ADF/Cofilin) with actin filaments*. Journal of Biological Chemistry, 1999. **274**(22): p. 15538-15546.
150. Pollard, T.D. and M.S. Mooseker, *Direct measurement of actin polymerization rate constants by electron microscopy of actin filaments nucleated by isolated microvillus cores*. The Journal of cell biology, 1981. **88**(3): p. 654-659.
151. Carlier, M.-F., et al., *Actin depolymerizing factor (ADF/cofilin) enhances the rate of filament turnover: implication in actin-based motility*. The Journal of cell biology, 1997. **136**(6): p. 1307-1322.
152. Gao, J. and F. Nakamura, *Actin-associated proteins and small molecules targeting the actin cytoskeleton*. International journal of molecular sciences, 2022. **23**(4): p. 2118.
153. Funk, J., et al., *Profilin and formin constitute a pacemaker system for robust actin filament growth*. Elife, 2019. **8**: p. e50963.
154. Small, J.V., M. Herzog, and K. Anderson, *Actin filament organization in the fish keratocyte lamellipodium*. The Journal of cell biology, 1995. **129**(5): p. 1275-1286.
155. Svitkina, T.M. and G.G. Borisy, *Arp2/3 complex and actin depolymerizing factor/cofilin in dendritic organization and treadmilling of actin filament array in lamellipodia*. The Journal of cell biology, 1999. **145**(5): p. 1009-1026.
156. Svitkina, T.M., et al., *Analysis of the actin-myosin II system in fish epidermal keratocytes: mechanism of cell body translocation*. The Journal of cell biology, 1997. **139**(2): p. 397-415.
157. Smilenov, L.B., et al., *Focal adhesion motility revealed in stationary fibroblasts*. Science, 1999. **286**(5442): p. 1172-1174.

158. Tseng, Y. and D. Wirtz, *Mechanics and multiple-particle tracking microheterogeneity of  $\alpha$ -actinin-cross-linked actin filament networks*. Biophysical journal, 2001. **81**(3): p. 1643-1656.
159. Beltzner, C.C. and T.D. Pollard, *Pathway of actin filament branch formation by Arp2/3 complex*. Journal of Biological Chemistry, 2008. **283**(11): p. 7135-7144.
160. Volkmann, N., et al., *Structure of Arp2/3 complex in its activated state and in actin filament branch junctions*. science, 2001. **293**(5539): p. 2456-2459.
161. Giannone, G., et al., *Periodic lamellipodial contractions correlate with rearward actin waves*. Cell, 2004. **116**(3): p. 431-443.
162. Tseng, Y., T.P. Kole, and D. Wirtz, *Micromechanical mapping of live cells by multiple-particle-tracking microrheology*. Biophysical journal, 2002. **83**(6): p. 3162-3176.
163. Welch, M.D., et al., *The human Arp2/3 complex is composed of evolutionarily conserved subunits and is localized to cellular regions of dynamic actin filament assembly*. The Journal of cell biology, 1997. **138**(2): p. 375-384.
164. Welch, M.D. and R.D. Mullins, *Cellular control of actin nucleation*. Annual review of cell and developmental biology, 2002. **18**(1): p. 247-288.
165. Pollard, T.D. and G.G. Borisy, *Cellular motility driven by assembly and disassembly of actin filaments*. Cell, 2003. **112**(4): p. 453-465.
166. Kovar, D.R., *Molecular details of formin-mediated actin assembly*. Current opinion in cell biology, 2006. **18**(1): p. 11-17.
167. Insall, R., et al., *Dynamics of the Dictyostelium Arp2/3 complex in endocytosis, cytokinesis, and chemotaxis*. Cell motility and the cytoskeleton, 2001. **50**(3): p. 115-128.
168. De Lozanne, A. and J.A. Spudich, *Disruption of the Dictyostelium myosin heavy chain gene by homologous recombination*. Science, 1987. **236**(4805): p. 1086-1091.
169. Friedl, P. and K. Wolf, *Plasticity of cell migration: a multiscale tuning model*. Journal of Cell Biology, 2010. **188**(1): p. 11-19.
170. Guck, J., et al., *Critical review: cellular mechanobiology and amoeboid migration*. Integrative biology, 2010. **2**(11-12): p. 575-583.
171. Chambers, A.F., A.C. Groom, and I.C. MacDonald, *Dissemination and growth of cancer cells in metastatic sites*. Nature Reviews Cancer, 2002. **2**(8): p. 563-572.
172. Friedl, P. and K. Wolf, *Tumour-cell invasion and migration: diversity and escape mechanisms*. Nature reviews cancer, 2003. **3**(5): p. 362-374.
173. Wang, W., et al., *Identification and testing of a gene expression signature of invasive carcinoma cells within primary mammary tumors*. Cancer research, 2004. **64**(23): p. 8585-8594.
174. Wang, W., et al., *Tumor cells caught in the act of invading: their strategy for enhanced cell motility*. Trends in cell biology, 2005. **15**(3): p. 138-145.
175. Condeelis, J. and J.E. Segall, *Intravital imaging of cell movement in tumours*. Nature Reviews Cancer, 2003. **3**(12): p. 921-930.
176. Wang, W., et al., *Single cell behavior in metastatic primary mammary tumors correlated with gene expression patterns revealed by molecular profiling*. Cancer research, 2002. **62**(21): p. 6278-6288.
177. Sahai, E., *Mechanisms of cancer cell invasion*. Current opinion in genetics & development, 2005. **15**(1): p. 87-96.
178. Friedl, P. and B. Weigelin, *Interstitial leukocyte migration and immune function*. Nature immunology, 2008. **9**(9): p. 960-969.

179. Paňková, K., et al., *The molecular mechanisms of transition between mesenchymal and amoeboid invasiveness in tumor cells*. Cellular and molecular life sciences, 2010. **67**: p. 63-71.
180. Ellenbroek, S.I., S. Iden, and J.G. Collard. *Cell polarity proteins and cancer*. in *Seminars in cancer biology*. 2012. Elsevier.
181. Nishimura, T., et al., *PAR-6-PAR-3 mediates Cdc42-induced Rac activation through the Rac GEFs STEF/Tiam1*. Nature cell biology, 2005. **7**(3): p. 270-277.
182. Iden, S. and J.G. Collard, *Crosstalk between small GTPases and polarity proteins in cell polarization*. Nature reviews Molecular cell biology, 2008. **9**(11): p. 846-859.
183. Ibarra, N., et al., *Nap1 regulates Dictyostelium cell motility and adhesion through SCAR-dependent and-independent pathways*. Current biology, 2006. **16**(7): p. 717-722.
184. Weiner, O.D., et al., *An actin-based wave generator organizes cell motility*. PLoS biology, 2007. **5**(9): p. e221.
185. Zencheck, W.D., et al., *Nucleotide-and activator-dependent structural and dynamic changes of arp2/3 complex monitored by hydrogen/deuterium exchange and mass spectrometry*. Journal of molecular biology, 2009. **390**(3): p. 414-427.
186. Kiselar, J.G., et al., *Visualizing Arp2/3 complex activation mediated by binding of ATP and WASp using structural mass spectrometry*. Proceedings of the National Academy of Sciences, 2007. **104**(5): p. 1552-1557.
187. Goley, E.D., et al., *Critical conformational changes in the Arp2/3 complex are induced by nucleotide and nucleation promoting factor*. Molecular cell, 2004. **16**(2): p. 269-279.
188. Peskin, C.S., G.M. Odell, and G.F. Oster, *Cellular motions and thermal fluctuations: the Brownian ratchet*. Biophysical journal, 1993. **65**(1): p. 316-324.
189. Tseng, Y., et al., *How actin crosslinking and bundling proteins cooperate to generate an enhanced cell mechanical response*. Biochemical and biophysical research communications, 2005. **334**(1): p. 183-192.
190. Mogilner, A. and G. Oster, *Cell motility driven by actin polymerization*. Biophysical journal, 1996. **71**(6): p. 3030-3045.
191. Pollard, T.D. and J.A. Cooper, *Quantitative analysis of the effect of Acanthamoeba profilin on actin filament nucleation and elongation*. Biochemistry, 1984. **23**(26): p. 6631-6641.
192. Schafer, D.A., P.B. Jennings, and J.A. Cooper, *Dynamics of capping protein and actin assembly in vitro: uncapping barbed ends by polyphosphoinositides*. The Journal of cell biology, 1996. **135**(1): p. 169-179.
193. Kuimova, M.K., *Mapping viscosity in cells using molecular rotors*. Physical Chemistry Chemical Physics, 2012. **14**(37): p. 12671-12686.
194. López-Duarte, I., et al., *A molecular rotor for measuring viscosity in plasma membranes of live cells*. Chemical Communications, 2014. **50**(40): p. 5282-5284.
195. Harris, A.R. and G. Charras, *Experimental validation of atomic force microscopy-based cell elasticity measurements*. Nanotechnology, 2011. **22**(34): p. 345102.
196. Kuznetsova, T.G., et al., *Atomic force microscopy probing of cell elasticity*. Micron, 2007. **38**(8): p. 824-833.
197. Ventre, M., F. Causa, and P.A. Netti, *Determinants of cell-material crosstalk at the interface: towards engineering of cell instructive materials*. Journal of the Royal Society Interface, 2012: p. rsif20120308.
198. Chen, D.T., et al., *Rheology of soft materials*. Condensed Matter Physics, 2010. **1**.
199. Natale, C.F., M. Ventre, and P.A. Netti, *Tuning the material-cytoskeleton crosstalk via nanoconfinement of focal adhesions*. Biomaterials, 2014. **35**(9): p. 2743-2751.

200. Yamaguchi, H. and J. Condeelis, *Regulation of the actin cytoskeleton in cancer cell migration and invasion*. Biochimica et Biophysica Acta (BBA)-Molecular Cell Research, 2007. **1773**(5): p. 642-652.
201. Kumar, S., et al., *Viscoelastic retraction of single living stress fibers and its impact on cell shape, cytoskeletal organization, and extracellular matrix mechanics*. Biophysical journal, 2006. **90**(10): p. 3762-3773.
202. Rianna, C., et al., *Micropatterned azopolymer surfaces modulate cell mechanics and cytoskeleton structure*. ACS applied materials & interfaces, 2015. **7**(38): p. 21503-21510.
203. Wu, G., et al., *Bioassay of prostate-specific antigen (PSA) using microcantilevers*. Nature biotechnology, 2001. **19**(9): p. 856-860.
204. Subramanian, A., et al., *Glucose biosensing using an enzyme-coated microcantilever*. Applied Physics Letters, 2002. **81**(2): p. 385-387.
205. Vashist, S.K., *A review of microcantilevers for sensing applications*. J. of Nanotechnology, 2007. **3**: p. 1-18.
206. Gates, R.S. and J.R. Pratt, *Accurate and precise calibration of AFM cantilever spring constants using laser Doppler vibrometry*. Nanotechnology, 2012. **23**(37): p. 375702.
207. Grutzik, S.J., et al., *Accurate spring constant calibration for very stiff atomic force microscopy cantilevers*. Review of Scientific Instruments, 2013. **84**(11): p. 113706.
208. Tortonese, M. and M. Kirk. *Characterization of application-specific probes for SPMs*. in *Photonics West'97*. 1997. International Society for Optics and Photonics.
209. Gates, R.S. and M.G. Reitsma, *Precise atomic force microscope cantilever spring constant calibration using a reference cantilever array*. Review of Scientific Instruments, 2007. **78**(8): p. 086101.
210. Gates, R.S., et al., *Atomic force microscope cantilever flexural stiffness calibration: toward a standard traceable method*. Journal of research of the National Institute of Standards and Technology, 2011. **116**(4): p. 703.
211. Song, Y., et al. *Calibration of the lateral spring constant of atomic force microscope cantilevers*. in *Applied Optics and Photonics China (AOPC2015)*. 2015. International Society for Optics and Photonics.
212. Sader, J.E., *Susceptibility of atomic force microscope cantilevers to lateral forces*. Review of Scientific Instruments, 2003. **74**(4): p. 2438-2443.
213. Clifford, C.A. and M.P. Seah, *The determination of atomic force microscope cantilever spring constants via dimensional methods for nanomechanical analysis*. Nanotechnology, 2005. **16**(9): p. 1666.
214. Tasci, T., et al., *Surface-enabled propulsion and control of colloidal microwheels*. Nature communications, 2016. **7**.
215. Sadiku, M.N., *Elements of electromagnetics*. Vol. 428. 2010, New York: Oxford university press New York.
216. Bishop, K.J., et al., *Nanoscale forces and their uses in self - assembly*. small, 2009. **5**(14): p. 1600-1630.
217. Gupta, A.K. and M. Gupta, *Synthesis and surface engineering of iron oxide nanoparticles for biomedical applications*. Biomaterials, 2005. **26**(18): p. 3995-4021.
218. Tse, J.R. and A.J. Engler, *Preparation of hydrogel substrates with tunable mechanical properties*. Current protocols in cell biology, 2010: p. 10.16. 1-10.16. 16.
219. DREHMELE. *Dremeleurope.com*. 2017 [cited 2017 January 04 2017]; Available from: <https://www.dremeleurope.com/nl/nl/imprint/>.

220. UHU. *2-Komponenten Klebstoffe*. 2016 [cited 2016 Febraury 02]; Available from: <http://www.uhu-profishop.de/klebstoffe/2-komponenten-klebstoffe.html?gclid=CNGU6Zm3qNECFVW4GwodATENuw>.
221. AG, C.Z.M. *Germany, Oberkochen - Company Location | Carl Zeiss Meditec AG*. 2017 [cited 2017 January 04]; Available from: <https://www.zeiss.com/meditec-ag/about-us/locations/germany-oberkochen-company.html>.
222. Attard, P., A. Carambassis, and M.W. Rutland, *Dynamic surface force measurement. 2. Friction and the atomic force microscope*. Langmuir, 1999. **15**(2): p. 553-563.
223. Stiernstedt, J., M.W. Rutland, and P. Attard, *A novel technique for the in situ calibration and measurement of friction with the atomic force microscope*. Review of Scientific Instruments, 2005. **76**(8): p. 083710.
224. Stiernstedt, J., et al., *Friction and forces between cellulose model surfaces: A comparison*. Journal of colloid and interface science, 2006. **303**(1): p. 117-123.
225. Warmack, R., et al., *Friction effects in the deflection of atomic force microscope cantilevers*. Review of scientific instruments, 1994. **65**(2): p. 394-399.
226. Piner, R. and R.S. Ruoff, *Cross talk between friction and height signals in atomic force microscopy*. Review of scientific instruments, 2002. **73**(9): p. 3392-3394.
227. Hoffmann, S., et al., *Fracture strength and Young's modulus of ZnO nanowires*. Nanotechnology, 2007. **18**(20): p. 205503.
228. Yu, Z., et al., *A force calibration standard for magnetic tweezers*. Review of Scientific Instruments, 2014. **85**(12): p. 123114.
229. Rico, F., et al., *Cell dynamic adhesion and elastic properties probed with cylindrical atomic force microscopy cantilever tips*. Journal of Molecular Recognition, 2007. **20**(6): p. 459-466.
230. Janmey, P.A. and R.T. Miller, *Mechanisms of mechanical signaling in development and disease*. J Cell Sci, 2011. **124**(1): p. 9-18.
231. Bao, G. and S. Suresh, *Cell and molecular mechanics of biological materials*. Nature materials, 2003. **2**(11): p. 715-725.
232. Needham, D. and R. Hochmuth, *Rapid flow of passive neutrophils into a 4 m pipet and measurement of cytoplasmic viscosity*. J. Biomech. Eng, 1990. **112**: p. 269-276.
233. Herant, M., W.A. Marganski, and M. Dembo, *The mechanics of neutrophils: synthetic modeling of three experiments*. Biophysical Journal, 2003. **84**(5): p. 3389-3413.